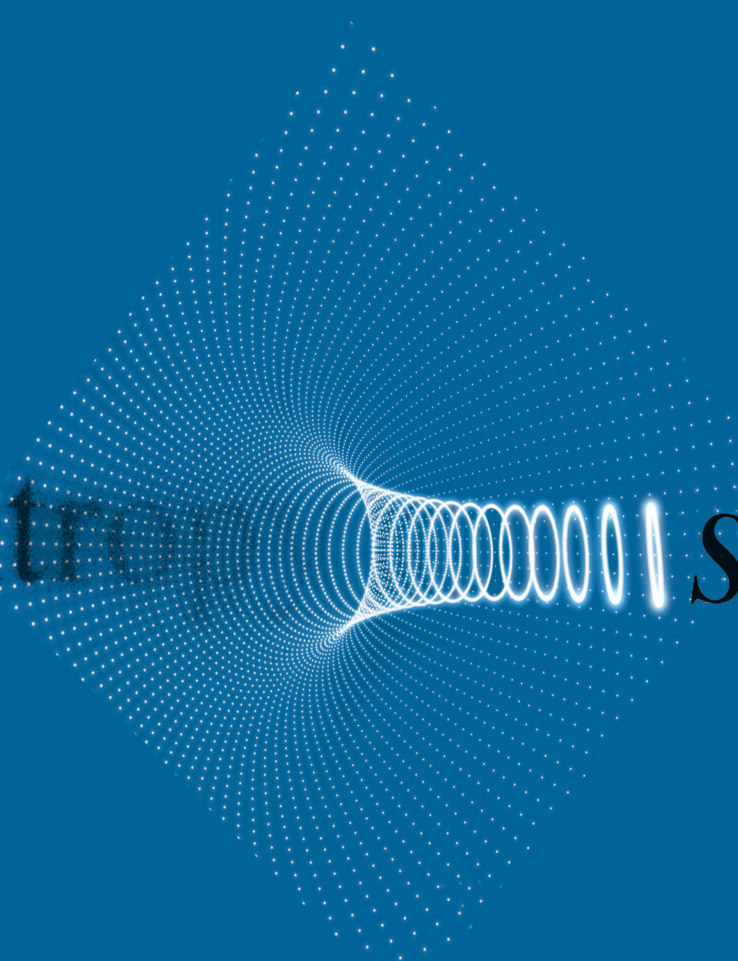


Yıl  
Year **2018**

Cilt  
Volume **2**

Sayı  
Number **1**

p-ISSN: 2587-0742  
e-ISSN: 2587-1749



entropi  $S = \frac{\pi A k c^3}{2 h G}$

*In memory of S. Hawking*

**Owner:**

Dr. Hamza KANDEMİR

**Editor in Chief:**

Prof. Dr. Kürşad ÖZKAN

**Co-Editor:**

Prof. Dr. Alireza HEIDARI  
Asst. Prof. Dr. Mustafa KARABOYACI

**Technical Editors:**

Res. Asst. Abdullah BERAM  
Instructor Serkan ÖZDEMİR

**Technical Assistant:**

Alican ÇIVGA  
Aslan MERDİN  
Tunahan ÇINAR  
Uysal Utku TURHAN  
Ahmet ACARER  
Hasan ÇULHACI

**Office Work:**

Instructor Doğan AKDEMİR

**Cover designer:**

Instructor Serkan ÖZDEMİR

**Press:**

Copy32 press-Isparta

**Contact:**

Kutbilge Association of Academicians,  
32040, Isparta, TURKEY

**Web** : [dergipark.gov.tr/bilgesci](http://dergipark.gov.tr/bilgesci)

**E-mail** : [kutbilgescience@gmail.com](mailto:kutbilgescience@gmail.com)

**Editorial Advisory Board:**

Ahmet AKSOY, Prof. Dr.  
*Akdeniz University, Turkey*

Amer KANAN, Prof. Dr.  
*Al-Quds University, Palestine*

Cüneyt ÇIRAK, Prof. Dr.  
*Ondokuz Mayıs University, Turkey*

Ender MAKİNECİ, Prof. Dr.  
*İstanbul University, Turkey*

Gülcan ÖZKAN, Prof. Dr.  
*Süleyman Demirel University, Turkey*

İbrahim ÖZDEMİR, Prof. Dr.  
*Süleyman Demirel University, Turkey*

Kari HELİÖVAARA, Prof. Dr.  
*University of Helsinki, Finland*

Kırali MÜRTEZAOĞLU, Prof. Dr.  
*Gazi University, Turkey*

Mehmet KILIÇ, Prof. Dr.  
*Süleyman Demirel University, Turkey*

Mehmet KİTİŞ, Prof. Dr.  
*Süleyman Demirel University, Turkey*

Mohamed Lahbib BEN JAMAA, Prof. Dr.  
*INRGREF, Tunisia*

Rene van den HOVEN, Prof. Dr.  
*University of Vet. Med. Vienna, Austria*

Semra KILIÇ, Prof. Dr.  
*Süleyman Demirel University, Turkey*

Steve WOODWARD, Prof. Dr.  
*University of Aberdeen, United Kingdom*

**Editorial Board:**

Ali Cesur ONMAZ, Assoc. Prof. Dr.  
*Erciyes University, Turkey*

Asko Tapio LEHTIJÄRVİ, Assoc. Prof. Dr.  
*Bursa Technical University, Turkey*

Halil GÖKÇE, Assoc. Prof. Dr.  
*Giresun University, Turkey*

Kubilay AKÇAÖZOĞLU, Assoc. Prof. Dr.  
*Niğde Ömer Halisdemir University, Turkey*

Ahmet MERT, Asst. Prof. Dr.  
*Süleyman Demirel University, Turkey*

Ayşe KOCABIYIK, Asst. Prof. Dr.  
*Süleyman Demirel University, Turkey*

Aziz ŞENCAN, Asst. Prof. Dr.  
*Süleyman Demirel University, Turkey*

Fecir DURAN, Asst. Prof. Dr.  
*Gazi University, Turkey*

Kubilay TAŞDELEN, Asst. Prof. Dr.  
*Süleyman Demirel University, Turkey*

Nuri ÖZTÜRK, Asst. Prof. Dr.  
*Giresun University, Turkey*

Ramazan ŞENOL, Asst. Prof. Dr.  
*Süleyman Demirel University, Turkey*

Şule Sultan UĞUR, Asst. Prof. Dr.  
*Süleyman Demirel University, Turkey*

**İmtiyaz Sahibi:**  
Dr. Hamza KANDEMİR

**Editör:**  
Prof. Dr. Kürşad ÖZKAN

**Yardımcı Editörler:**

Prof. Dr. Alireza HEIDARI  
Yrd. Doç. Dr. Mustafa KARABOYACI

**Teknik Editörler:**

Arş. Gör. Abdullah BERAM  
Öğr. Gör. Serkan ÖZDEMİR

**Teknik Yardımcılar:**

Alican ÇIVGA  
Aslan MERDİN  
Tunahan ÇINAR  
Uysal Utku TURHAN  
Ahmet ACARER  
Hasan ÇULHACI

**Büro İşleri:**

Öğr. Gör. Doğan AKDEMİR

**Kapak Tasarım:**

Öğr. Gör. Serkan ÖZDEMİR

**Baskı:**

Copy32 Matbaa-Isparta

**İletişim:**

Kutbilge Akademisyenler Derneği,  
32040, Isparta, TÜRKİYE

**Web** : dergipark.gov.tr/bilgesci

**E-mail** : kutbilgescience@gmail.com

**Danışma Kurulu:**

Ahmet AKSOY, Prof. Dr.  
*Akdeniz Üniversitesi, Türkiye*

Amer KANAN, Prof. Dr.  
*Al-Quds Üniversitesi, Filistin*

Cüneyt ÇIRAK, Prof. Dr.  
*Ondokuz Mayıs Üniversitesi, Türkiye*

Ender MAKİNECİ, Prof. Dr.  
*İstanbul Üniversitesi, Türkiye*

Gülcan ÖZKAN, Prof. Dr.  
*Süleyman Demirel Üniversitesi, Türkiye*

İbrahim ÖZDEMİR, Prof. Dr.  
*Süleyman Demirel Üniversitesi, Türkiye*

Kari HELİÖVAARA, Prof. Dr.  
*Helsinki Üniversitesi, Finlandiya*

Kıralı MÜRTEZAOĞLU, Prof. Dr.  
*Gazi Üniversitesi, Türkiye*

Mehmet KILIÇ, Prof. Dr.  
*Süleyman Demirel Üniversitesi, Türkiye*

Mehmet KİTİŞ, Prof. Dr.  
*Süleyman Demirel Üniversitesi, Türkiye*

Mohamed Lahbib BEN JAMAA, Prof. Dr.  
*INRGREF, Tunus*

Rene van den HOVEN, Prof. Dr.  
*Viyana Veterinerlik Üniversitesi, Avusturya*

Semra KILIÇ, Prof. Dr.  
*Süleyman Demirel Üniversitesi, Türkiye*

Steve WOODWARD, Prof. Dr.  
*Aberdeen Üniversitesi, Birleşik Krallık*

**Editör Kurulu:**

Ali Cesur ONMAZ, Doç. Dr.  
*Erciyes Üniversitesi, Türkiye*

Asko Tapio LEHTIJÄRVİ, Doç. Dr.  
*Bursa Teknik Üniversitesi, Türkiye*

Halil GÖKÇE, Doç. Dr.  
*Giresun Üniversitesi, Türkiye*

Kubilay AKÇAÖZOĞLU, Doç. Dr.  
*Niğde Ömer Halisdemir Üniversitesi, Türkiye*

Ahmet MERT, Yrd. Doç. Dr.  
*Süleyman Demirel Üniversitesi, Türkiye*

Ayşe KOCABIYIK, Yrd. Doç. Dr.  
*Süleyman Demirel Üniversitesi, Türkiye*

Aziz ŞENCAN, Yrd. Doç. Dr.  
*Süleyman Demirel Üniversitesi, Türkiye*

Fecir DURAN, Yrd. Doç. Dr.  
*Gazi Üniversitesi, Türkiye*

Kubilay TAŞDELEN, Yrd. Doç. Dr.  
*Süleyman Demirel Üniversitesi, Türkiye*

Nuri ÖZTÜRK, Yrd. Doç. Dr.  
*Giresun Üniversitesi, Türkiye*

Ramazan ŞENOL, Yrd. Doç. Dr.  
*Süleyman Demirel Üniversitesi, Türkiye*

Şule Sultan UĞUR, Yrd. Doç. Dr.  
*Süleyman Demirel Üniversitesi, Türkiye*

# Bilge International Journal of Science and Technology Research

Year: 2018, Volume: 2, Issue: 1

## CONTENTS

### Research

- Numerical Analyses of the Effects of Fuel Load Variation on Combustion Performance of a Pellet Fuelled Boiler  
*Bilal Sungur, Bahattin Topaloğlu* ..... 1-8
- An Assessment of Shallow Groundwater Wells in An Agricultural And Coastal Area in Göksu Delta, Turkey  
*Esra Deniz Güner, Senem Tekin, Galip Seçkin* ..... 9-16
- Numerical Computation of Fission-Product Poisoning Build-up and Burn-up Rate in a Finite Cylindrical Nuclear Reactor Core  
*Mathew Ademola Jayeola, Musbaudeen Kewulere Fasasi, Adebimpe Amos Amosun Ayodeji Olalekan Salau, Babatunde Michael Ojo* ..... 17-30
- Changes in Quality Parameters of Deep Fat Fried Carrot Slices Under The Effect of Ultrasound Assisted Pre-Drying Process  
*Erkan Karacabey, Merve Seçil Turan* ..... 31-39
- Real-time Parental Voice Recognition System For Persons Having Impaired Hearing  
*Mete Yağanoğlu, Cemal Köse* ..... 40-46
- Investigation in Electrical and Thermal Efficiency of An Active Cooling Photovoltaic Thermal (Pv/T) Solar System with Taguchi Method  
*Gökhan Ömeroğlu* ..... 47-55
- Experimental (FT-IR, Raman and NMR) and Theoretical (B3LYP, B3PW91, M06-2X and CAM-B3LYP) Analyses of P-Tert-Butylphenyl Salicylate  
*Nuri Öztürk, Tuba Özdemir, Yelda Bingöl Alpaslan, Halil Gökçe, Gökhan Alpaslan* ..... 56-73
- Infrared and NMR Spectral Analyses and Computational Studies of 2-amino-3-methylbenzoic acid  
*Muhammet Hakkı Yıldırım* ..... 74-82
- Sapwood Area Related to Tree Size, Tree Age, and Leaf Area Index in *Cedrus libani*  
*Aylin Güney* ..... 83-91
- Chemical Characterization and Biological Activity Evaluation of Essential Oils of *Achillea Sipikorensis*, an Endemic Plant from Turkey  
*Nuraniye Eruygur, Özge Çevik, Mehmet Atas, Mehmet Tekin* ..... 92-97
- A Study on the Classification of Woody Vegetation in Forest Ecology (Isparta-Yenişarbademli Case)  
*Esra Özge Kurt, Mehmet Güvenç Negiz* ..... 98-109
- Wildlife Diversity in Reed beds Around Beyşehir Lake  
*Ahmet Mert, Ahmet Acarer* ..... 110-119



# Bilge International Journal of Science and Technology Research

Yıl: 2018, Cilt: 2, Sayı: 1

## İÇİNDEKİLER

### Araştırma

- Numerical Analyses of the Effects of Fuel Load Variation on Combustion Performance of a Pellet Fuelled Boiler  
*Bilal Sungur, Bahattin Topaloğlu* ..... 1-8
- An Assessment of Shallow Groundwater Wells In An Agricultural And Coastal Area in Göksu Delta, Turkey  
*Esra Deniz Güner, Senem Tekin, Galip Seçkin* ..... 9-16
- Numerical Computation of Fission-Product Poisoning Build-up and Burn-up Rate in a Finite Cylindrical Nuclear Reactor Core  
*Mathew Ademola Jayeola, Musbaudeen Kewulere Fasasi, Adebimpe Amos Amosun Ayodeji Olalekan Salau, Babatunde Michael Ojo* ..... 17-30
- Changes in Quality Parameters of Deep Fat Fried Carrot Slices Under The Effect of Ultrasound Assisted Pre-Drying Process  
*Erkan Karacabey, Merve Seçil Turan* ..... 31-39
- Real-time Parental Voice Recognition System For Persons Having Impaired Hearing  
*Mete Yağanoğlu, Cemal Köse* ..... 40-46
- Investigation in Electrical and Thermal Efficiency of An Active Cooling Photovoltaic Thermal (Pv/T) Solar System with Taguchi Method  
*Gökhan Ömeroğlu* ..... 47-55
- Experimental (FT-IR, Raman and NMR) and Theoretical (B3LYP, B3PW91, M06-2X and CAM-B3LYP) Analyses of P-Tert-Butylphenyl Salicylate  
*Nuri Öztürk, Tuba Özdemir, Yelda Bingöl Alpaslan, Halil Gökçe, Gökhan Alpaslan* ..... 56-73
- Infrared and NMR Spectral Analyses and Computational Studies of 2-amino-3-methylbenzoic acid  
*Muhammet Hakkı Yıldırım* ..... 74-82
- Sapwood Area Related to Tree Size, Tree Age, and Leaf Area Index in *Cedrus libani*  
*Aylin Günay* ..... 83-91
- Chemical Characterization and Biological Activity Evaluation of Essential Oils of *Achillea Sipikorensis*, an Endemic Plant from Turkey  
*Nuraniye Eruygur, Özge Çevik, Mehmet Atas, Mehmet Tekin* ..... 92-97
- Orman Ekolojisinde Odunsu Vejetasyonun Sınıflandırmasına Yönelik Bir Çalışma (Isparta-Yenişarbademli Örneği)  
*Esra Özge Kurt, Mehmet Güvenç Negiz* ..... 98-109
- Beyşehir Gölü Çevresindeki Sazlık Alanların Yaban Hayatı Çeşitliliği  
*Ahmet Mert, Ahmet Acarer* ..... 110-119

# BİLGE INTERNATIONAL JOURNAL OF SCIENCE AND TECHNOLOGY RESEARCH

ISSN: 2587-0742  
e-ISSN: 2587-1749

A peer reviewed journal, published biannually by  
Kutbilge Association of Academicians.

Yılda iki sayı olarak yayımlanan hakemli bir dergidir.  
Kutbilge Akademisyenler Derneği tarafından  
yayımlanmaktadır.

Year/Yıl: 2018, Volume/Cilt: 2, Issue/Sayı: 1

The journal is indexed in Researchbib, AcademicKey, International Institute of Organized Research (I2OR),  
Cosmos Index, Google Scholar, Journal Factor, Index Copernicus, JIFACTOR, Science Library Index,  
Sindex, Rootindexing, Eurasian Scientific Journal Index (ESJI), Directory of Research Journals Indexing  
(DRJI).

Dergimiz Researchbib, AcademicKey, International Institute of Organized Research (I2OR), Cosmos Index,  
Google Scholar, Journal Factor, Index Copernicus, JIFACTOR, Science Library Index, Sindex,  
Rootindexing, Eurasian Scientific Journal Index (ESJI), Directory of Research Journals Indexing (DRJI) 'de  
taranmaktadır.



## Numerical Analyses of the Effects of Fuel Load Variation on Combustion Performance of a Pellet Fuelled Boiler

Bilal Sungur<sup>1</sup>, Bahattin Topaloğlu<sup>1\*</sup>

**Abstract:** Domestic and industrial energy requirements since the beginning of industrial revolution have been largely met by fossil fuels. This leads to a continuous increase in the Earth's atmosphere of carbon dioxide and other harmful components. Also, fossil energy resources decreasing day by day and scientists have turned to new research. In this context alternative energy sources have an important role to reduce dependence on fossil fuels. One of the alternative energy sources is biomass and pellet fuel is one of them. In this study, combustion characteristics of pellet fuel in a model smoke tube boiler at different loading conditions were investigated numerically. As a Computational Fluid Dynamic (CFD) program FLUENT package program was used. Calculations were performed at two dimensional conditions. According to various loading conditions, temperature and stream function contours, velocity vectors, exhaust gas temperatures and efficiencies were investigated and results were discussed. With decreasing thermal load, the exhaust gas temperatures decreased and boiler efficiencies increased. By reducing thermal power from the maximum value of 75 kW to the minimum value of 30 kW, the exhaust gas temperature decreased from 585 K to 429 K, whereas the thermal efficiency increased from 76% to 89%

**Keywords:** Biofuels, Numerical modeling, Pellet, Pellet boilers

### 1. Introduction

Today, saving energy and studies on the renewable energy resources is gaining importance day by day in the face of declining fossil-based resources. According to the sources, the distribution of energy consumption performed by taking the average of the last 5 years (2011-2015), the highest consumption is oil with 33% and it is followed by coal with 30% (Sungur et al., 2017). Studies on biomass which is one of the renewable energy sources has gained importance recently. Positive features of biomass fuels in terms of economic and environmental are among the reasons to prefer this renewable source. Some countries see bioenergy as the main energy source of the future and benefit from this energy source with a significant amount. Boilers can be defined as closed vessels in which combustion occurs and heat from combustion is transferred to a fluid. In general, boilers are used for heating purposes in houses and in many industries which

require energy. The energy efficiency of boilers is dependent on combustion quality and amount of the combustion energy transferred to the fluid. However, flue gas emissions dependent on combustion quality, grate type, the amount of the contaminants in the fuel and operating conditions of the combustion system.

Pellet fuels are one of the biomass energy sources and can be made from sawdust, wood chips, bark, waste, agricultural products, stems of crops, hazelnut, almond and walnut shells etc. These materials, compressed under

high pressure after grinding and typically 6-8 mm in diameter, 10-11 mm in length, with a cylindrical structure and it's called with the name of pellet. Pellet fuel is a sustainable resource and has many advantages: reduces fossil fuel imports, contributes to the economy, leaves less waste after usage, and leads to exhaust emissions within acceptable limits.

<sup>1</sup>Ondokuz Mayıs University, Faculty of Engineering, Department of Mechanical Engineering, Samsun/Turkey.

\*Corresponding author: [btopal@omu.edu.tr](mailto:btopal@omu.edu.tr)

Citation: Sungur, B., Topaloğlu, B. (2018). Numerical Analyses of the Effects of Fuel Load Variation on Combustion Performance of a Pellet Fuelled Boiler. *Bilge International Journal of Science and Technology Research*, 2 (1): 1-8.

Considering the scope of this study a literature search was carried out on the numerical modeling of the combustion of solid fuel boilers. (Begum et al., 2014) investigated the fluidized bed gasification of solid waste experimentally and numerically. They did their experiments on a pilot scale gasifier and they used Advanced System for Process Engineering (Aspen) Plus software for numerical calculations. They stated that experimental and numerical methods were in good agreement and they said that the model could be useful to predict the temperature, pressure, air-fuel ratio and steam-fuel ratio of a gasification plant. (Porteiro et al., 2009) carried out numerical analyses with Fluent 6.3 program on 24 kW pellet boiler in their work. They used k- $\epsilon$  model for modeling the turbulence, Discrete Ordinate (DO) model for modeling the radiation and Arrhenius Finite rate/Eddy dissipation model for modeling the gas phase. They presumed that biomass volatiles consist of CO, CO<sub>2</sub>, H<sub>2</sub>O, H<sub>2</sub>, light hydrocarbons (CH<sub>4</sub>) and heavy hydrocarbons (C<sub>6</sub>H<sub>6</sub>). As a result they compared the gas temperatures and concentrations with numerical and experimental methods and they stated that the results were in good agreement. (Chaney et al., 2012) investigated the combustion performance and NO<sub>x</sub> emissions optimization of 50 kW pellet boiler. They said that there are many parameters which can improve the combustion performance and NO<sub>x</sub> emissions like primary and secondary air adjustment, secondary air inlet number etc. For modeling the gas phase they used Eddy Dissipation model and as a CFD program, they used Fluent program in their calculations. (Collazo et al., 2012) simulated the domestic pellet boiler with CFD program and they used Finite rate/Eddy dissipation model for modeling the gas phase. They stated that the numerical results were in good agreement with the experimental results. As a result of the boiler analyses, they specified that the positions of water tubes and air inlet distributions were important factors which can cause the high emissions in such systems. (Klason and Bai, 2007) investigated the effect of secondary air on the combustion characteristics of wood pellets in a grate-fired furnace. They compared flame temperatures, distributions of CO and NO concentrations experimentally and numerically. They stated that the biomass combustion can be powerfully controlled by the secondary and tertiary air injection. (Lee et al., 2011) researched to optimize the furnace design of a pellet stove with 30000 kcal/h capacity experimentally and numerically. As a result of their study, they said that for good gaseous mixing and combustion efficient

use of furnace volume is necessary. (Zhou et al., 2005) aimed to optimize operating conditions and design parameters of straw combustion in a fixed bed. They observed that the simulation results (gas concentrations at the bed surface, ignition flame front, and bed temperature) were in good agreement with experimental results. (Sui et al., 2013) numerically investigated the biomass briquette combustion in the grate. They presented temperature, oxygen and carbon dioxide distribution as numerical results and evaluated them. (Dong and Blasiak, 2001) numerically analyzed the systems distributed the secondary air into to the boiler, which aims to reduce emissions by more efficient combustion for 15 MW solid biomass-fired and 29 MW coal-fired boilers, respectively. They used Arrhenius finite-rate reaction mechanism and the Magnussen and Hjertager eddy-dissipation model to calculate the relationship between turbulence and chemistry. They took the biomass and coal gas reactions chemical data's directly adopted from the data generated by methane combustion reactions from the Fluent program and they stated that the numerical results were successful. (Gómez et al., 2012) compared the heat transfer, temperature and species concentration of a domestic pellet boiler. As a result, they stated that the numerical results were in acceptable level of accuracy in comparison to experiments. Also, they numerically investigated the effect of water temperature on a pellet boiler and they showed that low water temperature increased the heat transfer. (Ahn and Kim, 2014) designed a pellet fuelled boiler and then they carried out experiments and numerical simulation with this boiler. They stated that the flame forms an arch from the second grate and this issue was predicted well by numerical simulations.

From the literature, it can be seen that the studies mainly focused on investigating the amount, number and positions of the secondary air, air inlet distributions, positions of the water tubes and comparing these effects on the performance and emissions of a boiler. In this study, combustion characteristics of a model pellet boiler for various loading conditions were analyzed numerically with Fluent program. Calculations were made for two-dimensional conditions. As the turbulence model RNG k- $\epsilon$  model, as the combustion model Finite rate/Eddy dissipation model and as the radiation model P1 approach was used. Temperature and stream function contours, velocity vectors, exhaust gas temperatures and efficiencies were investigated

for various loading conditions and results were discussed.

## 2. Material and Method

Pellet fuel combustion occurs in four stages, like other solid fuels which are drying (evaporation of water), pyrolysis (separation of the volatile components), and combustion of volatile components and combustion of fixed carbon as shown in Figure 1 (Pelletsatlas, 2009).

In the solution of combustion problems analytical, experimental and numerical methods can be applied. These methods can be applied separately, or they can be used together. Due to developments of powerful computers, numerical methods have been used quite often in recent years. In this study Fluent program was used as CFD program and therefore some information was given about the details of the submodels which were used in this program.

Fluent is a computational fluid dynamics program (CFD) which can model various processes like fluid motion, heat transfer, particle motion, and combustion. It transforms the partial differential equations to algebraic equation form and solves these equations numerically. Various options are available for combustion modeling in Fluent program (Fluent, 2006). These are species transport model, non-premixed model, premixed model, partially premixed model, composition PDF model.

For the combustion modeling, species transport model was used in this study so brief description of this model are given below:

**Species Transport Model:** This model can be used to solve the problems as non-premixed combustion, premixed combustion, and partial premixed combustion. In this approach, the conservation of the species mass fractions is defined by the user contains a solution of chemical reactions. The reaction rates and the relationship of turbulence-reaction are taken into account with Arrhenius equation and/or Magnussen-Hjertager equations by the following models: laminar finite rate, finite-rate/eddy dissipation, eddy dissipation and eddy dissipation concept models (Fluent, 2006). Finite rate/Eddy dissipation model computes both the Arrhenius and the Eddy dissipation rates and uses the smaller value as the reaction rate.

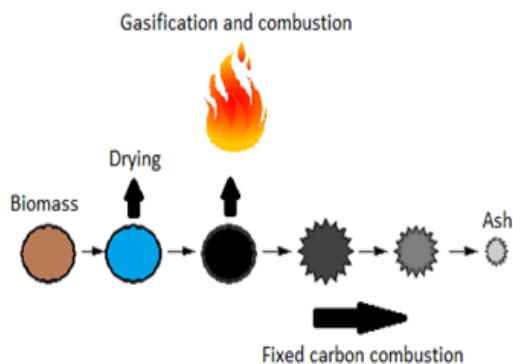
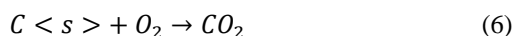
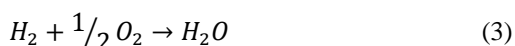
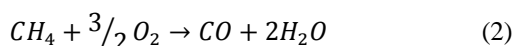
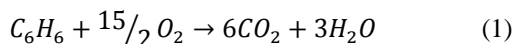


**Figure 1.** Pellet fuel combustion steps (Pelletsatlas, 2009)

In this study, volatile components of pellet fuel were modeled at a gas phase in a model boiler. The part of the fixed carbon was modeled by injecting carbon particles above the grate. Calculations were made at two-dimensional conditions. For modeling the turbulence RNG k-ε model, for modeling the combustion Finite rate/Eddy dissipation model and for modeling the radiation P1 approach were used.

In reaction model, calculations were performed by entering the following equations into the program:



The geometric dimension of the model boiler is given in Figure 2. Because of the boiler considered as symmetric, calculations were carried out for only one half of the boiler.

The mesh structure of the boiler which was used in this study was shown in Figure 3. This mesh has a 102704 cell with interval size of 1mm (medium mesh). Also coarser (interval size of 2.5 mm and finer (interval size of 0.5 mm) mesh structures were tried by pre-calculations. These calculations showed that the results of medium and fine mesh structures were close to each other (Table 1), so in this study, medium mesh was used.

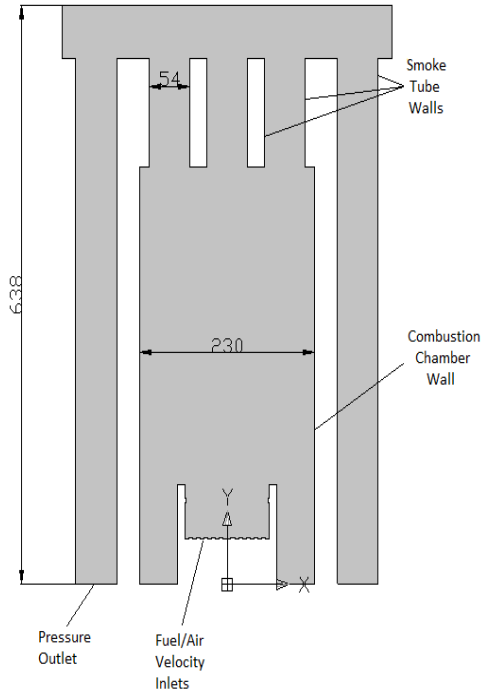


**Figure 2.** Dimensions of the pellet boiler

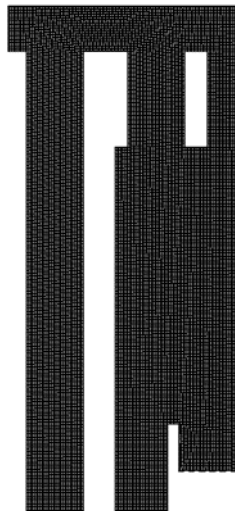


**Figure 3.** Mesh structure of the pellet boiler

**Table 1.** Effect of the mesh size for 30 kW boiler power

Mesh Size	Max Temp (K)	Exhaust Temp. (K)
Coarse	1663,7	454,48
Medium	1832,2	428,5
Fine	1853,6	422,4

Calculations were performed with the boiler power of 30 kW which is the minimum loading, 45 kW, 60 kW, and 75 kW which is defined by full loading conditions. Properties of the pellet fuels were given in Table 2. The amount of moisture content in the fuel is considered by adding it to the gas phase. It is assumed that the volatile components consist of CO, CO<sub>2</sub>, H<sub>2</sub>, H<sub>2</sub>O, NH<sub>3</sub>, light hydrocarbons (CH<sub>4</sub>) and tar (C<sub>6</sub>H<sub>6</sub>) (Gómez et al., 2012).

**Table 2.** Properties of the pellet fuel (Gómez et al., 2012)

Proximate analyses	
Moisture [wt %]	8.50
Ash [wt %]	0.62
Fixed carbon [wt.%]	16.20
Volatile matter [wt.%]	74.68
Lower heating value [kJ/kg]	18330

All the calculations were made for the constant value of excess air coefficient  $\lambda=2$ . All surfaces in contact with water considered as the wall temperature of 353 K. Outlet region introduced as pressure outlet where atmospheric pressure prevails, air inlet and fuel inlet are introduced as velocity inlet. Iterations were continued up to the value of 10<sup>-6</sup> for continuity and energy convergence criteria.

### 3. Results and Discussions

The temperature contours of pellet fuel combustion are shown in Figure 4. As can be seen from the figure, in all cases flame temperatures reached to their maximum values in areas near to the grate, and temperatures decreased toward the exit because of the hot gases areas surrounded by water. In the case of full loading conditions (75 kW), mean temperatures in the boiler are higher than the other cases because of the effect of increasing power. In the case of minimum loading conditions (30 kW) the maximum flame temperature (1897 K) occurred near to the grate region and was higher than the other cases due to the effect of low gas velocities. The maximum flame temperature values were close to each other in other loading conditions with the temperature of about 1845 K. In the combustion chamber, regions close to the water jackets, temperatures were about 561-626 K in the case of 30 kW, 618 - 682 K in the case of 45 kW, 679 - 743 K in the case of 60 kW and 743 - 807 K in the case of 75 kW. In the inlet section of the central smoke tube of the first pass (located above the flame) gas

temperatures were about 1020 - 1080 K at 30 kW, 1130 K-1190 K at 45 kW, 1190 - 1250 K at 60 kW and 1250 - 1310 K at 75 kW. The gas temperatures in the inlet section of side tubes of the first pass were about 822 - 887 K, 873 - 936 K, 996 - 1060 K and 1060 - 1120 K in the case of 30 kW, 45 kW, 60 kW and 75 kW, respectively. From the first pass, the gas flow turned to the second pass and cooled further towards the exit.

Figure 5 shows the stream function contours. The flow of hot gases which occurred as a result of fuel combustion created a vortex in the combustion chamber and near to the water channel, then turned towards the smoke tubes and exited the boiler properly. Gas velocities decreased with the effect of decreasing loading conditions from full load to low load and consequently the stream function values decreased too. Also velocity vectors were given in Figure 6. As can be seen from this figure the gas velocities increased with increasing boiler heat power.

The efficiency of a boiler can be calculated with Eq.(7) as follows (Sungur et al., 2016), if losses are neglected except sensible heat of flue gases:

$$\eta = 1 - (1 + \lambda A_{sto})(T_{exh} - T_0)c_{p,exh} / H_U \quad (7)$$

In this equation  $\lambda$  is excess air coefficient,  $A_{sto}$  is stoichiometric air fuel ratio,  $c_{p,exh}$  is specific heat of exhaust gases,  $T_{exh}$  is exhaust gas temperature,  $T_{amb}$  is ambient air temperature and  $H_U$  is lower heating value of the fuel.

According to this equation the exhaust gas temperatures can be used for comparison the boiler efficiency by changing loading conditions. In Figure 7, exhaust gas temperatures and efficiencies are given for various loading conditions. The maximum exhaust gas temperature occurs in the case of full loading conditions with the temperature of 585 K, and the minimum exhaust gas temperature occurs in the case of minimum loading conditions with the temperature of 429 K. Accordingly, with the increasing heating power the exhaust gas temperatures increased and boiler efficiencies decreased. The maximum boiler efficiency was 89% at 30 kW heat power and the minimum efficiency value is 76% at 75 kW heat power.

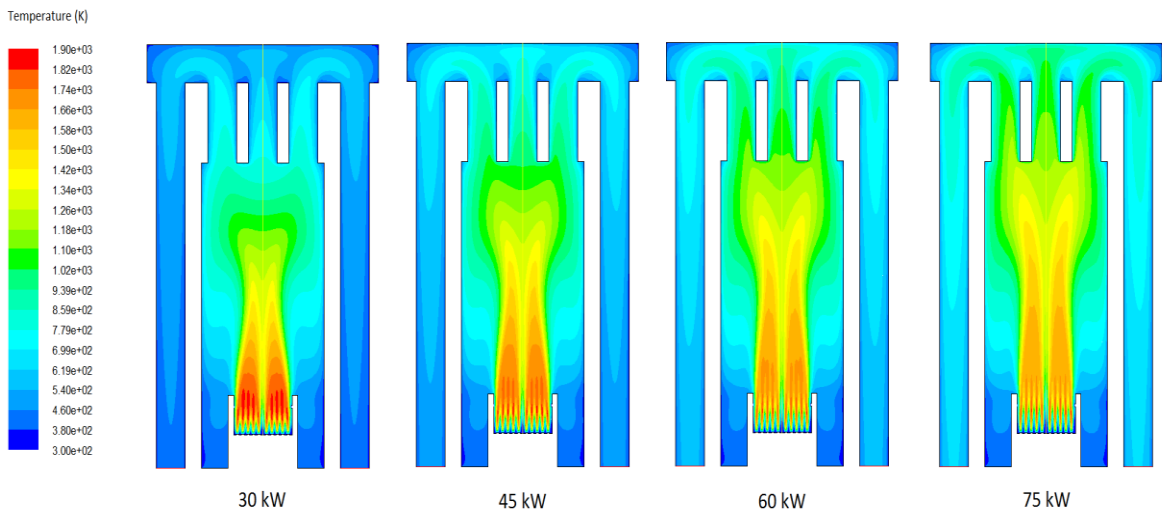


**Figure 4.** Temperature contours for various loading conditions



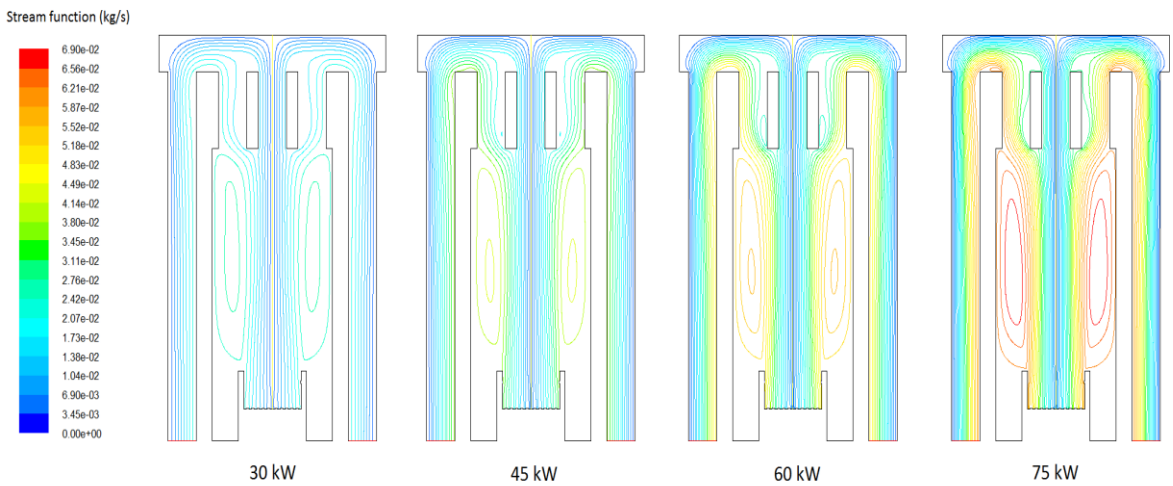


**Figure 5.** Stream function contours for various loading conditions

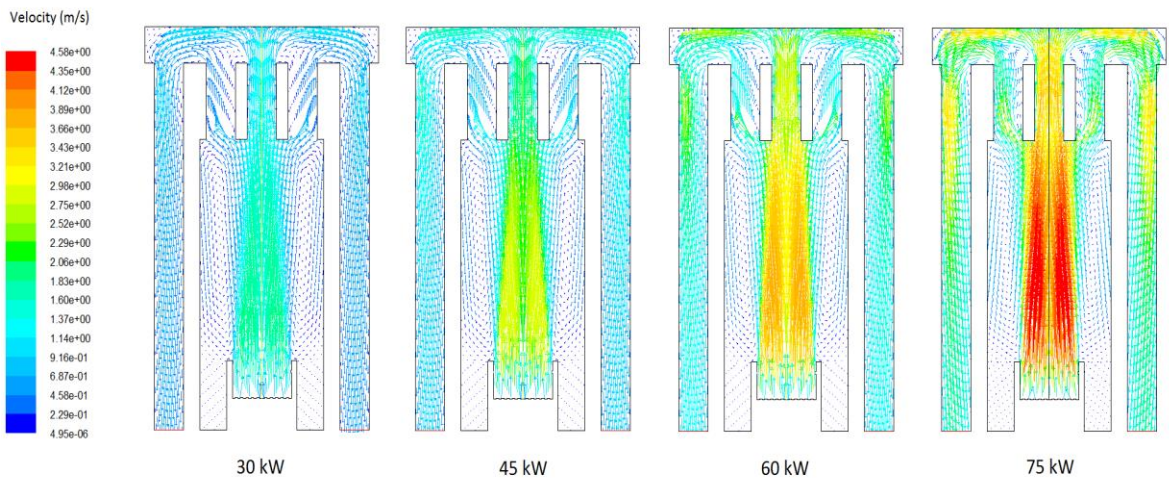


**Figure 6.** Velocity vectors for various loading conditions

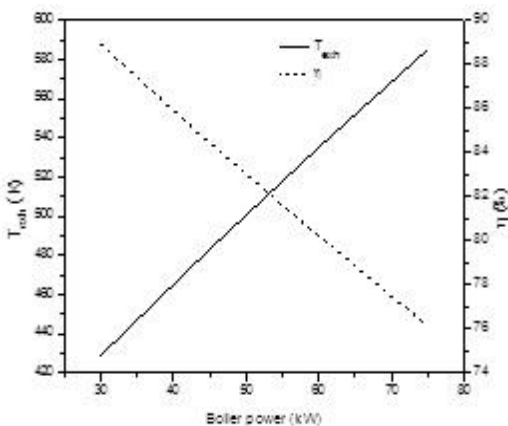


**Figure 7.** Exhaust gas temperatures and efficiencies for various loading conditions

These values are compatible with the literature. In the study of (Gómez et al., 2012), they numerically investigated the 18 kW domestic pellet boiler performance and they reported that the maximum temperatures were about 1873 K and occurred close to the grate, exhaust gas temperature was 461 K and efficiency was 77.2%. (Lee et al., 2011) investigated the domestic pellet boiler with 35 kW capacity and aimed to design an optimal furnace for the boiler. They experimentally and numerically investigated different furnace geometries and stated that the maximum flame temperatures were about 1530 K-1760 K. They also said that in the existing pellet boiler the exhaust gas temperature was about 443 K. (Collazo et al., 2012) experimentally and numerically analyzed the domestic pellet boiler



with 18 kW capacity. They obtained from the numerical simulations that at  $\lambda=2.1$ , the exhaust temperature was nearly 423 K, at  $\lambda=2.25$  the exhaust temperature was about 428 K, at  $\lambda=2.6$  the exhaust temperature was about 443 K and at  $\lambda=3$  the exhaust temperature was about 448 K. Maximum gas temperatures were about 1773 K and occurred near to the grate. With increasing, air/fuel excess ratio hot gas regions increased through the combustion chamber.

#### 4. Conclusions

In this study, combustion in a model pellet boiler is analyzed numerically for various loading conditions. Temperature and stream function contours, velocity vectors, exhaust gas temperatures and efficiencies were determined for various loading conditions and results were evaluated. As a result of calculations, the exhaust gas temperatures increased and boiler efficiencies decreased with the increasing heating power. In the case of full loading conditions, the maximum exhaust gas temperature occurred with a value of 585 K, whereas the minimum exhaust gas temperature occurred with a value of 429 K in the case of minimum loading conditions. The efficiency of the boiler increased as the temperature of the exhaust gas decreased. The maximum boiler efficiency was obtained at 30 kW heat power with the value of 89% and the minimum efficiency value was obtained at 75 kW heat power with the value of 76%.

To improve the efficiency different methods can be developed according to the boiler loading conditions. For example, turbulators can be inserted to the smoke tubes in the boiler for prevent the high exhaust gas temperatures in the case of full loading conditions. In future studies, the combustion model can be developed by applying more detailed calculation for the combustion process (drying, gasification, fixed carbon combustion) of solid fuels. In this way, the effect of various loading variations on the harmful exhaust emissions such as NO<sub>x</sub> can be also calculated.

#### References

- Ahn, J., Kim, J.J. (2014). Combustion and heat transfer characteristics inside the combustion chamber of a wood pellet boiler. *J Mech Sci Technol* 28(2), 789-795.
- Begum, S., Rasul, M., Akbar, D., Cork, D. (2014). An Experimental and Numerical Investigation of Fluidized Bed Gasification of Solid Waste. *Energies* 7(1), 43.
- Chaney, J., Liu, H., Li, J. (2012). An overview of CFD modelling of small-scale fixed-bed biomass pellet boilers with preliminary results from a simplified approach. *Energ Convers Manage* 63, 149-156.
- Collazo, J., Porteiro, J., Míguez, J.L., Granada, E., Gómez, M.A. (2012). Numerical simulation of a small-scale biomass boiler. *Energ Convers Manage* 64, 87-96.
- Dong, W., Blasiak, W. (2001). CFD modeling of ecotube system in coal and waste grate combustion. *Energ Convers Manage* 42(15-17), 1887-1896.
- Fluent, (2006). *Fluent User's Guide*.
- Gómez, M.A., Comesaña, R., Feijoo, M.A.Á., Eguía, P., (2012). Simulation of the Effect of Water Temperature on Domestic Biomass Boiler Performance. *Energies* 5(4), 1044.
- Klason, T., Bai, X.S. (2007). Computational study of the combustion process and NO formation in a small-scale wood pellet furnace. *Fuel* 86(10-11), 1465-1474.
- Lee, Y.-W., Ryu, C., Lee, W.-J., Park, Y.-K. (2011). Assessment of wood pellet combustion in a domestic stove. *Journal of Material Cycles and Waste Management* 13(3), 165-172.
- Pelletsatlas, (2009). *English Handbook for Wood Pellet Combustion*. European Biomass Industry Association.
- Porteiro, J., Collazo, J., Patiño, D., Granada, E., Moran Gonzalez, J.C., Míguez, J.L. (2009). Numerical Modeling of a Biomass Pellet Domestic Boiler. *Energ Fuel* 23(2), 1067-1075.
- Sui, J., Xu, X., Zhang, B., Huang, C., Lv, J. (2013). A Mathematical Model of Biomass Briquette Fuel Combustion. *Energy and Power Engineering* 5, 1-5.
- Sungur, B., Ozdogan, M., Topaloglu, B., Namli, L. (2017). Technical and Economical Evaluation of Micro-Cogeneration Systems in the Context of Global Energy Consumption. *Engineer and Machinery* 58(686), 1-20.
- Sungur, B., Topaloglu, B., Ozcan, H. (2016). Effects of nanoparticle additives to diesel on

the combustion performance and emissions of a flame tube boiler. *Energy* 113, 44-51.

Zhou, H., Jensen, A.D., Glarborg, P., Jensen, P.A., Kavaliauskas, A. (2005). Numerical modeling of straw combustion in a fixed bed. *Fuel* 84(4), 389-403.

## An Assessment of Shallow Groundwater Wells in an Agricultural and Coastal Area in Göksu Delta, Turkey

Esra Deniz Güner<sup>1\*</sup>, Senem Tekin<sup>2</sup>, Galip Seckin<sup>1</sup>

**Abstract:** The Göksu Delta of Turkey is an alluvial delta with intense agricultural activity and has great ecological and economic significance. The delta is environmental protection area in term of remarkable in natural life. In particular, water birds are an important point, delta chosen as Ramsar site. So, this special area is important in terms of monitoring water quality and effects of anthropogenic activities (such as agricultural). Water samples were collected monthly from 24 wells in the study area, and 13 water quality parameters were examined. The objective of the study was also to determination the water quality in wells of the Göksu Delta and assess levels of salinisation in the region. Piper diagrams and the Geographic Information Systems (GIS) was used to generate ionic ratios to evaluate water quality in the study area in an efficient manner. Overall, the groundwater examined has medium levels of salinity and low sodium content. Piper diagram shows that all the samples collected from the region are located in NaCl, KCl, Na<sub>2</sub>SO<sub>4</sub> zone. The increase in groundwater salinity and amounts of Na<sup>+</sup> and Cl<sup>-</sup> are indicators of saltwater intrusion. Rock dissolution and ion exchange were also found to play an active role in the region. All of these factors affect the sustainability of the freshwater aquifers and lower their quality for wildlife species.

**Keywords:** Groundwater quality, diagram, seawater intrusion, salinity, geographical information systems (GIS)

### 1. Introduction

The demand for freshwater resources has been increasing gradually due to population growth, and consequently, the use of underground water resources as a source of fresh water has increased over a short period. Shallow groundwater resources are currently being used for agricultural production in many parts of Turkey. Agricultural activity results in the intense use of groundwater, which in turn can have significant effects on the quality of groundwater, particularly in shallow coastal aquifers (Trabelsi et al., 2012; Huang et al., 2013; Knight et al., 2013; Kastridis and Kamperidou, 2015). Additionally, there is natural groundwater pollution, which is due to geological formation with shallow groundwater mass, infiltration from low-quality surface water bodies,

seawater intrusion, geothermal fluids and anthropogenic groundwater pollution (Baba and Ayyildiz, 2006).

The precincts is an important part of the Mediterranean region with its tourism potential, important natural, historical and ecological heritage area. The region host a wetland site which is classified as a Wetland of International Importance according to the Ramsar Convention due to its location along bird migration route. Besides that, the area has a particular significance for being one of the few remaining areas where sea turtles lay their eggs in the world. In this area there are significant and intense agricultural activities each month of the year due to it being characterised by a typical Mediterranean Climate. With these properties, a careful examination of the

<sup>1</sup>Cukurova University, Faculty of Engineering and Architecture, Department of Environmental Engineering, 01330, Adana, Turkey.

<sup>2</sup>Cukurova University, Faculty of Engineering and Architecture, Department of Geology Engineering, 01330, Adana, Turkey.

\* Corresponding author: \*egunerr@cu.edu.tr

Citation: Güner, E.D., Tekin, S., Seckin, G. (2018). An Assessment of Shallow Groundwater Wells in an Agricultural and Coastal Area in Göksu Delta, Turkey. *Bilge International Journal of Science and Technology Research*, 2 (1): 9-16.

hydro-chemical qualities of coastal aquifer systems is crucial to assess the current condition of the aquifers, levels of saltwater intrusion, and impacts of human-environment interaction.

In this study, the water quality was examined from 24 wells samples. Physical and chemical water quality parameters were analysed over the period of a year. This study provides both an overview of the hydrochemical parameters in the delta, using hydro-chemical parameters, and evaluates the distribution of geochemical parameters and their variations using graphs and GIS maps.

## 2. Material and Method

### 2.1. Description of the study area

The Göksu Delta is situated in the Mediterranean Sea region of Turkey between latitude 35°35' N and longitudes 33°17' E (Figure 1). The Göksu Delta was formed by the deposition of alluvial material carried by the Göksu River. A wide flatness characterizes the geomorphology of the study area that has an elevation that ranges from 0 to 5 m in height above the sea. Göksu delta is in the east of the Paradeniz and Akgöl lagoons. The total area is about 15 000 ha which 226 km<sup>2</sup> is the protection area.

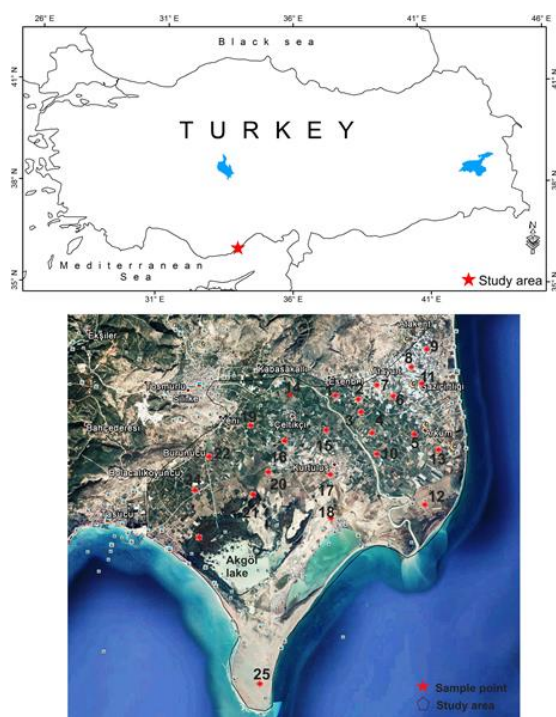


**Figure 1.** Sample sites in the Göksu Delta.

Meteorological data have obtained from Silifke Meteorology Directorate's TUMAS (Turkish Meteorological Archiving System) which has the most eligible data for study site and database via formal request (Table 1). Wet and mild winter combined with dry and hot summers are typical for the coastal zone around the Mediterranean Sea. The meteorological data of Silifke indicates that annual average temperature was 20.89°C, total annual precipitation was 606.8 mm, and average annual relative humidity was 55.5%, the mean annual precipitation is 43.3 mm in the Göksu Delta between May 2011 and April 2012.

**Table 1.** Range of meteorological parameters in the Göksu Delta

Temperature (°C)	Relative humidity (%)	Precipitation (mm)	Temperature (°C)
Maximum	25.4	77.1	37.5
Minimum	17.0	30.1	14.8
Average	21.0	55.5	21.4

### 2.2. Sample collection and analysis

A total of 24 water wells were selected, in the Göksu Delta to represent all the study areas. Water samples from the selected wells were collected on a monthly basis over a year. pH and EC values of the samples were measured on site using; WTW brand pH-meter and an Orion brand conductivity meter. A Shimadzu ion chromatography (IC) device was used for Anion (SO<sub>4</sub><sup>2-</sup>, Cl<sup>-</sup>, NO<sub>3</sub><sup>-</sup>) analyses, and Optical Emission Spectrometry (ICP-OES) was used for the analysis of Cations (Ca<sup>2+</sup>, Mg<sup>2+</sup>, Na<sup>+</sup>, K<sup>+</sup>). The detection of carbonate (CO<sub>3</sub><sup>2-</sup>) and bicarbonate (HCO<sub>3</sub><sup>-</sup>) in water was made using titration of H<sub>2</sub>SO<sub>4</sub> acid solution with methyl orange and phenolphthalein as indicators. Total dissolved solids (TDS) analysis was carried out using Method 2540 C. Standards to check the accuracy and precision of the analyses were provided before and during the analysis. Sodium adsorption ratio (SAR) used in the classification of water, the residual sodium carbonate (RSC) and %Na are calculated respectively according to the following formulas below. All ionic values used in these formulas are in meq/l.

The sodium adsorption ratio (SAR) was calculated by using the following formula (Raghunath, 1987):

$$SAR = \frac{Na^+}{\sqrt{\frac{Ca^{2+} + Mg^{2+}}{2}}}$$

The residual sodium carbonate (RSC) was determined as follows (Eaton, 1950):

$$RSC = (CO_3^{2-} + HCO_3^-) - (Ca^{2+} + Mg^{2+})$$

The %Na was determined as follows (Wilcox, 1955):

$$\%Na = \frac{100 \times Na^+}{Na^+ + Ca^{2+} + K^+ + Mg^{2+}}$$

### 3. Results and Discussion

The descriptive statistical overview of the hydrochemical data of the groundwater is presented in Table 2. The water samples obtained from the wells in the study area had pH values ranging from 7.5 to 8.19 with mean ± s.d. of 7.82-0.04, which indicates slightly alkalinity.

Distribution maps for EC, Cl<sup>-</sup>, TDS and SO<sub>4</sub><sup>2-</sup> which are strong indicators of seawater intrusion, are displayed in Figure 3, clearly showing that these parameters are higher in the Göksu region. The average annual EC was measured as 1471.74 ± 1262.63 µS/cm (mean ± sd). TDS values varied from 156.61 to 3941.3, with an annual average of 807.88 ± 821.98 mg/L (mean ± sd). The examination of seawater intrusion using EC values, with the threshold value set at 1000 µS/cm, shows indicators of high EC seawater intrusion into the wells, varies with the time of the year, and possess a serious threat to water quality. The assessment of groundwater samples for salinity from the Göksu Delta showed that none of the samples met the criteria for freshwater classification (TDS<500 mg/L) in terms of total dissolved solids, all samples are classified as brackish water. Increasing salinity in coastal groundwaters is an indicator of saltwater intrusion and results in decreasing the use of the aquifer as it no longer provides high-quality irrigation water.

**Table 2.** Average of 12-months analytical results of water quality parameters from Göksu Delta

Sample Point	T	PH	EC	TDS	Ca <sup>2+</sup>	Mg <sup>2+</sup>	K <sup>+</sup>	Na <sup>+</sup>	Cl <sup>-</sup>	SO <sub>4</sub> <sup>2-</sup>	NO <sub>3</sub> <sup>-</sup>	HCO <sub>3</sub> <sup>-</sup>	CO <sub>3</sub> <sup>2-</sup>
1	20.7	7.7	1014	605.15	88.61	51.91	5.05	31.6	94.8	228.8	12.4	347.9	5.93
2	20.2	7.7	1324.6	796.88	100.4	48.04	5.69	77.5	127.74	251.3	12.2	381.6	2.58
3	20.3	8	667.42	574.69	85.52	45.52	4.89	88.2	212.77	169.3	12.1	191.1	17.6
4	20.4	8	883.67	392.82	78.23	20.56	4.88	108.7	94.02	226.6	12.1	211.3	17.1
5	21.2	7.6	1632	817.65	15.83	14.77	7.43	282	308.89	172	12.4	311	5.58
6	22.8	7.6	1208.5	728.74	63.66	48.29	14.7	89.34	98.5	253.7	12.2	453.7	2.05
7	21.2	8	1106.2	555.87	43.61	63.39	11.7	191.7	171.61	321.5	12.1	285.7	11.4
8	20.8	8.2	1014	523.32	21.39	20.46	13.6	134.3	136.69	138.7	12.4	240.4	22.4
9	20.4	8	1171.4	548.93	19.36	21.55	13.9	149.1	154.93	151	12.1	251.9	11.8
10	20.4	8	832.08	405.14	21.55	19.28	6.19	110.4	111.92	124.1	12.1	229	14.4
11	20.9	8.1	1104.9	551.18	28.07	18.22	11.3	155.9	123.13	245.7	12.5	264.9	21.4
12	22.3	7.7	5677.5	3941.3	124.8	125.6	34.5	880.1	1597.6	299.8	12.4	211.6	2.33
13	22.3	7.8	4629.2	2695.1	100.8	96.22	31.8	741.8	1279.4	207.8	12.9	234	4.98
14	20.7	7.8	753.33	322.7	56.28	31.54	3.27	25.72	112.64	105.6	12.6	233.6	9.55
15	20.7	7.7	949.75	488.31	136.4	64.44	4.2	42.05	185.13	250	12.7	289.2	5.08
16	20.5	7.8	1429.3	610.05	44.36	44.39	3.02	169.3	332.06	123.3	13	205.2	7.63
17	22.7	7.9	1277.6	568.92	37.35	27.65	5.99	149.6	254.34	130.8	13.3	196.5	13.8
18	22	8.2	3352.5	1517.1	36.68	29.98	20.4	452	543.51	223.5	13.3	267.6	23.1
19	21.6	7.8	265.57	156.61	31.57	13.4	4.66	411.1	100.51	302.3	12.3	77.75	9.88
20	20.9	7.9	601.25	256.4	45.06	25.96	2.41	31.8	72.02	114.2	12.5	203.5	9.97
21	20.7	7.6	633.42	308.15	36.86	16.64	2.71	53.44	77.32	115.7	12.5	221.7	2.6
22	23.1	7.6	924.75	528.17	96.81	30.69	6.32	19.51	123.47	160.7	12.7	260.7	2.57
23	21.3	7.7	2041.6	994.67	74.45	34.29	5.11	255.5	362.65	205.8	12.5	273.6	2.58
24	22.4	7.5	827.33	501.29	110.8	35.84	2.51	23.54	145.61	181.4	12.3	305.5	2.48

\*The water temperature (T) is in °C, electrical conductivity (EC) is in µS/cm, and the other parameters are in mg/L.

The amount of  $\text{Cl}^-$  in the water from sample sites varied between 72 and 1598 mg/L and the  $\text{Cl}^-$  in groundwater comes from rocks, from rain water and melting snow, and from the atmosphere (Belkhir et al., 2012). Apart from these sources, the only other source of chloride in groundwater is seawater. Surface water in coastal areas has very high  $\text{Cl}^-$  content, which makes up more than half of all elements dissolved in seawater (Demir, 2008). Studies show that when  $\text{Cl}^-$  amounts are over 250 mg/L, the groundwater in question is either already intruded by saltwater or is under serious threat of intrusion (Andreasen and Fleck, 1997; Essink, 2001; Demirel, 2004; Arslan, 2011). Examining seawater intrusion using  $\text{Cl}^-$  content, with the threshold value set at 250 mg/L, we have observed indicators of seawater intrusion in wells 12, 13, 18 and 23. High levels of sulphate in groundwater may be an indicator of seawater intrusion into the coastal aquifers (Wang and Jiao, 2012; Huang et al., 2013). Examining seawater intrusion using  $\text{SO}_4^{2-}$  contents, with the threshold value set at 250 mg/L, we have observed in wells 2, 6, 7, 12, 15 and 19 that  $\text{SO}_4^{2-}$  contents were above the threshold. The average annual  $\text{SO}_4^{2-}$  amount in the Paradeniz region was found to be 914.8 mg/L. Previous studies show that, compared with seawater, clean shallow coastal aquifers have lower concentrations of sulphate (Werner et al., 2013).

The average annual values  $\text{Ca}^{2+}$  and  $\text{Mg}^{2+}$  ranged from 15.83 mg/L to 136.43 mg/L and 13.4 mg/L to 134.8 mg/L, with mean  $\pm$  s.d. of 62.43-7.35 mg/L and 39.9-5.73 mg/L, respectively. The  $\text{Ca}^{2+}$  content was higher wells in the limestone bedrocks, and the  $\text{Mg}^{2+}$  content was higher wells in the dolomite area (Jiang et al., 2009).

The  $\text{Na}^+$  and  $\text{K}^+$  values ranged from 19.5 mg/L to 880.0 mg/L and 2.41 mg/L to 34.46 mg/L, with mean  $\pm$  s.d. of 194.75-45.42 mg/L and 9.42-1.76 mg/L, respectively.  $\text{Na}^+$  was relatively high compared with  $\text{Ca}^{2+}$  which indicate the probable high TDS, hardness and alkalinity of the water samples.

The average annual  $\text{NO}_3^-$  and  $\text{K}^+$  concentrations have been observed to be 12.49 mg/L and 9.42 mg/L respectively in the study area. These value are a clear indicator of groundwater pollution in the region by agricultural activities. Several different studies have shown that the source for nitrate pollution is from different agricultural practices (Kim et al., 2005; Zhao et al., 2010;

Landon et al., 2011; Güler et al., 2012; Qin et al., 2013).

Taking into consideration the intensive agricultural activities in this area and the commercial composites that have been applied for an extended period, the high  $\text{NO}_3^-$  content may be due to agricultural fertilizers. The main component of fertiliser,  $\text{NH}_4^+$  is easily oxidized into  $\text{NO}_3^-$  by the nitrification process (Kim et al., 2005). Also,  $\text{K}^+$  concentration in natural groundwater is usually expected to be less than 5 mg/L (Ltd., 2004).  $\text{K}^+$  concentrations above this level might be an indication of fertilizer-related pollution. The average annual  $\text{K}^+$  value of 9.42 mg/L observed in the study area is a clear indicator of agricultural pollution in the groundwater of the region.

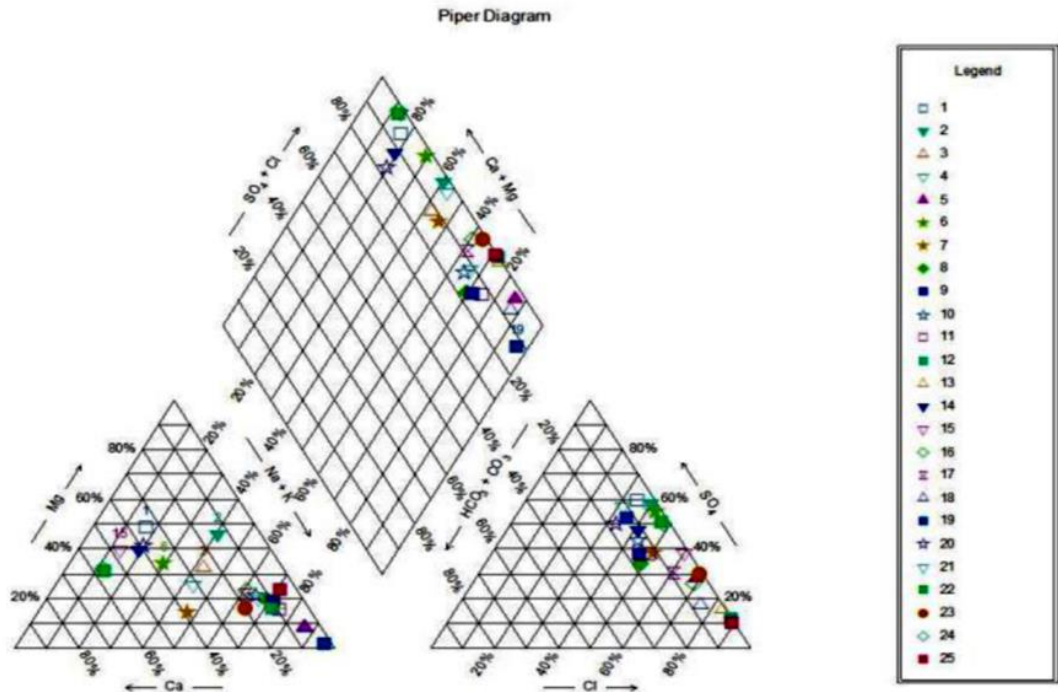


**Figure 2.** Major ion composition of groundwater at Göksu Delta represented using the Piper diagram (Piper, 1944)

Piper diagrams is developed to display different types of waters understand and define the water composition of different classes. Piper diagram was used to conduct origin and hydro-chemical facies analyses of the sampling sites (Fig.2). Piper diagram shows that all the samples collected from the region are located in NaCl, KCl, Na<sub>2</sub>SO<sub>4</sub> zone. Waters located in this zone, such as seawater and highly brackish water, have high chloride, sodium or potassium content. In addition, in Relatively high amounts of SO<sub>4</sub><sup>2-</sup> and Ca<sup>2+</sup> shown in the piper diagram indicate a process of mixing. Sulfate may have remained in the region due to the dissolution of the small amount of gypsum rocks found throughout the delta and due to vaporization as a result of over-irrigation, and calcium may have resulted from the dissolution of calcite rocks. Also, the samples are very rich in the anionic species, especially the chloride content is high. The main reason for this is the deep sea circulation in the northern part of the well field. According to Figure 2 wells 11, 14, 20 and 22 are most likely calcium sulphate and anhydrite origin. Sulphate enrichment throughout the region indicates that the

groundwater aquifer it is recharged by water from evaporitic lithologies. Samples 9, 13, 23 and 25 show that clearly intrusion salt water. When looking at well 23, it shows that Akgöl lake has been subjected to saltwater intrusion. In terms of contents anions, Cl<sup>-</sup> > SO<sub>4</sub><sup>2-</sup> > HCO<sub>3</sub><sup>-</sup>+CO<sub>3</sub><sup>2-</sup> whereas the cation contents show the following relationship: Na<sup>+</sup>+K<sup>+</sup> > Mg<sup>2+</sup> > Ca<sup>2+</sup>

On the basis of RSC and SAR values, which are parameters commonly used to assess water salinity, the water samples are classified as “fresh water” (RSC and SAR values, respectively, were - 1.93 ± 3.65 and 5.13 ± 4.86 (mean ± sd) as seen in Table 3. The %Na value is an important parameter for groundwater that indicates whether the water is suitable for use as irrigation water in agriculture. The average annual %Na value was found to be 47.59 ± 24.08 (mean ± sd) in the study area. On this basis,, the water samples are classified as having “moderate salinity”. Over the one-year period of study, during which several parameters were measured, total hardness varied between 101.11 and 835.48, with an average value of 320.93 ± 181.74 mg CaCO<sub>3</sub>/L (mean ± s d). This average value measured in the delta indicated



“very high salinity”. In terms of Cl<sup>-</sup> amounts measured throughout the year ( $8 \pm 10.57$  meq/L

(mean  $\pm$  sd)), the groundwater in the delta is classified as having “moderate salinity”.

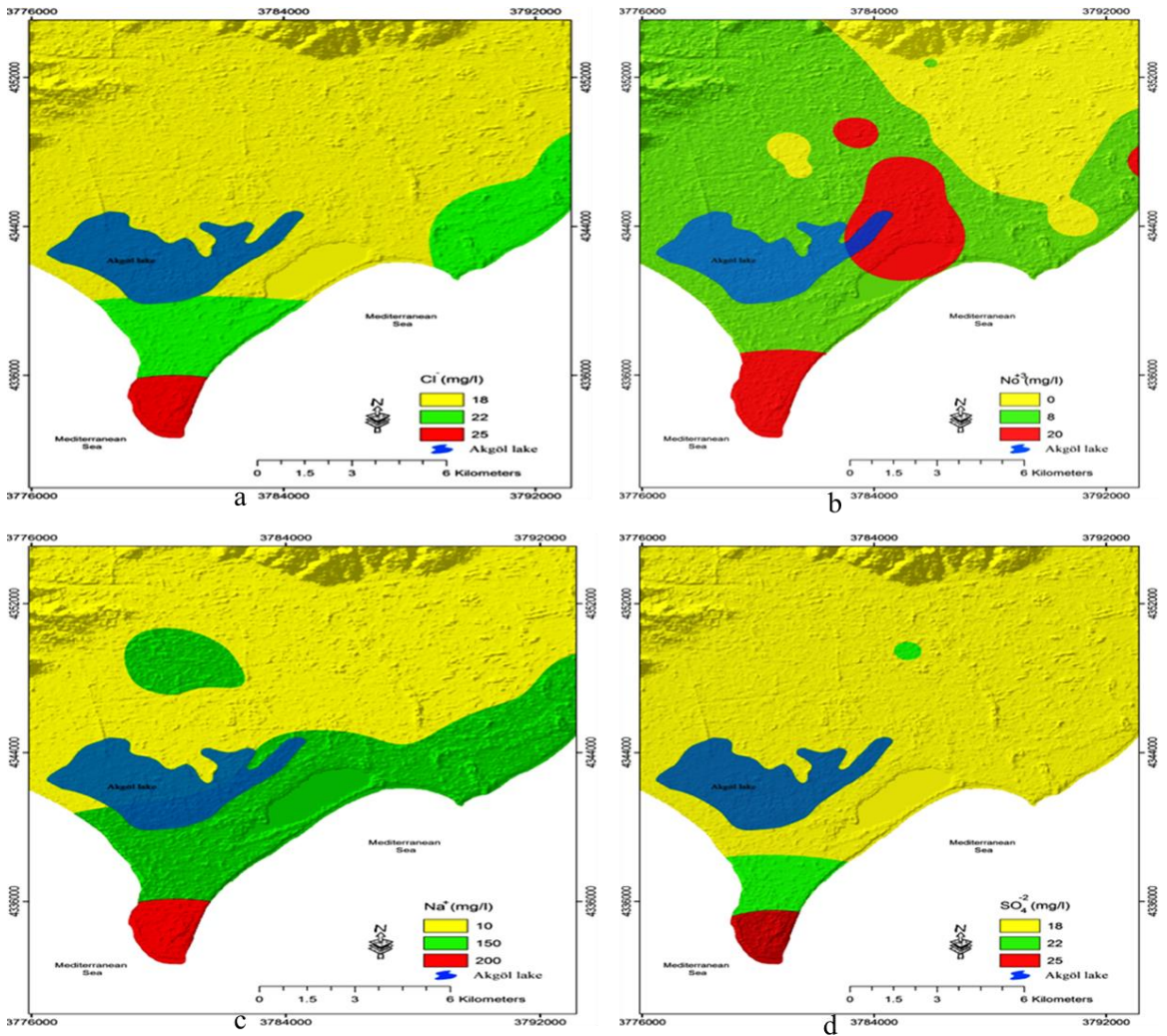


**Figure 3.** GIS maps showing the distribution for Cl<sup>-</sup> (a), NO<sub>3</sub><sup>-</sup> (b), Na<sup>+</sup> (c), and SO<sub>4</sub><sup>2-</sup> (d) in Göksu Delta

**Table 3.** Groundwater classification based on parameters

Class	Fresh	Slightly saline	Moderately saline	Highly saline	Very highly saline	Seawater	Avegare This work
Cl <sup>-</sup> (meq/L)	<2.8	2.8-7.1	7.1-14.1	14.1-28.2	28.2-282.2	>282.2	8
TDS (mg/L)	0-500	500-1500	1500-7000	7000-15000	15000-35000	>35000	807.88
EC (μS/cm)	<700	700-2000	2000-10000	10000-25000	25000-45000	>45000	1471.74
Total Hardness (mg CaCO <sub>3</sub> /L)	<75	-	75-150	150-300	>300	-	320.93
%Na	<20	20-40	40-60	60-80	>80	-	47.59
RSC (meq/L)	<1.25	-	1.25-2.5	>2.5	-	-	<1.25
SAR	<6	6-10	10-18	18-26	>26	-	5.13

Adapted from (Konikow, 1999; Rhoades, 1992; Wilcox, 1955)



#### 4. Conclusions

The findings of the present study show that  $\text{Cl}^-$ ,  $\text{SO}_4^{2-}$ ,  $\text{Na}^+$  and  $\text{HCO}_3^-$  are the dominant ions in the region, which is a reliable indicator of seawater intrusion in the region. The EC and TDS contents varied in a range that was much wider than is normal for fresh water, which might be another indicator of seawater intrusion in the region. The Piper diagrams showed that water samples were in the same zone with seawater and brackish water, which are  $\text{Cl}^-$  and  $\text{Na}^+$  type waters. The presence of  $\text{NO}_3^-$ , which, together with seawater intrusion, represents an issue for groundwater management in the region, may be due to the use of fertilisers.

Relatively high amounts of  $\text{SO}_4^{2-}$  and  $\text{Ca}^{2+}$  shown in the piper diagram indicate a process of mixing. Sulfate may have remained in the region due to the dissolution of gypsum rocks found throughout the delta and due to vaporisation as a result of over-irrigation, and calcium may have resulted from the dissolution of calcite rocks. Pollution distribution maps created using GIS visualize the predicted effects of seawater on the groundwater. Water extraction from the inland wells for irrigation purposes is also problematic and should be prevented. Aquifers can be fed from the surface by precipitation, or by water from rivers or other aquifers. Thus, alluvial water may have different characteristics at different points. Water resource 'planning' in the region should be replaced a 'water management' approach.

#### References

- Andreasen, D.C., Fleck, W.B. (1997). Use of bromide: chloride ratios to differentiate potential sources of chloride in a shallow, unconfined aquifer affected by the brackish-water intrusion. *Hydrogeology Journal* 5, 17-26.
- Arslan, H., Demir, Y. (2011). Bafra Ovasında Deniz Suyu Girişiminin Yerli Suyu Kalitesi Üzerine Etkisi *Anadolu Journal of Agricultural Sciences* 26, 136-144.
- Baba, A., Ayyıldız, O. (2006). Urban groundwater pollution in turkey, *Urban Groundwater Management and Sustainability*. Springer 93-110.
- Belkhir, L., Mouni, L., Boudoukha, A. (2012). Geochemical evolution of groundwater in an alluvial aquifer: Case of El Eulma aquifer, East Algeria. *Journal of African Earth Sciences* 66, 46-55.
- Demir, A. (2008). Akyatan Lagününde Tuzluluk ve Bazı Kirlilik Düzeylerinin Saptanarak Coğrafi Bilgi Sistemi Destekli Dağılımlarının Belirlenmesi. Çukurova Üniversitesi Fen Bilimleri Enstitüsü, Çevre Bilimleri Anabilim Dalı yüksek lisans tezi.
- Demirel, Z. (2004). The history and evaluation of saltwater intrusion into a coastal aquifer in Mersin, Turkey. *Journal of environmental management* 70, 275-282.
- Eaton, F.M. (1950). Significance of carbonates in irrigation waters. *Soil science* 69(2), 123-134.
- Essink, G.H.O. (2001). Improving fresh groundwater supply—problems and solutions. *Ocean & Coastal Management* 44, 429-449.
- Güler, C., Kurt, M.A., Alpaslan, M., Akbulut, C. (2012). Assessment of the impact of anthropogenic activities on the groundwater hydrology and chemistry in Tarsus coastal plain (Mersin, SE Turkey) using fuzzy clustering, multivariate statistics and GIS techniques. *Journal of Hydrology* 414, 435-451.
- Huang, G., Sun, J., Zhang, Y., Chen, Z., Liu, F. (2013). Impact of anthropogenic and natural processes on the evolution of groundwater chemistry in a rapidly urbanized coastal area, South China. *Science of the Total Environment* 463, 209-221.
- Jiang, Y., Wu, Y., Groves, C., Yuan, D., Kambesis, P. (2009). Natural and anthropogenic factors affecting the groundwater quality in the Nandong karst underground river system in Yunan, China. *Journal of contaminant hydrology* 109, 49-61.
- Kastridis, A., Kamperidou, V. (2015). Influence of Land Use Changes on Alluviation of Volvi Lake Wetland (North Greece). *Soil & Water Res* 10, 2.
- Kim, J.H., Kim, R.H., Lee, J., Cheong, T.J., Yum, B.W., Chang, H.W. (2005). Multivariate statistical analysis to identify the major

- factors governing groundwater quality in the coastal area of Kimje, South Korea. *Hydrological Processes* 19, 1261-1276.
- Knight, S.S., Locke, M.A., Smith Jr, S. (2013). Effects of agricultural conservation practices on oxbow lake watersheds in the Mississippi River alluvial plain. *Soil and Water Research* 8, 113-123.
- Konikow, L.F., Reilly, T.E. (1999). Seawater intrusion in the United States. *Seawater Intrusion in Coastal Aquifers—Concepts, Methods and Practices*. Springer Netherlands, 463-506.
- Landon, M.K., Green, C.T., Belitz, K., Singleton, M.J., Esser, B.K. (2011). Relations of hydrogeologic factors, groundwater reduction-oxidation conditions, and temporal and spatial distributions of nitrate, Central-Eastside San Joaquin Valley, California, USA. *Hydrogeology Journal* 19, 1203-1224.
- Ltd, H.C. (2004). Clearwater county regional groundwater assessment. Prepared for Clearwater County in conjunction with Agriculture and Agri-Food Canada. .
- Qin, R., Wu, Y., Xu, Z., Xie, D., Zhang, C. (2013). Assessing the impact of natural and anthropogenic activities on groundwater quality in coastal alluvial aquifers of the lower Liaohe River Plain, NE China. *Applied Geochemistry* 31, 142-158.
- Raghunath, I.M. (1987). The sodium adsorption ratio (SAR) was calculated by using the following formula, *Groundwater*. 2nd Edn., Wiley Eastern Ltd., New Delhi, India.
- Rhoades, J.D., Kandiah, A., Mashali A.M. (1992). *The use of saline waters for crop production*, Rome: FAO.
- Piper A.M. (1944). A graphic procedure in the geochemical interpretation of water-analyses. *Eos, Transactions American Geophysical Union* 25(6), 914-928.
- Trabelsi, R., Abid, K., Zouari, K., Yahyaoui, H. (2012). Groundwater salinization processes in shallow coastal aquifer of Djeffara plain of Medenine, Southeastern Tunisia. *Environmental Earth Sciences* 66, 641-653.
- Wang, Y., Jiao, J.J. (2012). Origin of groundwater salinity and hydrogeochemical processes in the confined Quaternary aquifer of the Pearl River Delta, China. *Journal of hydrology* 438, 112-124.
- Werner, A.D., Bakker, M., Post, V.E., Vandenbohede, A., Lu, C., Ataie-Ashtiani, B., Simmons, C.T., Barry, D.A. (2013). Seawater intrusion processes, investigation and management: recent advances and future challenges. *Advances in Water Resources* 51, 3-26.
- Wilcox, L. (1955). Classification and use of irrigation waters.
- Zhao, M., Zeng, C., Liu, Z., Wang, S. (2010). Effect of different land use/land cover on karst hydrogeochemistry: a paired catchment study of Chenqi and Dengzhanhe, Puding, Guizhou, SW China. *Journal of Hydrology* 388, 121-130.

## Numerical Computation of Fission-Product Poisoning Build-up and Burn-up Rate in a Finite Cylindrical Nuclear Reactor Core

Mathew Ademola Jayeola<sup>1\*</sup>, Musbaudeen Kewulere Fasasi<sup>2</sup>,  
Adebimpe Amos Amosun<sup>1</sup>, Ayodeji Olalekan Salau<sup>3</sup>, Babatunde Michael Ojo<sup>1</sup>

**Abstract:** All fission products are classified as reactor poisons because they absorb neutrons to some extent, most of which buildup slowly as the fuel burns up and eventually constitutes a long term reactivity effect in the core. Amidst the numerous fission fragments produced per fission, the presence of Xenon-135 and Samarium-149 has the greatest effect on a reactor core multiplication factor because of their large absorption cross-sections. In this study, we present a modified one-group time independent neutron diffusion equation using the method of Eigen functions and also provided an algorithm to calculate the temperature variations of the neutron fluxes. The solution obtained from the diffusion equation was used to determine the initial thermal neutron flux needed for the reactor startup. The four basic fission-product poisoning buildup and burn-up rate equations were solved using direct integration method and constant flux approximation over a particular time interval. Furthermore, a computer algorithm called Java code for Fission-Product Poisoning Build-up and Burn-up (Jac-FPPB) code was designed to calculate the temperature variations of the neutron fluxes, fission - isotopes cross sections and the atom concentrations of the fission products over a given time interval. The result from Jac-FPPB code show that the neutron fluxes and neutron energies increase as the temperature of the fuel increases. In addition, the computed atom concentrations of each fission isotopes at any given time interval show that the isotopes increasingly build up steadily at the initial time interval and rises to a constant level where the buildup rate of the isotopes approximately equals its burn up rate. This study concluded that the designed algorithm (JaC-FPBB code) proved efficient as it could compute the build-up and burn-up rates for the two important fission fragments in a nuclear reactor core. The code is easily accessible and can serve as a tool for the development of nuclear energy in developing countries, especially Nigeria.

**Keywords:** Numerical computation, Cylindrical reactor core, Fission-Products poisoning, Neutron diffusion equation, Samarium-149 and Xenon-135

### 1. Introduction

All nuclear reactors operate on the principle of nuclear fission (Marcum and Spinrad, 2013). This is the process in which a heavy atomic nucleus splits into two smaller fragments (Fermi, 1940). The fission fragments are in very excited states and they emit neutrons, other subatomic particles, and photons. The emitted neutrons may then cause new fissions which in turn yield more neutrons, and so forth. Such self-sustaining series of fissions

constitutes a fission chain reaction. In addition, as the fission chain reaction continues, many fission fragments popularly called nuclear reactor poisons buildup in the reactor core. However, some of these poisonings particularly Xenon-135 and Samarium-149 have large absorption cross sections for thermal neutrons, thereby constituting significant threat to the normal operation of the reactor system.

The remainder of this paper is organized as follows. The related work done is presented in Section 2.

<sup>1</sup>Obafemi Awolowo University, Faculty of Science, Department of Physics and Engineering Physics, Ile-Ife, Nigeria.

<sup>2</sup>Obafemi Awolowo University, Center for Energy Research and Development, Ile-Ife, Nigeria.

<sup>3</sup>Obafemi Awolowo University, Faculty of Technology, Department of Electronic and Electrical Engineering, Ile-Ife, Nigeria.

\*Corresponding author: [senatormao6@gmail.com](mailto:senatormao6@gmail.com)

Citation: Jayeola, M.A., Fasasi, M.K., Amosun, A.A., Salau, A.O., Ojo, B.M. (2018). Numerical Computation of Fission-Product Poisoning Build-up and Burn-up Rate in a Finite Cylindrical Nuclear Reactor Core. *Bilge International Journal of Science and Technology Research*. 2(1), 17-30.

Section 3 explains our proposed method in detail. Section 4 presents and discusses the results, and the paper is finally concluded in section 5.

## 2. Related Works

In recent years, several studies related to the numerical computation of poison build-up and burn-up in the core of a cylindrical nuclear reactor as well as the general computer codes to solving these equations were carried out but were not made accessible to people inside or outside the scientific communities where they were developed. Fission isotopes buildup/burnup and fuel depletion codes have been developed and used in the nuclear industry since the introduction of digital computing. Codes used today to calculate fission product buildup and burnup as well as their reactivity transient effects include coupled neutronics calculation and fission poisoning formation codes and post-processing modules.

Yesilyurt et al. (2011) developed a multi-physics code system called Oak Ridge Isotope Generation and Depletion Scale (ORIGEN-S). This code solves a set of ordinary differential equations to compute the time dependent quantity of nuclides that vary due to radioactive decay, isotopic transmutation, and nuclear fission. In ORIGEN-S, nuclide number densities at a given time,  $t$ , decay constants, monoenergetic microscopic cross sections and neutron flux were all computed and incorporated into the code. The neutron flux does vary with time, due to changes in the spectrum and isotopic concentrations. Advanced depletion code systems like ORIGEN-S generally involve coupling between lattice physics transport methods that solve for the neutron flux spectrum and generate problem-dependent cross sections and depletion methods that simulate the time-dependent isotopic evolution. Whether this is done in one integrated code or as several modular codes, the functional requirements are largely the same: neutron transport (or diffusion) codes generate accurate problem-dependent cross sections for use in the depletion calculation, and the nuclide concentrations from the depletion calculation are applied in the transport (or diffusion) calculation in order to reflect the time-dependent composition changes associated with irradiation.

Meanwhile, earlier in 1998, ORIGEN-S program was first developed by the Chemical Technology Division of Oak-ridge national laboratory (ORNL) to provides reliable bench mark result for such

computation which includes multi-group neutron diffusion calculations, fuel burnup analysis and fission product poisoning buildup and burnup calculations. The numerical methods used in ORIGEN SCALE or ORIGEN-S (Hermann and Wesfall, 1998) solve for arbitrary matrix element coupling using a hybrid approach that combines the matrix exponential method with Bateman equations for short-lived nuclides to obtain stable numerical solutions for all nuclides. The method allows for cyclical transition feedback, eliminating the need of analytical methods to use linearized chains. However, the highest fidelity approach simply uses neutron absorption and fission reaction information and fissile material cross sections generated in the code to determine the nuclide concentration at the next time step. This type of model allows for all of the neutron flux information to be integrated into the calculation without post-processing and additional manipulation of the neutron flux and cross-sections of fissile materials. Fission isotope's absorption and fission cross sections data for individual nuclides are available as output for Monte Carlo codes like Monte Carlo N-Particle (MCNP), (Briesmeister, 1993). The major requirement is that some sets of energy-dependent cross-sections are made available for each nuclide of interest at the required material temperature. The neutronics code is used to calculate core criticality ( $k_{eff}$ ) and the energy dependent neutron flux for a reactor or a region within the reactor. Typical neutronics code such as MCNP Code uses the neutron flux information and power density to compute the fission nuclides composition for the different time step. The process is repeated for an extensive duration of fuel burnup cycle. Usually a one-group thermal neutron flux generation code is used to perform the fission buildup and burnup analysis. Typical depletion/fission-product generation codes include ORIGEN (Kord and Lulu, 2012) and EPRI-CINDER (England et al., 1976).

Parma, (2002) presented a Fortran computer code design. This design was used to aid the analysis, prediction, and optimization of fuel burnup performance in a nuclear reactor. This computer program is called BURNCAL- A Nuclear Reactor Burnup Code Using MCNP Tallies. The code uses output parameters generated by the Monte Carlo neutronics code MCNP to determine the isotopic inventory as a function of time and power density. BURNCAL was also designed to study the reactivity effects and isotopic inventory as a function of time for a nuclear reactor system. Neutron transmutation, fission and radioactive

decay are included in the modeling of the production and removal terms for each isotope of interest. For a fueled region, neutron transmutation, fuel depletion, fission-product poisoning, actinide generation, burnable poison loading and depletion effects are included in the calculation. In addition, its flexibility feature makes it useful in fission product poisoning calculation. Furthermore, BURNCAL uses the neutron absorption and fission information generated from the neutronics code in calculating the nuclide mixture for the next time step of interest.

Arshad (1994) presented a study on Xenon and Samarium's behavior in a typical PARR-1 core comprising 22 low enriched uranium (LEU) fuel elements operating at 5MW and 10MW using a point model. In the point model, the core power is represented by average thermal flux. For this purpose, the flux-power correlation was taken from the core calculation results and the fuel parameters were taken from the lattice studies carried out in the context of conversion and upgradation of PARR- 1.

In another model called cell model, Xenon concentration is evaluated using the actual fission density and flux values which were obtained from cell calculations. Using this methodology and employing the parameters of low enriched uranium (LEU) core, the equilibrium Xenon and post-shutdown Xenon effects were studied. The analysis also pointed out that equilibrium xenon reactivities were also evaluated using cell model and 3-dimensional core model. The core calculations were carried out with the help of a developed computer code called FCAP. The result indicated that when the core is fresh or the reactor has been in a shutdown state for a few days, the amount of xenon in the core is zero. After reactor start-up the concentration of Xe-135 starts increasing immediately. In contrast with Sm-149 it attains the equilibrium value rather quickly.

Hence, this study considered the buildup and burnup rate of the aforementioned fission-product poisonings in a cylindrical nuclear reactor core with

the aim of laying a computational foundation for the calculation of the corresponding reactivity poisoning effects that may be introduced due to the presence of the two fission products in an operating reactor.

### 3. Methods and Approximations Used

The solution to the steady state neutron diffusion equation with appropriate boundary conditions is presented in this section. Furthermore, the analytical solution to the four (4) fission rate equations were solved.

#### 3.1. Neutron flux

The production and consumption of these isotopes (Xenon-135 and Samarium-149) depend on the neutron flux in the reactor and its operation history. Any change in the neutron flux which occurs during reactor start-up or shut down, is accompanied by a corresponding change in the concentration of these isotopes. Therefore, it is important to recall that the basic processes governing the behavior of the core of a nuclear reactor include variations in the distribution of neutrons in the reactor core. Neutron flux is a measure of the combined effect of the motions of neutrons. The description of the neutron distribution is based on the neutron transport equation. This equation is a linear form of the Boltzmann equation used in the study of gases. The analytical solution of the Boltzmann equation cannot be obtained as a result of its complexities which includes the presence of too many independent variables, complicated energy variations of microscopic cross-sections and complex geometrical structure of the core materials.

Hence for simplicity, an approximation of the transport equation known as the multi-group neutron diffusion equation is best used for reactor calculations in order to obtain reasonably accurate results. The multigroup time-independent neutron diffusion equation can be written as Eq. (1) (Larmash, 1966):

$$D_g \nabla^2 \Phi_g - \Sigma_{ag} \Phi_g - \sum_{h=g+1}^N \Sigma_{g \rightarrow h} \Phi_h + \sum_{h=1}^{g-1} \Sigma_{h \rightarrow g} \Phi_h = -S_g \quad (1)$$

Describing Eq. (1), we have:

$D_g \nabla^2 \Phi_g$  is the diffusion term in group g.

where  $D_g$  is the diffusion coefficient of the neutron flux in group  $g$  and  $\Phi_g$  is the neutron flux of energy group  $g$ .

Also,  $\Sigma_{ag}\Phi_g$  is the absorption rate in group  $g$ ,  $\Sigma_{h=g+1}^N \Sigma_{g \rightarrow h} \Phi_g$  is the total rate at which neutrons scatter out of  $g^{th}$  group into  $h^{th}$  group,  $\Sigma_{h=1}^{g-1} \Sigma_{h \rightarrow g} \Phi_g$  is the transfer rate into  $g^{th}$  group from  $h^{th}$  group.

Lastly,  $S_g$  is the total neutrons emitted into the groups from the sources.

However, a modified one-group time-dependent neutron diffusion equation is presented and is sufficient to describe the behavior of the thermal neutron flux present in the reactor core and this is considered the starting point for fission product-poisoning formation. The group transfer terms in the multi-group equation will be omitted, so that the rate at which neutrons are produced and absorbed is given as:

$$D\nabla^2\phi(\vec{r}, t) - \Sigma_a\phi(\vec{r}, t) + S(\vec{r}, t) = \frac{1}{v} \frac{\partial\phi(\vec{r}, t)}{\partial t} \quad (2)$$

Here,  $\phi$  is the one-group flux,  $D$  and  $\Sigma_a$  are the one-group diffusion coefficient and macroscopic absorption cross-section for the fuel-coolant mixture,  $S$  is the source density (i.e. the number of neutrons emitted per  $cm^3/sec$ ), and  $v$  is the

neutron speed. The modified one-group neutron diffusion equation is obtained by making the derivative term to be equal to zero so that it is properly termed steady-state neutron diffusion equation as given in Eq. (3).

$$D\nabla^2\phi(\vec{r}, t) - \Sigma_a\phi(\vec{r}, t) + S(\vec{r}, t) = 0 \quad (3)$$

### 3.2. Neutron cross section

The probability of a particular reaction occurring between a neutron and a nucleus of an atom is called the microscopic cross section ( $\sigma(E)$ ) of the nucleus for the particular reaction. This cross section varies with the energy of the neutron. The microscopic

absorption cross section decreases steadily with increasing neutron energy in a low energy region ( $E < 1 eV$ ) (Lamarsh, 1966). Microscopic absorption and fission cross section of any nucleus can be obtained using these relations:

$$\sigma_a(E) = \frac{\sqrt{\pi}}{2} g_a(T) \left(\frac{T_0}{T}\right)^{\frac{1}{2}} \sigma(E_0) \quad (4)$$

and

$$\sigma_f(E) = \frac{\sqrt{\pi}}{2} g_f(T) \left(\frac{T_0}{T}\right)^{\frac{1}{2}} \sigma(E_0) \quad (5)$$

where,  $\sigma_a(E)$  is the microscopic absorption cross section at higher temperature ( $> 20$  °C),  $\sigma_a(E_0)$  is the microscopic absorption cross section at the ambient temperature,  $\sigma_f(E)$  is the microscopic fission cross section at higher temperature ( $> 20$  °C),  $\sigma_f(E_0)$  is the microscopic fission cross section at the ambient temperature,  $g_f(T)$  is the non -  $\frac{1}{v}$  fission factor and  $g_a(T)$  is the non -  $\frac{1}{v}$  absorption factor.  $T$  and  $T_0$  are the absolute temperature and ambient temperature respectively of the neutron at

20 °C; where  $T_0 = 273.15 + 20.46 = 293.61$ °K and  $E_0 = 0.0253$ ev. However, the tendency of having a neutron interacting with a certain volume of nuclei depends not only on the microscopic cross section of the individual nuclei but also on the number of nuclei within that volume. Therefore, it is essential to define another kind of cross section termed as the macroscopic cross section ( $\Sigma$ ). The macroscopic cross section is the probability of a given reaction occurring per unit travel of the neutron.  $\Sigma$  is related to the microscopic cross section ( $\sigma(E)$ ) as follows:

$$\Sigma = N\sigma(E) \quad (6)$$

where  $\Sigma$  is the macroscopic cross section ( $cm^{-1}$ ),  $\sigma(E)$  is the microscopic cross section ( $cm^2$ ) and  $N$  is the atom density of material ( $atoms/cm^3$ ).

### 3.3. Solution to the steady state neutron diffusion equation and initial neutron flux calculation

The solution to the steady state neutron diffusion equation is obtained by employing the eigenfunction method. The central idea of the eigenfunction method is that it is possible to obtain

a solution to a diffusion equation in term of solutions of a differential equation (Lamarsh, 1966). The geometry of the reactor under study is cylindrical, the neutron source density is assumed to be distributed within the finite medium of the core in such a pattern that the diffusion equation is reduced to an ordinary differential equation (ODE). Therefore, from Eq. (3), we have

$$D\nabla^2\phi(r, z) - \Sigma_a\phi(r, z) = -S(r, z) . \tag{7}$$

$$\nabla^2 = \frac{1}{r} \frac{\partial}{\partial r} \left( r \frac{\partial}{\partial r} \right) + \frac{1}{r^2} \frac{\partial^2}{\partial \varphi^2} + \frac{\partial^2}{\partial z^2} . \tag{8}$$

$$\phi(r, z) = \frac{2S}{V\Sigma_a} \sum_{mn} \frac{1}{[B_{mn}^2 L^2 + 1] J_1^2(x_m)} J_0 \left( \frac{x_m r}{R_0} \right) \cos \left( \frac{n\pi z}{H} \right) . \tag{9}$$

$$B_{mn}^2 = \left( \frac{m\pi}{H} \right)^2 + \left( \frac{x_n}{R} \right)^2 . \tag{10}$$

where  $\nabla^2$  denotes the Laplacian operator for the cylindrical reactor as shown in Eq. (8). By applying all appropriate approximations and boundary conditions, Eq. (7) is solved to obtained Eq. (9) which is the complete solution to the neutron flux problem. where  $B_{mn}^2$  is the reactor buckling and is expressed in Eq. (10).

pellet and water ( $H_2O$ ) is considered. The reactor is assumed to be critical and operates at a power level of 25 Megawatts. The density of the fuel ( $UO_2$ ) is  $10.5 \text{ g/cm}^3$  with the  $^{235}U$  enrichment of 20.5. Furthermore, the molecular weight and atom density of the fuel as well as the core buckling were computed and used in the initial neutron flux calculation.

However, in order to obtain the analytical solution for the initial neutron flux (i.e. flux at the start of a clean core), in this study, a finite cylindrical reactor core of radius 120 cm and height 300 cm consisting of a homogenous mixture of uranium dioxide ( $UO_2$ )

From Eq. (9), The fundamental neutron distribution function denoted by a constant  $A_{11}$  can be obtained from the power level  $P$  of the reactor (Lamarsh and Baratta, 2001).

$$A_{11} = \frac{2S}{V\Sigma_a[B_{11}^2 L^2 + 1] J_1^2(2.405)} = \frac{3.63 P}{V E_R \Sigma_f} . \tag{11}$$

$$A_{11} = \frac{3.63 P}{V E_R \Sigma_f} = 2.9875 \times 10^{13} \tag{12}$$

$$\Phi(r, z) = 2.9875 \times 10^{13} J_0 \left( \frac{x_m r}{R_0} \right) \cos \left( \frac{n\pi z}{H} \right) \tag{13}$$

$$\Phi(0,0) \equiv \Phi_0 = 2.9875 \times 10^{13} \text{ neutron/cm}^2\text{s} . \tag{14}$$

$$\Phi_T = \frac{2}{\sqrt{\pi}} \left( \frac{T}{T_0} \right)^{\frac{1}{2}} \Phi_0 , \tag{15}$$

From Eq. (11),  $E_R$  is the recoverable energy of the reactor,  $\Sigma_f$  is the macroscopic fission cross section

of the fuel,  $P$  is the reactor power and  $V$  is the volume of the reactor. Numerical evaluation of

constant  $A_{11}$  is obtained using some assumed values of a typical thermal reactor. Hence, Eq. (11) is solved and its value is shown in Eq. (12). Eq. (13) is obtained when Eq. (12) is substituted into Eq. (9). Hence, since the maximum value of the thermal neutron flux occurs at  $r = 0$  and  $z = 0$ , the thermal neutron flux is obtained by explicitly solving Eq. (13) and its result is presented in Eq. (14).

In order to compute subsequent values of the thermal neutron flux at different temperatures, Eq. (15) was used to carry out the computation (Lamarsh, 2001), where  $\Phi_0$  is the initial thermal neutron flux obtained in Eq. (14),  $T_0$  is the absolute temperature of the neutron and  $T$  is the ambient temperature of the neutron at 20 °C.

### 3.4. Solution to fission-product poisoning coupled rate equations

#### (i) Iodine -135

The iodine rate equation is:

$$\frac{\partial I(\vec{r}, t)}{\partial t} = \gamma_I \bar{\Sigma}_f(\vec{r}, t) \phi(\vec{r}, t) - \lambda_I I(\vec{r}, t), \quad (16)$$

$$e^{\lambda_I t} \frac{\partial I(\vec{r}, t)}{\partial t} + \lambda_I I(\vec{r}, t) e^{\lambda_I t} = \gamma_I \bar{\Sigma}_f(\vec{r}, t) \phi(\vec{r}, t) e^{\lambda_I t}, \quad (17)$$

$$\frac{\partial [I(\vec{r}, t) e^{\lambda_I t}]}{\partial t} = \gamma_I \bar{\Sigma}_f(\vec{r}, t) \phi(\vec{r}, t) e^{\lambda_I t}, \quad (18)$$

$$\int_0^{\Delta t} dI(\vec{r}, t) e^{\lambda_I t} dt = \gamma_I \bar{\Sigma}_f(\vec{r}, 0) \phi(\vec{r}, 0) \int_0^{\Delta t} e^{\lambda_I t} dt. \quad (19)$$

$$I(\vec{r}, \Delta t) e^{\lambda_I \Delta t} - I(\vec{r}, 0) = \frac{\gamma_I}{\lambda_I} \bar{\Sigma}_f(\vec{r}, 0) \phi(\vec{r}, 0) [e^{\lambda_I \Delta t} - 1]. \quad (20)$$

$$I(\vec{r}, \Delta t) e^{\lambda_I \Delta t} = \frac{\gamma_I}{\lambda_I} \bar{\Sigma}_f(\vec{r}, 0) \phi(\vec{r}, 0) [e^{\lambda_I \Delta t} - 1]. \quad (21)$$

$$I(\vec{r}, \Delta t) = \frac{\gamma_I}{\lambda_I} \bar{\Sigma}_f(\vec{r}, 0) \phi(\vec{r}, 0) [1 - e^{-\lambda_I \Delta t}]. \quad (22)$$

$$e^{-\lambda_I \Delta t} = 1 - \frac{\lambda_I \Delta t}{1!} + \frac{(\lambda_I \Delta t)^2}{2!} - \frac{(\lambda_I \Delta t)^3}{3!}. \quad (23)$$

$$I(\vec{r}, \Delta t) = \frac{\gamma_I}{\lambda_I} \bar{\Sigma}_f(\vec{r}, 0) \phi(\vec{r}, 0) [1 - (1 - \lambda_I \Delta t)]. \quad (24)$$

$$I(\vec{r}, \Delta t) = \frac{\gamma_I}{\lambda_I} \bar{\Sigma}_f(\vec{r}, 0) \phi(\vec{r}, 0) [\lambda_I \Delta t]. \quad (25)$$

$$\int_t^{t+\Delta t} \partial I(\vec{r}, t) e^{\lambda_I t} = \gamma_I \bar{\Sigma}_f(\vec{r}, t) \phi(\vec{r}, t) \int_t^{t+\Delta t} e^{\lambda_I t} dt. \quad (26)$$

Equation (16) is the buildup and burn up rate equation for Iodine-135 where  $I$  is the number of  $^{135}\text{I}$  atoms/cm<sup>3</sup> i.e. the atom density of iodine,  $\gamma_I$  is

This section presents the buildup and burnup rate equations for Xenon-135, its precursor Iodine-135 and Samarium-149 as well as its precursor-Promethium-149. These production-destruction rate equations distinctively depicts how the individual fission isotopes are formed and how they dissappeared. The analytical solution to the coupled rate equations were equally presented.

#### 3.4.1. Derivation of Xenon-135 rate equation

Xenon-135 is produced in the reactor fuel in two ways (Lamarsh, (2001):

- a) Directly from fission. About 0.3% of all fission products are Xenon-135.
- b) Indirectly from the decay of Iodine-135, this is either produced as a fission product or from the decay of the fission product Tellurium-135.

the effective yield of the isotope, and  $\bar{\Sigma}_f$  is the average thermal fission cross section.



Multiplying both sides of Eq. (16) by the integration factor;  $e^{\lambda_I t}$ , we have Eq. (17). By simplifying Eq. (17), Eq. (18) is obtained.

However, assuming we are dealing with a “clean core” at the start of the reactor, the concentration of iodine-135 isotope is zero at  $t = 0$  and the neutron flux in the reactor is assumed to be constant in the interval  $0 < t < \Delta t$ , by applying this approximation to Eq. (18), we obtained Eq. (19). By carrying out the Integration on Eq. (19) over the limit  $0 \rightarrow \Delta t$ , we have Eq. (20). Since the reactor core is assumed

to be clean within this time interval where  $I(\vec{r}, 0) = 0$ , therefore, Eq. (20) results to Eq. (21). By multiplying both sides of Eq. (21) by  $e^{-\lambda_I \Delta t}$ , Eq. (22) is obtained.

In a bid to simplify Eq. (22), we must apply Taylor’s expansion approximation stated in Eq. (23), hence, we obtain Eq. (24). with further simplification of Eq. (24), we have Eq. (25). However, it is very important to derive a more general solution for  $^{135}\text{I}$  concentration at  $t + \Delta t$ , in terms of its concentration at time  $t$ . Applying the constant flux approximation to Eq. (18), we have Eq. (26).

$$I(\vec{r}, t + \Delta t)e^{\lambda_I(t+\Delta t)} - I(\vec{r}, t)e^{\lambda_I t} = \frac{\gamma_I}{\lambda_I} \bar{\Sigma}_f(\vec{r}, t)\phi(\vec{r}, t) [e^{\lambda_I(t+\Delta t)} - e^{\lambda_I t}]. \quad (27)$$

$$I(\vec{r}, t + \Delta t) = I(\vec{r}, t)e^{-\lambda_I \Delta t} + \frac{\gamma_I}{\lambda_I} \bar{\Sigma}_f(\vec{r}, t)\phi(\vec{r}, t)[1 - e^{-\lambda_I \Delta t}]. \quad (28)$$

$$I(\vec{r}, t + \Delta t) = I(\vec{r}, t)[1 - \lambda_I \Delta t] + \frac{\gamma_I}{\lambda_I} \bar{\Sigma}_f(\vec{r}, t)\phi(\vec{r}, t)[\lambda_I \Delta t]. \quad (29)$$

By re-arranging Eq. (27) and multiplying both sides by  $e^{-\lambda_I(t+\Delta t)}$ , we obtain Eq. (28). Introducing Taylor’s expansion approximation into Eq. (28), the

general solution for  $^{135}\text{I}$  concentration at  $t + \Delta t$ , in terms of its concentration at time  $t$  is thus presented in Eq. (29).

**(ii) Xenon-135**

The xenon rate equation is:

$$\frac{\partial X_e(r,t)}{\partial t} = \lambda_I I(\vec{r}, t) + \gamma_X \Sigma_f(\vec{r}, t)\phi(\vec{r}, t) - \lambda_X X(\vec{r}, t) - \sigma_{ax} X(\vec{r}, t)\phi(\vec{r}, t). \quad (30)$$

$$\lambda_I I(\vec{r}, t) + \gamma_X \Sigma_f(\vec{r}, t)\phi(\vec{r}, t) - \lambda_X X(\vec{r}, t) - \sigma_{ax} X(\vec{r}, t)\phi(\vec{r}, t) = 0. \quad (31)$$

$$\lambda_I I(\vec{r}, t) + \gamma_X \Sigma_f(\vec{r}, t)\phi(\vec{r}, t) = \lambda_X X(\vec{r}, t) - \sigma_{ax} X(\vec{r}, t)\phi(\vec{r}, t). \quad (32)$$

$$\lambda_I I(\vec{r}, t) + \gamma_X \Sigma_f(\vec{r}, t)\phi(\vec{r}, t) [\lambda_X - \sigma_{ax}\phi(\vec{r}, t)] X(\vec{r}, t) \quad (33)$$

$$X(\vec{r}, t) = \frac{\lambda_I I(\vec{r}, t) + \gamma_X \Sigma_f(\vec{r}, t)\phi(\vec{r}, t)}{\lambda_X + \sigma_{ax}\phi(\vec{r}, t)}. \quad (34)$$

$$\frac{\partial I(\vec{r}, t)}{\partial t} = \gamma_I \Sigma_f(\vec{r}, t)\phi(\vec{r}, t) - \lambda_I I(\vec{r}, t), \quad (35)$$

$$\frac{\partial I(\vec{r}, t)}{\partial t} = 0. \quad (36)$$

$$\lambda_I I(\vec{r}, t) = \gamma_I \Sigma_f(\vec{r}, t)\phi(\vec{r}, t). \quad (37)$$

$$I(\vec{r}, t) = \frac{\gamma_X \Sigma_f(\vec{r}, t) \phi(\vec{r}, t)}{\lambda_I} \quad (38)$$

$$X(\vec{r}, t)_\infty = \frac{\gamma_I \Sigma_f(\vec{r}, t) \phi(\vec{r}, t) + \gamma_X \Sigma_f(\vec{r}, t) \phi(\vec{r}, t)}{\lambda_X + \sigma_{aX} \phi(\vec{r}, t)} \quad (39)$$

Since the half-lives of I-135 and Xe-135 are so short and the absorption cross-section of the xenon-135 isotope is so large, the concentration of these isotopes quickly rise to saturation or equilibrium values. This concentration can be formed by placing the time derivative in Eq. (16) and Eq. (30) equal to zero, (Lamarsh, 2001). Therefore, by evaluating

these two (2) equations carefully, Eq. (30) is translated into Eq. (34) and Eq. (16) into Eq. (38) respectively. By substituting Eq. (38) into Eq. (34), we obtain Eq. (39) which is the equation for equilibrium xenon.

$$\frac{\partial X(\vec{r}, t)}{\partial t} + \lambda_X X(\vec{r}, t) + \overline{\sigma_{aX}} \phi(\vec{r}, t) X(\vec{r}, t) = \lambda_I I(\vec{r}, t) + \gamma_X \overline{\Sigma_f}(\vec{r}, t) \phi(\vec{r}, t), \quad (40)$$

$$\frac{\partial X(\vec{r}, t)}{\partial t} + [\lambda_X + \overline{\sigma_{aX}} \phi(\vec{r}, t)] X(\vec{r}, t) = \lambda_I I(\vec{r}, t) + \gamma_X \overline{\Sigma_f}(\vec{r}, t) \phi(\vec{r}, t). \quad (41)$$

$$e^{[\lambda_X + \overline{\sigma_{aX}} \phi(\vec{r}, t)] t} \frac{\partial X(\vec{r}, t)}{\partial t} + [\lambda_X + \overline{\sigma_{aX}} \phi(\vec{r}, t)] X(\vec{r}, t) e^{[\lambda_X + \overline{\sigma_{aX}} \phi(\vec{r}, t)] t} = \lambda_I I(\vec{r}, t) e^{[\lambda_X + \overline{\sigma_{aX}} \phi(\vec{r}, t)] t} + \gamma_X \overline{\Sigma_f}(\vec{r}, t) \phi(\vec{r}, t) e^{[\lambda_X + \overline{\sigma_{aX}} \phi(\vec{r}, t)] t}. \quad (42)$$

$$\frac{\partial [X(\vec{r}, t) e^{[\lambda_X + \overline{\sigma_{aX}} \phi(\vec{r}, t)] t}]}{\partial t} = \lambda_I I(\vec{r}, t) e^{[\lambda_X + \overline{\sigma_{aX}} \phi(\vec{r}, t)] t} + \gamma_X \overline{\Sigma_f}(\vec{r}, t) \phi(\vec{r}, t) e^{[\lambda_X + \overline{\sigma_{aX}} \phi(\vec{r}, t)] t}. \quad (43)$$

$$\int_0^{\Delta t} \partial [X(\vec{r}, t) e^{[\lambda_X + \overline{\sigma_{aX}} \phi(\vec{r}, t)] t}] dt = \lambda_I I(\vec{r}, 0) \int_0^{\Delta t} e^{[\lambda_X + \overline{\sigma_{aX}} \phi(\vec{r}, 0)] t} dt + \gamma_X \overline{\Sigma_f}(\vec{r}, 0) \phi(\vec{r}, 0) \int_0^{\Delta t} e^{[\lambda_X + \overline{\sigma_{aX}} \phi(\vec{r}, 0)] t} dt. \quad (44)$$

$$X(\vec{r}, \Delta t) e^{[\lambda_X + \overline{\sigma_{aX}} \phi(\vec{r}, 0)] \Delta t} = \frac{\lambda_I I(\vec{r}, 0)}{\lambda_X + \overline{\sigma_{aX}} \phi(\vec{r}, 0)} [e^{[\lambda_X + \overline{\sigma_{aX}} \phi(\vec{r}, 0)] \Delta t} - 1] + \frac{\gamma_X \overline{\Sigma_f}(\vec{r}, 0) \phi(\vec{r}, 0)}{\lambda_X + \overline{\sigma_{aX}} \phi(\vec{r}, 0)} [e^{[\lambda_X + \overline{\sigma_{aX}} \phi(\vec{r}, 0)] \Delta t} - 1]. \quad (45)$$

$$X(\vec{r}, \Delta t) e^{[\lambda_X + \overline{\sigma_{aX}} \phi(\vec{r}, 0)] \Delta t} = \left[ \frac{\lambda_I I(\vec{r}, 0)}{\lambda_X + \overline{\sigma_{aX}} \phi(\vec{r}, 0)} + \frac{\gamma_X \overline{\Sigma_f}(\vec{r}, 0) \phi(\vec{r}, 0)}{\lambda_X + \overline{\sigma_{aX}} \phi(\vec{r}, 0)} \right] [e^{[\lambda_X + \overline{\sigma_{aX}} \phi(\vec{r}, 0)] \Delta t} - 1], \quad (46)$$

$$X(\vec{r}, \Delta t) e^{[\lambda_X + \overline{\sigma_{aX}} \phi(\vec{r}, 0)] \Delta t} = \left[ \frac{\lambda_I I(\vec{r}, 0) + \gamma_X \overline{\Sigma_f}(\vec{r}, 0) \phi(\vec{r}, 0)}{\lambda_X + \overline{\sigma_{aX}} \phi(\vec{r}, 0)} \right] [e^{[\lambda_X + \overline{\sigma_{aX}} \phi(\vec{r}, 0)] \Delta t} - 1]. \quad (47)$$

$$X(\vec{r}, \Delta t) = \left[ \frac{\lambda_I I(\vec{r}, 0) + \gamma_X \overline{\Sigma_f}(\vec{r}, 0) \phi(\vec{r}, 0)}{\lambda_X + \overline{\sigma_{aX}} \phi(\vec{r}, 0)} \right] [1 - e^{-[\lambda_X + \overline{\sigma_{aX}} \phi(\vec{r}, 0)] \Delta t}], \quad (48)$$

$$I(\vec{r}, 0) = \frac{\gamma_I \overline{\Sigma_f}(\vec{r}, 0) \phi(\vec{r}, 0)}{\lambda_I}. \quad (49)$$

$$X(\vec{r}, \Delta t) = \left[ \frac{\gamma_I \overline{\Sigma_f}(\vec{r}, 0) \phi(\vec{r}, 0) + \gamma_X \overline{\Sigma_f}(\vec{r}, 0) \phi(\vec{r}, 0)}{\lambda_X + \overline{\sigma_{aX}} \phi(\vec{r}, 0)} \right] [1 - e^{-[\lambda_X + \overline{\sigma_{aX}} \phi(\vec{r}, 0)] \Delta t}]. \quad (50)$$

$$X(\vec{r}, \Delta t) = \left[ \frac{[\gamma_I + \gamma_X] \overline{\Sigma_f}(\vec{r}, 0) \phi(\vec{r}, 0)}{\lambda_X + \overline{\sigma_{aX}} \phi(\vec{r}, 0)} \right] [1 - e^{-[\lambda_X + \overline{\sigma_{aX}} \phi(\vec{r}, 0)] \Delta t}]. \quad (51)$$

$$\int_t^{t+\Delta t} \partial X(\vec{r}, t) e^{[\lambda_X + \overline{\sigma_{aX}}\phi(\vec{r}, t)]t} dt = \int_t^{t+\Delta t} \lambda_I I(\vec{r}, t) e^{[\lambda_X + \overline{\sigma_{aX}}\phi(\vec{r}, t)]t} dt + \int_t^{t+\Delta t} \gamma_X \overline{\Sigma_f}(\vec{r}, t) \phi(\vec{r}, t) e^{[\lambda_X + \overline{\sigma_{aX}}\phi(\vec{r}, t)]t} dt, \tag{52}$$

$$\int_t^{t+\Delta t} \partial X(\vec{r}, t) e^{[\lambda_X + \overline{\sigma_{aX}}\phi(\vec{r}, t)]t} dt = \lambda_I I(\vec{r}, t) \int_t^{t+\Delta t} e^{[\lambda_X + \overline{\sigma_{aX}}\phi(\vec{r}, t)]t} dt + \gamma_X \overline{\Sigma_f}(\vec{r}, t) \phi(\vec{r}, t) \int_t^{t+\Delta t} e^{[\lambda_X + \overline{\sigma_{aX}}\phi(\vec{r}, t)]t} dt. \tag{53}$$

$$X(\vec{r}, t + \Delta t) e^{[\lambda_X + \overline{\sigma_{aX}}\phi(\vec{r}, t)]t+\Delta t} = X(\vec{r}, t) e^{[\lambda_X + \overline{\sigma_{aX}}\phi(\vec{r}, t)]t} + \frac{[\lambda_I I(\vec{r}, t) + \gamma_X \overline{\Sigma_f}(\vec{r}, t) \phi(\vec{r}, t)]}{\lambda_X + \overline{\sigma_{aX}}\phi(\vec{r}, t)} [e^{[\lambda_X + \overline{\sigma_{aX}}\phi(\vec{r}, t)]t+\Delta t} - e^{[\lambda_X + \overline{\sigma_{aX}}\phi(\vec{r}, t)]t}]. \tag{54}$$

$$X(\vec{r}, t + \Delta t) = X(\vec{r}, t) e^{-[\lambda_X + \overline{\sigma_{aX}}\phi(\vec{r}, t)]\Delta t} + \frac{[\lambda_I I(\vec{r}, t) + \gamma_X \overline{\Sigma_f}(\vec{r}, t) \phi(\vec{r}, \Delta t)]}{\lambda_X + \overline{\sigma_{aX}}\phi(\vec{r}, 0)} [1 - e^{-[\lambda_X + \overline{\sigma_{aX}}\phi(\vec{r}, t)]\Delta t}]. \tag{55}$$

$$e^{-[\lambda_X + \overline{\sigma_{aX}}\phi(\vec{r}, t)]t} = 1 - \frac{[\lambda_X + \overline{\sigma_{aX}}\phi(\vec{r}, t)]t}{1!} + \frac{[\lambda_X + \overline{\sigma_{aX}}\phi(\vec{r}, t)]t^2}{2!} - \dots \tag{56}$$

$$X(\vec{r}, t + \Delta t) = X(\vec{r}, t) \{1 - [\lambda_X + \overline{\sigma_{aX}}\phi(\vec{r}, t)]\Delta t\} + \frac{[\lambda_I I(\vec{r}, t) + \gamma_X \overline{\Sigma_f}(\vec{r}, t) \phi(\vec{r}, t)]}{\lambda_X + \overline{\sigma_{aX}}\phi(\vec{r}, 0)} [[\lambda_X + \overline{\sigma_{aX}}\phi(\vec{r}, t)]\Delta t]. \tag{57}$$

By rearranging Eq. (40), we have Eq. (41). Eq. (42) is obtained by multiplying both sides of Eq. (41) by the integration factor  $e^{[\lambda_X + \overline{\sigma_{aX}}\phi(\vec{r}, t)]t}$ . This resulted into Eq. (43). Eq. (43) is further simplified extensively to obtain the atom concentration of Xe-135 just shortly after the reactor's startup (within the time interval  $0 \rightarrow \Delta t$ ) and this is expressed in Eq. (51). Moreover, as in the case of Iodine-135 atom concentration, in order to obtain the general solution of  $^{135}\text{Xe}$  at  $(t + \Delta t)$  in terms of its concentration at  $t$ , by applying all appropriate boundary conditions and approximations to Eq. (43), we have Eq. (57). Hence, Eq. (57) represents the atom concentration of  $^{135}\text{Xe}$  at  $(t + \Delta t)$  in terms of its concentration at  $t$  and therefore is used for the

numerical computation of xenon-135 atom concentration at subsequent time intervals.

### 3.4.2. Derivation of Samarium-149 rate equation

Samarium-149 is the most important of the stable fission products. It is formed in the fuel by the decay of fission products Neodymium-149 and Promethium-149 (Stacey, 2007).

Consequently, by adopting similar mathematical methods used in solving for the above Iodine-135 rate equations above (i.e. Eq. 16). The general solution to Pm-149 and Sm-149 concentration at  $(t + \Delta t)$ , in terms of its concentration at time  $t$ , are expressed respectively:

$$P(\vec{r}, t + \Delta t) = P(\vec{r}, \Delta t)[1 - \lambda_P t] + \frac{\gamma_P}{\lambda_P} \overline{\Sigma_f}(\vec{r}, \Delta t) \phi(\vec{r}, \Delta t) [\lambda_P t]. \tag{58}$$

and

$$S(\vec{r}, t + \Delta t) = S(\vec{r}, t)(1 - \sigma_{aS}\phi(\vec{r}, t)t) - \frac{\lambda_P P(\vec{r}, t)}{\sigma_{aS}\phi(\vec{r}, t)} [\sigma_{aS}\phi(\vec{r}, t)t]. \tag{59}$$

### 3.4.3. Nuclide burn-up time

The various time steps during which the fission nuclides concentrations were observed to buildup and burnup is calculated with the aid of nuclide burn-up time equation. The burnup time for any nuclide is the time necessary to transmuted by

neutron absorption to half of the quantity of a nuclide under neutron irradiation (Berthou *et al.*, 2003). It also refers to the disappearance of an isotope. The time evolution of a quantity  $N$  of an isotope under neutron irradiation is given by:

$$\frac{\partial N}{\partial t} = -(\lambda + \sigma\phi)N, \quad (60)$$

where  $\phi$  is the flux,  $\sigma$  the absorption cross-section, and  $\lambda$  the decay constant.

$$\frac{\partial N}{N} = -(\lambda + \sigma\phi)dt. \quad (61)$$

Applying integration to both sides of Eq. (61)

$$\ln \left[ \frac{N(t)}{N_0} \right] = -(\lambda + \sigma\phi)t, \quad (62)$$

$$\frac{N(t)}{N_0} = e^{-(\lambda + \sigma\phi)t}, \quad (63)$$

and

$$N(t) = N_0 e^{-(\lambda + \sigma\phi)t}. \quad (64)$$

Hence, for the selected nuclei, the individual nuclide burnout time is given by:

$$\tau_{BU} = \frac{\ln 2}{(\lambda + \sigma\phi)}. \quad (65)$$

where  $\tau_{BU}$  is the burnout time of the isotope.

### 3.4.4. JaC-FPBB code flow chart

Figure 3.1 shows the flow chart for JaC-FPBB Code (algorithm). In Figure 3.1, we show the calculated ambient temperature  $T_n$  in degree kelvin for seven different temperature levels. The temperatures

obtained are then used to compute new neutron energies and fluxes. The calculated new neutron energies as well as fluxes and values of other constants were used to calculate the fission product atom concentrations.

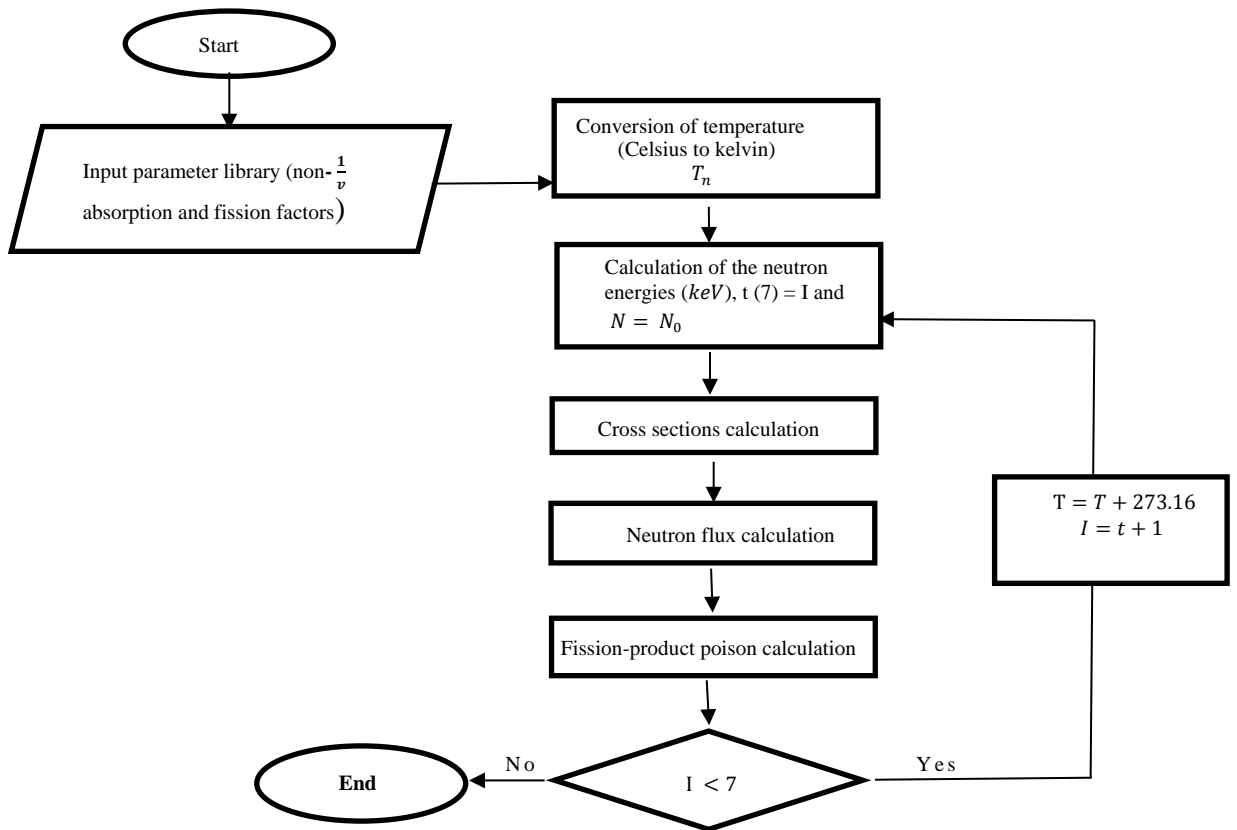


Figure 3.1. Flow chart for the Jac-FPBB code.

#### 4. Result and Discussion

This section presents the atom concentrations of the two vital fission product poisons relevant to this study (Xenon-135 and Samarium-149) when the program JaC-FPBB code is run. The temperature variations of the neutron flux and neutron energy in the reactor core as well as the computed cross-sections for, Xenon-135 and Samarium-149 needed for their respective atom concentration computations were also presented. The atom concentrations at only seven (7) different burnup times were conducted because the fluxes at temperatures higher than 1000 °C could not be calculated due to lack of nuclear data from available literatures.

##### 4.1. Temperature variation of neutron flux and neutron energy

Having obtained the initial thermal neutron flux  $\Phi_0$  from Eq. (14), the thermal neutron flux  $\Phi_T(E)$  at different available energies were calculated using the relationship between  $\Phi_T$  and  $\Phi_0$  from Eq. (15). Table 4.1 shows the temperature variation values of

neutron fluxes and neutron energies. From the Table 4.1, it is observed that the values of the neutron flux increases as the temperature of the fuel and the corresponding energy increase. The thermal neutron fluxes obtained were used in computing the atom concentrations of the fission products poison.

##### 4.2. Computed cross-sections for poison fission-products

The average microscopic and macroscopic absorption and fission cross-sections for Iodine-135, Xenon-135, Promethium-149 and Samarium-149 were computed using Eq. (4), Eq. (5) and Eq. (6) but, only the values obtained for Xenon-135 and Samarium-149 are presented in Table 4.2 and Table 4.3 respectively. It was observed from Table 4.2 and 4.3 that the computed cross-sections decrease with increasing fuel temperature. This is expected since the microscopic absorption and fission cross sections of the fissile material used (Uranium-235) are inversely proportional to the temperature of the fuel. These computed cross-sections were used to calculate the atom concentrations of Xenon-135 and Samarium-149.

**Table 4.1.** Temperature variation of neutron energies and fluxes.

Temperature (°C)	Neutron Energy (KeV)	Neutron Flux $\Phi_T(E)$
20	0.0253	$2.7219 \times 10^{13}$
100	0.0322	$3.0709 \times 10^{13}$
200	0.0408	$3.4580 \times 10^{13}$
400	0.0580	$4.1245 \times 10^{13}$
600	0.0752	$4.6975 \times 10^{13}$
800	0.0925	$5.2077 \times 10^{13}$
1000	0.1097	$5.6723 \times 10^{13}$

**Table 4.2.** Computed cross-sections for Xenon-135.

$T^{\circ}C$	$\bar{\sigma}_{aXe}$ (barn)	$\bar{\Sigma}_{aXe}$ ( $cm^{-1}$ )
20	$5.54 \times 10^{-6}$	47197.65
100	$5.13 \times 10^{-6}$	43719.20
200	$4.66 \times 10^{-6}$	39649.82
400	$3.75 \times 10^{-6}$	31907.93
600	$3.03 \times 10^{-6}$	25772.93
800	$2.47 \times 10^{-6}$	21060.03
1000	$2.03 \times 10^{-6}$	17322.91

**Table 4.3.** Computed cross-sections for Samarium-149.

$T^{\circ}C$	$\bar{\sigma}_{as}$ (barn)	$\bar{\Sigma}_{as}$ ( $cm^{-1}$ )
20	$1.17 \times 10^{-5}$	1144.80
100	$1.21 \times 10^{-5}$	1184.37
200	$1.19 \times 10^{-5}$	1164.86
400	$1.04 \times 10^{-5}$	1021.04
600	$8.74 \times 10^{-4}$	855.40
800	$7.24 \times 10^{-4}$	712.16
1000	$6.10 \times 10^{-4}$	596.83

**4.3. Graphical representation of time variation of Xenon-135 concentration**

Figure 4.2 shows the plot of atom concentration of Xenon-135 isotope against time. At the origin of time (at  $t = 0$ ), the concentration of Xenon-135 is zero, which signified that the reactor was clean and free of poison before it is being put to use. Three segments of the plot are considered in the following time intervals: 0-17 hours, 17-18 hours and 18-21 hours. At the time interval 0-17 hours the concentration of Xenon-135 buildup linearly from  $6.96 \times 10^{13}$  atoms/cm<sup>3</sup> to  $3.83 \times 10^{14}$  atoms/cm<sup>3</sup>. This buildup was mainly due to contributions from both

fission of Uranium-235 and decay of Iodine-135 ( $T_{1/2}$  of Iodine-135 is 6.6 hours) at this stage. within the time interval 17-18 hours, the concentration of Xenon-135 isotope shown in the profile depicts a little deviation from the original linear shape. This marks the starting point for Xenon-135 buildup from fission of Uranium-235 and decay of Iodine-135 equals its disappearance due to neutron absorption to form Xenon-136 and beta decay to form Cesium-135. Shortly after this time interval, i.e. between 18 hours to approximately 21 hours of the simulation, the equilibrium buildup of Xenon-135 begins to surface.

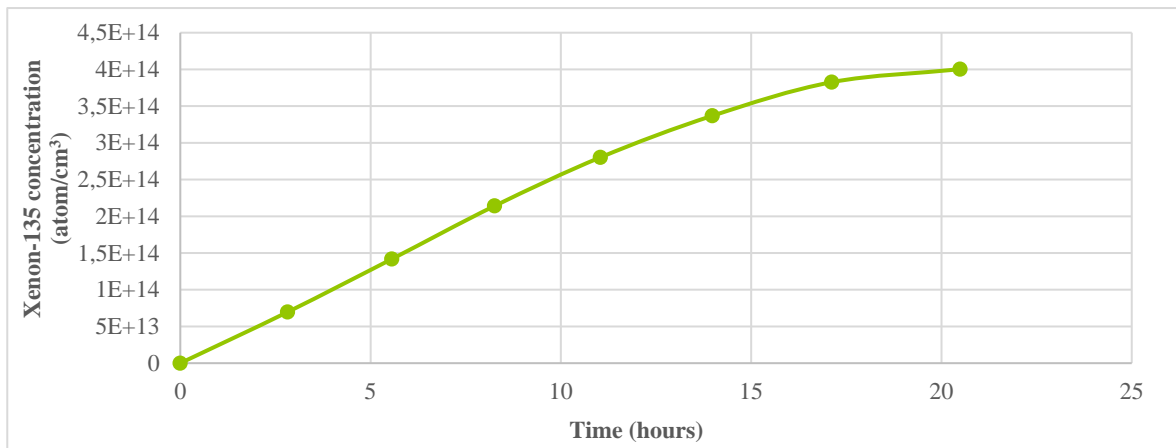


**Figure 4.2.** Plot of Xenon-135 concentration against time.

**4.4. Graphical representation of time variation of Samarium-149 concentration**

Figure 4.4 shows the profile of Samarium-149 concentration against time in an operating reactor that startup from a clean core. At the initial time of the analysis (at  $t = 0$ ) the concentration of Samarium-149 was zero. This validates one of the assumptions made that at the start of the reactor the concentration of all poisons were zero. From time 0-510 hours the concentration of Samarium-149

increases linearly to  $5.3 \times 10^{16}$  atom/cm<sup>3</sup> own to its production from the decay of Promethium-149 and removal solely by neutron absorption to produce to Samarium-150 isotope. As shown by the Samarium-149 profile, at exactly 510 hours of this simulation, equilibrium Samarium-149 began to form till 605 hours of the simulation. It should be noted that, the long duration taken to simulate Samarium-149 concentration is as a result of its lone production from the decay of Promethium-149 which have a half-life of 54 hours. By implication,

this means that Samarium-149 is expected to begin its significant buildup after 54 hours of Promethium-149 formation.

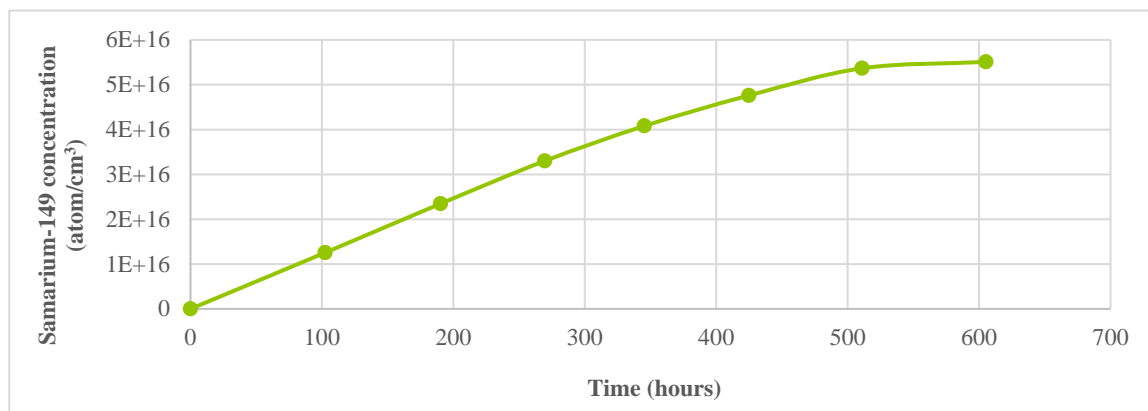


**Figure 4.4.** Plot of Samarium-149 concentration against time.

## 5. Conclusion

In this paper, four important fission products were investigated which includes: Iodine-135, Xenon-135, Promethium-149 and Samarium-149 but with special focus and consideration on Xenon-135 and Samarium-149 because of their large absorption cross sections. The result from JaC-FPBB computed the temperature variations of neutron energies and fluxes, the fission isotopes microscopic and macroscopic cross sections and most importantly, the fission-product poisoning atom concentrations within a computed time. In this study, the result obtained show that it takes Xenon-135 and Samarium-149, 17 hours and 510 hours respectively to buildup and attain equilibrium. The discrepancy between the two fission nuclide's equilibrium attainment time is not far fetch. Since, there is no direct production of Samarium-149 from fission as with Xenon-135; aside from beta decay of Promethium-149 which has a considerable long half-life coupled with the fact that Samarium-149 has a much lower cross section ( $4.2 \times 10^6$  barn) than Xenon-135, Consequentially, it will correspondingly take longer time for Samarium-149 to attain equilibrium than Xenon-135 as shown in this study. This study concluded that the designed algorithm (JaC-FPBB code) proved efficient as it could compute the build-up and burn-up rates for

the two important fission fragments in a nuclear reactor core. The code is easily accessible and could serve as a tool for the development of nuclear energy in developing countries, especially Nigeria.

## Acknowledgements

Authors wish to acknowledge the support provided by the Department of Physics and Engineering Physics, the Center for Energy Research and Development and the Department of Electronic and Electrical Engineering, Obafemi Awolowo University, Ile-Ife, Osun State, Nigeria.

## References

- Arshad, M. (1994). Study Of Xenon And Samarium behaviour in the LEU Parr-1 Cores. Pakistan: Nuclear Engineering Division, Pakistan Institute of Nuclear Science & Technology, 4(28), pp. 1-21.
- Briesmeister, J. F. (1993). MCNP - A General Monte Carlo N-Particle Transport Code, Los Alamos National Laboratory, New Mexico, USA, pp. 4-12.
- Berthou, V., Degueudre, C., Magill, J. (2003). Transmutation Characteristics in Thermal and Fast Neutron Spectra: Application to Americium, Journal of Nuclear Materials, pp. 156-162.

- England, T.R., Wilson. W.B., Stamatelatos, M.G. (1976). Fission product data for thermal reactors- A data set for EPRI-CINDER using ENDF/B-IV. USA: Los Alamos Scientific Laboratory, 8(9), 81p.
- Fermi, E. (1940). Nuclear disintegrations, In: Electrical Engineering, 59(2), pp. 57-58.
- Hermann, O. W., Wesfall, R. M. (1998). ORIGEN-S: Scale System Module to Calculated Fuel Depletion Actinide Transmutation, Fission Product Build-up, Decay and Associated Radiation Source Terms. Tennessee, USA: Oak Ridge National Laboratory, 6(2), pp. 1-122.
- Marcum, W., Spinrad, B. I. (2013). Nuclear reactor device, pp. 1-8. [Online]. Available: [www.britannica.com/technology/nuclear-reactor](http://www.britannica.com/technology/nuclear-reactor).
- Kord, S., Lulu, L. (2012). Nuclear Reactor Physics, Massachusetts Institute of Technology, 372p.
- Lamarsh, J. R. (1966). Introduction to Nuclear Reactor Theory. New york: Addison-Wesley Publishing Company, pp. 255-256.
- Lamarsh, J. R. (2001). Introduction to Nuclear Reactor Theory. New york: Addison-Wesley Publishing Company, 501p.
- Lamarsh, J. R, Baratta, A. J. (2001). Introduction to Nuclear Engineering. Newjersy: Prentice-Hall, Inc. Publishing Company, 3, pp. 272-281.
- Parma, E. J. (2002). BURNCAL- A Nuclear Reactor Burnup Code Using MCNP Tallies. California: Sandia National Laboratories, pp. 3-102.
- Stacey, W. M. (2007). Nuclear Reactor Physics, New york: Wiley-VCH Publishing Company, 2, pp. 211-215.
- Yesilyurt, G., Clarno, K. T., Gauld, I. C. (2011). Modular Origen-S for Multi-Physics Code Systems. International Conference on Mathematics and Computational Methods Applied to Nuclear Science and Engineering, Rio de Janeiro, Brazil, pp. 1-14.



## Changes in Quality Parameters of Deep Fat Fried Carrot Slices Under the Effect of Ultrasound Assisted Pre-drying Process

Merve Secil Turan<sup>1\*</sup>, Erkan Karacabey<sup>1</sup>

**Abstract:** Oil absorption is partially associated to the initial moisture content of frying material, thus controlling the moisture level could result in decreased oil absorption during frying with accompanying changes in other physical properties. As a result, in the current study, in order to figure out the changes in moisture and oil contents of fried carrot slices, the effects of process parameters of ultrasound (U/S) assisted pre-drying was examined. As process conditions of U/S, power levels of 30%, 50%, and 70%, temperature levels of 30 and 50 °C, and time periods of 5, 10 and 15 min were studied. Additionally texture and color preferences were studied. Any reduction in oil absorption was achieved by U/S-predrying, whereas it was observed that there was an increase in brightness (L\*) value of carrot slices as well as generally a decrease in a\* values compared to the control group (directly deep-fat-fried 4mm-carrot slices at 160°C for 120 seconds). Effect of temperature was found to be significant over a\* and L\* values for all power levels. Additionally, no statistically significant change was observed for the textural properties with applied ultrasound power levels.

**Keywords:** frying; food drying; texture; oils; color.

### 1. Introduction

Frying is a common cooking method with a wide range of applications all over the world. In the frying process, product is immersed in pre-heated oil at certain temperature level being far above the boiling point of water. Thus, water movement throughout the solid matrix occurs with accompanying oil absorption and product is removed from oil, when color and textural characteristics meet the sensorial expectations (Gupta, 2005; Dueik et al., 2010; Medina et al., 2015; Esturk et al., 2000). This oil absorption is crucial parameter, since high amount of fat intake is known to potentially cause disorders such as coronary heart disease, diabetes (Saguy and Dana, 2003). Therefore, people are willing to consume low-fat products (Esturk et al., 2000). Studies show that reduction in moisture content encourages positively oil absorption and final product has high oil content which could be potentially hazard for health (Pedreschi and Moyano, 2005; Krokida et al., 2001; Moreira et al.,

1999; Vitrac, 2000; Lamberg et al., 1990; Moreira et al., 1997). Consequently, many techniques to apply before frying have been developed in food industry such as; drying (Pedreschi and Moyano, 2005), microwave drying (Gamble and Rice, 1987), vacuum assisted microwave drying (Song et al., 2007), vacuum frying (Dueik et al., 2010), osmotic dehydration (Ikoko and Kuri, 2007), application of coating material (García et al., 2004; Esturk et al., 2000; Lalam et al., 2013).

In literature there are a plenty number of research works about potato chips being pre-dried with different techniques before frying. However, there is no any literature focusing on the ultrasound assisted hot air pre-drying prior to deep fat frying for fried carrot slice manufacturing.

In reported studies, improvements in drying characteristics of different plant materials have been achieved by ultrasound assisted drying technique as a result of the sponge effect occurring in micro channels (Garcia-Perez et al., 2007;

<sup>1</sup>Suleyman Demirel University, Engineering Faculty, Food Engineering Department, 32260, Isparta, Turkey.

\*Corresponding author: [erkankaracabey@sdu.edu.tr](mailto:erkankaracabey@sdu.edu.tr)

Citation: Turan, M.S., Karacabey, E. (2018). Changes in Quality Parameters of Deep Fat Fried Carrot Slices Under the Effect of Ultrasound Assisted Pre-drying Process. *Bilge International Journal of Science and Technology Research*, 2 (1): 31-39.

Ortuño et al., 2010; Nowacka et al., 2012). Therefore, with sonication, it was supposed to achieve a reduction in moisture content and also oil absorption.

In this study, it was aimed to facilitate drying characteristics by means of the effect of ultrasound application, as a result, to achieve the encouraged moisture movement throughout the carrot slices during drying. Additionally, the influences of ultrasound assisted pre-drying and frying of carrot slices on the quality parameters like color and texture values were examined.

## 2. Material and Method

### 2.1. Sample preparation

Carrots (*Daucus carota* L. subsp. *Sativus*, Nanco) were purchased five days after the harvest from a local market in Isparta, Turkey, and were stored in a polyethylene bags in a refrigerator at 4°C before use. Initial moisture content of carrot samples were determined as  $897.0 \pm 2.0 \text{ g.kg}^{-1}$ , which was coincidence with the range (873 – 910  $\text{g.kg}^{-1}$ ) reported by Gichuhi et al. (2009). Before the analyses, carrot was washed, cleaned and peeled. Peeled carrots were sliced at 4 mm thickness using an industrial type slicer (Arisco, HBS-200, Turkey). Carrot slices having diameter of  $2.5 \pm 0.5$  cm were selected for remaining process steps. Afterwards, carrot slices were subjected to blanching for 90 s in a hot water at 85°C and then cooled down using tap water for 120 seconds. Excess surface water was removed using absorbent paper.

### 2.2. Ultrasound pretreatments and hot air drying

Boiled carrot slices have been immersed in a beaker filled with distilled water. Sonication was conducted by using an ultrasonic probe having ultrasonic frequency of 20 kHz and density of 500  $\text{W.m}^{-2}$  (Ultrasonic-Homogenizer, Cy-500, Spain). The ratio of sample in water for all groups was adjusted 1: 4 (w/v) in order to avoid environment effect on sonication influence (Fernandes et al., 2006). Ultrasonic treatments were carried out at power levels of 30%, 50%, and 70% under temperature levels of 30 and 50 °C for time periods of 5, 10 and 15 min. All conducted trials and relevant process conditions were given in Table 1.

A bunch of carrot slices (~50 g) of previously pretreated by ultrasound (at different temperature, time and power) were arranged as a single layer on a tray and dried in a convectional hot air dryer (Mikrotest, MKD, Turkey) at air flow rate of  $1.3 \pm 0.02 \text{ m s}^{-1}$ . Temperature and weight loss during drying were set according to optimal drying conditions (63.4°C for drying temperature, 16% for weight loss during drying) determined in our previous study (Karacabey et al., 2016).

**Table 1.** Ultrasonic Pretreatments

Label	Power (%)	Temperature (°C)	Time (min)
A	50	30	5
B	50	30	10
C	50	30	15
D	50	50	5
E	50	50	10
F	50	50	15
G	30	30	15
H	50	30	15
I	70	30	15

### 2.3. Deep fat frying

When the target weight loss on samples was attained, frying was conducted using 3 L of sunflower oil (Marsa Oil Industry Co. Ltd., İstanbul, Turkey) in an industrial type fryer (Remta Co. Ltd, İstanbul, Turkey) under specified optimal conditions determined as 152°C for frying temperature, and 207 s for frying time (Karacabey et al., 2016).

After frying, the fried carrot slices were removed from the oil and drained for about 300 s over a wire screen to drain the most of the surface oil, and then the slices were transferred to an absorbent towel. Frying oil was replaced with fresh one, after each run was completed. In order to determine the reference values for untreated samples, one group of carrot slices were directly fried after blanching without pre-treatment steps. Oil content, moisture content, breaking force, and  $L^*$ ,  $a^*$ ,  $b^*$  value were measured in these fried slices. Temperature (160°C) and time (120 sec.) were the corresponding values of directly deep-fat-frying process which was determined according to our previous study. In that study, sensory analysis was conducted to determine the process conditions, fried carrot slices (4 mm thickness) at which took the highest score. Texture values,  $L^*$ ,  $a^*$ , and  $b^*$ ,

oil content and moisture content of control group is shown in Table 2.

#### 2.4. Analyses of samples

##### Moisture content

The method of Fan, Zhang was used (Fan et al., 2005). Carrot slices were ground after frying. Five gram of ground samples were used for moisture content ( $\text{g.kg}^{-1}$ ). Ground samples were dried in an oven (FN300, Nuve, Turkey) at  $105 \pm 0.5^\circ\text{C}$ , until no weight change was attained. Test was performed in duplicate.

**Table 2.** The Results of Control Group

MC,%	OC*,%	CV			TP	
		L*	a*	b*	H, g force	BF, g force
48	32.50	50.3	30.4	41.8	462.8	549.0

\*Oil content (%) is calculated based on the dry weight. MC: moisture content; OC: Oil content; CV: Color values; TP: Texture properties; H: Hardness; BF: Breaking force

##### Oil content

The oil determination method reported by Sulaeman et al. (2001) was used with modification. Briefly, oil extraction was performed in a Soxhlet extractor (Büchi Universal Extraction System B-811, Germany) using hexane as a solvent to determine the oil content of fried carrot slices. Before extraction, fried samples (5 g) were dried in a vacuum oven and then ground (James, 1998). Oil content ( $\text{g.kg}^{-1}$ ) was calculated as wet bases. The test was performed in duplicate.

##### Surface Color

Color parameters ( $L^*$ ,  $a^*$ , and  $b^*$ ) were measured using a colorimeter (NH310, 3nh Tech. Co., Ltd. China) (Robertson, 1977). The equipment was standardized each time with white and black references. Five carrot slices and at five different locations for each slice were used for color measurements and mean values were reported.

##### Texture Values

Texture analysis was conducted by a texture analyzer (TA.XT Plus, Stable Micro System Co. Ltd., Godalming, UK). The PS / 30 probe and LKB probe were used to measure the slice hardness and firmness, respectively. PS / 30 probe movement speed was  $1 \times 10^{-3} \text{ m s}^{-1}$  and initial distance from the platform was set as  $50 \times 10^{-3} \text{ m}$ .

LKB probe movement speed was  $1 \times 10^{-3} \text{ m s}^{-1}$  and initial distance from the platform was set as  $25 \times 10^{-3} \text{ m}$ . The result for each trial was given as a mean of 5 measurements.

### 3. Results and Discussion

The results of texture, surface color, moisture and oil content of fried carrot slices previously ultrasound assisted pre-dried were given in Table 3.

#### 3.1. Texture

As can be seen in Table 3, the hardness values of ultrasound-assisted pre-dried and fried carrot slices were lower than the control group in case of almost all treatments, except for B and D, but this reduction in the slice hardness was not enormous, instead, limited. Statistical analysis has also supported this fact by indicating that the differences in control and pretreated carrot slices as none significant almost for all cases ( $p > 0.05$ ) (Table 3). In order to analyses the effects of process variables of ultrasound assisted pre-drying, temperature and treatment time were statistically analyzed and the results were given in Table 4.

**Table 3.** Results of texture, color and moisture and oil content of fried carrot slices pretreated by ultrasound-assisted pre-drying

Groups	Hardness, g force	Firmness, g force	L*	a*	b*	Moisture Content, %	Oil Content, %
A	409.58±282.57 <sup>ab</sup>	569.95±227.38 <sup>a</sup>	53.34±3.46 <sup>f</sup>	23.41±2.91 <sup>c</sup>	44.55±4.01 <sup>d</sup>	51.36±0.85 <sup>c,d</sup>	33.57±0.58 <sup>c</sup>
B	538.35±345.76 <sup>a</sup>	499.41±188.81 <sup>ab</sup>	56.80±3.10 <sup>b,c</sup>	28.42±3.00 <sup>b</sup>	50.64±3.20 <sup>a,b</sup>	58.03±1.02 <sup>a,b</sup>	33.60±1.58 <sup>c</sup>
C	154.31±242.74 <sup>b</sup>	239.01±143.40 <sup>c</sup>	54.83±1.80 <sup>d,e</sup>	30.65±1.92 <sup>a</sup>	49.89±2.42 <sup>a,b</sup>	47.05±0.27 <sup>d,e,f</sup>	40.64±1.80 <sup>b</sup>
D	485.86±517.51 <sup>ab</sup>	225.44±116.68 <sup>c</sup>	51.19±2.21 <sup>g</sup>	31.19±1.73 <sup>a</sup>	47.95±3.91 <sup>c</sup>	44.19±6.21 <sup>e,f</sup>	34.72±2.04 <sup>c</sup>
E	141.47±190.80 <sup>b</sup>	368.23±178.03 <sup>ab,c</sup>	57.35±3.17 <sup>b</sup>	24.16±3.81 <sup>c</sup>	51.19±2.24 <sup>a</sup>	42.00±0.72 <sup>f</sup>	47.11±0.81 <sup>a</sup>
F	308.15±183.80 <sup>ab</sup>	290.04±142.78 <sup>c</sup>	63.52±1.36 <sup>a</sup>	18.64±3.04 <sup>d</sup>	49.52±2.75 <sup>b</sup>	51.29±1.02 <sup>c,d</sup>	39.97±5.51 <sup>b</sup>
G	410.80±283.89 <sup>ab</sup>	329.43±216.45 <sup>b,c</sup>	54.34±1.22 <sup>e,f</sup>	28.43±1.46 <sup>b</sup>	46.53±2.03 <sup>c</sup>	53.47±2.72 <sup>b,c</sup>	34.44±1.67 <sup>c</sup>
H	358.49±416.32 <sup>ab</sup>	511.17±275.01 <sup>ab</sup>	55.65±1.30 <sup>c,d</sup>	28.59±1.55 <sup>b</sup>	47.40±2.78 <sup>c</sup>	46.67±2.11 <sup>d,e,f</sup>	36.22±0.83 <sup>b,c</sup>
I	181.29±222.14 <sup>b</sup>	542.60±188.97 <sup>a</sup>	57.64±1.16 <sup>b</sup>	30.61±1.35 <sup>a</sup>	47.67±1.38 <sup>c</sup>	59.72±0.43 <sup>a</sup>	32.19±0.06 <sup>c</sup>
Control	462.75±443.18 <sup>ab</sup>	549.02±231.48 <sup>a</sup>	50.25±2.86 <sup>g</sup>	30.35±1.43 <sup>a</sup>	41.76±3.21 <sup>e</sup>	48.00±0.70 <sup>c,d,e</sup>	32.50±1.35 <sup>c</sup>

Different letters in the same column indicate a significant difference ( $p \leq 0.05$ )

**Table 4.** Effects of temperatures and time of the ultrasound assisted pre-drying on the hardness of fried carrot slices

Hardness (g, force)	Temperature (°C)	
	30	50
Time (min)		
5	409.58±282.57 <sup>A,a,b</sup>	485.86±517.51 <sup>A,a</sup>
10	538.35±345.76 <sup>A,a</sup>	141.47±190.80 <sup>B,b</sup>
15	154.31±242.74 <sup>A,b</sup>	308.15±183.80 <sup>A,a,b</sup>

Different capital letters in the same row indicate a significant difference in terms of application temperatures ( $p \leq 0.05$ )  
 Different lowercase letters in the same column indicate a significant difference in terms of application time ( $p \leq 0.05$ )

The difference among the application time of the ultrasonic pre-treatment carried out for 10 and 15 minutes at 30°C were significant ( $p \leq 0.05$ ). Hardness of carrot slices were only changed with temperature rise from 30°C to 50°C, when the ultrasound assisted pre-drying was performed for 10 min (Table 4).

Similar to the hardness values of carrot slices, it was seen that treatments C, D, F, and G caused significant changes in firmness value compared to that of control group ( $p \leq 0.05$ ). Remaining ones were found to be statistically same as control (Table 3). Change in firmness of fried carrot slices depending on the process conditions of pre-dried by ultrasound assisted drying technique were displayed in Table 5. The influence of temperature increasing from 30 °C to 50 °C was only found to be significant when pretreatment was applied for 5 min ( $p \leq 0.05$ ). Treatment time caused any significant change in firmness of carrot slices, when it was performed at 10 min and 15 min ( $p > 0.05$ ). For both temperature levels, it was seen that the firmness decreased with increasing time (Table 5).

**Table 5.** Effects of temperatures and time of the ultrasound assisted pre-drying on the firmness of fried carrot slices

Firmness (g, force)	Temperature (°C)	
	30	50
Time (min)		
5	569.95±227.38 <sup>A,a</sup>	225.44±116.68 <sup>B,b</sup>
10	499.41±188.81 <sup>A,a</sup>	368.23±178.03 <sup>A,a</sup>
15	239.01±143.40 <sup>A,b</sup>	290.04±142.78 <sup>A,a,b</sup>

Different capital letters in the same row indicate a significant difference in terms of application temperatures ( $p \leq 0.05$ ).  
 Different lowercase letters in the same column indicate a significant difference in terms of application time ( $p \leq 0.05$ )

**Table 6.** The effects different intensity ultrasound power on textural properties of fried carrot slices

Experiments	Power (%)	Hardness, g force	Firmness, g force
G	30	410.80±283.89 <sup>a</sup>	329.43±216.45 <sup>a</sup>
H	50	358.49±416.32 <sup>a</sup>	511.17±275.01 <sup>a</sup>
I	70	181.29±222.14 <sup>a</sup>	542.60±188.97 <sup>a</sup>

Different letters in the same column indicate a significant difference ( $p \leq 0.05$ )

According to the results given in Table 6, it is seen that there is no any significant change in hardness or firmness values of fried carrot slices with changing ultrasound power ( $p > 0.05$ ). Brncic et al. (2010) studied the ultrasound assisted drying at different ultrasound power and reported the absence of significant effect on the textural properties or a limited effect. In another study conducted by Dujmić et al. (2013), increasing ultrasound power was found to cause a decrease in hardness values but noted that this effect was not statistically significant. These results are coincidence with the finding in this current study.

### 3.2. Surface Color Values

As can be seen in Table 3,  $L^*$  values, representing surface brightness of fried carrot slices pre-dried by ultrasound assisted drying technique, displayed that the nearest brightness value to control group was achieved for the carrot slices processed at the conditions coded as D among all experiments. Besides to D group,  $L^*$  values of remaining ones are shown to be higher than control group (Table 3). Color change from green to red is defined with  $a^*$  value. The results indicated that the general trend in  $a^*$  value was a decrease compared to control group ( $p \leq 0.05$ ), but few exceptions being coded treatments of C, D, and I ( $p > 0.05$ ).  $b^*$  value is another surface color parameter measured in current study. Table 3 shows that compared to  $b^*$  value of control group, there is an increase in this color parameter of fried carrot slices if they were pretreated by ultrasound assisted drying technique before frying ( $p \leq 0.05$ ). Ultrasound parameters (temperature and time) were also investigated to figure out their influences on  $L^*$ ,  $a^*$  and  $b^*$  values. Figure 1, Figure 2 and Figure 3 display the change in surface color parameters with temperature and time as well as their statistical differences. It is seen that at constant temperature level, increasing sonication time caused an increase in  $L^*$  value and this is more apparent when medium temperature was  $50^\circ\text{C}$  (Figure 1). The temperature was found not to create any certain effect on  $L^*$  value of fried carrot slices as seen from Figure 1. For 5 min treatment, as changing temperature value from  $30^\circ\text{C}$  to  $50^\circ\text{C}$  lowered the  $L^*$  value. On the other hand, an increase in brightness was seen with increasing temperature, when sonication was 15 min (Figure 1). No statistically significant change was observed with temperature for 10 min treatment. The temperature significantly affected  $a^*$  value for all treatment durations ( $p \leq 0.05$ ), but this effect was different in between 5 min and 10 or 15 min treatments. There was an increase in  $a^*$  value for 5 min treatment, whereas  $a^*$  value decreased for the treatments of 10 min and 15 min (Figure 2). This may be related to the effect of temperature-time on carotenoid content of carrot slices. Because, for short term application, carotenoids may turn to free form with effects of temperature and ultrasound, but further increase in process time resulted in adverse effect of temperature like that was seen for treatments of 10 min and 15 min and carotenoids degraded and  $a^*$  value partially decreased. As can be seen from Figure 2 that an increase in  $a^*$  value was seen with increasing sonication time from 5 min to 15 min at

$30^\circ\text{C}$ , but this influence was reversed and increasing process time caused a decrease for sonication processes carried at  $50^\circ\text{C}$ . Another color parameter  $b^*$  was also studied and temperature and process time were found to affect it in limited extent (Figure 3). Except for 5 min treatment ( $p \leq 0.05$ ),  $b^*$  value did not change with temperature ( $p > 0.05$ ). There was also no change in  $b^*$  value with time when sonication was at  $30^\circ\text{C}$ . However, time affected  $b^*$  value ( $p \leq 0.05$ ) when sonication temperature was increased to  $50^\circ\text{C}$ , but this effect did not have a clear trend, instead fluctuated.

Ultrasound power was another process variable controlled in this study and the effect of its change was investigated in terms of surface color. The results were shown in Figure 4. An increase in ultrasound power was seen to increase brightness ( $L^*$  value) and redness ( $a^*$  value) of carrot slices ( $p \leq 0.05$ ), but no significant change in  $b^*$  value was detected ( $p > 0.05$ ) (Figure 4). An increase in  $L^*$  value was continued throughout the power levels. Power change was effective for  $a^*$  value after it was shifted from 30% to 70% ( $p \leq 0.05$ ), there was no difference between  $a^*$  values measured for samples processed at 30% and 50% power levels ( $p > 0.05$ ) (Figure 4). The change in color may be attributed to the cavitation occurred as a result of ultrasound. Tiwari et al. (2008) have reported change in color parameters after ultrasound application and they have associated these changes with the effects of ultrasound. An intensification in  $a^*$  value may also be attributed to the isomerization of carotenoids and reduction in degradation of  $\beta$ -carotene (Chen et al., 1995; Sun et al., 2010).

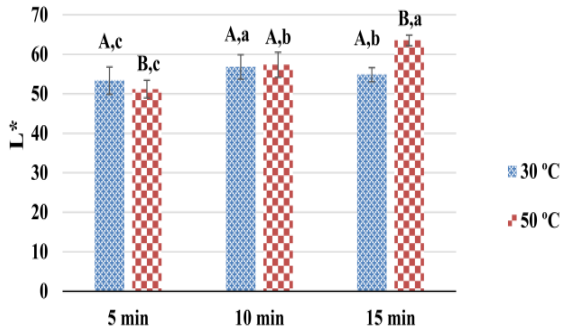


**Figure 1.** Effects of temperatures and time of the ultrasound assisted pre-drying on the brightness of fried carrot slices  
 Different lowercase letters indicate a significant difference in terms of ultrasound application time separately for each temperature ( $p \leq 0.05$ )  
 Different capital letters in the per column indicate a significant difference in terms of application temperatures for each time ( $p \leq 0.05$ )

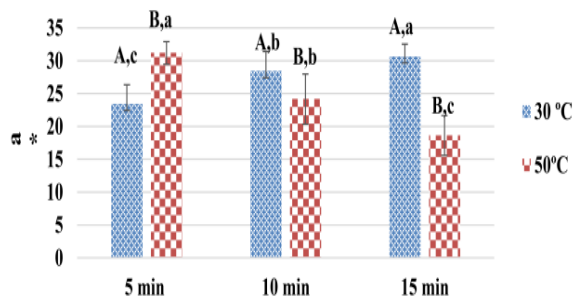


**Figure 2.** Effects of temperatures and time of the ultrasound assisted pre-drying on the a\* values of fried carrot slices  
 Different lowercase letters indicate a significant difference in terms of ultrasound application time separately for each temperature ( $p \leq 0.05$ )  
 Different capital letters in the per column indicate a significant difference in terms of application temperatures for each time ( $p \leq 0.05$ )

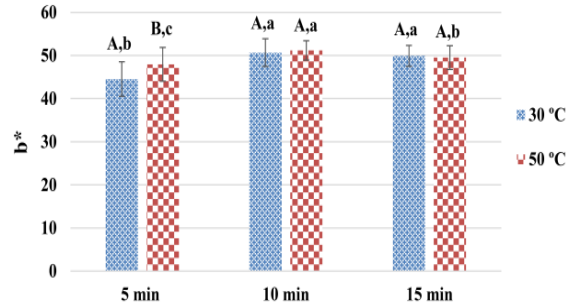


**Figure 3.** Effects of temperatures and time of the ultrasound assisted pre-drying on the b\* values of fried carrot slices  
 Different lowercase letters indicate a significant difference in terms of ultrasound application time separately for each temperature ( $p \leq 0.05$ )  
 Different capital letters in the per column indicate a significant difference in terms of application temperatures for each time ( $p \leq 0.05$ )

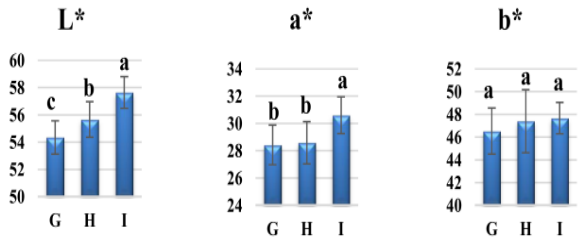


**Figure 4.** The effects of ultrasound power on surface color of fried carrot slices  
 Different letters indicate a significant difference for each color parameters separately ( $p \leq 0.05$ )

**3.3. Moisture Content**

Compared to control group, the moisture content of fried carrot slices differed depending on the conditions of ultrasound applications ( $p \leq 0.05$ ) (Table 3). Change in moisture content of final product occurred as a decrease or an increase. Thus, the influence of sonication conditions on moisture content of fried carrots was also investigated and temperature and time effects were analyzed in Table 7.

**Table 7.** Effects of temperatures and time of the ultrasound assisted pre-drying on the moisture content of fried carrot slices

Moisture Content (%)	Time (min)	Temperature (°C)	
		30	50
	5	51.36±0.85 <sup>A,b</sup>	44.19±6.21 <sup>A,a</sup>
	10	58.03±1.02 <sup>A,a</sup>	42.00±0.72 <sup>B,a</sup>
	15	47.05±0.27 <sup>A,c</sup>	51.29±1.02 <sup>B,a</sup>

Different capital letters in the same row indicate a significant difference in terms of application temperatures ( $p \leq 0.05$ )

Different lowercase letters in the same column indicate a significant difference in terms of application time ( $p \leq 0.05$ )

Tabulated results indicated that temperature elevation was only effective on moisture content, when application time was higher than 10 minutes ( $p \leq 0.05$ ), in other words there was no change in moisture content with sonication temperature for 5 min- treatment ( $p > 0.05$ ). Process time was also considered and it was found to cause a change in moisture content only application temperature was 30°C ( $p \leq 0.05$ ). Although moisture content increased especially after treatment time of 10 min, this change did not occur at significant level when sonication was conducted at the temperature level of 50°C. The last parameter of ultrasound application was power level and the influence of different sonication power in the fix time and temperature applications was shown in Figure 5. A decrease in moisture content at certain level was seen with increasing ultrasound power from 30% to 50%, but further increase up to 70% caused an increase in moisture content again. This variation in moisture content under the effect of power level was found to be statistically significant ( $p \leq 0.05$ ). Gallego-Juárez et al. (2007) reported that increasing the ultrasonic power raised the diffusion coefficient and accordingly it was supposed that the amount of moisture away from the product was increased by rising the ultrasound power. In this study similar effect was seen for power level of 30% and 50% and this effect was thought to be relevant to the occurrence of micro channels in solid matrix and thus moisture level decreased. However, at 70% power there was an increase in moisture content. This increase occurring in moisture content of product was attributed to the failure to remove moisture from the structure due to the collapses in the micro channel with the high ultrasonic effect, at 70% level (Figure 5).

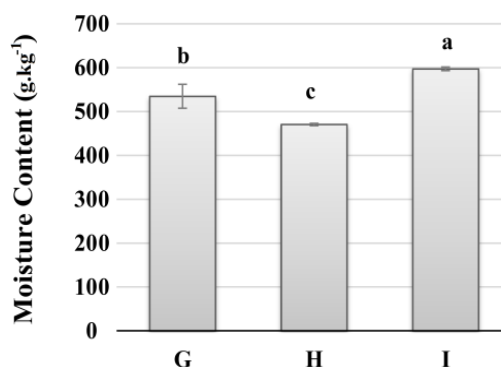


**Figure 5.** The effects different intensity ultrasound power on moisture content of fried carrot slices. Different letters indicate a significant difference ( $p \leq 0.05$ )

### 3.4. Oil Content

Oil content of ultrasound assisted dried and fried carrot slices were tabulated in Table 3. Oil content of final fried carrot slices were generally higher than that measured for control group samples ( $p \leq 0.05$ ). This may be explained with the effects of ultrasound on structure of carrot slices, since the cavitation occurred as a result of sonication caused mechanical effects on layers close to surface and this accelerates the mass transfer throughout/ into the solid matrix. Thus, oil absorption increased during frying as well that occurred for moisture transfer out of solid. Temperature and time effects on oil absorption of fried carrot slices were given in Table 8 where it was seen that both variables caused significant changes in oil content ( $p \leq 0.05$ ). At constant temperature level, in general manner, an increase in process time resulted in an increase in oil content. Temperature change was found only to affect oil content for 10 min treatment (Table 8).

**Table 8.** Effects of temperatures and time of the ultrasound assisted pre-drying on the oil content of fried carrot slices

Oil Content	Time (min)	Temperature (°C)	
		30	50
	5	33.57±0.58 <sup>A,b</sup>	34.72±2.0 <sup>A,b</sup>
	10	33.60±1.58 <sup>A,b</sup>	47.11±0.81 <sup>B,a</sup>
	15	40.64±1.80 <sup>A,a</sup>	39.97±5.51 <sup>A,a,b</sup>

Different capital letters in the same row indicate a significant difference in terms of application temperatures ( $p \leq 0.05$ )

Different lowercase letters in the same column indicate a significant difference in terms of application time ( $p \leq 0.05$ )

Power level of sonication was another variable and its effect on oil content of fried carrot slices were seen in Figure 6. Increased power level of



sonication was found to create statistically significant difference for 50% power level compared to 30% and 70% power levels (Figure 6). When oil absorption was taken into account, it was compatible with that observed for moisture content change in general trend (Figure 6).

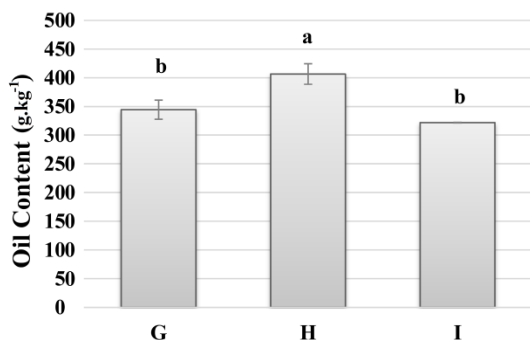


**Figure 6.** The effects different intensity ultrasound power on oil content of fried carrot slices  
Different letters indicate a significant difference ( $p \leq 0.05$ )

## Conclusion

The effect of ultrasound applied during drying was found not to change the oil absorption in the studied conditions. However, there are some differences in other investigated properties including color. As a result, although ultrasound application in drying have been reported to provide some changes in drying characteristics being relevant to the textural variations, these changes were not enough to affect the oil absorption taking place during frying process being contrast to expectations. Briefly, it could be said that further studies including different process conditions are required to evaluate the effect of ultrasound application on oil absorption.

## Acknowledgement

This work was supported by Süleyman Demirel University Scientific Research Projects Coordination Unit (grant number 4207-YL1-14); and The Scientific and Technological Research Council of Turkey (grant number 113R015).

## References

Brncic M., Karlovic S., Rimac B.S., Bosiljkov T., Ježek D., Tripalo B. (2010). Textural properties of infra red dried apple slices as affected by high power ultrasound pre-

treatment. *African Journal of Biotechnology*, 9(41), 6907-6915.

Chen B.H., Peng H.Y., Chen H.E. (1995). Changes of Carotenoids, Color, and Vitamin A Contents during Processing of Carrot Juice. *Journal of Agricultural and Food Chemistry*, 43(7), 1912-1918.

Dueik V., Robert P., Bouchon P. (2010). Vacuum frying reduces oil uptake and improves the quality parameters of carrot crisps. *Food Chemistry*, 119(3), 1143-1149.

Dujmić F., Brnčić M., Karlović S., Bosiljkov T., Ježek D., Tripalo B., Mofardin I. (2013). Ultrasound- Assisted Infrared Drying of Pear Slices: Textural Issues. *Journal of Food Process Engineering*, 36(3), 397-406.

Esturk O., Kayacier A., Singh R.K. (2000). Reduction of oil uptake in deep fried tortilla chips Reducción de la absorción de aceite en la fritura de tiras de maíz. *Revista de Agroquímica y Tecnología de Alimentos*, 6(5), 425-431.

Fan L.-p., Zhang M., Mujumdar A.S. (2005). Vacuum frying of carrot chips. *Drying Technology*, 23(3), 645-656.

Fernandes F.A., Rodrigues S., Gaspareto O.C., Oliveira E.L. (2006). Optimization of osmotic dehydration of bananas followed by air-drying. *Journal of Food Engineering*, 77(1), 188-193.

Gallego-Juárez J.A., Riera E., De la Fuente Blanco S., Rodríguez-Corral G., Acosta-Aparicio V.M., Blanco A. (2007). Application of high-power ultrasound for dehydration of vegetables: processes and devices. *Drying Technology*, 25(11), 1893-1901.

Gamble M., Rice P. (1987). Effect of pre- fry drying of oil uptake and distribution in potato crisp manufacture. *International Journal of Food Science & Technology*, 22(5), 535-548.

García-Perez J., Cárcel J., Benedito J., Mulet A. (2007). Power ultrasound mass transfer enhancement in food drying. *Food and Bioproducts Processing*, 85(3), 247-254.

García M.A., Ferrero C., Campana A., Bértola N., Martino M., Zaritzky N. (2004). Methylcellulose Coatings Applied to Reduce Oil Uptake in Fried Products. *Revista de Agroquímica y Tecnología de Alimentos*, 10(5), 339-346.



- Gichuhi P., Mortley D., Bromfield E., Bovell-Benjamin A. (2009). Nutritional, physical, and sensory evaluation of hydroponic carrots (*Daucus carota* L.) from different nutrient delivery systems. *Journal of Food Science*, 74(9), S403-S412.
- Gupta, M.K. (2005). *Frying Oils*.
- Ikoko J., Kuri V. (2007). Osmotic pre-treatment effect on fat intake reduction and eating quality of deep-fried plantain. *Food Chemistry*, 102(2), 523-531.
- James C.S. (1998). *Analytical Chemistry Of Foods*. James C.S. (Ed.) Springer.
- Karacabey E., Turan M.S., Özçelik Ş.G., Baltacıoğlu C., Küçüköner E. (2016). Optimisation of pre- drying and deep- fat-frying conditions for production of low- fat fried carrot slices. *Journal of the Science of Food and Agriculture*.
- Krokida M., Oreopoulou V., Maroulis Z., Marinou-Kouris D. (2001). Deep fat frying of potato strips—quality issues. *Drying Technology*, 19(5), 879-935.
- Lalam S., Sandhu J.S., Takhar P.S., Thompson L.D., Alvarado C. (2013). Experimental study on transport mechanisms during deep fat frying of chicken nuggets. *LWT-Food Science and Technology*, 50(1), 110-119.
- Lamberg I., Hallstroem B., Olsson H. (1990). Fat uptake in a potato drying/frying process. *Lebensmittel Wissenschaft und Technologie*, 23(4), 295-300.
- Medina M., Antequera T., Ruiz J., Jiménez-Martín E., Pérez-Palacios T. (2015). Quality characteristics of fried lamb nuggets from low-value meat cuts: Effect of formulation and freezing storage. *Revista de Agroquímica y Tecnología de Alimentos*, 21(7), 503-511.
- Moreira R.G., Castell-Perez M.E., Barrufet M.A. (1999). Deep fat frying: Fundamentals and applications.
- Moreira R.G., Sun X., Chen Y. (1997). Factors affecting oil uptake in tortilla chips in deep-fat frying. *Journal of Food Engineering*, 31(4), 485-498.
- Nowacka M., Wiktor A., Śledź M., Jurek N., Witrowa-Rajchert D. (2012). Drying of ultrasound pretreated apple and its selected physical properties. *Journal of Food Engineering*, 113(3), 427-433.
- Ortuño C., Pérez-Munuera I., Puig A., Riera E., Garcia-Perez J. (2010). Influence of power ultrasound application on mass transport and microstructure of orange peel during hot air drying. *Physics Procedia*, 3(1), 153-159.
- Pedreschi F., Moyano P. (2005). Effect of pre-drying on texture and oil uptake of potato chips. *LWT - Food Science and Technology*, 38(6), 599-604.
- Robertson A.R. (1977). The CIE 1976 Color-Difference Formulae. *Color Research and Application*, 2(1), 7-11.
- Saguy I.S., Dana D. (2003). Integrated approach to deep fat frying: engineering, nutrition, health and consumer aspects. *Journal of Food Engineering*, 56(2), 143-152.
- Song X.-j., Zhang M., Mujumdar A.S. (2007). Optimization of vacuum microwave predrying and vacuum frying conditions to produce fried potato chips. *Drying Technology*, 25(12), 2027-2034.
- Sulaeman A., Keeler L., Giraud D., Taylor S.L., Wehling R., Driskell J. (2001). Carotenoid Content and Physicochemical and Sensory Characteristics of Carrot Chips Deep- Fried in Different Oils at Several Temperatures. *Journal of Food Science*, 66(9), 1257-1264.
- Sun Y., Ma G., Ye X., Kakuda Y., Meng R. (2010). Stability of all-trans- $\beta$ -carotene under ultrasound treatment in a model system: Effects of different factors, kinetics and newly formed compounds. *Ultrasonics Sonochemistry*, 17(4), 654-661.
- Tiwari B., Muthukumarappan K., O'donnell C., Cullen P. (2008). Colour degradation and quality parameters of sonicated orange juice using response surface methodology. *LWT-Food Science and Technology*, 41(10), 1876-1883.
- Vitrac O. (2000). *Caractérisation expérimentale et modélisation de l'opération de friture*. (Doctoral dissertation, Massy, ENSIA).

## Real-time Parental Voice Recognition System For Persons Having Impaired Hearing

Mete Yağanoğlu<sup>1\*</sup>, Cemal Köse<sup>2</sup>

**Abstract:** Persons having impaired hearing do not live a comfortable life because they can't hear sounds when they are asleep or alone at home. In this study, a parental voice recognition system was proposed for those people. Persons having impaired hearing are informed by vibration about which one of their parents is speaking. By this means, the person having impaired hearing real timely perceives who is calling or who is speaking to him. The wearable device that we developed can real timely perceive parental voice very easily, and transmits it to person having impaired hearing, while he/she is asleep or at home. A wearable device has been developed for persons having impaired hearing to use easily at home environment. Our device is placed on user's back, and just a ring-sized vibration motor is attached to the finger of person. Our device consists of Raspberry Pi, usb sound card, microphone, power supply and vibration motor. First of all, the sound is received by a microphone, and sampling is made. According to the Nyquist Theorem, 44100 samples are made per second. Normalization during preprocessing phase, Mel Frequency Cepstral Coefficients (MFCC) during feature extraction stage, k nearest neighbor (knn) during the classification phase were used. Statistical or Z-score normalization was used in the pre-processing phase. By means of normalization of the data, it is ensured that each parameter in the training input set contributes equally to the prediction of the model. MFCC is one of the feature extraction methods that are frequently used in voice recognition applications. MFCC represents the short-time power spectrum of the audio signal, and models the manner of perception of human ear. Knn is an educational learning algorithm, and its aim is to classify the existing learning data when a new sampling arrives. The sound data received via microphone were estimated through preprocessing, feature extraction and classification stages, and the person having impaired hearing was informed through real time vibrations about to whom this voice belongs. This study was tested on 2 deaf, 3 normal hearing persons. The ears of normal hearing persons were covered with a earphone that gives out loud noise. Persons having impaired hearing estimated their mothers' voice by 76%, and fathers' voice by 81% accuracy in real-time tests. The success rate decreases due to the noise of environment especially while watching tv. In the tests performed while these persons are asleep, a person having impaired hearing perceives his/her mother's voice by 78%, and father's voice by 83% accuracy. In this study it was aimed for persons having impaired hearing to perceive their parents' voice and accordingly have a more prosperous standard of living.

**Keywords:** Wearable Processing, MFCC, Raspberry Pi, Vibration for Deaf.

### 1. Introduction

Engineers have been working on technological developments providing the relation between machines imitating human behaviors and humans for many years. Human-being wants discoveries

that would understand him and make meeting his expenses easier with developed technology. One of the most remarkable discoveries is speech recognition applications. Speech is the most appropriate and effective way of communication for people. The technology of speech recognition aims

<sup>1</sup>Ataturk University, Faculty of Engineering, Department of Computer Engineering, 25240, Erzurum, Turkey.

<sup>2</sup>Karadeniz Technical University, Faculty of Engineering, Department of Computer Engineering, 61080, Trabzon, Turkey.

\*Corresponding author: [yaganoglu@atauni.edu.tr](mailto:yaganoglu@atauni.edu.tr)

Citation: Yaganoglu, M., Kose, C. (2018). Real-time Parental Voice Recognition System for Persons Having Impaired Hearing. Bilge International Journal of Science and Technology Research, 2 (1): 40-46.

at developing and producing systems that can get data by talk and move on data. At the same time, it aims at providing data not only from humans to machines but also from machines to humans through speech synthesis. Works on speech recognition can be considered part of a function of artificial intelligence machines that can get, understand talked messages, turn them into text, move according to these messages and complete data transmission by talking. Speech recognition systems are in the first place in research subjects providing this kind of developments and are the systems including the recognition of voices recorded by a microphone through computer programs. The problem of speech recognition has had a very large place and a lot of various systems have been developed from the past to today in the literature. Speech processing is a place of study many various signal processing techniques can be applied.

It is too complicated problem to rapidly realize speech recognition process that people can easily do in daily life through an algorithm on computer. By getting rid of this problem, an important step would be taken in realizing a capability belonging to people by means of machines. This way, an application, which can rapidly work in a simple embedded system, be used by disabled people for example and place of use under the control of a device, can be developed.

The most important benefit in speech recognition applications is to be able to design a system deaf and blind people can understand. In this kind of applications, it is purposed to make a disabled person's life better than normal. For example, it can be provided that a blind reader can read records gotten before at any speed (Schafer and Rabiner, 1975). In this study, a system that deaf people can sense father and mother voices is designed. A deaf person doesn't hear his parents talking to him and his standard of life decreases. For example, he can understand during sleeping when his parents talk to him especially in emergency.

In the study of Phoophuangpairoj, multiple Hidden Markov Model (HMM) voice recognition system is used. The used system is composed of the results of acoustic model, spelling dictionary, robot command grammar, recognition of robot command and voice recognition algorithms. An average success at 98% is obtained with the system developed by using three different user groups as gender-dependent,

gender-independent and those whose genders are known (Phoophuangpairoj, 2011).

In the studies of Muda et al., various commands are separately tried for women and men by using Mel Frequency Cepstrum Coefficients (MFCC) and Dynamic Time Bending algorithms (Muda et al., 2010).

In the studies of Fezari and Salah, trials for voice recognition application are done under 4 different conditions. Average success at 85%, 73%, 78% and 65% is respectively obtained in the end of the trials as regular and irregular noisy inside and outside lab (Fezari and Salah, 2006).

In the studies of Babu et al., Linear Predictive Coding, Vector Quantization algorithms and HMM algorithm are separately used. In the developed system, environment noisy is determined and used as threshold value, numbers between 0 and 9 are firstly sensed through voice determination system independently from time and voice processing techniques are used. In various gain values, an average success at 80% is obtained (Babu et al., 2012).

In the studies of Leechor et al., while an average success at 98% is obtained noiseless environment a remote-control car is controlled by voice commands, it decreases up to 44% in a noisy room (Leechor et al., 2010).

In the studies of Jiang et al., MFCC and Chirp Z Transform algorithms are used. An average success at 86% is obtained in the study on 120 voice examples with the numbers between 0 and 9 (Jiang et al., 2009).

In their studies, Shearme and Leach develops an application providing the recognition of disjoint words voiced by any speaker. In their experiments, they express each one of words with a value sets obtained with specific intervals of the normalized spectrum and thus realize the recognition process by comparing the values for every one of words. They create a dictionary composed of 32 words and test their applications with 10 speakers. They determine recognition percentages as 90% (Shearme and Leach, 1968).

Chang et al. obtain 90% as the lowest success and 95% as the highest success for a speech recognition system which MFCC is used as feature and whose

education is realized with DTW (Chang et al., 2012).

Nandyala and Kumar realizes DTW algorithm whose education phase is very short compared to HMM, YSA and SVM with dynamic programming and a speaker-dependent Hindi disjoint speech recognition system which MFCCs are used as feature and suggest a success of recognition at 82% (Nandyala and Kumar, 2010).

## 2. Material and Method

While game consoles, computers, smart phones and tablets take place in the revolution of technology, smart and wearable devices are taking the first place today. Wearable devices particularly have an important place for blind and deaf people. Because of them, their life quality is tried to be increased. In this study, a wearable device is developed to make disabled people's usage. Our wearable device (see in Fig.1.) is placed on back of the user. The wearable device we develop is composed of Raspberry Pi, Usb sound card, Microphone, power supply and vibration motor.

Raspberry Pi (Rpi) is developed to improve computer-based education and teach computers to children at schools. It is at the size of a credit card and Linux, Android and Windows can be set up on it. Rpi is defined a mini computer with ARM architecture. Because of its low cost, power consumption and little size, Rpi's popularity has increased recently. You can get footage by connecting it onto TV and connect a keyboard. For example, you can do work you do on desktop computers and play various games working with Word processors and calculation programs by Rpi we call capable little computer (Balasubramanian and Manivannan, 2016).

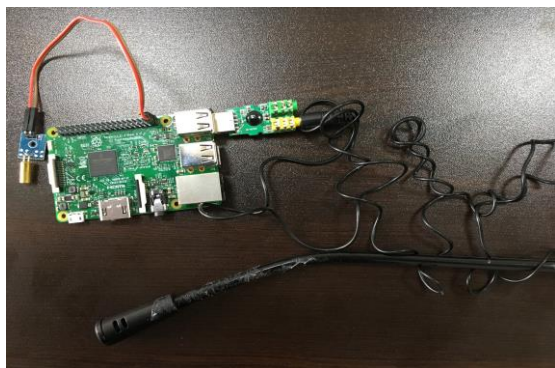


**Figure 1.** Our Wearable Device



**Figure 2.** Raspberry Pi

The Raspberry Pi 3 technical features are:

- 4× ARM Cortex-A53, 1.2GHz CPU
- 1GB RAM
- 10/100 Ethernet, 2.4GHz 802.11n wireless
- Bluetooth 4.1 Classic
- GPIO: 40-pin header
- HDMI, 3.5mm analogue audio-video jack, 4× USB 2.0, Ethernet, Camera Serial Interface (CSI), Display Serial Interface (DSI)

There should be Usb sound cart to connect microphone. Because there is no sound card on Rpi, Usb sound card is used to get sound. Microphone is plugged onto Usb sound card and used to sense sound. Sound is transmitted into Rpi by getting it by microphone. Thus, necessary processes are done for determined sound. As power supply, chargeable battery or usb power supply can be used. In this study, usb power supply is used. Vibration motor is placed on finger of the user. By giving different vibrations for mother and father voice with vibration motor, it is provided that users sense who talks.

The first step of speaker recognition is to obtain voiced expression. For this purpose, microphone or telephone is generally used. Speech signal obtained in this step is analogue. First, analogue signal in continuous time should turn into discrete time. The process of transformation into discrete time is done with sampling. Value of signal is measured at specific time intervals and this obtained value is called sample. If analogue signal has high frequency components, you should do sampling at higher rates not to lose data. Generally, we need sampling as much as double highest frequency not to lose data from analogue signal. This is known as Nyquist ratio. Otherwise, degradation occurs because of aliasing and original signal cannot be obtained

again. In this study, sound is gotten by microphone firstly and sampling is done. According to Nyquist Theorem, 44100 samplings are done per second. A general structure of sound recognition systems is given in Figure 3.



**Figure 3.** Speech Recognition System

### 2.1. Preprocessing

In the step of preprocessing, Statistical or Z-Score normalization is used. The fact that some values on the same data set are below 0 and some are bigger than it suggests that these distances between data and data at the initial or final point would be more effective on results. Because of data normalization, it is provided that every parameter on the input set equally contributes to prediction process of the model. By normalizing data, the distances between them are removed and extreme points on data are decreased (Yağanoğlu et al., 2014).

### 2.2. Feature Extraction

In the step of feature extraction, Mel Frequency Cepstrum Coefficients (MFCC) is used. MFCC features model human ear. Because it is obtained by using filter group, it shows a better success compared to farseeing coefficients in noisy sounds. MFCC is used in both speech recognition and speaker recognition applications and gives successful results. That's why, today's most widely used characteristic is vectors. The method of revealing feature taking human ear's hearing as example is one of the most widely used algorithms giving the highest success. In Figure 4, steps of deriving MFCCs are shown. MFCCs compose features by using mel scale taking human's hearing as model.

Characteristics of speech signals remain stable at a sufficiently little time interval. That's why, sound signals are processed at little time intervals (Schafer and Rabiner, 1975). Researches suggest that characteristics of sound signal remain stable at a sufficiently little time interval. Therefore, sound signals are processed at little time intervals. Signals are divided by frames with length varying from 20 to 100 milliseconds generally. Mostly, the most effective time interval is between 20 and 30 ms

(Atal, 1976). Every frame includes  $N$  speech examples and  $M$  ( $M < N$ ) examples of the previous neighboring frame. So, every frame covers a specific part of the previous frame. The goal of the method of covering is to provide that transition from a frame to another one would be soft

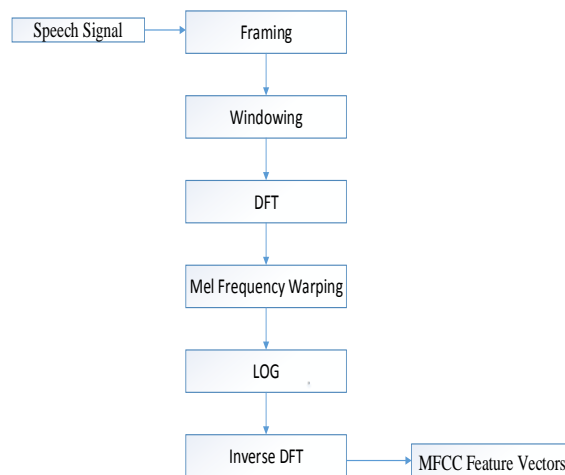


**Figure 4.** MFCC Steps

Windowing is the process done to prevent discontinuity in the beginning and end of every one of frames. Types of windowing are Hamming, Hanning, Rectangular, Barlett, Kaiser Mel Cepstrum Framing Windowing FFT Mel-frequency transform Keprum 9 and Blackman windows. The most widely used structure of window is Hamming. It is used to derive frequency components of windowed signal.

In the step of DFT, Fast Fourier Transform (FFT) is applied to transform every frame with  $N$  samples from the domain of time into of frequency. Methods allowing for rapid calculation of discrete fourier transform are fast fourier transform. Fast fourier transform provides that discrete fourier transform is widely used in signal processing application. Discrete fourier transform of a sign can be calculated the following equation. In that case, there should be  $N$  complicated multiplication and  $N-1$  complicated addition operations for every  $k$  value of the transform.

According to Mel frequency skewness, width of triangle filters changes and therefore daily total energy in a critical band around central frequency is included. Numbers of coefficients are yielded after warp. In the end, inverse DFT is used to calculate cepstral coefficient (Bhattacharyya, 2015).



As the last step of revealing feature, every frame is exposed to inverse fourier transform and the domain of frequency is turned into the domain of time again. As a result of it, Mel-Frequency Cepstral Coefficients are yielded.

### 2.3. Classification

K Nearest Neighbor (Knn) is one of the mostly preferred machine learning and classification methods in different applications. In this preference, the main reason is simplicity of the method. The method of Knn was firstly recommended by Fix and Hodges as the method of nonparametric pattern classification in 1951. In the classification of Knn, the first step is the process of learning. In this process, data in the form of feature vectors is taught to classification system and it is determined what class it belongs to. The next step is testing. In the step of testing, distance metrics of test data to learning data are simply calculated. After calculating distance metrics, results are increasingly listed (Yağanoğlu and Köse, 2017).

Bozkurt et al. used Knn in their study and obtained the classification results with 10-fold cross validation (Bozkurt et al., 2018). In our study, Leave-one-out cross validation was used in order to select the most suitable k value. Knn is a trained learning algorithm and its goal is to classify on the existing learning data when a new sample comes. The algorithm decides class of the example by considering a new sample's nearest k neighbor when it comes. In the algorithm of Knn, k value should be determined firstly. The best k value becomes determined. k = 5 value, having the best rate, is selected. After determining k value, its distance between all learning samples should be calculated. Then, the process of listing with respect to minimum distance is done. After the process of listing, what class value it belongs to is found.

### 3. Results

This study has been tested on 2 deaf and 3 normally hearing people for 30 days. Ears of normally hearing people are covered by loud sound earphones. Our device mounted on backs of the people gives data to deaf person. Thus, deaf person could very comfortably predict parent's voice. While sleeping, our device put with his side warns of the person when he hears parent's voice.

In Figure 5, success rates of deaf and normally hearing people in home environment are seen. While deaf people's rate of prediction of mother's voice is 74% on average, normally hearing people's rate of prediction of mother's voice is 79% on average. While deaf people's rate of prediction of father's voice is 78% on average, normally hearing people's rate of prediction of father's voice is 83% on average. Considering general average, mother's and father's voices are respectively predicted at 76% and 81% in home environment.

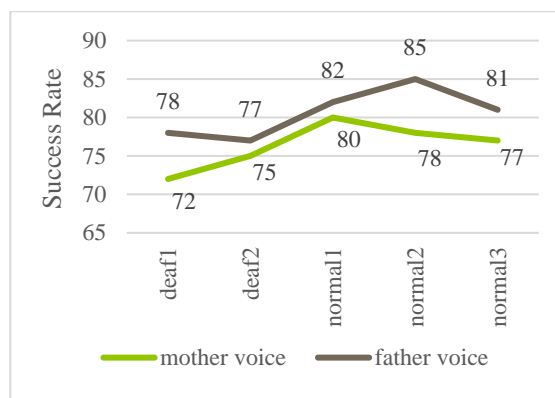


**Figure 5.** Success rates of deaf and normally hearing people in home environment

In Figure 6, success rates of deaf and normally hearing people while sleeping are seen. While deaf people's rate of prediction of mother's voice is 76% on average, normally hearing people's rate of prediction of mother's voice is 80% on average. While deaf people's rate of prediction of father's voice is 79% on average, normally hearing people's rate of prediction of father's voice is 83% on average. Considering general average, mother's and father's voices while sleeping are respectively predicted at 78% and 83%.

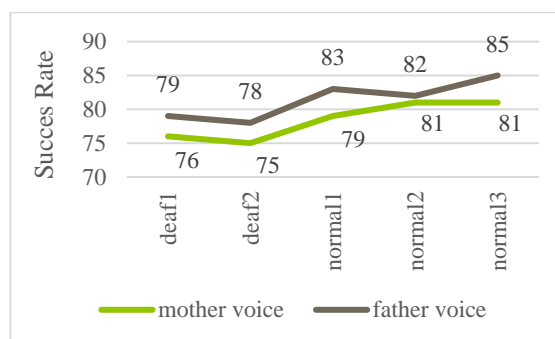


**Figure 6.** Success rates of deaf and normally hearing people while sleeping

Only success rates of deaf people are like in Figure 7. Deaf people respectively predicted mother's voice at 74% and 76% in home environment. While sleeping, they respectively predicted father's voice at 78% and 79%.

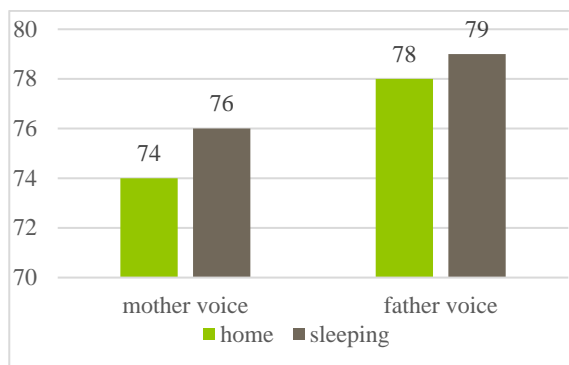


**Figure 7.** Success rates of deaf people

#### 4. Discussion and Conclusions

Telling the device to deaf people and educational process take time. Understandability in telling the device to them and first usages decreased. However, the user could better sense after using the device.

Because of noise in home environment, lower rates of success are obtained. Especially due to such sounds as TV and telephone sounds, success rates become lower. However, success rates increase while sleeping because there is no a lot of noise.

In this study, normalization in the step of pre-processing, MFCC in the step of feature extraction, Knn for classification are used. In the next studies, success rate would be tried to be increased by other methods of revealing feature and classification.

In this study, wearable device is designed to increase life quality of deaf people. Deaf people could sense who talks from parent's voice. Particularly in emergency, deaf people can sense that they are called when somebody calls them or while sleeping.

#### References

Atal, B.S. (1976). Automatic recognition of speakers from their voices, *Proceedings of the IEEE*, vol. 64, pp. 460-475, 1976.

Bhattacharyya, S. (2015). *Handbook of Research on Advanced Hybrid Intelligent Techniques and Applications*, IGI Global.

Babu, C.G., Kumar, R.H., Vanathi, P. (2012). Performance analysis of hybrid robust automatic speech recognition system, in *Signal Processing, Computing and Control (ISPPCC), 2012 IEEE International Conference on*, 2012, pp. 1-4.

Balasubramaniyan, C., Manivannan, D. (2016). IoT Enabled Air Quality Monitoring System (AQMS) using Raspberry Pi, *Indian Journal of Science and Technology*, vol. 9.

Bozkurt, F., Köse, C., Sarı, A. (2018). An inverse approach for automatic segmentation of carotid and vertebral arteries in CTA. *Expert Systems with Applications*, 93, 358-375.

Chang C.-H., Zhou, Z.-H., Lin, S.-H., Wang, J.-C. And Wang J.-F. (2012). Intelligent appliance control using a low-cost embedded speech recognizer, in *Computing and Networking Technology (ICCNT), 2012 8th International Conference on*, 2012, pp. 311-314.

Fezari, M., Bousbia-Salah, M. (2006). A voice command system for autonomous robots guidance," in *Advanced Motion Control, 9th IEEE International Workshop on*, 2006, pp. 261-265.

Jiang, Z., Huang, H., Yang, S., Lu, S., Hao, Z. (2009). Acoustic feature comparison of MFCC and CZT-based cepstrum for speech recognition, in *Natural Computation, 2009. ICNC'09. Fifth International Conference on*, 2009, pp. 55-59.

Leechor, P., Pompanomchai, C., Sukklay, P. (2010). Operation of a radio-controlled car by voice commands, *Mechanical and Electronics Engineering (ICMEE)*, pp. V1-14-V1-17.

Muda, L., Begram, M., Elamvazuthi, I. (2010). Voice recognition algorithms using mel frequency cepstral coefficient (MFCC) and dynamic time warping (DTW) techniques, *Journal of Computing*, Volume 2, Issue 3.

Nandyala, S.P., Kumar D.T.K. (2010). Real Time Isolated Word Speech Recognition System for Human Computer Interaction, *International Journal of Computer Applications*, vol. 12, pp. 1-7.

- Phoophuangpairoj, R. (2011). Using multiple HMM recognizers and the maximum accuracy method to improve voice-controlled robots, Intelligent Signal Processing and Communications Systems (ISPACS), pp. 1-6.
- Schafer, R.W., Rabiner, L.R. (1975). Digital representations of speech signals, Proceedings of the IEEE, vol. 63, pp. 662-677.
- Shearme, J, Leach, P. (1968). Some experiments with a simple word recognition system, IEEE Transactions on Audio and Electroacoustics, vol. 16, pp. 256-261.
- Yağanoğlu, M, Bozkurt, F., Günay, F.B. (2014). Feature Extraction Methods for EEG Based Brain-Computer Interface Systems, Journal of Engineering Sciences and Design, vol. 2, pp. 313-318.
- Yağanoğlu, M., Köse, C. (2017). Wearable Vibration Based Computer Interaction and Communication System for Deaf. Appl. Sci. 2017, 7, 1296.



## Investigation in Electrical and Thermal Efficiency of an Active Cooling Photovoltaic Thermal (Pv/T) Solar System with Taguchi Method

Gökhan Ömeroğlu<sup>1\*</sup>

**Abstract:** In this study, an attempt was made to optimize the default parameters in various experiments to improve the performance and heat transfer properties of the flat plate solar collector using the Taguchi method. An experimental investigation was carried out using air as working fluid at certain speeds (3.3, 3.9 & 4.5 m/s) on a PV/T collector. In this study, experiments were conducted to investigate the effects of heat transfer characteristics on performance, and the results are evaluated, since the above parameters have a great effect on the performance and heat transfer properties of the flat plate solar collector. Test Design for experiments were the Taguchi L36 Orthogonal Array Design. Experiments were carried out using the results of the outlet temperature of the air, the electrical and thermal efficiency of the collector, and the design of experiments by Taguchi method. The Verification results showed a significant improvement in the performance characteristics of the flat plate solar collector. The obtained results were analyzed in the ANSYS fluent program.

**Keywords:** PV/T, Taguchi Method, ANSYS fluent, Solar system, Electrical and Thermal efficiency

### 1. Introduction

Solar energy is a very important source of renewable energy with minimal environmental impact. Nowadays, solar energy is used for heat, electricity and so on. The conversion into useful form is the most important condition of this age. The daily solar flux on the Earth's surface provides more energy than that required by all people. In order to use solar energy efficiently, it is necessary to replace conventional energy conversion methods. Increasing the heat transfer by increasing the surface is one of the most commonly used methods. Fins are used in these methods through which the base heat transfer surface is increased.

The beneficial effects of turbulators on heat transfer were first investigated in 1921 by Royds (Royds). Eimsa-Ard et al., (2009) developed empirical relationships by experimentally examining the effects of propeller-type turbulators

in different numbers and manufactured at different angles on heat transfer, pressure loss and efficiency. In another study, Kim et al. (2007) developed an advanced nanotechnology, which is able to provide an effective platform in the field of heat transfer. In heat transfer applications, the nano-liquid is used as a heat transfer medium to absorb more heat than base air. Bulck (1991) reviewed the optimum design parameters for the cross flow heat exchanger. Vollara et al. (1999) investigated the optimum design for vertical position turbulators in the form of a rectangle. Bonjour et al. (2004) investigated the optimization in a coaxial heat exchanger where crystal-shaped fins were used as rotation generators. Yakut et al., (2005) investigated the effects of design parameters on heat transfer and pressure loss using the Taguchi Method. The suspended nanoparticles enhance the thermal, physical, radiative and transport properties of the base air. Due to the improved properties, better heat transfer

<sup>1</sup>Ataturk University, Engineering Faculty, 25240, Erzurum, Turkey.

\* Corresponding author: [gomeroglu@atauni.edu.tr](mailto:gomeroglu@atauni.edu.tr)

Citation: Omeroglu, G. (2018). Investigation in Electrical And Thermal Efficiency of an Active Cooling Photovoltaic Thermal (Pv/T) Solar System with Taguchi Method. *Bilge International Journal of Science and Technology Research*, 2 (1): 47-55.

characteristics are obtained in the flat plate solar collector. Asiltürk and Akkuş, (2011) experimentally investigated the effects of increasing thermal conductivity in nano-liquids. Qi et al. (2007) investigated the effect of selected parameters on the performance of a heat exchanger using louver fins with the Taguchi approach. Numerous researches have been made in the literature by Taguchi experimental design method (Sahin and Demir, 2008; Sahin et al., 2005). As to what another study reports, air mass is a critical factor affecting the amount of energy absorbed on the ground surface. It has been depending on the presence of particulate matter in the atmosphere and the length of the path through which the sunlight travels in the atmosphere, the AM0 (Air Mass Zero) radiation level -just above the atmosphere- falls from 1367 to 1000W/m<sup>2</sup> corresponding to AM1 at sea level, and AM1.5 is the standard test conditions (Virtuani et al., 2006).

**2. Material and Method**

The objective for using Taguchi method in this study is to obtain minimum number of experiments in investigating the effects of parameters, such as material, the number of fins, the velocity of air flow, the humidity, the fin arrangement and radiation level on thermal and electrical yields. The optimal input parameter combination was determined using the Taguchi method. The Taguchi method (de Lieto Vollaro et al., 1999) is an experimental design technique used to considerably reduce the number of experiments using appropriate orthogonal arrays. Using Taguchi experimental design method, optimum values of design parameters in different systems, such as radiation, different materials, and different humidity values have been tried to be determined.

The thermal and electrical efficiencies obtained for all given test cases are compared with the baseline data obtained with the empty channel. Local and average thermal and electrical efficiencies are presented and total heat transfer improvement is investigated. The aim is to reduce the experimenting time and cost and obtain higher Signal to Noise (S/N) ratios and to reduce the noise factors and consequently increase the signal value. The standard deviation also decreases The purpose of this experiment is; to identify and measure the parameters with the greatest potential to improve the electrical and thermal efficiencies and performance characteristics of the system as well as to optimize selected design and operating

parameters by modifying experimental variable parameters such as the actual transfer and speed.

Taguchi's Experimental Design (DOE) was conducted to determine the improved heat transfer properties of the airflows and the airflow that maximized performance of the photovoltaic solar panel, and to test 36 combinations of airborne species and materials.

Choosing an Orthogonal Array: An Orthogonal Array (OA) is a fractional factorial matrix that allows a balanced comparison of the interaction levels of any factor or factors. This is a matrix of numbers arranged in rows and columns, each row representing the level of the factors, and each column representing a specific factor that can be changed in each run. This sequence is called orthogonal because all columns can be evaluated independently of each other. OA has many design parameters at the same time. In this experimental study, parameters having three and two levels of control factor require 6 degrees of freedom. Mathematically:

$$L_{36} = 3^4 \cdot 2^2$$

The L36 can occupy three three-level parameters. Table 1 shows the design values of the L36 orthogonal array.

**Table 1.** Independent variables and levels.

Parameters		Levels	
Material (A)	Al	Cu	
Number of Fins (B)	54	108	
Irradiation (C)	900 W/m <sup>2</sup>	1100 W/m <sup>2</sup>	1350 W/m <sup>2</sup>
Arrangement (D)	In-Line	Shifted Type 1	Shifted Type 2
Air Velocity (E)	3.3 m/s	3.9 m/s	4.5 m/s
Humidity (F)	7.5	8	9.4

**Parameter selection:** When selecting the parameters, 6 basic operating parameters such as air velocity, radiation, humidity ratio, fin arrangement, material types, number of fins and incident solar radiation are selected. It is assumed that these parameters have a significant effect on the performance characteristics and they were tested using photovoltaic solar. In the Taguchi design experiment, two levels are considered for materials and the number of fins, and three levels for back channel parameters. The physical

properties of the base air, the heat transfer properties, and the fins for the turbulence formation. It is estimated that the collector performance depends on the solar irradiation.

For this reason, the Reynolds number, the number of fins and the incident solar power were chosen as the affected features. In the engineering system, manipulated production and performance factors behave in three categories: (Asiltürk, Akkuş, 2011).

- Control factors affecting the process variability measured by the S/N ratio.
- Signal factors affecting the S/N ratio or average of the process
- Factors affecting the S/N ratio or the average of the transactions

S/N ratio properties can be divided into three categories given by the following three equations when the properties are continuous (Shetty, Pai, Rao, Nayak, 2009).

- Nominal is the best feature;

$$\frac{S}{N} = 10 \log \frac{\bar{y}}{s_y^2} \quad (1)$$

- Smaller feature is better;

$$\frac{S}{N} = -10 \log \frac{1}{n} (\sum Y^2) \quad (2)$$

- Greater feature is better;

$$\frac{S}{N} = -10 \log \frac{1}{n} (\sum \frac{1}{Y^2}) \quad (3)$$

Here,  $\bar{Y}$  is the average of the observed data, ( $S_{Y^2}$ ); ( $Y$ ) is variation,  $n$  is the number of experimental observations. In Taguchi method, some factors rise or fall is good or bad. For example, the thinning of the boundary layer and the decrease in heat transfer coefficient slapping, causing an increase in heat transfer and this is good I mean S-N, S or older I prefer to be low. How good is the result when considering it? In this experiment, better characteristics are taken into consideration, since reactions in parameters such as outlet temperature, collector efficiency and heat transfer rate must be higher. The experiments were carried out based on the design values obtained from the L36 vertical alignment. Mean fluid velocity, inlet air temperature and solar radiation source has a constant value in all experiments. Experiments were validated and verified by carrying out multiple repetitions. If the deviation of the experimental reading measured for a given air velocity is lower than the specified limits during the constant temperature time, it is assumed that the collector is operating under

steady state conditions. The air velocity is between 3.3, 3.9 and 4.5m/s and the irradiation level is around 900, 1100 and 1350 W per square meter of photovoltaic surface area.

The flat plate photovoltaic is tested against Reynolds number. The block diagram of the flat plate solar collector is shown in Figure 2. Once the steady-state condition is satisfied, the data averages are taken for each test period and the Taguchi method is used for optimization.

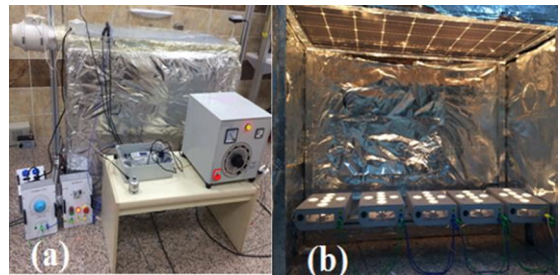


**Figure 1.** Solar flat photovoltaic plate collector test setup

A test setup was designed to investigate the thermal and electrical performance of the PV/T air system. This system was built in the engineering faculty laboratory at Ataturk University in Erzurum. A schematic diagram of the whole experimental setup is shown in detail in Figure 1. This experimental study was designed to investigate how temperature affects the efficiency and power output of a PV panel during operation and by using various fin numbers and arrangements.

The amount of radiation was tried to be kept constant at 900, 1100 and 1350 W/m<sup>2</sup> by using light bulbs during experiments. This radiation intensity cannot be measured by direct solar radiation on earth. However, this, or even higher intensities are possible in condensed (lens, mirror etc.) photovoltaic systems.

### 3. Mathematical Formulation

The law of conservation of mass (also referred to as the first law), the most basic law of thermodynamics, applies to all thermodynamic calculations. Before performing the thermodynamic analysis of the photovoltaic thermal (PV/T) system, which is the subject of this study, it should be noted that the system is a control volume with continuous flow (an open

system). A control volume is the general name for systems with a mass flow through their boundaries. The mass transfer from any system to the control volume or from the control volume to the system in a  $\Delta t$  time interval is equal to the change of mass in the control volume at that time interval.

$$\dot{m}_{inlet} - \dot{m}_{outlet} = \Delta \dot{m}_{cv} \quad [\text{kg/s}] \quad (4)$$

The energy equation for a continuous flow system is:.

**Table 2.** L36 orthogonal array design and thermal & electrical signal noise values

Ex No	Material	Number of fins	Irradiation	Fin arrangement	Air Velocity	Humidity	$\eta$ Thermal	S/N1	$\eta$ Electrical	S/N2
1	1	1	1	1	1	1	49	33.8039216	11	20.8318
2	1	1	2	2	2	2	52	34.32006687	11.05	20.879
3	1	1	3	3	3	3	56	34.96376054	11.12	20.96464
4	1	1	1	1	1	1	49	*	11.01	*
5	1	1	2	2	2	2	52	*	11.08	*
6	1	1	3	3	3	3	56	*	11.23	*
7	1	1	1	1	2	3	50	33.97940009	11	20.82785
8	1	1	2	2	3	1	53	34.48551739	11.03	20.85151
9	1	1	3	3	1	2	50	33.97940009	11.01	20.83575
10	1	2	1	1	3	2	68	36.65017825	11.8	21.43764
11	1	2	2	2	1	3	58	35.26855987	11.3	21.06157
12	1	2	3	3	2	1	65	36.25826713	11.73	21.38596
13	1	2	1	2	3	1	69	36.77698181	11.88	21.49633
14	1	2	2	3	1	2	57	35.11749711	11.28	21.04618
15	1	2	3	1	2	3	63	35.98681099	11.56	21.25916
16	1	2	1	2	3	2	67.5	36.58607546	11.6	21.28916
17	1	2	2	3	1	3	69.6	36.85218479	11.9	21.51094
18	1	2	3	1	2	1	63.2	36.01434157	11.58	21.27417
19	2	1	1	2	1	3	52	34.32006687	11.03	20.85151
20	2	1	2	3	2	1	56	34.96376054	11.09	20.89863
21	2	1	3	1	3	2	57	35.11749711	11.1	20.90646
22	2	1	1	2	2	3	55	34.80725379	11.08	20.8908
23	2	1	2	3	3	1	60	35.56302501	11.2	20.98436
24	2	1	3	1	1	2	52	34.32006687	11.02	20.84363
25	2	1	1	3	2	1	56	34.96376054	11.07	20.88295
26	2	1	2	1	3	2	57	35.11749711	11.25	21.02305
27	2	1	3	2	1	3	52	34.32006687	11.02	20.84363
28	2	2	1	3	2	2	69.5	36.83969609	11.9	21.51094
29	2	2	2	1	3	3	71.3	37.0617906	11.95	21.54736

30	2	2	3	2	1	1	65	36.25826713	11.89	21.50364
<b>31</b>	<b>2</b>	<b>2</b>	<b>1</b>	<b>3</b>	<b>3</b>	<b>3</b>	<b>74</b>	<b>37.38463439</b>	<b>12</b>	<b>21.58362</b>
32	2	2	2	1	1	1	63.6	36.06914231	11.45	21.17611
33	2	2	3	2	2	2	68.4	36.70112203	11.5	21.21396
34	2	2	1	3	1	2	66.3	36.43027057	11.87	21.48901
35	2	2	2	1	2	3	67.4	36.57319793	11.9	21.51094
36	2	2	3	2	3	1	71	37.02516697	11.95	21.54736

$$\dot{Q}_U = \dot{m} \cdot c_p (T_{inlet} - T_{outlet}) \quad [\text{kW}] \quad (5)$$

The total solar power from the sun is the sum of the thermal power gain and the electrical power production ( $\dot{Q}_e = I \cdot V$ ) and is given as below:

$$\dot{Q}_{gain} = \dot{m} [c_p (T_{inlet} - T_{outlet})] + I \cdot V [\text{kW}] \quad (6)$$

and the first-law efficiency is:

$$\eta_U = \frac{\dot{Q}_u + \dot{Q}_e - W_{fan}}{\dot{Q}_{solar}} = \frac{\dot{Q}_{gain} - W_{fan}}{\dot{Q}_{solar}} \quad (7)$$

When there is a flow in the system, regarding the calculations, it is important to determine whether the flow is compressible or incompressible. Where is concluded to be the Newtonian flow.

$$Q = h \cdot A_{pv} \cdot (\Delta T_{air} - T_{pv}) \quad [\text{kW}] \quad (8)$$

Using Equation 6, with the help of the energy the air has gained within the designed control volume, the total heat transfer coefficient for the system can be calculated.

Against each Reynolds value for the air acting as the refrigerant in the system, a different thermal and electrical efficiency will correspond.

The finned part of the test system, which is placed in the control volume in the test setup and ensured to fully contact with the panel, is the most important part of the system. In the control volume, two different arrangement configurations, a frequent arrangement with 54 pcs and 108 pcs and a sparse arrangement with 54 and 108 pcs, were used for both aluminum and copper cylindrical fins. In order to investigate the effects of the fins on the heat transfer rate, a baseline data has also been acquired with no fins installed in the control volume. Experiments were carried out

using artificial solar radiation on a mono crystalline photovoltaic panel and measurements were taken.

**Table 3.** Parts of the experimental setup

Test Section	Control Section
1 Air Outlet	10 Pyranometer
2 Fan	11 Data Logger
3 Temperature Humidity Transmitter	12 Computer
4 Input Velocity Anemometer	13 DC-AC Inverter
5 Photovoltaic Panel	14 Acidic Gel Battery
6 Thermocouple	15 Solar Charger Regulator
7 Control Volume	16 Air Inlet
8 Photovoltaic Power Transmission	17 Cooling Fins
9 Artificial Solar Radiation	

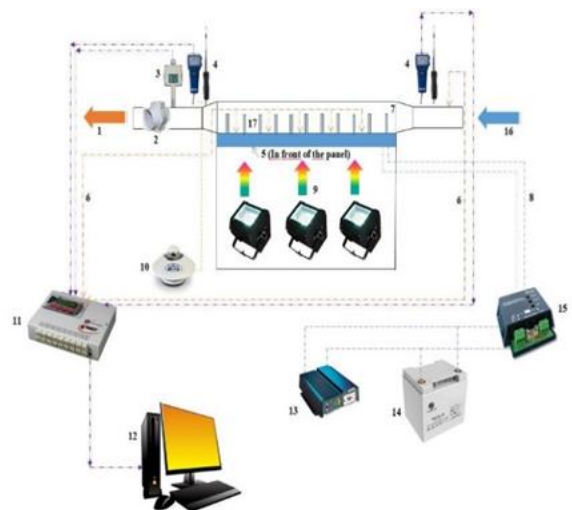


**Figure 2.** Experimental schematic setup



**Figure 3.** The control volume for the experimental setup

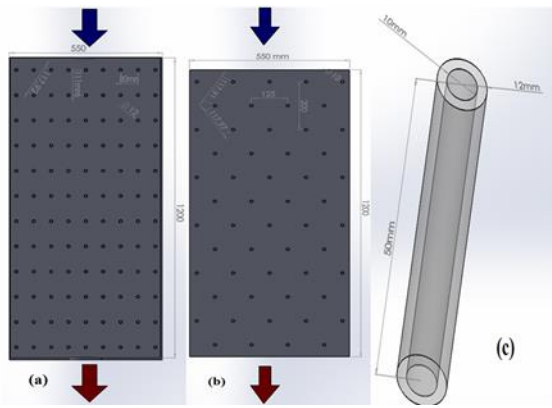


**Figure 4.** Fin numbers and arrangements a) 108 pcs in-line b) 54 pcs shifted c) fin geometry

**4. Results and Discussion**

Experimental studies were carried out according to the Taguchi design. The boundary conditions of each experiment were constant and the obtained data were analyzed using Taguchi analysis. The signal-to-noise ratio is an important part of the experimental data when analyzed by the Taguchi method. According to the Taguchi method, the maximum (S/N) ratio is required to obtain optimum heat transfer properties.

The level values of the factors obtained according to Taguchi design for thermal and electrical efficiency are given in Table 3 and Table 4. Better characteristics are selected and the thermal and electrical efficiency of the input parameters in Fig. 5. Therefore, interpretations can be made based on the level values of the factors A, B, C, D, E and F given in Table 3, Table 4 and in Fig. 4, when the optimum heat transfer parameters of the experiments to be performed under the same conditions are determined. Different values of the ratios (S/N) between maximum and minimum (main effect) are shown in Table 3 and Table 4.

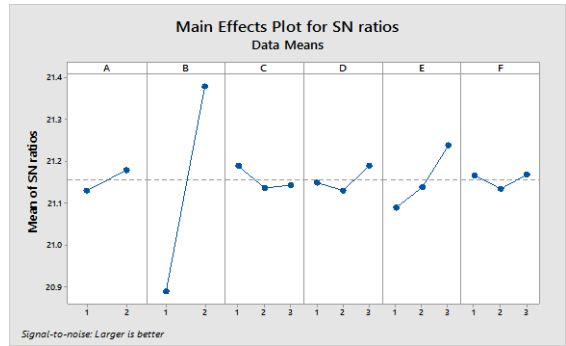


**Figure 5.** Mean S/N Ratios Versus Factor Levels for Electrical Efficiency

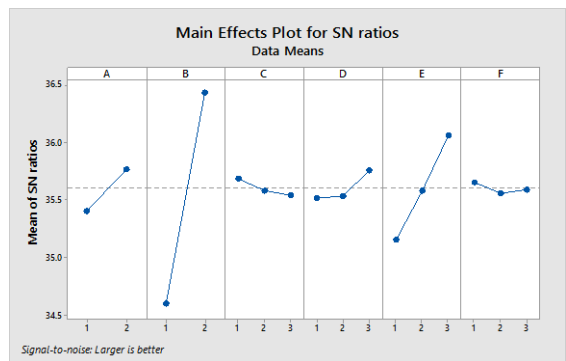


**Figure 6.** Mean S/N Ratios Versus Factor Levels for Thermal Efficiency

**Table 4.** Taguchi Analysis for Thermal Efficiency (Impact Rate)

Level	A	B	C	D	E	F
1	35,4	34,6	35,69	35,52	35,16	35,65
2	35,77	36,44	35,58	35,53	35,58	35,56
3	35,54	35,76	36,07	35,59	36,07	35,5
Delta	0,37	1,83	0,15	0,24	0,91	0,09
Rank	3	1	5	4	2	6

**Table 5.** Taguchi Analysis for Electrical Efficiency (Impact Rate)

Level	A	B	C	D	E	F
1	21,13	20,89	21,19	21,15	21,09	21,17
2	21,18	21,38	21,14	21,13	21,14	21,13
3	21,14	21,19	21,24	21,17	21,24	21,17
Delta	0,05	0,49	0,05	0,06	0,15	0,03
Rank	5	1	4	3	2	6



**Table 6.** Statistical studies prepared in Minitab program.

Sample	N	Mean	StDev	SE Mean	95% CI for $\mu$
C1	200	0,7424	0,0589	0,0525	(0,6395; 0,8452)

$\mu$ : mean of C1

The error analysis was performed for Exp. No: 31 which gives the best results. This analysis was conducted at a 95% confidence level. As a result of the analysis, the error rate is calculated to be 16% approx. The analysis of the wear test results was carried out using the "Biggest-Best" calculation method. As can be seen from Table 3, Table 4, Fig. 4 and Fig. 5, the arrangement of the fins and the material are considered to be the most influential factors in the experiments.

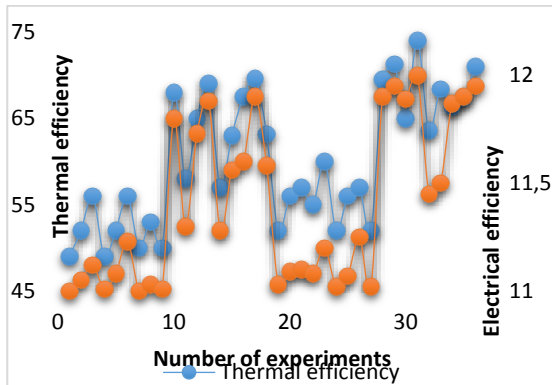
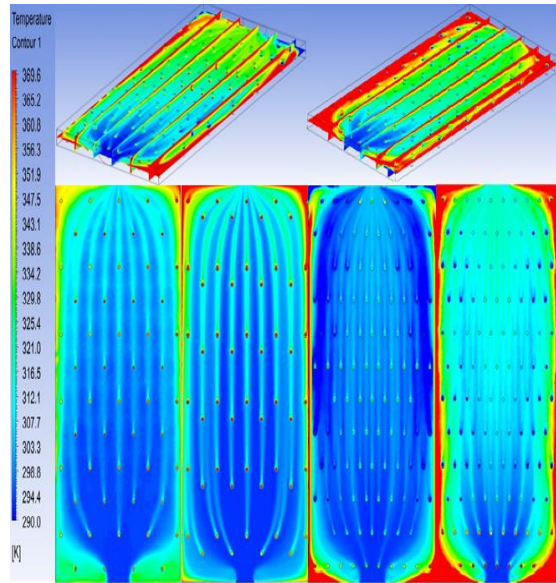
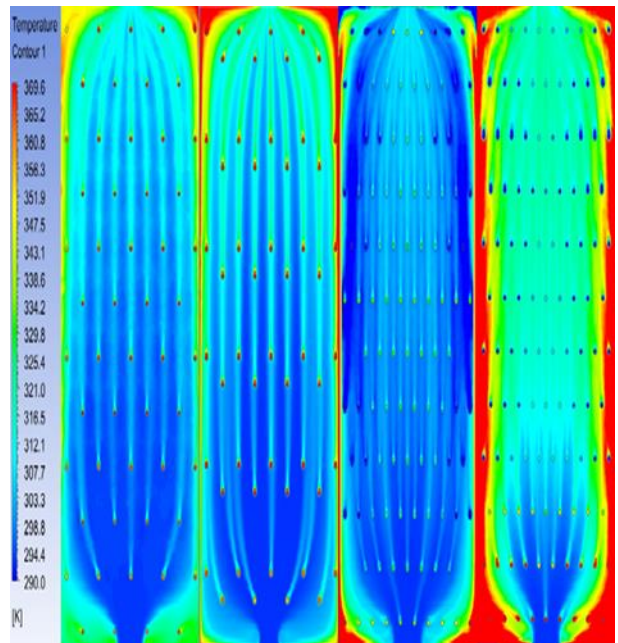


**Figure 7.** Electrical and Thermal Efficiency versus each Experiment of Taguchi



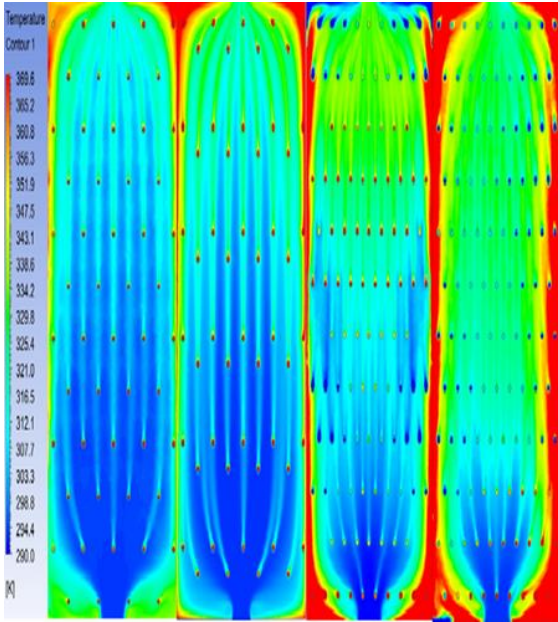
(54 Type-1) (54 Type-2) (108 Type-1) (108 Type-2)

**Figure 8.** Temperature contours for copper 108 pcs type 1&2 and 54 pcs type 1&2, at 4.5m/s



(54 Type-1) (54 Type-2) (108 Type-1) (108 Type-2)

**Figure 9.** Temperature contours for copper 108 pcs type 1&2 and 54 pcs type 1&2, at 3.9m/s



(54 Type-1) (54 Type-2) (108 Type-1) (108 Type-2)

**Figure 10.** Temperature contours for copper 108 pcs type 1&2 and 54 pcs type 1&2, at 3.3m/s

**5. Conclusion**

The Taguchi experimental design was used to obtain optimum heat transfer properties of the flat plate solar collector. Experiments were carried out using air as the heat transfer medium. Test results were analyzed using ANOVA and obtained results are given below.

Using the Taguchi method, the L36 vertical array has four different performance levels: air velocity, number of fins, fins material and incident solar radiation. instead of carrying out the full factorial number of experiments, only 36 experiments were carried out. (S/N) ratio was found to be the main influent factor. Variance analysis was applied to obtain the rates (S/N) to discover the interactions between the factors related to electrical and thermal efficiency and heat transfer rate. An attempt was made to reckon the best combination of variable values.

The results are as given below:

1. The most effective factor on thermal efficiency was found to be the Number of Fins (B), while the next most prominent being Air Velocity (E). The importance ratings were found to be Material (A),

Arrangement (D), Radiation (C) and Humidity (F) respectively.

2. The most effective factor on electrical efficiency was found to be the Number of Fins (B), while the next most prominent being Air Velocity (E). The importance ratings were found to be Arrangement (D), Radiation (C), Material (A) and Humidity (F) respectively.

3. According to applied Taguchi method, for the optimal resulting value; 2 values for Material (A), 2 values for Number of Fins (B), 1 value for Radiation (C), 3 values for Arrangement (D), 3 values for Air Velocity (E), 3 values or 1 value for Humidity (F) have been found to be optimal values. As a result; Material (Cu), Number of Fins (108), Radiation (900 w), Arrangement (Shifted Type 2), Air Velocity (4.5 m/s) and Humidity (7.5 or 9.4) were chosen to be optimal values for variable system parameters.

4. Prior to this study, the most important parameter to be most effective on these experiments was assumed to be the material. But it turned out that the most important parameter for the study is the number of fins.

5. While the number of experiments to be carried out with 2 variable 2 parameters and 3 variable 4 parameters is 324, thanks to the implementation of Taguchi method, the problem could be solved in 36 experiments and it provides equipment savings.

**Acknowledgement**

I would like to thank Atatürk University Engineering Faculty Mechanical Engineering laboratory staff for the time being.

**Nomenclature:**

$A_{pv}$	Aperture area of PV module ( $m^2$ )
$C$	Velocity of sound (m/s)
$c_p$	Specific heat capacity (J/kg K)
$\dot{Q}_e$	Electrical power production(W)
$\dot{Q}_u$	Usable thermal power (W)
$\dot{Q}_{solar}$	Solar radiation ( $W/m^2$ )
$\Delta\dot{m}_{cv}$	Difference of mass in control volume (kg/s)
$\dot{m}_{inlet}$	Inlet mass of air (kg/s)
$\dot{m}_{outlet}$	Outlet mass of air (kg/s)
$I$	Direct current (Ampere)
$h$	Heat transfer coefficient in air duct



	$(W/m^2 K)$
$T_{pv}$	Surface temperature of PV module(K)
$T_{inlet}$	Inlet air temperature ( $^{\circ}C$ )
$T_{outlet}$	Outlet air temperature ( $^{\circ}C$ )
$v$	Velocity of air (m/s)
$w_{fan}$	Work of fan (W)
$V$	Voltage (Volt)
$\dot{Q}_{gain}$	Gained total power (W)
$k$	Heat transfer coefficient for conduction (W/m K)
$Y$	Average of observed data
$n$	the number of experimental
$S_Y^2$	variation of Y,

## References

- Asiltürk, I., Akkuş, H. (2011). Determining the effect of cutting parameters on surface roughness in hard turning using the Taguchi method. *Measurement*, 44(9), 1697-1704.
- Bonjour, J., Rocha, L., Bejan, A., Meunier, F. (2004). Dendritic fins optimization for a coaxial two-stream heat exchanger. *International Journal of Heat and Mass Transfer*, 47(1), 111-124.
- De Lieto Vollaro, A., Grignaffini, S., Gugliemetti, F. (1999). Optimum design of vertical rectangular fin arrays. *International Journal of Thermal Sciences*, 38(6), 525-529.
- Eiamsa-Ard, S., Rattanawong, S., Promvong, P. (2009). Turbulent convection in round tube equipped with propeller type swirl generators. *International Communications in Heat and Mass Transfer*, 36(4), 357-364.
- Kim, S. H., Choi, S. R., Kim, D. (2007). Thermal conductivity of metal-oxide nanofluids: particle size dependence and effect of laser irradiation. *Journal of Heat Transfer*, 129(3), 298-307.
- Qi, Z.-g., Chen, J.-p., Chen, Z.-j. (2007). Parametric study on the performance of a heat exchanger with corrugated louvered fins. *Applied Thermal Engineering*, 27(2), 539-544.
- Royds, R. *Heat Transmission by Radiation, Conduction and Convection*. First Edition Company, 191-201.
- Sahin, B., Demir, A. (2008). Thermal performance analysis and optimum design parameters of heat exchanger having perforated pin fins. *Energy Conversion and Management*, 49(6), 1684-1695.
- Sahin, B., Yakut, K., Kotcioglu, I., Celik, C. (2005). Optimum design parameters of a heat exchanger. *Applied Energy*, 82(1), 90-106.
- Shetty, R., Pai, R. B., Rao, S. S., Nayak, R. (2009). Taguchi's technique in machining of metal matrix composites. *Journal of the Brazilian Society of Mechanical Sciences and Engineering*, 31(1), 12-20.
- Van den Bulck, E. (1991). Optimal design of crossflow heat exchangers. *Journal of Heat Transfer*, 113(2), 341-347.
- Virtuani, A., Lotter, E., Powalla, M. (2006). Influence of the light source on the low-irradiance performance of Cu (In, Ga) Se 2 solar cells. *Solar energy materials and solar cells*, 90(14), 2141-2149.

## Experimental (FT-IR, Raman and NMR) and Theoretical (B3LYP, B3PW91, M06-2X and CAM-B3LYP) Analyses of P-Tert-Butylphenyl Salicylate

Nuri Öztürk<sup>1\*</sup>, Tuba Özdemir<sup>2</sup>, Yelda Bingöl Alpaslan<sup>3</sup>, Halil Gökçe<sup>4</sup>, Gökhan Alpaslan<sup>4</sup>

**Abstract:** The spectroscopic investigations of p-tert-butylphenyl salicylate (C<sub>17</sub>H<sub>18</sub>O<sub>3</sub>) molecule were performed using <sup>13</sup>C and <sup>1</sup>H NMR chemical shifts, FT-IR and Raman spectroscopies. Molecular geometric optimizations, vibrational frequencies, Carbon-13 and Proton NMR chemical shifts (in vacuum and chloroform), HOMO-LUMO properties, natural bond orbital (NBO) analysis, nonlinear optical properties and thermodynamic parameters of p-tert-butylphenyl salicylate molecule was studied using B3LYP, B3PW91, M06-2X and CAM-B3LYP functionals in DFT method at the 6-311++G(d,p) basis set. NBO analysis was carried out to investigate the intramolecular hydrogen bonding (O-H...O) in the title molecule. Some of the molecular properties such as ionization potential (*I*), electron affinity (*A*), chemical hardness (*η*), chemical softness (*ζ*), electronegativity (*χ*), chemical potential (*μ*) and electrophilicity index (*ω*) parameters were determined via HOMO and LUMO energies of the title molecule. Also, quantum chemical computations were performed to determine the dipole moment (*μ<sub>total</sub>*), mean polarizability (*α*), anisotropy of the polarizability (*Δα*) and first hyperpolarizability (*β<sub>0</sub>*) values. Thermochemical properties of the title molecule were investigated with the aforementioned calculation levels. The recorded experimental spectroscopic results were found to be in good agreement with the computed data.

**Keywords:** P-tert-butylphenyl salicylate, Vibrational spectroscopy, NMR chemical shifts, NLO properties, Thermodynamic properties, HOMO-LUMO analysis.

### 1. Introduction

P-tert-butylphenyl salicylate (TBS) is well-known commercial ultraviolet stabilizer and ultraviolet absorber (UVA). Ultraviolet absorbers (UVA) have been extensively studied due to the importance of protecting polymeric materials from photooxidation (Schmitt and Hirt, 1960; Gottfried and Dutzer, 1961; Newland and Tamblyn, 1964; Dobashi and Ohkatsu, 2008). As a salicylic acid derivative, 4-tert-butylphenyl salicylate (4-TBPS) exhibits anti-inflammatory activity. Choi et al. investigated the anti-inflammatory effects of 4-tert-butylphenyl

salicylate (4-TBPS) (Choi et al., 2016). Salicylic acid derivatives are used for medicinal and cosmetic purposes. They are used as antipyretics, vitamins, antioxidants, NSAIDs, food preservatives, bactericidal agents, antiseptics, etc. (Hutchinson, 2003; Madan and Levitt, 2014). The molecular chemical formula and molecular weight of p-tert-butylphenyl salicylate are C<sub>17</sub>H<sub>18</sub>O<sub>3</sub> and 270.328 g/mol, respectively and its melting point is reported as 65-66 °C (Pubchem, 2017). Kasumov and Köksal studied new bidentate N-(2,5-di-tert-butylphenyl)salicylaldimines that involve X=H, HO, CH<sub>3</sub>O, Br, NO<sub>2</sub>, 3,5-di-Br, 3-NO<sub>2</sub>-5-Br and

<sup>1</sup>Giresun University, Dereli Vocational School, 28950, Giresun, Turkey

<sup>2</sup>Bartın University, Vocational School of Health Services, 74100, Bartın, Turkey

<sup>3</sup>Giresun University, Faculty of Medicine, Department of Biophysics, 28100, Giresun, Turkey

<sup>4</sup>Giresun University, Vocational School of Health Services, 28200, Giresun, Turkey

Corresponding author: \*[nuri.ozturk@giresun.edu.tr](mailto:nuri.ozturk@giresun.edu.tr)

Citation: Öztürk, N., Özdemir, T., Alpaslan, Y.B., Gökçe, H., Alpaslan, G. (2018). Experimental (FT-IR, Raman and NMR) and Theoretical (B3LYP, B3PW91, M06-2X and CAM-B3LYP) Analyses of P-Tert-Butylphenyl Salicylate. Bilge International Journal of Science and Technology Research, 2(1), 56-73.

5,6-benzo substituents on the salicylaldehyde moiety,  $L_xH$ , and their mononuclear bis [N-(2,5-di-tertbutylphenyl) salicylaldiminato] copper (II) complexes,  $Cu(L_x)_2$  using IR, UV-visible,  $^1H$  NMR, ESR spectroscopy, magnetic measurements (Kasumov and Köksal, 2002). Raja et al., investigated the molecular vibrations of 1-Naphthol in polycrystalline sample, at room temperature, using FT-IR and FT-Raman spectroscopy (Raja et al., 2013).

In this study, vibrational frequencies (FT-IR and Raman), NMR chemical shifts, optimized molecular geometric parameters, HOMO-LUMO analyses, NBO analysis, NLO properties and thermodynamic parameters of p-tert-butylphenyl salicylate were investigated both experimentally and theoretically. No detailed work was found on structural, spectral, electronic, nonlinear optical properties and thermodynamic investigations of the title molecule in the literature. The theoretical computations were performed using B3LYP, B3PW91, M06-2X and CAM-B3LYP functionals in DFT method with the 6-311++G(d,p) basis set. As theoretical analyses provide a powerful support for experimental studies, quantum chemical computations have been used by many researchers to determine the structural, spectroscopic, magnetic, electronic, optical and thermodynamic properties of the molecular systems in the literature (Buyukuslu et al., 2010; Ceylan et al., 2016; Kavitha and Velraj, 2016; Öztürk and Gökce, 2017).

## 2. Computational Details

Molecular geometric optimizations, vibrational wavenumbers, Proton and Carbon NMR chemical shifts (in vacuum and chloroform), NBO analysis, NLO properties, HOMO-LUMO analyses and thermodynamic parameters of the title molecule were studied using Gaussian 09W software package (Frisch et al., 2009). The calculated results were visualized via GaussView5.0 program (Dennington et al., 2009).

All quantum chemical computations were performed with B3LYP, B3PW91, M06-2X and CAM-B3LYP functionals in DFT method (Lee et al., 1988; Becke, 1993; Perdew et al., 1996; Yanai et al., 2004) at the 6-311++G(d,p) basis set in the

ground state of the title molecule. The calculated harmonic vibrational wavenumbers were scaled with 0.9671 for B3LYP/6-311++G(d,p) level, 0.9576 for B3PW91/6-311++G(d,p) level, 0.9489 for M06-2X/6-311++G(d,p) level and 0.9665 for CAM-B3LYP/6-311++G(d,p) level (Cruz et al., 2015; Kanagathara et al., 2015; Chase et al., 2016).

Using optimized molecular geometries,  $^1H$  and  $^{13}C$  NMR isotropic chemical shift were computed with aforementioned computational levels using integral equation formalism polarizable continuum model (IEFPCM), solvent model and gauge invariant atomic orbital (GIAO) approach (London, 1937; Ditchfield, 1974; Wolinski et al., 1990). The HOMO and LUMO analyses were performed using aforementioned computational levels. According to HOMO and LUMO energy values, the quantum molecular descriptors such as ionization potential ( $I$ ), electron affinity ( $A$ ), chemical hardness ( $\eta$ ), chemical softness ( $\zeta$ ), electronegativity ( $\chi$ ), chemical potential ( $\mu$ ) and electrophilicity index ( $\omega$ ) parameters were computed. Nonlinear optical (NLO) properties such as dipole moment ( $\mu$ ), mean polarizability ( $\alpha_{total}$ ), anisotropy of the polarizability ( $\Delta\alpha$ ) and first hyperpolarizability ( $\beta_0$ ) were computed with the mentioned computational levels. NBO analysis was performed to investigate the intramolecular hydrogen bonding interaction (O-H...O) in the title compound molecule. Finally, thermodynamic properties (thermal energy (E), heat capacity ( $C_v$ ), entropy (S), zero-point energy, etc.) were calculated at B3LYP, B3PW91, M06-2X and CAM-B3LYP/6-311++G(d,p) levels.

## 3. Results and Discussion

### 3.1. Molecular structure analysis

The optimized molecular structure of p-tert-butylphenyl salicylate was given in Figure 1 with numbering of the atoms. The optimized molecular geometric parameters including bond lengths and angles, as given in Table 1, were calculated using B3LYP, B3PW91, M06-2X and CAM-B3LYP/6-311++G(d,p) theoretical methods.

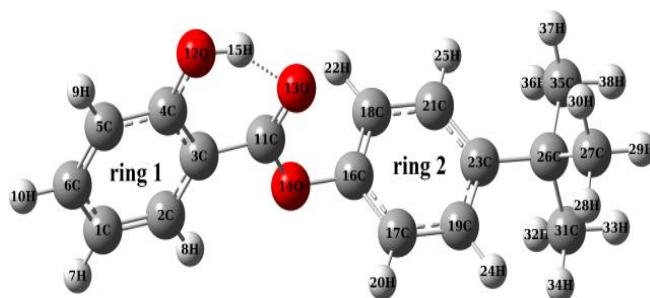


**Figure 1.** The optimized molecular structure with the B3LYP/6-311++G(d,p) level of p-tert-butylphenyl salicylate

**Table 1.** The optimized molecular geometric parameters of p-tert-butylphenyl salicylate.

Bond lengths (Å)	B3LYP	B3PW91	M06-2X	CAM-B3LYP	Bond angles (°)	B3LYP	B3PW91	M06-2X	CAM-B3LYP
C1-C2	1.383	1.381	1.380	1.377	C2-C1-C6	119.3	119.3	119.2	119.2
C1-C6	1.402	1.400	1.399	1.397	C1-C2-C3	121.0	120.9	120.9	120.9
C2-C3	1.407	1.404	1.403	1.401	C2-C3-C4	119.2	119.4	119.5	119.4
C3-C4	1.417	1.415	1.409	1.408	C2-C3-C11	122.0	122.1	121.6	121.8
C3-C11	1.469	1.465	1.473	1.467	C4-C3-C11	118.7	118.5	118.9	118.8
C4-C5	1.402	1.400	1.399	1.397	C3-C4-O12	123.0	122.9	123.5	123.0
C4-O12	1.344	1.337	1.339	1.338	C5-C4-O12	117.7	118.0	117.3	117.7
C5-C6	1.385	1.382	1.381	1.378	C4-C5-C6	120.3	120.2	120.3	120.2
C11-O13	1.221	1.220	1.212	1.215	C1-C6-C5	120.9	121.0	121.0	121.0
C11-O14	1.356	1.350	1.347	1.346	C3-C11-O13	124.3	124.2	124.4	124.2
O14-C16	1.405	1.398	1.395	1.399	C3-C11-O14	113.3	113.4	112.9	113.5
C16-C17	1.388	1.386	1.386	1.382	O13-C11-O14	122.4	122.4	122.8	122.3
C16-C18	1.385	1.383	1.382	1.378	C4-O12-H15	107.9	107.2	108.7	108.2
C17-C19	1.391	1.389	1.388	1.385	C11-O14-C16	119.0	118.7	119.4	118.5
C18-C21	1.395	1.392	1.392	1.390	O14-C16-C17	118.4	118.3	117.2	118.8
C19-C23	1.403	1.401	1.399	1.397	O14-C16-C18	120.7	120.7	121.7	120.1
C21-C23	1.400	1.397	1.396	1.393	C17-C16-C18	120.9	120.9	121.1	121.0
C23-C26	1.539	1.533	1.530	1.532	C16-C17-C19	119.2	119.1	119.1	119.1
C26-C27	1.547	1.540	1.538	1.538	C16-C18-C21	119.2	119.2	119.0	119.2
C26-C31	1.547	1.540	1.538	1.538	C17-C19-C23	121.8	121.8	121.6	121.8
C26-C35	1.540	1.533	1.532	1.532	C18-C21-C23	121.8	121.8	121.7	121.6
O13...H15	1.752	1.720	1.788	1.745	C19-C23-C21	117.2	117.2	117.5	117.4
O12...O13	2.619	2.598	2.635	2.608	C19-C23-C26	119.9	119.9	119.7	119.8
					C21-C23-C26	122.9	122.9	122.9	122.8
					C23-C26-C27	109.4	109.3	109.4	109.4
					C23-C26-C31	109.5	109.4	109.2	109.4
					C23-C26-C35	112.3	112.2	112.1	112.2
					C27-C26-C31	109.4	109.4	109.4	109.4
					C27-C26-C35	108.1	108.2	108.3	108.2
					C31-C26-C35	108.2	108.2	108.3	108.2
					O12- H15...O13	145.3	146.6	143.5	144.9

The calculated molecular geometric parameters were compared with the experimental and theoretical geometric parameters of similar structures in the literature (Bilgram et al., 1982; Hammond et al., 2002; Hanuza et al., 2004). C11-O14 and C11=O13 bond lengths in the salicylate

group of the title compound were computed as 1.356 Å, 1.350 Å, 1.347 Å, 1.346 Å and 1.221 Å, 1.220 Å, 1.212 Å, 1.215 Å respectively, using B3LYP, B3PW91, M06-2X, CAM-B3LYP/6-311++G(d,p) levels. Likewise, the C4-O12 bond length was found as 1.344 Å for B3LYP, 1.337 Å

for B3PW91, 1.339 Å for M06-2X and 1.338 Å. C11-O14, C11=O13 and C4-O12 bond lengths for salol (phenyl salicylate or benzoic acid 2-hydroxyphenylester) molecule were reported as 1.354 Å, 1.215 Å and 1.356 Å with experimental X-Ray analysis by Bilgram et al. (Bilgram et al., 1982), respectively. For salol molecule, Hanuza et al. (Hanuza et al., 2004) calculated C11-O14 bond length as 1.349 Å, C11=O13 bond length as 1.224 Å and C4-O12 bond length as 1.333 Å using MPW1PQ91/6-31G(d,p) level. Similarly, Hammond et al. (Hammond et al., 2002) reported the molecular structure and molecular geometric parameters of salol molecule in meta-stable phase using X-Ray powder diffraction analysis. C3-C11 and C16-O14 bond lengths were respectively found as 1.469 Å, 1.465 Å, 1.473 Å, 1.467 Å and 1.405 Å, 1.398 Å, 1.395 Å, 1.399 Å with the aforementioned computational methods. Experimental values of these bond lengths were reported as 1.464 Å and 1.411 Å, respectively (Bilgram et al., 1982). The C-C bond lengths in ring 1 and ring 2 of the title compound were calculated at the interval of 1.383-1.417 Å and 1.385-1.403 Å for B3LYP, 1.381-1.415 Å and 1.383-1.401 Å for B3PW91, 1.380-1.409 Å and 1.382-1.399 Å for M06-2X and 1.377-1.408 Å and 1.378-1.397 Å for CAM-B3LYP, respectively. The hydrogen bonding parameters for O12-H15, O13...H15, O12...O13 and O12-H15...O13 were computed as 0.982 Å, 1.752 Å, 2.619 Å and 145.3° for B3LYP, 0.983 Å, 1.720 Å, 2.598 Å and 146.6° for B3PW91, 0.974 Å, 1.788 Å, 2.635 Å and 143.5° for M06-2X and 0.979 Å, 1.745 Å, 2.608 Å and 144.9° for CAM-B3LYP. C3-C11-O13, O13-C11-O14, C4-O12-H15 and C11-O14-C16 bond angles were computed as 124.3°, 122.4°, 107.9° and 119.0° for B3LYP, 124.2°, 122.4°, 107.2° and 118.7° for B3PW91, 124.4°, 122.8°, 108.7° and 119.4° for M06-2X and 124.2°, 122.3°, 108.2° and 118.5° for CAM-B3LYP, whereas their experimental values were reported as 125.1°, 121.9°, 105.7° and 117.6°, respectively (Bilgram et al., 1982). C4-C3-C11-O14, C3-C11-O14-C16, C11-O14-C16-C17 and C19-C23-C26-C31 dihedral angle values were calculated as 179.5°, 179.4°, 109.1° and 60.0° for B3LYP, 179.4°, 179.1°, 110.3° and 60.0° for B3PW91, -180.0°, -179.9°, 124.7° and 60.7° for M06-2X and 179.8°, -180.0°, 101.2° and 59.9° for CAM-B3LYP, respectively.

We can see from computed vibrational wavenumbers given in Table 2 that imaginary frequency value is not found at B3LYP, B3PW91 and M06-2X/6-311++G(d,p) levels, whereas one

imaginary frequency value (mode no:  $\nu_1 = -3.2 \text{ cm}^{-1}$ ) is computed at CAM-B3LYP/6-311++G(d,p) level. This situation shows that the minimum energy state in the available conformation was not achieved for CAM-B3LYP/6-311++G(d,p) level. This molecular structure is an unstable conformational form for CAM-B3LYP/6-311++G(d,p) level and it can be a saddle point or transition state or non-minimum energy point over PES of the title compound. The vibrational assignment corresponding to this vibrational mode (mode no:  $\nu_1$ ) in all computational methods is torsional mode ( $\tau_{\text{C}_{11}\text{O}_{14}\text{C}_{16}\text{C}_{17}}$ ) between salicylate group and p-tert-butylphenyl group in the title compound.

### 3.2. Vibrational frequency analysis

P-tert-butylphenyl salicylate molecule has 38 atoms and 108 fundamental vibrational modes. The recorded (AIST, 2017) and calculated vibrational wavenumbers, IR intensities, Raman scattering activities and vibrational assignments were summarized in Table 2. The recorded (AIST, 2017) and calculated IR and Raman spectra of the title molecule were presented in Figures. 2 and 3, respectively. The OH, CH, CC, C-O and C=O vibrational results obtained with experimental and computational methods are in good agreement with the results given in the literature (Nyquist et al., 1996; Kalampounias et al., 2003; Baran and Davydova, 2010). The linear correlation coefficients ( $R^2$ ) between experimental and computed vibrational wavenumbers were also given in Table 2.

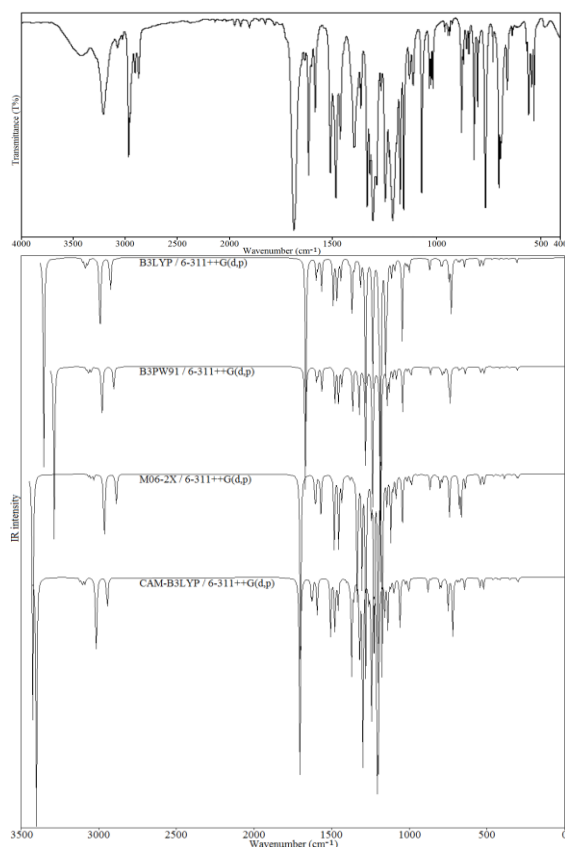


**Figure 2.** The experimental (AIST, 2017) (top) and simulated (bottom) IR spectra of p-tert-butylphenyl salicylate.

The OH vibrations are very sensitive due to effect of hydrogen bonding and the OH stretching modes observe in the region of 2800-3250  $\text{cm}^{-1}$  (Colthup et al., 1964; Bellamy, 1975). Due to O12-H15...O13 intramolecular hydrogen bonding in the title molecule, the OH stretching band was observed at 3207  $\text{cm}^{-1}$  in IR spectrum and 3208  $\text{cm}^{-1}$  in Raman spectrum. This stretching band was computed at 3353.0  $\text{cm}^{-1}$  with B3LYP, 3286.9  $\text{cm}^{-1}$  with B3PW91, 3424.6  $\text{cm}^{-1}$  with M06-2X and 3401.3  $\text{cm}^{-1}$  with CAM-B3LYP. OH in-plane bending modes were observed and computed as mixed with other vibrations in the region of 1200-1600  $\text{cm}^{-1}$ . However, the OH out-of-plane bending mode was obtained as individual bands. The OH out-of-plane bending bands were not observed in IR and Raman spectra of the title molecule. These bands were computed at 728.2 (mode no:  $\nu_{35}$ ) and 775.6 (mode no:  $\nu_{37}$ )  $\text{cm}^{-1}$  with B3LYP, 744.3 (mode no:  $\nu_{36}$ ) and 773.7 (mode no:  $\nu_{37}$ )  $\text{cm}^{-1}$  with B3PW91, 663.9 (mode no:  $\nu_{32}$ ) and 677.2 (mode no:  $\nu_{34}$ )  $\text{cm}^{-1}$  with M06-2X and 727.5 (mode no:  $\nu_{34}$ ) and 791.1 (mode no:  $\nu_{37}$ )  $\text{cm}^{-1}$  with CAM-B3LYP.

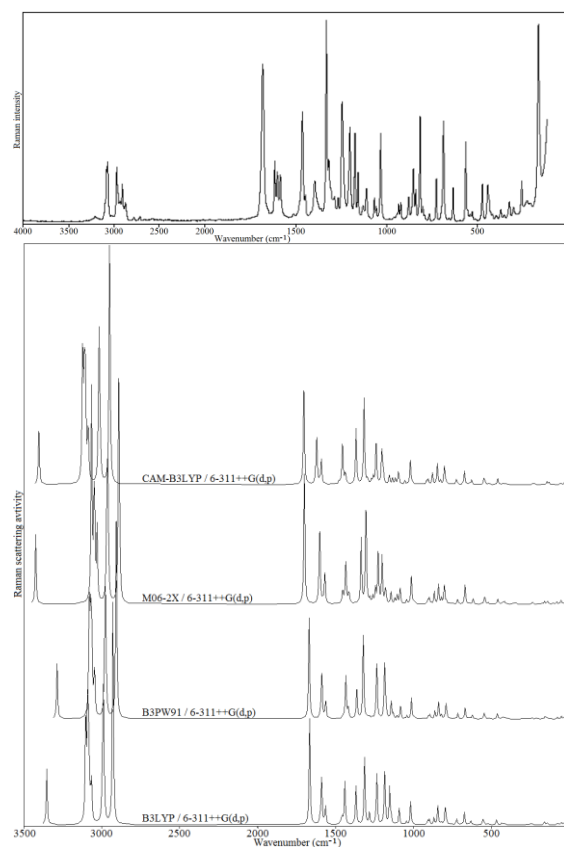


**Figure 3.** The experimental (AIST, 2017) (top) and simulated (bottom) Raman spectra of p-tert-butylphenyl salicylate.

The aromatic CH stretching vibrational modes occur in the region of 3000-3100  $\text{cm}^{-1}$  (Colthup et al., 1964; Bellamy, 1975; Silverstein and Webster, 1998; Stuart, 2004). The bands recorded at 3023, 3068 and 3073  $\text{cm}^{-1}$  in IR and Raman spectra of the title compound can be attributed to the aromatic CH stretching modes. These modes were computed at the interval of 3065.4-3104.3  $\text{cm}^{-1}$  for B3LYP, 3045.2-3081.7  $\text{cm}^{-1}$  for B3PW91, 3029.7-3066.4  $\text{cm}^{-1}$  for M06-2X and 3086.2-3123.6  $\text{cm}^{-1}$  for CAM-B3LYP. Symmetric and asymmetric stretching modes for methyl and methylene groups were observed between 2800  $\text{cm}^{-1}$  and 3000  $\text{cm}^{-1}$  (Colthup et al., 1964; Bellamy, 1975; Silverstein and Webster, 1998; Stuart, 2004). As seen in Table 2, CH<sub>3</sub> symmetric stretching bands were appeared at 2869 and 2900  $\text{cm}^{-1}$  in IR spectrum and at 2872, 2905 and 2932  $\text{cm}^{-1}$  in Raman spectrum and the corresponding calculated scaled frequencies were computed in the regions of 2921.5-2929.3  $\text{cm}^{-1}$ , 2900.6-2907.4  $\text{cm}^{-1}$ , 2883.8-2891.3  $\text{cm}^{-1}$ , 2944.1-2951.2  $\text{cm}^{-1}$  with B3LYP, B3PW91, M06-2X and CAM-B3LYP functionals using 6-311++G(d,p)

basis set, respectively. Similarly, the asymmetric  $\text{CH}_3$  stretching modes were observed at 2969 (IR)-2968 (R)  $\text{cm}^{-1}$  and computed in the region 2981.6-2996.6  $\text{cm}^{-1}$  for B3LYP, 2970.1-2983.8  $\text{cm}^{-1}$  for B3PW91, 2956.4-2969.0  $\text{cm}^{-1}$  for M06-2X and 3008.1-3022.1  $\text{cm}^{-1}$  for CAM-B3LYP. The other vibrational modes (in-plane bending, out-of-plane bending, rocking, scissoring and symmetric bending) of the aromatic and methyl groups in the title compound were summarized in Table 2.

Carbonyl (C=O) groups cause strong C=O stretching absorption bands in the region of 1540-1870  $\text{cm}^{-1}$  in IR and Raman spectra (Silverstein and Webster, 1998). The peak at 1686 (IR)-1681 (R)  $\text{cm}^{-1}$ , observed as a strong band in IR and Raman spectra of the title compound, can be assigned to C=O stretching mode. This mode was calculated at 1665.6  $\text{cm}^{-1}$  for B3LYP, 1669.1  $\text{cm}^{-1}$  for B3PW91, 1699.6  $\text{cm}^{-1}$  for M06-2X and 1709.6  $\text{cm}^{-1}$  for CAM-B3LYP. The C4-O12 stretching mode in phenolic group of the title compound was obtained in mode no:  $\nu_{66}$ ,  $\nu_{68}$  and  $\nu_{69}$  with B3LYP, mode no:  $\nu_{66}$ ,  $\nu_{67}$

and  $\nu_{69}$  with B3PW91, mode no:  $\nu_{66}$ ,  $\nu_{70}$  and  $\nu_{71}$  with M06-2X and mode no:  $\nu_{66}$ ,  $\nu_{70}$  and  $\nu_{71}$  with CAM-B3LYP. Likewise, the C11-O14 stretching mode was observed at 1057  $\text{cm}^{-1}$  in Raman spectrum and it is calculated at 1044.1, 1041.7, 1043.0 and 1066.8  $\text{cm}^{-1}$  with all mentioned computational levels (mode no:  $\nu_{56}$ ). Additionally, C16-O14 stretching mode was found at mode no:  $\nu_{64}$  with B3LYP, mode no:  $\nu_{64}$  with B3PW91, mode no:  $\nu_{65}$  with M06-2X level and mode no:  $\nu_{65}$  with CAM-B3LYP.

The C23-C26 and C3-C11 stretching modes were observed at 1247 (IR)-1243 (R)  $\text{cm}^{-1}$  (mode no:  $\nu_{67}$ ) and 1304 (IR)-1307 (R)  $\text{cm}^{-1}$  (mode no:  $\nu_{71}$ ), respectively and they were computed at 1240.0  $\text{cm}^{-1}$  and 1313.0  $\text{cm}^{-1}$  for B3LYP, 1236.6  $\text{cm}^{-1}$  and 1321.2  $\text{cm}^{-1}$  for B3PW91, 1243.3  $\text{cm}^{-1}$  and 1304.2  $\text{cm}^{-1}$  for M06-2X level and 1267.7  $\text{cm}^{-1}$  and 1326.2  $\text{cm}^{-1}$  for CAM-B3LYP. The vibrations in aromatic groups and other groups of the title molecule were summarized in Table 2.

**Table 2.** The experimental (AIST, 2017) and computed vibrational wavenumbers and their assignments of p-tert-butylphenyl salicylate.

Mode	Assignments	Exp. freq. (cm <sup>-1</sup> )		B3LYP/6-311++G(d,p)			B3PW91/6-311++G(d,p)			M06-2X/6-311++G(d,p)			CAM-B3LYP/6-311++G(d,p)		
		IR	Raman	Freq.	I <sub>IR</sub>	S <sub>Raman</sub>	Freq.	I <sub>IR</sub>	S <sub>Raman</sub>	Freq.	I <sub>IR</sub>	S <sub>Raman</sub>	Freq.	I <sub>IR</sub>	S <sub>Raman</sub>
V <sub>1</sub>	Lattice mode	-	-	10.3	0.30	6.00	9.5	0.30	5.85	13.2	0.44	3.85	-3.2	0.26	6.26
V <sub>2</sub>	Lattice mode	-	-	27.8	0.37	2.05	27.5	0.37	2.07	24.6	0.23	1.28	28.9	0.37	2.09
V <sub>3</sub>	Lattice mode	-	-	37.0	0.47	0.69	37.7	0.47	0.68	39.5	0.37	0.73	34.7	0.51	0.47
V <sub>4</sub>	Lattice mode	-	-	49.3	0.03	2.95	49.5	0.03	3.11	52.1	0.02	3.33	48.1	0.02	1.80
V <sub>5</sub>	Lattice mode	-	-	74.0	0.07	1.82	74.5	0.09	1.97	79.4	0.15	2.09	73.3	0.03	1.33
V <sub>6</sub>	δC <sub>23</sub> C <sub>26</sub> C <sub>27,31,35</sub> +δC <sub>16</sub> O <sub>14</sub> C <sub>11</sub>	-	-	103.2	0.13	0.79	102.0	0.12	0.75	102.0	0.07	0.71	104.5	0.18	0.81
V <sub>7</sub>	τring1+τO <sub>13</sub> C <sub>11</sub> C <sub>3</sub> C <sub>2</sub>	-	-	140.4	0.01	2.33	139.9	0.02	2.29	137.8	0.01	2.81	143.5	0.02	2.28
V <sub>8</sub>	δO <sub>14</sub> C <sub>11</sub> C <sub>3</sub> +δC <sub>16</sub> O <sub>14</sub> C <sub>11</sub>	-	160	156.2	0.81	3.59	154.7	0.79	3.41	157.3	0.80	2.68	157.5	0.73	3.24
V <sub>9</sub>	δC <sub>21</sub> C <sub>23</sub> C <sub>26</sub> +δC <sub>23</sub> C <sub>26</sub> C <sub>35</sub> +δC <sub>17</sub> C <sub>16</sub> O <sub>14</sub>	-	-	196.6	0.02	0.44	193.1	0.02	0.47	194.5	0.07	0.48	201.0	0.01	0.30
V <sub>10</sub>	τCH <sub>3</sub>	-	207	214.1	0.02	0.87	212.0	0.03	0.86	203.5	0.10	0.32	212.0	0.07	0.50
V <sub>11</sub>	τCH <sub>3</sub> +τring1	-	225	239.0	0.32	1.04	237.3	0.27	1.05	233.5	0.37	1.60	240.7	0.40	1.22
V <sub>12</sub>	τCH <sub>3</sub> +τring1	-	-	242.9	0.29	0.87	240.6	0.43	0.81	242.5	0.59	0.61	245.7	0.06	0.97
V <sub>13</sub>	τCH <sub>3</sub>	-	255	267.7	0.28	0.04	266.6	0.27	0.04	263.7	0.35	0.05	266.9	0.18	0.06
V <sub>14</sub>	τCH <sub>3</sub> +δC <sub>11</sub> C <sub>3</sub> C <sub>4</sub>	-	302	304.2	7.20	0.09	301.8	7.56	0.29	296.4	5.07	0.84	307.1	6.13	0.36
V <sub>15</sub>	δC <sub>27</sub> C <sub>26</sub> C <sub>31</sub> +τCH <sub>3</sub>	-	-	306.4	1.07	0.88	302.4	3.09	0.89	305.1	5.19	0.51	313.6	4.96	0.53
V <sub>16</sub>	τCH <sub>3</sub>	-	323	308.6	3.05	0.29	306.9	0.63	0.12	323.4	0.12	0.04	320.8	0.14	0.03
V <sub>17</sub>	δC-CH <sub>3</sub> (sym. bendig)	-	353	342.4	1.67	0.87	337.8	1.98	0.80	341.0	1.72	1.38	346.5	1.32	0.90
V <sub>18</sub>	δC <sub>27</sub> C <sub>26</sub> C <sub>35</sub> +δC <sub>31</sub> C <sub>26</sub> C <sub>35</sub>	-	370	358.8	3.52	0.32	351.2	3.60	0.31	356.8	1.78	0.32	361.5	4.37	0.28
V <sub>19</sub>	δC <sub>17</sub> C <sub>16</sub> O <sub>14</sub> +δC <sub>27</sub> C <sub>26</sub> C <sub>31</sub> +τring2	-	396	392.4	3.30	0.05	387.4	3.74	0.04	386.2	7.37	0.11	398.2	2.00	0.03
V <sub>20</sub>	τring2	-	-	409.6	0.09	0.72	403.5	0.08	0.83	403.4	0.15	0.42	415.3	0.25	0.10
V <sub>21</sub>	δO <sub>13</sub> C <sub>11</sub> C <sub>3</sub> +τring2+τring1	-	416	420.5	3.67	1.59	416.4	4.70	1.27	414.0	3.67	2.01	425.4	4.14	1.59
V <sub>22</sub>	τring1+τO <sub>13</sub> C <sub>11</sub> O <sub>14</sub> C <sub>16</sub> +δC <sub>27</sub> C <sub>26</sub> C <sub>31</sub>	-	428	428.1	0.44	0.61	422.9	0.20	0.65	419.2	0.21	1.30	434.5	0.58	0.32
V <sub>23</sub>	δC <sub>27</sub> C <sub>26</sub> C <sub>31</sub> +τring2+τring1	-	442	434.1	1.53	1.87	429.2	1.49	2.11	431.0	1.89	1.34	439.4	2.67	1.25
V <sub>24</sub>	δC <sub>26</sub> C <sub>23</sub> C <sub>31</sub> +δO <sub>14</sub> C <sub>16</sub> C <sub>17</sub> +δC <sub>27</sub> C <sub>26</sub> C <sub>31</sub>	-	-	461.0	0.67	0.36	455.0	0.61	0.32	451.9	1.08	0.56	466.9	0.66	0.31
V <sub>25</sub>	δO <sub>12</sub> C <sub>4</sub> C <sub>3</sub> +δC-CH <sub>3</sub> (sym. bending)	471	470	466.1	3.81	6.40	461.0	3.54	7.10	458.2	3.48	4.75	470.9	3.73	6.34
V <sub>26</sub>	τring1+γC <sub>3</sub> O <sub>12</sub> C <sub>3</sub> C <sub>4</sub>	-	-	520.4	8.36	0.18	514.7	8.93	0.19	514.3	8.03	0.19	529.6	8.90	0.13
V <sub>27</sub>	δC-CH <sub>3</sub> (sym. bending)+δring2+δO <sub>12</sub> C <sub>4</sub> C <sub>3</sub>	525	527	524.8	11.15	1.41	518.2	12.52	1.06	519.1	12.47	1.41	530.7	12.10	1.41
V <sub>28</sub>	γC <sub>19</sub> C <sub>21</sub> C <sub>26</sub> C <sub>23</sub> +γC <sub>17</sub> C <sub>18</sub> O <sub>14</sub> C <sub>16</sub> + τHCCC in ring 2	536	538	544.4	16.88	2.08	537.8	16.61	2.04	539.5	12.81	4.86	552.6	17.31	2.23
V <sub>29</sub>	[τHCCC+τCCCC]in ring 2+δring1	554	562	552.8	1.08	7.59	545.8	1.18	7.43	544.7	6.57	4.11	559.4	1.36	6.71
V <sub>30</sub>	δring2	630	633	630.8	0.68	5.55	621.1	0.57	5.54	615.6	0.71	5.58	637.5	0.21	5.61
V <sub>31</sub>	νC <sub>23</sub> C <sub>26</sub> +δring2+δring1+δO <sub>13</sub> C <sub>11</sub> C <sub>3</sub>	654	657	643.9	18.48	1.97	638.6	21.07	1.34	638.4	21.95	1.18	652.7	21.16	1.39
V <sub>32</sub>	[τHCCC+τCCCC] in ring 2+νC <sub>26</sub> C <sub>27,31,35</sub>	684	685	672.3	7.06	16.58	667.5	5.94	16.21	663.9	63.47	1.02	683.2	6.14	14.74
V <sub>33</sub>	γC <sub>3</sub> O <sub>13</sub> O <sub>14</sub> C <sub>11</sub> +γO <sub>12</sub> C <sub>3</sub> C <sub>3</sub> C <sub>4</sub> +τHCCC in ring 1	694	-	684.1	7.66	0.33	678.3	10.11	0.35	668.3	4.76	18.51	696.8	6.57	0.19
V <sub>34</sub>	τring2	723	724	720.6	5.10	8.14	714.4	2.73	7.58	677.2	48.64	0.18	727.5	106.45	0.44
V <sub>35</sub>	τHOCC	-	-	728.2	109.89	0.81	735.5	90.03	0.32	716.4	1.88	4.98	734.9	3.39	6.11
V <sub>36</sub>	τHCCC in ring 1+τHOCC+γO <sub>12</sub> C <sub>3</sub> C <sub>3</sub> C <sub>4</sub> + γO <sub>13</sub> O <sub>14</sub> C <sub>3</sub> C <sub>11</sub>	760	764	743.4	40.19	0.23	744.3	47.14	0.56	740.1	67.55	0.20	757.9	56.71	0.25
V <sub>37</sub>	γC <sub>3</sub> O <sub>13</sub> O <sub>14</sub> C <sub>11</sub> +τHOCC+τHCCC in ring 1	-	-	775.6	3.22	0.53	773.7	15.32	0.41	770.0	1.10	0.57	791.1	2.47	0.57



V <sub>38</sub>	δring2+δring1+vC <sub>26</sub> C <sub>27,31,35</sub> +δO <sub>13</sub> C <sub>11</sub> C <sub>3</sub>	790	790	786.5	12.78	3.68	784.6	15.84	5.83	787.0	11.23	2.92	801.7	14.53	3.50
V <sub>39</sub>	τHCCC in ring 2+δO <sub>13</sub> C <sub>11</sub> O <sub>14</sub>	-	-	794.8	13.58	25.57	790.5	12.70	18.93	800.7	22.32	19.84	811.2	16.59	20.68
V <sub>40</sub>	τHCCC in ring 2	797	800	806.8	1.45	0.70	798.8	3.59	1.41	807.4	2.27	0.46	822.0	0.34	0.07
V <sub>41</sub>	ρCH <sub>3</sub> +vC <sub>26</sub> C <sub>27,31,35</sub> +vC <sub>26</sub> C <sub>23</sub> + τHCCC in ring 2	816	815	820.6	0.69	4.00	818.5	0.57	5.35	820.0	2.53	6.12	836.3	0.33	4.54
V <sub>42</sub>	δring1+δring2+vO <sub>14</sub> C <sub>16</sub>	839	838	842.8	1.03	26.83	837.5	0.48	24.66	838.4	0.26	19.45	856.3	0.33	23.55
V <sub>43</sub>	[τHCCC+τCCCC] in ring 1	851	850	848.7	2.22	0.05	838.9	1.65	0.97	852.3	3.01	0.03	866.9	2.80	0.05
V <sub>44</sub>	τHCCC in ring 2+γO <sub>14</sub> C <sub>17</sub> C <sub>18</sub> C <sub>16</sub> + δO <sub>14</sub> C <sub>11</sub> O <sub>13</sub> +δCCCC in ring 1	864	-	867.5	26.06	9.71	862.0	22.59	10.98	865.2	23.44	12.35	887.2	25.18	13.08
V <sub>45</sub>	ρCH <sub>3</sub> +vC <sub>27,31,35</sub> C <sub>26</sub>	876	878	896.6	1.99	7.43	893.5	1.82	6.01	897.2	1.54	6.04	913.8	2.18	6.06
V <sub>46</sub>	ρCH <sub>3</sub> +vC <sub>27,31,35</sub> C <sub>26</sub>	-	-	906.4	0.53	6.14	902.2	1.03	4.87	905.8	1.23	4.80	924.8	0.92	4.97
V <sub>47</sub>	ρCH <sub>3</sub> +τHCCC in ring 2	921	923	929.3	0.38	0.35	912.3	0.22	0.21	910.6	0.33	0.14	935.9	0.13	0.03
V <sub>48</sub>	τHCCC in ring 2+ρCH <sub>3</sub>	932	935	933.6	0.46	0.32	921.3	0.71	0.62	930.9	0.70	0.81	954.8	0.75	1.22
V <sub>49</sub>	τHCCC in ring 1	940	-	943.6	0.93	0.09	932.4	0.93	0.07	946.0	0.05	0.12	967.0	0.02	0.05
V <sub>50</sub>	τHCCC in ring 2	-	-	945.6	0.03	0.27	934.9	0.02	0.32	948.6	1.41	0.10	967.9	0.88	0.09
V <sub>51</sub>	τHCCC in ring 1	956	-	963.1	0.09	0.01	951.1	0.08	0.01	964.7	0.11	0.01	989.0	0.11	0.01
V <sub>52</sub>	δring2+ρCH <sub>3</sub>	-	-	998.4	24.70	0.41	986.3	21.81	0.48	983.4	16.63	0.52	1009.3	20.75	0.54
V <sub>53</sub>	ρCH <sub>3</sub>	1013	-	1007.8	9.97	1.39	993.9	11.18	1.40	992.6	8.10	1.46	1016.3	11.11	1.22
V <sub>54</sub>	ρCH <sub>3</sub>	1024	-	1014.9	0.05	1.24	999.1	0.23	1.27	999.6	0.03	1.34	1022.8	0.02	1.39
V <sub>55</sub>	[δCCC+vCC] in ring 1	1033	1032	1017.9	10.69	32.23	1012.1	10.20	30.16	1013.1	10.07	31.82	1031.8	10.53	29.91
V <sub>56</sub>	vO <sub>14</sub> C <sub>11</sub> +δring1	-	1057	1044.1	163.32	5.08	1041.7	118.31	4.71	1043.0	82.70	4.60	1066.8	87.65	4.87
V <sub>57</sub>	[δHCC+vCC+δCCCC] in ring 2+ vC <sub>23</sub> C <sub>26</sub> +ρCH <sub>3</sub>	1067	1066	1090.9	18.80	24.22	1082.0	24.67	19.45	1080.2	9.02	0.63	1102.1	12.03	3.25
V <sub>58</sub>	δHCC in ring 2	-	-	1096.7	7.17	0.14	1083.9	10.04	1.27	1084.8	29.11	17.39	1107.5	21.12	14.30
V <sub>59</sub>	[δHCC+vCC] in ring 1	1109	1110	1113.2	37.01	2.01	1105.2	27.58	4.25	1103.2	19.10	9.14	1126.8	14.44	7.67
V <sub>60</sub>	δHCC in ring 1	1128	1130	1142.1	83.04	11.32	1128.2	57.31	7.49	1118.1	97.45	6.21	1145.1	87.74	7.56
V <sub>61</sub>	δHCC in ring 2+vO <sub>14</sub> C <sub>16</sub>	1156	1156	1152.1	220.89	54.20	1141.7	94.54	26.05	1143.4	43.34	13.32	1165.1	60.81	11.74
V <sub>62</sub>	vC-CH <sub>3</sub> +ρCH <sub>3</sub>	1174	1172	1180.7	2.94	8.94	1173.9	2.95	8.44	1173.9	297.26	4.68	1202.1	14.15	7.20
V <sub>63</sub>	vC-CH <sub>3</sub> +ρCH <sub>3</sub> +δHCC in ring 2	-	-	1182.9	96.06	28.09	1177.8	3.02	8.85	1178.0	1.04	8.09	1205.6	261.50	4.26
V <sub>64</sub>	vO <sub>14</sub> C <sub>16</sub> +δHCC in ring 2 and 1+ vC-CH <sub>3</sub> +ρCH <sub>3</sub>	-	-	1184.5	382.18	51.38	1183.8	553.82	80.25	1181.3	2.60	8.63	1206.7	4.41	8.26
V <sub>65</sub>	δHCC in ring 1 and 2+δHOC	-	1201	1195.6	107.43	0.44	1188.0	43.08	8.33	1200.7	296.73	51.35	1213.3	333.33	41.78
V <sub>66</sub>	vO <sub>12</sub> C <sub>4</sub> +δHCC+vCC] in ring 1+vC <sub>3</sub> C <sub>11</sub>	1210	-	1234.0	239.49	73.73	1234.3	252.80	65.37	1225.9	301.05	62.25	1249.3	253.41	56.94
V <sub>67</sub>	vC <sub>23</sub> C <sub>26</sub> +ρCH <sub>3</sub>	1247	1243	1240.0	14.17	6.17	1236.6	156.79	25.92	1243.3	51.74	16.04	1267.7	32.91	9.17
V <sub>68</sub>	vO <sub>12</sub> C <sub>4</sub> +vC <sub>11</sub> C <sub>3</sub> + [vCC+δHCC+δCCCC] in ring 2 and 1	1264	1266	1279.2	173.61	4.87	1267.4	0.31	1.89	1259.9	2.56	7.90	1279.2	2.28	5.55
V <sub>69</sub>	[vCC+δHCC+δCCCC] in ring 2 and 1+ vC <sub>3</sub> C <sub>11</sub> +vO <sub>12</sub> C <sub>4</sub>	1286	1287	1282.6	151.29	14.45	1281.4	263.69	3.26	1266.8	1.77	0.78	1298.0	0.49	1.43
V <sub>70</sub>	δHCC in ring 2	-	-	1290.4	1.09	0.85	1294.4	8.25	2.50	1279.4	331.44	5.32	1305.4	331.68	4.87
V <sub>71</sub>	[vCC+δHCC] in ring 1+vC <sub>3</sub> C <sub>11</sub> +vO <sub>12</sub> C <sub>4</sub>	1304	1307	1313.0	54.01	105.19	1321.2	121.60	133.55	1304.2	160.86	118.65	1326.2	150.84	110.05
V <sub>72</sub>	δCH <sub>3</sub> (sym. bending)	1320	1320	1353.1	8.84	0.13	1330.1	11.02	0.11	1326.4	12.08	0.10	1362.9	14.16	0.27
V <sub>73</sub>	δCH <sub>3</sub> (sym. bending)	1335	1331	1354.2	9.50	0.44	1331.2	12.46	0.69	1329.3	13.67	0.58	1363.8	13.10	0.01
V <sub>74</sub>	δHOC+[δHCC+vCC] in ring 1	1364	1362	1368.4	113.65	60.55	1361.2	8.20	1.96	1335.1	194.76	71.83	1377.4	166.41	69.75
V <sub>75</sub>	δCH <sub>3</sub> (sym. bending)	-	-	1384.4	4.16	0.84	1362.9	115.01	50.06	1358.9	5.12	0.71	1392.6	5.97	0.50
V <sub>76</sub>	[vCC+δHCC] in ring 2+ δCH <sub>3</sub> (sym. bending)	1395	1396	1388.7	5.65	0.30	1378.7	5.23	0.35	1381.2	6.40	0.64	1409.7	5.86	0.17

V77	$\delta_s\text{CH}_3$	-	-	1434.8	0.03	0.62	1411.2	0.03	0.59	1408.2	0.05	1.35	1439.1	0.00	1.14
V78	[vCC+ $\delta\text{HCC}$ ] in ring 1	-	-	1439.4	41.32	52.68	1416.6	0.09	8.92	1410.9	0.08	7.54	1443.3	0.11	8.12
V79	$\delta_s\text{CH}_3$	-	-	1440.0	0.03	8.91	1419.4	1.50	9.31	1416.3	0.91	8.60	1447.6	0.99	8.51
V80	$\delta_s\text{CH}_3$	-	1445	1442.5	1.28	8.86	1433.1	35.86	54.06	1430.4	12.57	6.92	1461.5	12.00	7.34
V81	$\delta_s\text{CH}_3$	-	-	1455.2	12.60	6.97	1433.3	9.28	9.42	1434.2	23.45	40.21	1463.4	35.86	43.19
V82	$\delta_s\text{CH}_3$	1463	1462	1460.0	8.56	7.81	1437.7	8.97	8.01	1435.7	9.04	6.98	1465.5	9.04	8.16
V83	[vCC+ $\delta\text{HCC}$ ] in ring 1+ $\delta\text{HOC}$	-	-	1465.6	79.18	1.28	1449.8	6.05	3.32	1448.1	6.47	3.41	1477.1	8.38	2.36
V84	$\delta_s\text{CH}_3$	1483	-	1471.2	6.34	2.77	1455.4	103.58	2.19	1454.3	110.08	14.58	1485.7	95.08	4.44
V85	[vCC+ $\delta\text{HCC}$ ] in ring 2	1510	1510	1489.2	93.29	0.68	1477.6	98.82	0.63	1482.6	114.80	0.82	1512.5	103.95	0.53
V86	[vCC+ $\delta\text{HCC}$ ] in ring 1+ $\delta\text{HOC}$	-	-	1563.4	62.99	27.98	1562.0	68.53	30.67	1568.2	68.31	38.55	1598.5	66.54	33.49
V87	[vCC+ $\delta\text{HCC}$ ] in ring 2	1585	1586	1571.6	2.48	4.97	1570.3	2.66	4.51	1581.2	3.01	4.37	1609.8	2.57	5.28
V88	[vCC+ $\delta\text{HCC}$ ] in ring 2 and 1	1602	1601	1588.8	19.00	78.86	1587.9	23.43	81.79	1601.1	37.02	95.56	1628.1	32.24	66.66
V89	[vCC+ $\delta\text{HCC}$ ] in ring 1 and 2+ $\delta\text{HOC}$	1616	1615	1599.2	39.91	10.30	1597.5	40.08	7.27	1607.5	32.73	7.40	1636.3	33.60	8.00
V90	vO=C+ $\delta\text{HOC}$ +vCC in ring 1	1689	1681	1665.6	330.03	181.26	1669.1	327.52	176.99	1699.6	342.85	173.19	1709.6	360.72	147.66
V91	$\nu_s\text{CH}_3$	2869	2872	2921.5	27.29	10.92	2900.6	26.77	9.91	2883.8	20.55	28.88	2944.1	23.25	9.06
V92	$\nu_s\text{CH}_3$	2900	2905	2922.0	26.85	7.97	2901.7	26.32	8.75	2886.1	22.75	46.36	2944.4	22.62	7.55
V93	$\nu_s\text{CH}_3$	-	2932	2929.3	28.73	516.33	2907.4	27.82	521.18	2891.3	14.90	400.26	2951.2	22.20	476.11
V94	$\nu_{as}\text{CH}_3$	-	-	2981.6	3.42	17.61	2970.1	3.23	17.67	2956.4	2.30	18.56	3008.1	4.03	15.86
V95	$\nu_{as}\text{CH}_3$	-	-	2982.4	3.23	15.61	2971.1	2.77	13.33	2958.0	5.41	22.55	3009.1	6.47	25.63
V96	$\nu_{as}\text{CH}_3$	2969	2968	2988.3	21.24	32.99	2975.3	19.56	35.69	2961.3	17.44	42.95	3014.6	15.11	24.57
V97	$\nu_{as}\text{CH}_3$	-	-	2989.8	100.46	261.47	2976.9	95.06	259.11	2962.2	46.54	145.92	3016.6	85.05	222.48
V98	$\nu_{as}\text{CH}_3$	-	-	2994.1	20.12	40.99	2980.9	22.48	43.79	2964.4	20.66	45.96	3019.7	21.04	43.46
V99	$\nu_{as}\text{CH}_3$	-	-	2996.6	42.93	64.94	2983.8	32.21	55.00	2969.0	38.28	109.35	3022.1	34.94	57.85
V100	vCH in ring 1	3023	-	3065.4	5.36	88.24	3045.2	5.27	86.90	3029.7	3.76	90.44	3086.2	4.57	84.02
V101	vCH in ring 2	-	3068	3072.9	11.54	41.46	3050.3	11.59	45.26	3031.2	5.66	36.53	3091.0	9.90	40.41
V102	vCH in ring 1	3073	-	3083.9	9.10	120.46	3063.4	5.91	52.51	3045.0	2.29	106.94	3103.1	4.23	59.57
V103	vCH in ring 2	-	-	3084.1	5.51	60.39	3063.9	6.95	114.33	3049.9	2.99	102.02	3105.0	6.22	107.65
V104	vCH in ring 2	-	-	3089.3	6.67	109.03	3068.7	5.10	101.70	3051.1	2.56	48.41	3109.1	3.99	102.89
V105	vCH in ring 1	-	-	3092.3	6.30	181.09	3072.5	5.00	155.10	3063.8	0.81	36.63	3113.4	3.41	150.82
V106	vCH in ring 2	-	-	3102.4	4.42	121.66	3079.0	3.67	131.79	3065.6	1.25	112.94	3122.1	2.86	118.64
V107	vCH in ring 1	-	-	3104.3	3.76	140.17	3081.7	4.32	164.32	3066.4	2.00	229.27	3123.6	3.14	149.11
V108	vOH	3207	3208	3353.0	416.37	141.80	3286.9	464.78	146.35	3424.6	393.18	133.08	3401.3	440.23	127.81
The linear correlation coefficients ( $R^2$ )				0.99916 for IR wavenumbers and 0.99930 for Raman ones			0.99951 for IR wavenumbers and 0.99961 for Raman ones			0.99916 for IR wavenumbers and 0.99836 for Raman ones			0.99909 for IR wavenumbers and 0.99927 for Raman ones		

v, stretching;  $\delta$ , in-plane bending;  $\tau$ , torsion;  $\gamma$ , out-of-plane bending;  $\delta_s$ , scissoring;  $\delta_a$ , symmetric bending;  $\rho$ , rocking;  $I_{IR}$ , IR intensity (km/mol);  $S_{Raman}$ , Raman scattering activity.

### 3.3. NMR chemical shift analyses

The experimental (AIST, 2017)  $^1\text{H}$  and  $^{13}\text{C}$  NMR chemical shifts of the title molecule were measured in chloroform-d solvent. The  $^1\text{H}$  and  $^{13}\text{C}$  NMR chemical shifts of the title molecule were calculated at B3LYP, B3PW91, M06-2X and CAM-B3LYP/6-

311++G(d,p) levels in vacuum and chloroform solvent with IEFPCM solvent model using GIAO method. The experimental and calculated NMR chemical shift values were listed in Table 3. The linear correlation coefficients ( $R^2$ ) between the experimental and calculated proton and carbon-13 NMR chemical shifts were also given in Table 3.

**Table 3.** The experimental (AIST, 2017) and calculated  $^{13}\text{C}$  and  $^1\text{H}$  NMR isotropic chemical shifts (with respect to TMS, all values in ppm) of p-tert-butylphenyl salicylate.

Atoms	$\delta_{\text{exp}}$	B3LYP		B3PW91		M06-2X		CAM-B3LYP	
		vacuum	chloroform	vacuum	chloroform	vacuum	chloroform	vacuum	chloroform
C1	119.43	123.39	124.87	122.29	123.78	138.19	139.85	124.79	126.31
C2	130.37	137.24	138.05	136.07	136.92	151.95	152.83	140.35	141.19
C3	111.98	117.47	117.92	115.55	116.01	129.58	129.95	118.03	118.53
C4	162.26	173.10	172.85	170.74	170.52	185.29	184.95	175.15	174.84
C5	117.84	123.93	124.17	122.99	123.27	138.87	139.13	125.79	125.99
C6	136.39	142.52	144.06	141.59	143.15	158.39	160.09	145.85	147.38
C11	169.14	177.01	178.17	174.90	176.01	183.64	184.69	179.34	180.55
C16	147.81	157.49	157.34	155.15	155.04	168.31	168.26	158.63	158.47
C17	120.98	127.19	127.55	126.25	126.69	140.88	141.51	130.22	130.55
C18	120.98	128.87	128.88	127.91	127.97	144.21	144.15	131.16	131.27
C19	126.53	134.86	135.97	133.86	134.99	150.4	151.64	137.22	138.30
C21	126.53	131.03	131.94	130.16	131.08	145.95	146.79	133.58	134.51
C23	149.30	157.46	159.19	155.15	156.92	173.74	175.63	159.62	161.36
C26	34.55	42.28	42.94	39.73	40.42	41.35	42.01	38.96	39.61
C27	31.41	34.56	34.67	34.03	34.16	35.72	35.79	34.41	34.51
C31	31.41	34.78	34.85	34.22	34.30	36.17	36.19	34.39	34.45
C35	31.41	30.22	30.39	29.69	29.87	33.51	33.61	30.52	30.70
<b>R<sup>2</sup></b>		<b>0.99824</b>	<b>0.99840</b>	<b>0.99875</b>	<b>0.99888</b>	<b>0.99564</b>	<b>0.99534</b>	<b>0.99894</b>	<b>0.99907</b>
H7	6.96	6.97	7.15	6.99	7.19	7.72	7.91	7.03	7.21
H8	8.07	8.35	8.44	8.38	8.49	9.07	9.16	8.51	8.60
H9	7.03	7.18	7.26	7.20	7.29	7.93	8.00	7.30	7.37
H10	7.52	7.61	7.80	7.64	7.84	8.16	8.34	7.73	7.91
H15	10.56	10.95	10.90	11.34	11.31	10.92	10.88	10.96	10.91
H20	7.13	7.32	7.43	7.36	7.49	7.97	8.09	7.42	7.52
H22	7.13	7.24	7.32	7.28	7.38	8.09	8.15	7.36	7.45
H24	7.46	7.61	7.75	7.68	7.84	8.34	8.49	7.79	7.93
H25	7.76	7.61	7.73	7.68	7.82	8.38	8.49	7.65	7.77
H28	1.34	1.62	1.65	1.63	1.68	1.63	1.66	1.66	1.68
H29	1.34	1.30	1.35	1.30	1.36	1.30	1.35	1.17	1.21
H30	1.34	1.21	1.18	1.22	1.20	1.24	1.19	1.29	1.24
H32	1.34	1.16	1.14	1.17	1.16	1.07	1.03	1.17	1.13
H33	1.34	1.32	1.36	1.29	1.35	1.34	1.39	1.29	1.33
H34	1.34	1.60	1.63	1.62	1.67	1.50	1.52	1.59	1.61
H36	1.34	1.61	1.63	1.62	1.66	1.51	1.53	1.55	1.57
H37	1.34	1.64	1.65	1.67	1.69	1.54	1.55	1.59	1.59
H38	1.34	1.09	1.14	1.10	1.16	1.40	1.45	1.15	1.19
<b>R<sup>2</sup></b>		<b>0.99721</b>	<b>0.99748</b>	<b>0.99622</b>	<b>0.99699</b>	<b>0.99587</b>	<b>0.99449</b>	<b>0.99732</b>	<b>0.99736</b>

$^{13}\text{C}$  NMR chemical shifts were recorded in the interval of 31.41-169.14 ppm and they were computed in the region of 30.22-178.17 ppm for B3LYP, 29.69-176.01 ppm for B3PW91, 33.51-184.69 ppm for M06-2X and 30.52-180.55 ppm for CAM-B3LYP. Carbonyl carbons in esters, carboxylic acids, amides, ketones, phenols and

aldehydes have characteristic chemical shift signals at the interval of 160-220 ppm, as the highly electronegative O atom reduces the electron density of carbon atom. But, the aromatic carbons occur signals in the region of 100-150 ppm (Anderson et al., 2004; Wade, 2006; Pavia et al., 2009). The NMR chemical shift signals for the C4 phenolic

carbon atom and C11 ester atom were recorded at 162.26 ppm and 169.14 ppm, respectively. The computed values for these carbon atoms are 173.10/172.85 ppm and 177.01/178.17 ppm for B3LYP, 170.74/170.52 ppm and 174.90/176.01 ppm for B3PW91, 185.29/184.95 ppm and 183.64/184.69 ppm for M06-2X and 175.15/174.84 ppm and 179.34/180.55 ppm for CAM-B3LYP, respectively. As expected, the other aromatic carbons were recorded in the region of 111.98-149.30 ppm, while they were calculated at the interval of 117.47-159.19 ppm, 115.55-156.92 ppm, 129.58-175.63 ppm and 118.03-161.36 ppm for aforementioned computation levels, respectively. Methyl and methylene carbon atoms are shielded by their own hydrogen atoms. Therefore,  $^{13}\text{C}$  NMR resonance signals of these groups occur within the region of 15-35 ppm (Silverstein and Webster, 1998; Anderson et al., 2004; Stuart, 2004; Wade, 2006). The signals recorded at 31.41 ppm and 34.55 ppm in the Carbon-13 NMR isotropic chemical shift spectrum of the title molecule indicated presence of methyl groups (C26, C27, C31 and C35). The computed values corresponding to these carbon atoms were given in Table 3.

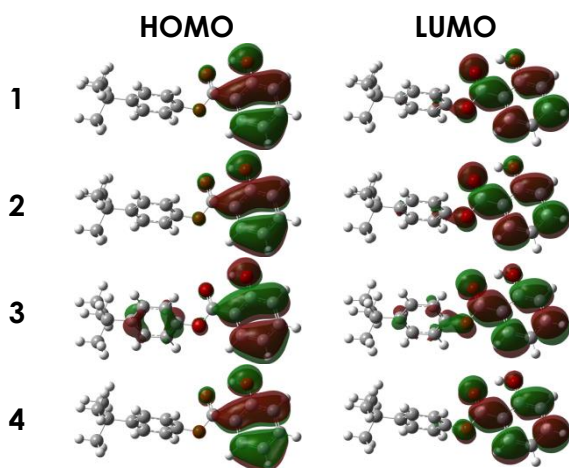
Due to intramolecular hydrogen bonding, phenolic protons shift to the approximate range of  $\delta$  10-12 ppm (Silverstein and Webster, 1998). The NMR chemical shift value for the phenolic H15 proton is observed at 10.56 ppm, while the computed values for this proton are between 10.90 ppm and 11.34 ppm in all mentioned computational levels. Aromatic hydrogens are deshielded at a higher level than those attached to double bonds due to the large anisotropic field that is generated by the circulation of the  $\pi$  electrons in the ring and they are easily identified in the region of 6.5-9.0 ppm (Pavia et al., 2009). The aromatic protons (H7, H8, H9 and H10) were experimentally recorded at the interval of 6.96-8.07 ppm, while they were theoretically computed at the regions of 6.97-8.44 ppm for B3LYP, 6.99-8.49 ppm for B3PW91, 7.72-9.16 ppm for M06-2X and 7.03-8.60 ppm for CAM-B3LYP. The methyl hydrogen atoms, shielded at the highest level, have chemical shift signals in the region of 0.7-1.3 ppm (Pavia et al., 2009). The methyl protons in the title molecule were experimentally and theoretically obtained at 1.34 ppm and at the interval of 1.09-1.68 ppm with the mentioned computational levels, respectively.

### 3.4. Frontier molecular orbitals analyses

The highest occupied molecular orbital (HOMO) and the lowest unoccupied molecular orbital (LUMO) are the main orbitals taking part in a chemical reaction (Fukui, 1982). The HOMO is the outermost orbital filled by electrons. It is represented by the ionization potential of a molecule. It can be considered as a valance band since it behaves as an electron donor. The LUMO represents the first empty innermost orbital unfilled by electrons. It is directly related to the electron affinity. Behaving as an electron acceptor, it can be thought as the conductance band of the system. The HOMO-LUMO energy band gap is an indication of molecular chemical stability. It is a very important parameter for determination of molecular electrical properties. Furthermore, the quantum molecular descriptors such as ionization potential, electron affinity, chemical reactivity, kinetic stability, polarizability, chemical hardness and softness, aromaticity and electronegativity can be found using HOMO-LUMO energy band gap (Alpaslan et al., 2015). HOMO and LUMO energy values and HOMO-LUMO band gap values, computed with the B3LYP, B3PW91, M06-2X and CAM-B3LYP/6-311++G(d,p) levels, were summarized in Table 4. Additionally, the ionization potential, chemical potential, electron affinity, electronegativity chemical hardness, softness and electrophilicity index parameters, found using the computed HOMO and LUMO energy values, were summarized in Table 4 (Alpaslan et al., 2015). HOMO and LUMO surfaces were given in Figure 4. As seen from Figure 4, both HOMO and LUMO plots simulated with all four-computational level were localized on salicylate group of p-tert-butylphenyl salicylate molecule.

**Table 4.** The calculated molecular electronic properties of p-tert-butylphenyl salicylate (vacuum/ethanol).

Parameters (eV)	B3LYP	B3PW91	M06-2X	CAM-B3LYP
$E_{LUMO}$	-1.8090/-1.9421	-1.8117/-1.9638	-0.8177/-0.9557	-0.5021/-0.6416
$E_{HOMO}$	-6.5686/-6.7218	-6.5914/-6.7658	-7.9003/-8.0584	-7.9572/-8.1275
Energy band gap $/E_{HOMO}-E_{LUMO}/$	4.7595/4.7797	4.7797/4.8020	7.0826/7.1027	7.4551/7.4859
Ionization potential ( $I = -E_{HOMO}$ )	6.5686/6.7218	6.5914/6.7658	7.9003/8.0584	7.9572/8.1275
Electron affinity ( $A = -E_{LUMO}$ )	1.8090/1.9421	1.8117/1.9638	0.8177/0.9557	0.5021/0.6416
Chemical hardness ( $\eta = (I-A)/2$ )	2.3798/2.3898	2.3898/2.4010	3.5413/3.5514	3.7276/3.7429
Chemical softness ( $\zeta = 1/2\eta$ )	0.2101/0.2092	0.2092/0.2082	0.1412/0.1408	0.1341/0.1336
Electronegativity ( $\chi = (I+A)/2$ )	4.1888/4.3319	4.2016/4.3648	4.3590/4.5070	4.2296/4.3846
Chemical potential ( $\mu = -(I+A)/2$ )	-4.1888/-4.3319	-4.2016/-4.3648	-4.3590/-4.5070	-4.2296/-4.3846
Electrophilicity index ( $\omega = \mu^2/2\eta$ )	3.6865/3.9261	3.6934/3.9675	2.6828/2.8599	2.3996/2.5681

**Figure 4.** The HOMO and LUMO plots of p-tert-butylphenyl salicylate (1= B3LYP, 2= B3PW91, 3= M06-2X and 4= CAM-B3LYP).

### 3.5. NBO analysis

NBO analysis is a powerful method to determine intra-molecular and inter-molecular bonding interactions, bond species, bond structures and hyperconjugation interactions in molecular systems. The stabilization energy,  $E(2)$ , depends on the interaction between Lewis type (bonding or lone pair) filled orbitals and non-Lewis type (antibonding or Rydberg) vacancy orbitals. For each donor NBO ( $i$ ) and acceptor NBO ( $j$ ), the stabilization energy  $E(2)$  associated with the electron delocalization between stabilization energy  $E(2)$  associated with the electron delocalization between the donor and the acceptor is estimated as (Wienhold and Landis, 2005);

$$E(2) = -q_i \frac{F_{ij}^2}{\Delta E} = -q_i \frac{\langle i|F|j \rangle^2}{\varepsilon_j - \varepsilon_i}$$

Where  $q_i$  is the donor orbital occupancy,  $\varepsilon_i$  and  $\varepsilon_j$  are diagonal elements (orbital energies), and  $F_{ij}$  is the off-diagonal NBO Fock matrix element. Table 5 shows the results of second-order perturbation theory analysis of the Fock Matrix computed with B3LYP, B3PW91, M06-2X and CAM-B3LYP/6-311++G(d,p) levels for the intra-molecular O-H $\cdots$ O interaction in the title molecule. According to the computed NBO results, the  $n(O13) \rightarrow \sigma^*(O12-H15)$  charge transfer for the intramolecular hydrogen bonding in the title molecule belongs to the stabilization energy of 17.24 kcal mol $^{-1}$  for B3LYP, 19.69 kcal mol $^{-1}$  for B3PW91, 14.85 kcal mol $^{-1}$  for M06-2X and 19.92 kcal mol $^{-1}$  for CAM-B3LYP.

**Table 5.** The calculated results with second order perturbation theory of Fock matrix in NBO of p-tert-butylphenyl salicylate.

Method	ED(i)(e)	Donor (i)	ED(j)(e)	Acceptor (j)	E(2) <sup>a</sup> (kcal/mol)	E(j)-E(i) <sup>b</sup> (a.u.)	F(i,j) <sup>c</sup> (a.u.)
B3LYP	1.97154	n(O13)	0.04433	$\sigma^*(\text{O12-H15})$	3.17	1.13	0.054
	1.83711	n(O13)	0.04433	$\sigma^*(\text{O12-H15})$	14.07	0.71	0.092
B3PW91	1.97112	n(O13)	0.04914	$\sigma^*(\text{O12-H15})$	3.63	1.13	0.057
	1.83281	n(O13)	0.04914	$\sigma^*(\text{O12-H15})$	16.06	0.72	0.099
M06-2X	1.97339	n(O13)	0.03336	$\sigma^*(\text{O12-H15})$	3.14	1.31	0.057
	1.85046	n(O13)	0.03336	$\sigma^*(\text{O12-H15})$	11.71	0.87	0.093
CAM-B3LYP	1.97088	n(O13)	0.04277	$\sigma^*(\text{O12-H15})$	3.92	1.27	0.063
	1.84407	n(O13)	0.04277	$\sigma^*(\text{O12-H15})$	16.00	0.85	0.107

ED is the electron density.

<sup>a</sup> E(2) is the energy of hyperconjugative interactions.

<sup>b</sup> Energy difference between donor (i) and acceptor (j) NBO.

<sup>c</sup> F(i,j) is the Fock matrix element between i and j NBO.

### 3.6. NLO analysis

Organic, inorganic and organometallic nonlinear optical (NLO) materials have drawn much interest in the fields of physics, chemistry and engineering, due to their potential for future applications in the fields of optoelectronics and microelectronics, such as optical telecommunications, signal processing, optical interconnections, optical computing, optical information processing, sensor protection, optical switching, dynamic image processing and various other photonic technologies (Nalwa and Miyata, 1997). Mean polarizability ( $\alpha_{total}$ ), anisotropy of polarizability ( $\Delta\alpha$ ) and first hyperpolarizability ( $\beta_0$ ) values are important factors to determine NLO

properties of molecular systems. Therefore, recent syntheses and investigations of novel nonlinear optic materials with high performance have created an interesting study area.

Dipole moments, polarizabilities and the first hyperpolarizabilities of the title molecule were computed with B3LYP, B3PW91, M06-2X and CAM-B3LYP functionals at the 6-311++G(d,p) basis set by using the finite-field approach and they were summarized in Table 6. Total dipole moment ( $\mu_{total}$ ), mean polarizability ( $\alpha_{total}$ ), anisotropy of the polarizability ( $\Delta\alpha$ ) and the first hyperpolarizability

**Table 6.** The computed dipole moments, polarizability and first hyperpolarizability values of p-tert-butylphenyl salicylate.

Parameters	B3LYP	B3PW91	M06-2X	CAM-B3LYP
$\alpha_{xx}$	45.857057	45.473318	43.918975	43.590784
$\alpha_{xy}$	-1.468724	-1.447369	-1.205952	-1.491938
$\alpha_{xz}$	0.449402	0.475443	0.498052	0.270501
$\alpha_{yy}$	27.495369	27.189745	27.844298	26.498934
$\alpha_{yz}$	0.469464	0.481560	0.619328	0.309205
$\alpha_{zz}$	23.023234	22.626691	21.211417	22.961580
$\alpha_{total}$	32.125220	31.763251	30.991563	31.017099
$\Delta\alpha$	21.142517	21.123398	20.378165	19.294768
$\mu_x$	-1.4442	-1.4885	-1.4025	-1.5652
$\mu_y$	-1.6647	-1.6355	-2.0823	-1.7500
$\mu_z$	0.7754	0.7834	0.4717	0.6313
$\mu_{total}$	2.3363	2.3461	2.5545	2.4312
$\beta_{xxx}$	-55.968084	-52.625296	-46.395861	-57.108908
$\beta_{yyy}$	4.261637	4.600238	3.859765	5.394967
$\beta_{zzz}$	-2.829172	2.527659	1.929119	3.227416
$\beta_{yyy}$	-17.457290	-16.207580	-16.276324	-16.228853
$\beta_{yxx}$	14.480956	14.150298	15.123341	12.616432

$\beta_{yzz}$	-6.695821	-6.313197	-5,074227	-6.136804
$\beta_{zzz}$	3.084199	2.925735	4,045505	1.341176
$\beta_{zxx}$	-2.916310	-2.832231	-3,601204	-1.264909
$\beta_{zyy}$	1.153410	1.220107	0.722601	1.530175
$\beta_0$	55.402438	46.279626	41.098253	49.463611

$\times 10^{-24}$  for  $\alpha$  in esu,  $\times 10^{-31}$  for  $\beta$  in esu,  $\mu$  in Debye, 1 a.u.=  $0.1482 \times 10^{-24}$  for  $\alpha$  in esu and 1 a.u.=  $8.6393 \times 10^{-33}$  for  $\beta$  in esu

( $\beta_0$ ) magnitudes were computed using the following equations (Temel et al., 2015);

$$\alpha_{total} = \frac{1}{3}(\alpha_{xx} + \alpha_{yy} + \alpha_{zz})$$

$$\Delta\alpha = \frac{1}{\sqrt{2}} \left[ (\alpha_{xx} - \alpha_{yy})^2 + (\alpha_{yy} - \alpha_{zz})^2 + (\alpha_{zz} - \alpha_{xx})^2 \right]^{\frac{1}{2}} + 6\alpha_{xz}^2 + 6\alpha_{xy}^2 + 6\alpha_{yz}^2$$

$$\beta_0 = \left[ (\beta_{xxx} + \beta_{yyy} + \beta_{zzz})^2 + (\beta_{yyy} + \beta_{yzz} + \beta_{yxx})^2 + (\beta_{zzz} + \beta_{zxx} + \beta_{zyy})^2 \right]^{\frac{1}{2}}$$

$$\mu_{total} = (\mu_x^2 + \mu_y^2 + \mu_z^2)^{\frac{1}{2}}$$

The calculated dipole moment ( $\mu_{total}$ ) values for the title molecule were found as 2.3363 Debye for B3LYP, 2.3461 Debye for B3PW91, 2.5545 Debye for M06-2X and 2.4312 Debye for CAM-B3LYP. The  $\alpha_{total}$ ,  $\Delta\alpha$  and  $\beta_0$  values were computed as  $32.125220 \times 10^{-24}$ ,  $21.142517 \times 10^{-24}$  and  $55.402438 \times 10^{-31}$  esu for B3LYP,  $31.763251 \times 10^{-24}$ ,  $21.123398 \times 10^{-24}$  and  $46.279626 \times 10^{-31}$  esu for B3PW91,  $30.991563 \times 10^{-24}$ ,  $20.378165 \times 10^{-24}$  and  $41.098253 \times 10^{-31}$  esu for M06-2X and  $31.017099 \times 10^{-24}$ ,  $19.294768 \times 10^{-24}$  and  $49.463611 \times 10^{-31}$  esu for CAM-B3LYP, respectively. Urea that is the most common organic NLO material can be usually compared with those of other organic compounds. By using B3LYP/6-311++G(d,p) level, computed values for urea are  $5.047959 \times 10^{-24}$  esu for  $\alpha_{total}$ ,  $2.036631 \times 10^{-24}$  esu for  $\Delta\alpha$  and  $7.878196 \times 10^{-31}$  esu for  $\beta_0$ . The  $\alpha_{total}$ ,  $\Delta\alpha$  and  $\beta_0$  values calculated with B3LYP/6-311++G(d,p) level of the title compound are approximately 6.364, 10.381 and 7.324 times greater than those of urea, respectively.

### 3.7. Thermodynamic properties

The thermodynamic parameters were calculated using B3LYP, B3PW91 and CAM-B3LYP methods with the 6-311++G(d,p) basis set at the room temperature of 298.15 K, under 1 atm pressure and in vacuum for the title molecule. The computed

thermodynamic parameters were given in Table 7. The partition function, indicating the statical properties of a system in thermodynamic equilibrium is very important for thermodynamic parameters. There are four types of partition functions, namely, translational, electronic, vibrational and rotational partition functions. Partition functions can be used to compute the thermodynamic variables (such as heat capacity, entropy, equilibrium constants, total energy, free energy, pressure, thermal energy and rate constants, etc.) of a system. As known, the total energy of any molecular system is the sum of electronic, vibrational, rotational and translation energies (or  $E = E_e + E_v + E_r + E_t$ ). The computed total energy values for the title molecule were obtained as -884.59282006 Hartrees for B3LYP, -884.24252309 Hartrees for B3PW91, -884.22227194 Hartrees for M06-2X and -884.13686115 Hartrees for CAM-B3LYP. The computed zero-point vibrational energy (ZPVE) values for all four levels were found as 195.37107, 195.84427, 197.44399 and 197.70185 kcal/mol, respectively. As seen from Table 7, the computed thermal energy (E), heat capacity ( $C_v$ ) and entropy (S) values for B3LYP, B3PW9, M06-2X and CAM-B3LYP/6-311++G(d,p) levels are 206.790, 207.257, 208.763 and 207.407 cal/mol×K, 71.656, 71.566, 71.003 and 68.641 cal/mol×K and 141.872, 141.859, 140.605 and 133.286 cal/mol×K, respectively. The major contributions to these values were from vibrational energies, whereas the minor contributions resulted from electronic, translational and rotational energies. The computed rotational temperatures (Kelvin), rotational constants (GHz) and other thermodynamic parameters for the title molecule were listed in Table 7.

**Table 7.** The computed thermodynamic parameters (at the temperature of 298.15 K, under the pressure of 1 atm and in vacuum) of p-tert-butylphenyl salicylate.

Parameters	B3LYP	B3PW91	M06-2X	CAM-B3LYP
Thermal energy, E (cal/mol K)				
Electronic	0.000	0.000	0.000	0.000
Translational	0.889	0.889	0.889	0.889
Rotational	0.889	0.889	0.889	0.889
Vibrational	205.013	205.479	206.986	206.630
Total	206.790	207.257	208.763	207.407
Heatcapacity, C <sub>v</sub> (cal/mol K)				
Electronic	0.000	0.000	0.000	0.000
Translational	2.981	2.981	2.981	2.981
Rotational	2.981	2.981	2.981	2.981
Vibrational	65.694	65.604	65.041	62.679
Total	71.656	71.566	71.003	68.641
Entropy, S (cal/mol K)				
Electronic	0.000	0.000	0.000	0.000
Translational	42.680	42.680	42.680	42.680
Rotational	34.185	34.164	34.166	34.152
Vibrational	65.007	65.014	63.759	56.454
Total	141.872	141.859	140.605	133.286
Rotational temperatures (Kelvin)				
A	0.05548	0.05580	0.05576	0.05598
B	0.00599	0.00604	0.00607	0.00606
C	0.00575	0.00579	0.00576	0.00583
Rotational constants (GHz)				
A	1.15611	1.16276	1.16182	1.16650
B	0.12490	0.12586	0.12649	0.12622
C	0.11978	0.12065	0.11996	0.12143
Zero-point vibrational energy (kcal/mol)	195.37107	195.84427	197.44399	197.70185
Zero-point correction*	0.311344	0.312098	0.314647	0.315058
Thermal correction to Energy*	0.329541	0.330285	0.332685	0.332118
Thermal correction to Enthalpy*	0.330485	0.331229	0.333629	0.333063
Thermal correction to Gibbs Free Energy*	0.263077	0.263827	0.266824	0.269734
Sum of electronic and zero-point energy*	-884.281476	-883.930425	-883.907625	-883.821803
Sum of electronic and thermal Energies*	-884.263279	-883.912238	-883.889587	-883.804743
Sum of electronic and thermal Enthalpies*	-884.262335	-883.911294	-883.888643	-883.803799
Sum of electronic and thermal Free Energies*	-884.329743	-883.978696	-883.955448	-883.867127
Total energy (Hartree)	-884.59282006	-884.24252309	-884.22227194	-884.13686115

\* in Hartree/particle

#### 4. Conclusions

The molecular geometric, spectroscopic (FT-IR, Raman and NMR), HOMO-LUMO, NBO, NLO and thermodynamic analyses for p-tert-butylphenyl salicylate molecule were investigated using experimental and theoretical methods. In order to support the experimental spectroscopic data, theoretical computations were performed using B3LYP, B3PW91, M06-2X and CAM-B3LYP methods with the 6-311++G(d,p) basis set. The computed total molecular energy was obtained in the following order: B3LYP<B3PW91<M06-

2X<CAM-B3LYP. As seen from the tables and figures, the computed structural, spectroscopic, electronic, nonlinear optical and thermodynamic properties varied depending on the calculation levels. In the present study, due to O-H...O intramolecular hydrogen bonding interaction in title compound, O-H vibrational frequencies, <sup>1</sup>H NMR isotropic chemical shifts for mentioned proton, and NBO analysis of n(O)→σ\*(O-H) interaction were investigated using experimental and theoretical methods. The calculated  $\alpha_{total}$ ,  $\Delta\alpha$  and  $\beta_0$  values show that p-tert-butylphenyl salicylate molecule may be a good nonlinear optical material. The



thermodynamic parameters were computed to understand the thermochemical properties (at the room temperature of 298.15 K, under 1 atm pressure and in vacuum) of the title compound.

## References

- AIST, (2017). National Institute of Advanced Industrial Science and Technology Spectral Database for Organic Compounds, SDBS. [http://sdbs.db.aist.go.jp/sdbs/cgi-bin/re\\_index.cgi](http://sdbs.db.aist.go.jp/sdbs/cgi-bin/re_index.cgi), (Accessed on 10 March 2017).
- Alpaslan, Y.B., Gökce, H., Alpaslan, G., Macit, M. (2015). Spectroscopic Characterization and Density Functional Studies of (Z)-1-[(2-methoxy-5-(trifluoromethyl) phenylamino) methylene] naphthalene-2(1H)-one, *Journal of Molecular Structure*, 1097, 171-180.
- Anderson, R.J., Bendell, D.J., Groundwater, P.W. (2004). *Organic Spectroscopic Analysis*, The Royal Society of Chemistry, Sanderland UK.
- Baran, J., Davydova, N.A. (2010). Infrared spectroscopy study of structural changes in glass-forming salol, *Physical Review E*, 031503.1-6.
- Becke, A.D. (1993). Density functional Thermochemistry. III. The Role of Exact Exchange. *The Journal of Chemical Physics*, 98, 5648-5652.
- Bellamy, L.J. (1975). *The Infrared Spectra of Complex Molecules*, 3rd ed. Wiley, New York.
- Bilgram, J.H., Dürig, U., Wächter, M., Seiler, P. (1982). Zone Refining and Structure Determination of Salol Crystals, *Journal of Crystal Growth*, 57, 1-5.
- Buyukuslu, H., Akdogan, M., Yildirim, G., Parlak, C. (2010). Ab Initio Hartree-Fock and Density Functional Theory Study on Characterization of 3-(5-methylthiazol-2-ylidiazonyl)-2-phenyl-1H-indole, *Spectrochimica Acta Part A: Molecular and Biomolecular Spectroscopy*, 75(4), 1362-1369.
- Ceylan, Ü., Tari, G.Ö., Gökce, H., Açar, E. (2016). Spectroscopic (FT-IR and UV-Vis) and Theoretical (HF and DFT) Investigation of 2-Ethyl-N-[(5-nitrothiophene-2-yl) methylidene] aniline, *Journal of Molecular Structure*, 1110, 1-10.
- Chase, H.M., Rudshteyn, B., Psciuk, B.T., Upshur, M.A., Strick, B.F., Thomson, R.J., Batista, V.S., Geiger, F.M. (2016). Assessment of DFT for Computing Sum Frequency Generation Spectra of an Epoxydiol and a Deuterated Isotopologue at Fused Silica/Vapor Interfaces, *The Journal of Physical Chemistry B*, 120(8), 1919-1927.
- Choi, Y.H., Na, B.H., Choi, Y.S., Rahman, M.S., Kim, M.R., Jee, J., Shin, J., Suh, J.W., Yoo, J.C. (2016). Anti-inflammatory Function of 4-Tert-butylphenyl Salicylate Through Down-Regulation of the NF-kappa B Pathway, *Archives of Pharmacal Research*, 39(3), 429-436.
- Colthup, N.B., Daly, L.H., Wiberley, E. (1964). *Introduction to Infrared and Raman Spectroscopy*, Academic Press, New York.
- Dennington, R., Keith, T., Millam J. (Eds.). (2009). *GaussView, Version 5*, Semicem Inc., Shawnee Mission KS.
- Ditchfield, R. (1974). Self-consistent Perturbation Theory of Diamagnetism. *Molecular Physics*, 27, 789-807.
- Dobashi, Y., Ohkatsu, Y. (2008). Dependence of Ultraviolet Absorbers' Performance on Ultraviolet Wavelength, *Polymer Degradation and Stability*, 93(2), 436-447.
- Frisch, M.J., Trucks, G.W., Schlegel, H.B., Scuseria, G.E., et al. (2009). *Gaussian 09, Revision C.01*, Gaussian, Inc., Wallingford CT.
- Fukui, K. (1982). Role of Frontier Orbitals in Chemical Reactions, *Science*, 218, 747-754.
- Gottfried, C., Dutzer, M.J. (1961). Status of Investigations for Improving Weatherability of Linear Polyethylene and Copolymers, *Journal of Applied Polymer Science*, 5(17), 612-619.
- Hammond, R.B., Jones, M.J., Roberts, K.J., Kutzke, H., Klapper, H. (2002). A Structural Study of Polymorphism in Phenyl Salicylate: Determination of the Crystal Structure of a Meta-Stable Phase from X-Ray Powder Diffraction Data Using a Direct Space Systematic Search Method, *Zeitschrift-fur-Kristallographie*, 217(9), 484-491.
- Hanuza, J., Sasiadek, W., Michalski, J., Lorenc, J.,

- Maczka, M., Kaminskii, A.A., Butashin, A.V., Klapper, H., Hulliger, J., Mohmed, A.F.A. (2004). Polarized Raman and Infrared Spectra of the Salol Crystal-Chemical Quantum Calculations of the Vibrational Normal Modes, *Vibrational Spectroscopy*, 34(2), 253-268.
- Hutchinson, E. (2003). An aspirin a day, *Nature Reviews Cancer*, 3(8), 552-552.
- Kalampounias, A.G., Yannopoulos, S.N., Steffen, W., Kirillova, L.I., Kirillov, S.A. (2003). Short-time Dynamics of Glass-Forming Liquids: Phenyl Salicylate (Salol) in Bulk Liquid, Dilute Solution, and Confining Geometries, *The Journal of Chemical Physics*, 118(18), 8340-8349.
- Kanagathara, N., Marchewka, M.K., Drozd, M., Gunasekaran, S., Rajakumar, P.R., Anbalagan, G. (2015). Structural and Vibrational Spectroscopic Studies on Charge Transfer and Ionic Hydrogen Bonding Interactions of Melaminium Benzoate Dihydrate, *Spectrochimica Acta Part A: Molecular and Biomolecular Spectroscopy*, 145, 394-409.
- Kasumov, V.T., Köksal, F. (2002). Synthesis, Spectroscopic Characterization and EPR Studies on Electron Transfer Reactions of Bis [N-(2,5-di-tert-butylphenyl) salicylaldiminato] copper Complexes with PPh<sub>3</sub>, *Spectrochimica Acta Part A: Molecular and Biomolecular Spectroscopy*, 58(10), 2199-2211.
- Kavitha, T., Velraj, G. (2016). Structural, Spectroscopic (FT-IR, FT-Raman, NMR) and Computational Analysis (DOS, NBO, Fukui) of 3,5-dimethylisoxazole and 4-(chloromethyl)-3,5-dimethylisoxazole: A DFT Study, *Journal of Theoretical and Computational Chemistry*, 15(05), 1650039.
- Lee, C., Yang, W., Parr, R.G. (1988). Development of the Colle-Salvetti Correlation-Energy Formula into a Functional of the Electron Density, *Physical Review B*, 37, 785-789.
- London, F. (1937). Théorie Quantique Des Courants Interatomiques Dans Les Combinaisons Aromatiques, *Journal de Physique et le Radium*, 8, 397-409.
- Schmitt, R.G., Hirt, R.C. (1960). Investigation of the Protective Ultraviolet Absorbers in a Space Environment. I. Rate of Evaporation and Vapor Pressure Studies, *Journal of Polymer Science Part A: Polymer Chemistry*, 45(145), 35-47.
- Madan, R.K., Levitt, J. (2014). A Review of Toxicity from Topical Salicylic Acid Preparations, *Journal of The American Academy of Dermatology*, 70(4), 788-792.
- Nalwa, H.S., Miyata, S. (1997). *Nonlinear Optics of Organic Molecules and Polymers*, CRC Press, Boca Raton, FL.
- Newland, G.C., Tambllyn, J.W. (1964). Mechanism of Ultraviolet Stabilization of Polymers by Aromatic Salicylates, *Journal of Applied Polymer Science*, 8(5), 1949-1956.
- Nyquist, R.A., Putzig, C.L., Clark, T.L., McDonald, A.T. (1996). Infrared Study of Intramolecularly Hydrogen Bonded Aromatic Carbonyl Containing Compounds in Various Solvents, *Vibrational Spectroscopy*, 12(1), 93-102.
- Ortiz, A.F.C., López, A.S., Ríos, A.G., Cabezas, F.C., Correa, C.E.R. (2015). Experimental and Theoretical Studies on the Structure and Spectroscopic Properties of (E)-1-(2-aminophenyl)-3-(pyridine-4-yl) prop-2-en-1-one, *Journal of Molecular Structure*, 1098, 216-228.
- Öztürk, N., Gökce, H. (2017). Structural and Spectroscopic (FT-IR and NMR) Analyses on (E)-pent-2-enoic Acid, *Bilge International Journal of Science and Technology Research*, 1(1), 9-15.
- Pavia, D.L., Lampman, G.M., Kriz, G.S., Vyvyan, J.R. (2009). *Introduction to Spectroscopy*, Brooks/Cole Cengage Learning, USA.
- Perdew, J.P., Burke, K., Wang, Y. (1996). Generalized Gradient Approximation for the Exchange-Correlation Hole of a Many-Electron System, *Physical Review B*, 54(23), 16533.
- Pubchem, (2017). U.S. National Library of Medicine, Open Chemistry Database, [https://pubchem.ncbi.nlm.nih.gov/compound/d/4-tert-Butylphenyl\\_salicylate](https://pubchem.ncbi.nlm.nih.gov/compound/d/4-tert-Butylphenyl_salicylate) (Accessed on 10 March 2017).
- Raja, G., Saravanan, K., Sivakumar, S. (2013). Structure and Vibrational Spectroscopic Studies of 1-Naphthol: Density Functional Theory Calculations, *International Journal on Applied Bioengineering*, 7(1), 45-56.

- Silverstein, R.M., Webster, F.X. (1998). Spectroscopic Identification of Organic Compound, 6nd ed., John Willey & Sons, New York.
- Stuart, B.H. (2004). Infrared Spectroscopy: Fundamentals and Applications, JohnWilley & Sons, England.
- Temel, E., Alaşalvar, C., Gökçe, H., Güder, A., Albayrak, Ç., Alpaslan, Y.B., Alpaslan, G., Dilek, N. (2015). DFT Calculations, Spectroscopy and Antioxidant Activity Studies on (E)-2-nitro-4-[(phenylimino) methyl] phenol, Spectrochimica Acta Part A: Molecular and Biomolecular Spectroscopy, 136, 534-546.
- Wade Jr, L.G. (2006). Organic Chemistry, Pearson Prentice Hall, New Jersey.
- Wienhold, F., Landis, C.R. (2005). Valency and Bonding-A Natural Bond Orbital Donor-Acceptor Perspective, Cambridge University Press, New York.
- Wolinski, K., Himton, J.F., Pulay, P. (1990). Efficient Implementation of the Gauge-Independent Atomic Orbital Method for NMR Chemical Shift Calculations, Journal of the American Chemical Society, 112, 8251-8260.
- Yanai, T., Tew, D.P., Handy, N.C. (2004). A New Hybrid Exchange-Correlation Functional Using the Coulomb-Attenuating Method (CAM-B3LYP), Chemical Physics Letters, 393(1), 51-57.

## Infrared and NMR Spectral Analyses and Computational Studies of 2-amino-3-methylbenzoic Acid

Muhammet Hakkı Yıldırım<sup>1\*</sup>

**Abstract:** Detailed infrared spectrum in gas phase, NMR spectra analyses and theoretical studies of 2-amino-3-methylbenzoic acid were performed with DFT/B3LYP/6-311G+(2d,p) level of method in Gaussian 09W. Ground state molecular geometries of monomeric and dimeric structures were calculated in vacuum and compared to the experimental XRD results. Potential energy surface graphics of the proton transfer and torsional tautomerism process were obtained. Also, HOMA aromaticity changing graphics were drowned in mentioned process. The IR band assignments and the decompositions of potential energy for each band were done using theoretical calculations. <sup>1</sup>H and <sup>13</sup>C NMR chemical shifts analyses were performed by using GIAO NMR calculations with SCRF solvent model.

**Keywords:** Anthranilic acid, FT-IR, NMR, DFT, HOMA analysis

### 1. Introduction

Anthranilic or aminobenzoic acid and its derivatives are used as a starting material for biological and chemical active material synthesis. Gichner et al. showed that the antimutagenic capacities of 2-, 3-, 4-aminobenzoic compounds depend on the location of amino group (Gichner et al., 1994). Detailed vibrational spectrum analysis and molecular characterizations with theoretical calculations of mentioned compounds were done by Samsonowicz et al. (Samsonowicz et al., 2005). Syahrani et al. reported that the biotransformation and structure elucidation of some aminobenzoic acid compound in suspension cultures of *S. mammosum* (Syahrani et al., 1999). The effect of p-aminobenzoic acid on the uptake of thymidine and uracil by *Escherichia coli* was published by Richards and Xing (Richards and Xing, 1995). X Ray crystal structure of title compound was published by Brown et al. (Brown and Marsh, 1963). Newman et al. obtained 3 Methylbenzylene from the reaction of 2-amino-3-methylbenzoic acid with 2-hydroxyiminoacet-o-toluidide (Newman and Kannan, 1976). Gerber et al. published synthesis and crystal structure a Rhenium(V) metal

complex which is obtained from the reaction of the cis  $\text{ReO}_2^+$  core with 2-amino-3-methylbenzoic acid (Gerber et al., 2003). Dong et al. prepared biological active compounds by using 2-amino-3-methylbenzoic acid (Dong et al., 2009).

Spectroscopic characterization with supported computational studies of organic compounds attract attention of researchers. Computational studies help us to better understand electronic properties of compounds, such as HOMO-LUMO (Öztürk and Gökçe, 2017), NLO (Eryılmaz et al., 2016), tautomeric equilibrium (Yıldırım et al., 2016) and prototropy (Albayrak Kaştaş et al., 2017). As a part of our ongoing studies about the derivatives of aminobenzoic acid (Yıldırım et al., 2015), we report spectroscopic and theoretical studies of 2-amino-3-methylbenzoic acid. To our knowledge, there is no study about its spectroscopic and computational characterization.

### 2. Material and Method

Initial geometry for optimization was directly taken from X-RD results (Brown and Marsh, 1963). All the calculations were performed on Gaussian 09W

<sup>1</sup>Giresun University, Dereli Vocational School, 28950, Giresun, Turkey

\*Corresponding author: [hakki.yildirim@giresun.edu.tr](mailto:hakki.yildirim@giresun.edu.tr)

Citation: Yıldırım, M. H. (2018). Infrared and NMR Spectral Analyses and Computational Studies of 2-amino-3-methylbenzoic Acid. *Bilge International Journal of Science and Technology Research*, 2 (1):74-82.

(Frisch et al., 2009) software with DFT theory. In the calculations, B3LYP hybrid functional (Becke, 1993) with 6-311G+(2d,p) basis set was used. For NMR calculations, GIAO method (Wolinski et al., 1990) was selected and solvent modelled with SCRF theory (Cossi et al., 2003; Tomasi et al., 2005). Because of title compound was found a dimeric structure in crystal phase, we performed the geometry optimizations for monomeric and dimeric structures.

### 3. Results and Discussions

#### 3.1. Molecular structure

Optimized molecular structure with atom labeled scheme was given in Figure 1 and intra-molecular hydrogen bonds were presented with dashed lines.

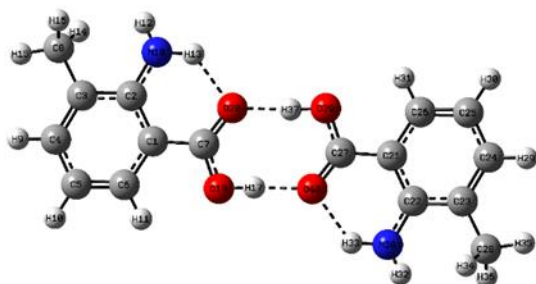


Figure 1. Optimized dimeric structure

To measure our computational level accuracy, experimental XRD and calculated bond lengths and angles were compared and a summary given in Table 1. Root mean square error values given in table were calculated for all bond lengths and angles.

As seen in Table 1, a good correlation can be found in between both monomeric and dimeric structure with the experimental one. The biggest differences between the experimental and calculated structure were occurred at atoms involved in a hydrogen bond. In the amino group, N-H bond lengths are found 0.88Å-0.91Å for x-ray while 1.01Å-1.00Å for calculated structure. Similarly, C7-O19-H17 bond angle was found 105.8° for monomeric structure while 110.2° for dimeric structure. In the inter-molecular hydrogen bond, hydrogen acceptor distance was 1.73Å for XRD while 1.66Å for dimeric structure. To make an overall comparison, the Root Mean Square Errors (RMSE) were given in Table 1. In the bond length, RMSE was 0.014 Å for both monomer and dimer structures, nearly equal to XRD deviation limit. 0.3° values were

founded for angles showed that perfect match between the XRD and simulated structure, the exception of the C-O-H bond angle. Consequently, calculations of molecular structure are very successful when considering experimental values are taken in crystal structure while calculated values are taken in vacuum media

Table 1. A comparison table of geometric bond parameters of 2-amino-3-methylbenzoic acid

Bond Lengths (Å)	Exp.*	Monomer	Dimer
C7-O20	1.24	1.22	1.24
C7-O19	1.32	1.36	1.32
O19-H17	0.93	0.97	1.00
C2-N18	1.37	1.37	1.37
N18-H13	0.88	1.01	1.01
N18-H12	0.91	1.00	1.00
H17-O40	1.73	-	1.66
H13...O20	2.05	1.91	1.91
O19...O40	2.65	-	2.66
RMSE**		0.014	0.014
Bond Angles (°)			
C7-O19-H17	108.1	105.8	110.2
C1-C7-O19	114.7	114.0	115.1
C1-C7-O20	124.5	126.2	123.7
O19-C7-O20	120.8	119.8	121.2
C7-C1-C2	121.5	120.4	121.5
O19-H17...O40	170.0		176.7
N18-H13...O20	131.0	130.9	130.3
RMSE**		0.30	0.28
Dihedral Angles(°)			
O20-C7-O19-H17	1.3	0.0	0.0
C1-C7-O19-H17	-179.1	179.7	179.6
C3-C2-N18-H12	-7.2	-15.8	-16.4
O20-C7-C1-C6	176.9	178.3	178.1
O19-C7-C1-C2	177.9	179.4	179.2
RMSE**		0.37	0.39

\*(Brown and Marsh, 1963), \*\*Calculated for the all parameters

There is well-known fact that, 2-aminobenzoic acid derivatives show two type transformations which are the proton exchange in dimers (Monte and Hillesheim, 2001) and the rotation of carboxyl acid group (Fleisher et al., 2011). To find energy gap values between these transformations, relaxed potential energy surface scan calculations were performed. In dimeric structure, O19-H17...O40 pathway selected as a redundant coordinate for a relaxed scan calculation and proton was migrated of 0.05 Å step size.

Relative energies were calculated with respect to minimum energy and obtained potential energy

graphic was presented in Figure 2. Total energy of the dimer increased after the proton transfer process because of changing structure of N-H...O intramolecular hydrogen bond. Potential energy barrier for this transformation was found as 7.00 kcal/mol.

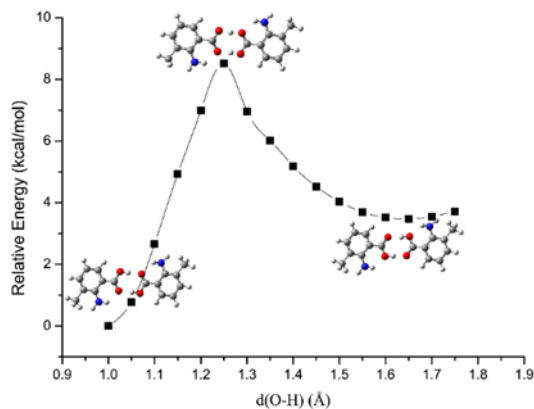


**Figure 2.** A relative energy graph for the proton transfer

Aromaticity indices were used to better understand the movement of  $\pi$  electrons in the ring. Bond parameter based aromaticity criteria was introduced by Kruszewski and Krygowski as HOMA (Harmonic Oscillator Model of Aromaticity). HOMA index of a ring is calculated by using the following equation:

$$HOMA = 1 - \frac{1}{n} \sum_{i=1}^n \alpha_i (R_i - R_{i,opt})^2 \quad (1)$$

where  $n$  is the number of bonds in the ring,  $\alpha_i$  is a normalization constant,  $R_i$  is the bond length and  $R_{i,opt}$  optimized bond length (Kruszewski and Krygowski, 1972). For the aromatic ring, HOMA value is expected in the range of 0.90-0.99 while for non-aromatic ring is in the range of 0.50-0.80 (Krygowski, 1993). HOMA indices were calculated for each step of scan calculations and summarized in Figure 3.

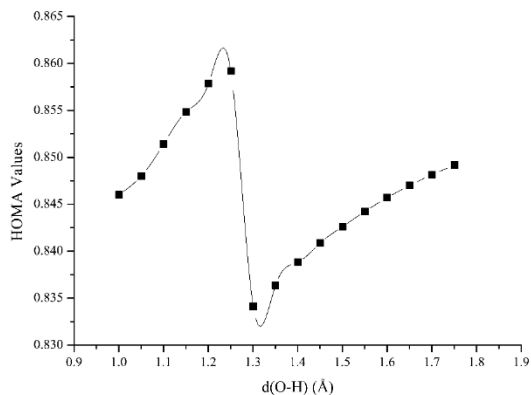


**Figure 3.** HOMA changing graphic during the proton transfer

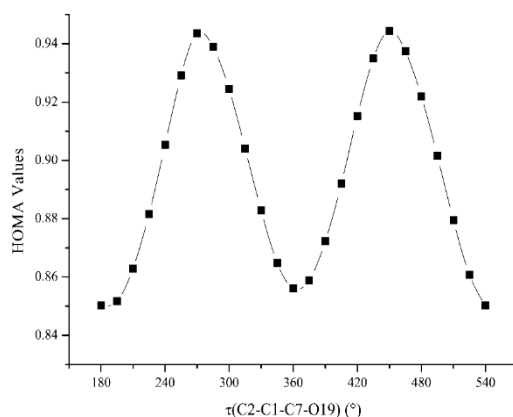


**Figure 4.** A torsional scan energy graph for the rotation

To draw a torsional potential energy profile for  $\tau(C2-C1-C7-O19)$  torsion angle, a relaxed potential energy scan with the step size of  $15^\circ$  was done. Figure 4 represents the results of this scan calculation. Relative energies in the figure were calculated with respect to minimum energy.

As shown in Figure 4, the torsional energy barrier is 12.68 kcal/mol. Also, the transformation of intramolecular hydrogen bond from NH-O to NH OH form increases the total energy by 3.23 kcal/mol. Also HOMA values are wagging to parallel of energy changing, as given in Figure 5.

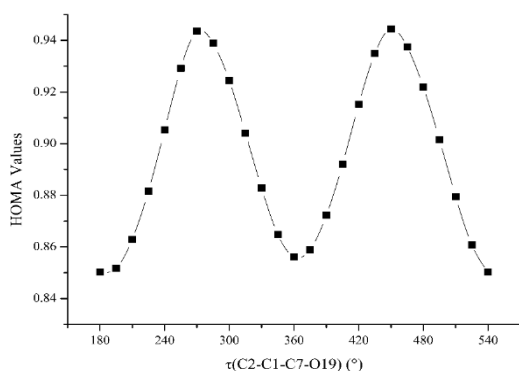


**Figure 5.** HOMA changing graphic during the proton transfer

### 3.2. Infrared spectroscopy analysis

Experimental gas phase IR spectrum data of the title compound were obtained from NIST Chemistry WebBook (Linstrom and Mallard, 2001) website. Due to overestimation problems of DFT calculations, calculated IR wavenumbers were scaled with two scale factor; 0.989 for lower than  $1600\text{ cm}^{-1}$  and 0.954 for higher than  $1600\text{ cm}^{-1}$  as in Wang's study (Wang et al., 2015). Experimental and calculated monomeric and dimeric IR spectra which were obtained in gas phase were given in Figure 6.

Due to the experimental IR spectrum was recorded in  $4000\text{-}600\text{ cm}^{-1}$ , Figure 1(a) has an interruption at  $600\text{-}400\text{ cm}^{-1}$  region. As seen in figure, there is a good coherence between the experimental and calculated spectra. Therefore, band assignments with calculation of their PED values were made by VEDA (Jamróz, 2013) software and the results were given in Table 2, comparatively.

Hydroxyl group stretching vibration peak has been located at  $3584\text{ cm}^{-1}$  and calculated as  $3595\text{ cm}^{-1}$ . The experimental peaks at  $3520\text{ cm}^{-1}$  and  $3383\text{ cm}^{-1}$  can be attributed to symmetric and asymmetric stretching vibrations of amino group. Theoretical values of amino group stretching vibrations are  $3531\text{ cm}^{-1}$   $3368\text{ cm}^{-1}$ . Aromatic C-H stretching vibrations are found at  $3085\text{ cm}^{-1}$ ,  $3049\text{ cm}^{-1}$  and  $3017\text{ cm}^{-1}$  in the experimental spectrum while their calculated values are  $3065\text{ cm}^{-1}$ ,  $3041\text{ cm}^{-1}$ ,  $3011\text{ cm}^{-1}$ . Methyl group stretching vibrations are in the region of  $2982\text{-}2879\text{ cm}^{-1}$ . The most intense peak ( $1725\text{ cm}^{-1}$ ) in the spectrum corresponds to the C=O stretching vibration. This peak caused maximum deviation between the experimental and calculated spectra with  $\Delta\nu$  is  $75\text{ cm}^{-1}$ , which may be originated from steric effect in gas phase. Other intense peaks founded at  $1166\text{ cm}^{-1}$  and  $1079\text{ cm}^{-1}$  arise from in-plane and out of plane vibrations of hydroxyl group (Gardner and Wright, 2011).

Comparing to the IR spectrum of 2-aminobenzoic acid in solid phase (Samsonowicz et al., 2005), the major shifts take place in the carboxyl group, due to the aminobenzoic acid derivatives prefer dimeric structure in solid state while IR spectrum of the title compound was obtained in gas phase. Stretching vibration of C=O group was assigned  $1670\text{ cm}^{-1}$  for 2-aminobenzoic acid while  $1725\text{ cm}^{-1}$  for the title compound. In the experimental spectrum of 2-amino-3-benzoic acid, the  $\nu(\text{C-N})$  vibration was found at  $1319\text{ cm}^{-1}$ , which is calculated as  $1307\text{ cm}^{-1}$ , while the same vibration was found at  $1326\text{ cm}^{-1}$  for 2-aminobenzoic acid.  $\nu(\text{C-OH})$  vibration peak located at  $1261\text{ cm}^{-1}$  (exp.)  $1213\text{ cm}^{-1}$  (calc.) and  $1253\text{ cm}^{-1}$  (2-aminobenzoic acid).

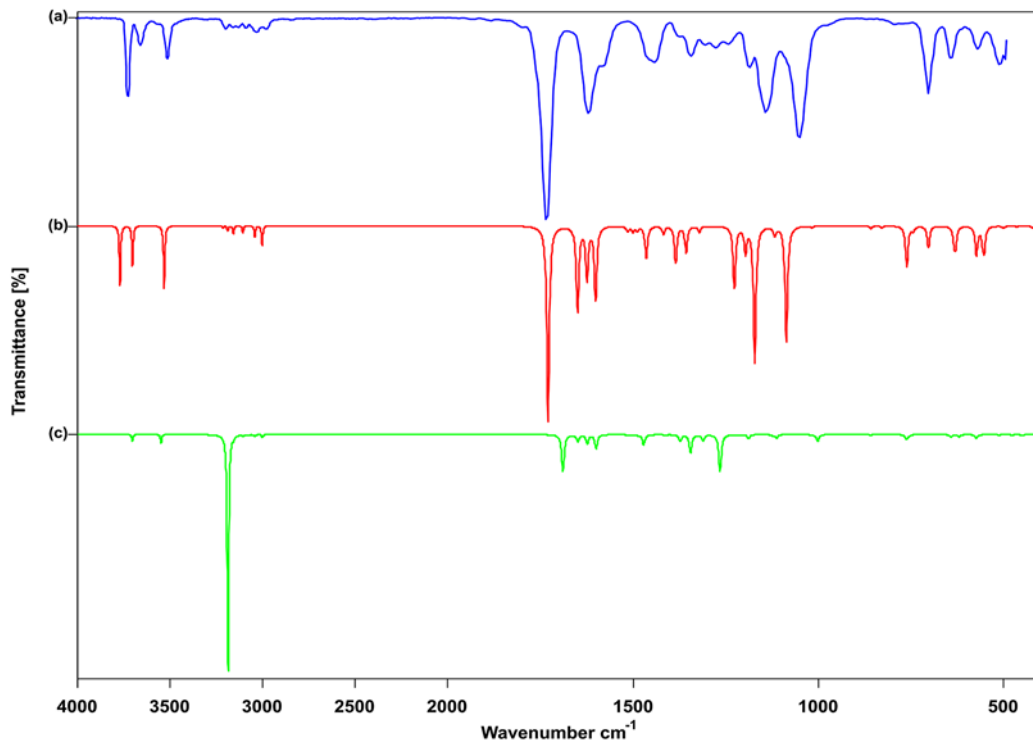


**Figure 6.** Experimental (a) and calculated monomeric (b), dimeric (c) gas phase IR spectra of the compound



**Table 2.** Infrared band assignments with their PED values of 2-amino-3-methylbenzoic acid

Exp. Freq	Calc. Freq.	Calc. Int.	Assignments with PED values (Only major contributions)
3584	3595	105	$\nu(\text{O19-H17})(\%100)$
3520	3531	70	$\nu(\text{N18-H12})(\%84) + \nu(\text{N18-H13})(\%15)$
3383	3368	111	$\nu(\text{N18-H12})(\%15) + \nu(\text{N18-H13})(\%84)$
3085	3065	3	$\nu(\text{C6-H11})(\%91)$
3047	3041	9	$\nu(\text{C5-H10})(\%85)$
3019	3011	13	$\nu(\text{C4-H9})(\%93)$
2982	2962	13	$\nu(\text{C8-H15})(\%91)$
2929	2901	19	$\nu(\text{C8-H14})(\%35) + \nu(\text{C8-H16})(\%64)$
2879	2863	35	$\nu(\text{C8-H14})(\%62) + \nu(\text{C8-H16})(\%30)$
1725	1650	346	$\nu(\text{O20-C7})(\%68)$
1618	1574	149	$\nu(\text{C4-C3})(\%12) + \nu(\text{C1-C6})(\%14) + \beta(\text{H13-N18-H12})(\%26)$
1582	1550	127	$\nu(\text{C6-C5})(\%14) + \beta(\text{H13-N18-H12})(\%31)$
	1527	92	$\nu(\text{C5-C4})(\%16) + \beta(\text{H13-N18-H12})(\%19)$
	1498	10	$\beta(\text{H14-C8-H16})(\%29) + \beta(\text{H15-C8-H14})(\%13)$
	1484	9	$\nu(\text{C1-C6})(\%12) + \beta(\text{H9-C4-C5})(\%10) + \beta(\text{H10-C5-C6})(\%22)$
	1472	8	$\beta(\text{H15-C8-H14})(\%38) + \beta(\text{H16-C8-H15})(\%42) + \tau(\text{H15-C8-C3-C4})(\%12)$
1449	1448	58	$\nu(\text{N18-C2})(\%17) + \beta(\text{H11-C6-C1})(\%10) + \beta(\text{H14-C8-H16})(\%14)$
	1403	14	$\beta(\text{H14-C8-H16})(\%32) + \beta(\text{H15-C8-H14})(\%25) + \beta(\text{H16-C8-H15})(\%28)$
1384	1370	65	$\nu(\text{C6-C5})(\%12) + \nu(\text{O19-C7})(\%13) + \nu(\text{C7-C1})(\%14) + \beta(\text{H17-O19-C7})(\%15)$
1355	1342	46	$\nu(\text{C4-C3})(\%20) + \nu(\text{C2-C3})(\%10)$
1319	1307	11	$\nu(\text{N18-C2})(\%20) + \beta(\text{H9-C4-C5})(\%31)$
1292	1282	2	$\nu(\text{C1-C6})(\%20) + \nu(\text{N18-C2})(\%12) + \beta(\text{H11-C6-C1})(\%25)$
1261	1213	107	$\nu(\text{C8-C3})(\%24) + \beta(\text{H17-O19-C7})(\%13) + \beta(\text{C1-C6-C5})(\%10)$
1206	1184	46	$\nu(\text{C6-C5})(\%11) + \beta(\text{H17-O19-C7})(\%10) + \beta(\text{H10-C5-C6})(\%41)$
1166	1159	239	$\nu(\text{O19-C7})(\%13) + \beta(\text{H17-O19-C7})(\%20) + \beta(\text{H12-N18-C2})(\%14) + \beta(\text{H10-C5-C6})(\%11) + \beta(\text{H11-C6-C1})(\%12)$
	1106	15	$\nu(\text{C6-C5})(\%22) + \nu(\text{C5-C4})(\%27) + \beta(\text{H9-C4-C5})(\%20)$
1079	1075	204	$\nu(\text{O19-C7})(\%33) + \beta(\text{H12-N18-C2})(\%25) + \beta(\text{C1-C6-C5})(\%13)$
	1053	1	$\beta(\text{H15-C8-H14})(\%11) + \beta(\text{H16-C8-H15})(\%11) + \tau(\text{H15-C8-C3-C4})(\%55) + \gamma(\text{C8-C4-C2-C3})(\%10)$
	1006	3	$\beta(\text{H14-C8-H16})(\%10) + \tau(\text{H14-C8-C3-C4})(\%27) + \tau(\text{H16-C8-C3-C4})(\%26)$
	963	0	$\tau(\text{H10-C5-C6-C1})(\%24) + \tau(\text{H11-C6-C1-C7})(\%43) + \tau(\text{C1-C6-C5-C4})(\%16)$
	928	0	$\tau(\text{H9-C4-C5-C6})(\%53) + \tau(\text{H11-C6-C1-C7})(\%26)$
891	870	1	$\nu(\text{C2-C3})(\%13) + \nu(\text{O19-C7})(\%13) + \nu(\text{C7-C1})(\%13) + \nu(\text{C8-C3})(\%20) + \beta(\text{C5-C4-C3})(\%10)$
836	849	5	$\nu(\text{N18-C2})(\%14) + \beta(\text{C2-C3-C4})(\%10) + \beta(\text{C6-C5-C4})(\%35) + \beta(\text{C5-C4-C3})(\%14)$
	820	3	$\tau(\text{H10-C5-C6-C1})(\%17) + \gamma(\text{O20-C1-O19-C7})(\%42) + \gamma(\text{C7-C6-C2-C1})(\%14) + \gamma(\text{N18-C3-C1-C2})(\%11)$
750	753	72	$\tau(\text{H9-C4-C5-C6})(\%13) + \tau(\text{H10-C5-C6-C1})(\%50) + \tau(\text{H11-C6-C1-C7})(\%19)$
	736	9	$\tau(\text{C2-C3-C4-C5})(\%14) + \gamma(\text{O20-C1-O19-C7})(\%29) + \gamma(\text{N18-C3-C1-C2})(\%22)$
	696	20	$\beta(\text{O20-C7-O19})(\%32)$
624	627	37	$\beta(\text{O20-C7-O19})(\%12) + \tau(\text{H13-N18-C2-C3})(\%45)$
599	623	34	$\beta(\text{O20-C7-O19})(\%16) + \beta(\text{C5-C4-C3})(\%10) + \tau(\text{H13-N18-C2-C3})(\%36)$
	568	51	$\tau(\text{H17-O19-C7-C1})(\%52) + \tau(\text{C1-C6-C5-C4})(\%11) + \gamma(\text{N18-C3-C1-C2})(\%13)$
	551	16	$\beta(\text{O19-C7-C1})(\%15) + \tau(\text{H17-O19-C7-C1})(\%12)$
	547	43	$\tau(\text{H17-O19-C7-C1})(\%19) + \tau(\text{C1-C6-C5-C4})(\%16) + \gamma(\text{N18-C3-C1-C2})(\%10)$
	496	4	$\nu(\text{C8-C3})(\%13) + \beta(\text{C2-C3-C4})(\%16) + \beta(\text{C7-C1-C6})(\%12)$
	460	1	$\tau(\text{H17-O19-C7-C1})(\%13) + \gamma(\text{C7-C6-C2-C1})(\%16) + \gamma(\text{C8-C4-C2-C3})(\%22)$
	418	3	$\beta(\text{N18-C2-C1})(\%40) + \beta(\text{O19-C7-C1})(\%20)$
	375	14	$\nu(\text{C7-C1})(\%18) + \beta(\text{C6-C5-C4})(\%11) + \beta(\text{C1-C6-C5})(\%24)$
	346	5	$\beta(\text{O19-C7-C1})(\%17) + \beta(\text{C8-C3-C2})(\%50)$
	300	138	$\tau(\text{H12-N18-C2-C3})(\%56)$
	266	6	$\beta(\text{C6-C5-C4-C3})(\%11) + \gamma(\text{C7-C6-C2-C1})(\%13) + \gamma(\text{N18-C3-C1-C2})(\%22) + \gamma(\text{C8-C4-C2-C3})(\%31)$
	230	3	$\beta(\text{O19-C7-C1})(\%19) + \beta(\text{C7-C1-C6})(\%49) + \beta(\text{C8-C3-C2})(\%12)$
	204	10	$\tau(\text{H14-C8-C3-C4})(\%33) + \tau(\text{H15-C8-C3-C4})(\%17) + \tau(\text{H16-C8-C3-C4})(\%35)$
	198	7	$\tau(\text{C2-C3-C4-C5})(\%35) + \gamma(\text{C7-C6-C2-C1})(\%19) + \gamma(\text{C8-C4-C2-C3})(\%13)$
	106	1	$\tau(\text{C6-C5-C4-C3})(\%35) + \tau(\text{C1-C6-C5-C4})(\%18) + \tau(\text{O19-C7-C1-C6})(\%13) + \gamma(\text{C7-C6-C2-C1})(\%15)$
	72	1	$\tau(\text{O19-C7-C1-C6})(\%77)$
RMSE	25		

v: Stretching,  $\beta$ : In-plane bending,  $\tau$ : Torsion,  $\gamma$ : Out-of-plane bending

### 3.3. NMR analysis

Experimental  $^1\text{H}$  and  $^{13}\text{C}$  NMR spectra of 2-amino-3-methoxybenzoic acid were obtained from AIST database (AIST, 2017) which were sample saturated in DMSO-d<sub>6</sub> and data acquired with an 89.56 MHz instrument. NMR chemical shifts of 2-aminobenzoic acid (Samsonowicz et al., 2005), 2-amino-3-methylbenzoic acid and calculated spectra were given in Table 3. In the experimental spectra of 2-amino-3-methylbenzoic acid, there was only a small shift on C3 atom, which methyl group is attached to C3, when compared to 2-aminobenzoic acid NMR spectra. On the other hand, there was a systematic small down-field shift in calculated spectra.

**Table 3.** Chemical shifts for 2-amino benzoic acid and 2-amino-3-methylbenzoic acid

Atom	$\delta_{\text{exp}}^*$	$\delta_{\text{exp}}^{**}$	$\delta_{\text{calc}}$
C1	109.69	109.39	109.89
C2	151.58	149.63	156.72
C3	114.69	122.91	128.37
C4	133.82	134.33	140.93
C5	116.42	114.27	117.56
C6	131.26	128.97	134.76
C7	169.69	169.96	176.16
C8		17.41	17.69
H9	7.21	7.16	7.56
H10	6.50	6.48	6.77
H11	7.70	7.63	8.11
H14, 15, 16	-	2.11	2.13

\*2-aminobenzoic acid (Samsonowicz et al., 2005),

\*\*2-amino-3-methylbenzoic acid (AIST, 2017)

These deviations can be reduced by using empirical scale factor proposed from Forsyth and Sebag (Forsyth and Sebag, 1997), but in this case was not necessary. Due to carboxyl and amino protons are constantly changing from one atom to another atom in solvent media, their proton NMR peaks are generally broad or lose (Anderson et al., 2004). Moreover, their shifts are depending on the solvent, concentration and temperature. Therefore, their peaks could not be assigned as in 2-aminobenzoic acid compound (Samsonowicz et al., 2005).

### 4. Conclusions

Geometry optimizations of title compound show a good agreement with experimental XRD values. Potential energy scan calculations with HOMA aromaticity index changing graphics were obtained.

Therefore, we decided to the selected theoretical method was sufficient. 2-amino-3-benzoic acid consists of 20 atoms which has 54 normal modes from 3N-6 rule. All the normal modes were assigned with their PED values. NMR spectra chemical shifts were not fully resolved due to the nature of both acidic and basic group included in the compound.

### References

- AIST, (2017). National Institute of Advanced Industrial Science and Technology Spectral Database for Organic Compounds, SDBS. <http://sdb.db.aist.go.jp/sdb/> (Accessed on: 09.09.2017).
- Albayrak Kaştaş, Ç., Kaştaş, G., Güder, A., Gür, M., Muğlu, H., Büyükgüngör, O. (2017). Investigation of two o-hydroxy Schiff bases in terms of prototropy and radical scavenging activity. *Journal of Molecular Structure*, 1130: 623–632.
- Anderson, R.J., Bendell, D.J., Groundwater, P.W. (2004). Nuclear magnetic resonance spectroscopy. Abel, E.W. (Ed.) *Organic Spectroscopic Analysis*. Cambridge, England.
- Becke, A.D. (1993). Density-functional thermochemistry. III. The role of exact exchange. *The Journal of Chemical Physics*, 98(7): 5648.
- Brown, G.M., Marsh, R.E. (1963). The crystal and molecular structure of 2-amino-3-methylbenzoic acid. *Acta Crystallographica*, 16(3): 191–202.
- Cossi, M., Rega, N., Scalmani, G., Barone, V. (2003). Energies, structures, and electronic properties of molecules in solution with the C-PCM solvation model. *Journal of Computational Chemistry*, 24(6): 669–681.
- Dong, W., Xu, J., Xiong, L., Liu, X., Li, Z. (2009). Synthesis, structure and biological activities of some novel anthranilic acid esters containing N-Pyridylpyrazole. *Chinese Journal of Chemistry*, 27(3): 579–586.
- Eryılmaz, S., Gül, M., İnkaya, E., İdil, Ö., Özdemir, N. (2016). Synthesis, crystal structure analysis, spectral characterization, quantum chemical calculations, antioxidant and antimicrobial activity of 3-(4-chlorophenyl)-3a,4,7,7a-tetrahydro-4,7-

- methanobenzo[d]isoxazole. *Journal of Molecular Structure*, 1122: 219–233.
- Fleisher, A.J., Morgan, P.J., Pratt, D.W. (2011). High-Resolution electronic spectroscopy studies of meta-aminobenzoic acid in the gas phase reveal the origins of its solvatochromic behavior. *ChemPhysChem*, 12(10): 1808–1815.
- Forsyth, D.A., Sebag, A.B. (1997). Computed <sup>13</sup>C NMR chemical shifts via empirically scaled GIAO shieldings and molecular mechanics geometries. Conformation and configuration from <sup>13</sup>C shifts. *Journal of the American Chemical Society*, 119(40): 9483–9494
- Frisch, M.J., Trucks, G.W., Schlegel, H.B., Scuseria, G.E., Robb, M.A., Cheeseman, J.R., Scalmani, G., Barone, V., Mennucci, B., Petersson, G.A., Nakatsuji, H., Caricato, M., Li, X., Hratchian, H.P., Izmaylov, A.F., Bloino, J., Zheng, G., Sonnenberg, J.L., Hada, M., Ehara, M., Toyota, K., Fukuda, R., Hasegawa, J., Ishida, M., Nakajima, T., Honda, Y., Kitao, O., Nakai, H., Vreven, T., Montgomery Jr., J.A., Peralta, J.E., Ogliaro, F., Bearpark, M., Heyd, J.J., Brothers, E., Kudin, K.N., Staroverov, V.N., Kobayashi, R., Normand, J., Raghavachari, K., Rendell, A., Burant, J.C., Iyengar, S.S., Tomasi, J., Cossi, M., Rega, N., Millam, J.M., Klene, M., Knox, J.E., Cross, J.B., Bakken, V., Adamo, C., Jaramillo, J., Gomperts, R., Stratmann, R.E., Yazyev, O., Austin, A.J., Cammi, R., Pomelli, C., Ochterski, J.W., Martin, R.L., Morokuma, K., Zakrzewski, V.G., Voth, G.A., Salvador, P., Dannenberg, J.J., Dapprich, S., Daniels, A.D., Farkas, Ö., Foresman, J.B., Ortiz, J.V., Cioslowski, J., Fox, D.J. (2009). *Gaussian 09, Revision C.01*, Gaussian, Inc., Wallingford CT.
- Gardner, A.M., Wright, T.G. (2011). Consistent assignment of the vibrations of monosubstituted benzenes. *Journal of Chemical Physics*, 135(11): 1–18.
- Gerber, T.I.A., Luzipo, D., Mayer, P. (2003). The Reaction of the cis -ReO<sub>2</sub><sup>+</sup> core with 2-amino-3-methylbenzoic acid. *Journal of Coordination Chemistry*, 56(18): 1549–1554.
- Gichner, T., Voutsinas, G., Patrinely, A., Kappas, A., Plewa, M.J. (1994). Antimutagenicity of three isomers of aminobenzoic acid in *Salmonella typhimurium*. *Mutation Research/Fundamental and Molecular Mechanisms of Mutagenesis*, 309(2): 201–210.
- Jamróz, M.H. (2013). Vibrational Energy Distribution Analysis (VEDA): Scopes and limitations. *Spectrochimica Acta Part A: Molecular and Biomolecular Spectroscopy*, 114: 220–230.
- Kruszewski, J., Krygowski, T.M. (1972). Definition of aromaticity basing on the harmonic oscillator model. *Tetrahedron Letters*, 13(36): 3839–3842.
- Krygowski, T.M. (1993). Crystallographic studies of inter- and intramolecular interactions reflected in aromatic character of pi-electron systems. *Journal of Chemical Information and Modeling*, 33(1): 70–78.
- Linstrom, P.J., Mallard, W.G. (2001). NIST Chemistry webbook; NIST standard reference database No. 69. NIST Chemistry WebBook, (69): 20899.
- Monte, M.J.S., Hillesheim, D.M. (2001). Thermodynamic study of the sublimation of six aminomethylbenzoic acids. *The Journal of Chemical Thermodynamics*, 33(7): 745–754.
- Newman, M.S., Kannan, R. (1976). Reactions of 3-methylbenzynes with 2-substituted furans. Steric effects. *The Journal of Organic Chemistry*, 41(21): 3356–3359.
- Öztürk, N., Gökçe, H. (2017). Structural and spectroscopic (FT-IR and NMR) analyses on (E)-pent-2-enoic acid. *Bilge International Journal of Science and Technology Research*, 1(1): 9–15.
- Richards, M.R.E., Xing, D.K.L. (1995). The effect of p-aminobenzoic acid on the uptake of thymidine and uracil by *Escherichia coli*. *International Journal of Pharmaceutics*, 116(2): 217–221.
- Samsonowicz, M., Hrynaskiewicz, T., Świsłocka, R., Regulska, E., Lewandowski, W. (2005). Experimental and theoretical IR, Raman, NMR spectra of 2-, 3- and 4-aminobenzoic acids. *Journal of Molecular Structure*, 744(2005): 345–352.
- Syahrani, A., Ratnasari, E., Indrayanto, G., Wilkins, A. (1999). Biotransformation of o- and p-aminobenzoic acids and N-acetyl p-aminobenzoic acid by cell suspension

cultures of Solanum. *Phytochemistry*, 51(5): 615–620.

Tomasi, J., Mennucci, B., Cammi, R. (2005). Quantum mechanical continuum solvation models. *Chemical Reviews*, 105(8): 2999–3094.

Wang, Z., Chen, J., Li, L., Zhou, Z., Geng, Y., Sun, T. (2015). Detailed structural study of  $\beta$ -artemether: Density functional theory (DFT) calculations of Infrared, Raman spectroscopy, and vibrational circular dichroism. *Journal of Molecular Structure*, 1097: 61–68.

Wolinski, K., Hinton, J.F., Pulay, P. (1990). Efficient implementation of the gauge-independent atomic orbital method for NMR chemical shift calculations. *Journal of the American Chemical Society*, 112(23): 8251–8260.

Yıldırım, A.Ö., Yıldırım, M.H., Kaştaş, Ç.A. (2016). Studies on the synthesis, spectroscopic analysis and DFT calculations on (E) 4,6 dichloro 2 [(2 chlorophenylimino) methyl] 3 methoxyphenol as a novel Schiff's base. *Journal of Molecular Structure*, 1113: 1–8.

Yıldırım, M.H., Paşaoğlu, H., Odabaşoğlu, H.Y., Odabaşoğlu, M., Yıldırım, A.Ö. (2015). Synthesis, structural and computational characterization of 2-amino-3,5-diodobenzoic acid and 2-amino-3,5-dibromobenzoic acid. *Spectrochimica Acta Part A: Molecular and Biomolecular Spectroscopy*, 146: 50–60.

## Sapwood Area Related to Tree Size, Tree Age, and Leaf Area Index in *Cedrus libani*

Aylin Güney<sup>1</sup>

**Abstract:** Sapwood includes the water conducting part of the stem which transports water and minerals from roots to leaves. Studies using sap flow gauges have to determine the area of the sapwood in order to scale measured sap flow densities to the tree or stand level. The aim of this study was to investigate the relationship between sapwood area at breast height and other tree parameters which are easy to measure of the montane Mediterranean conifer *Cedrus libani*, including a total number of 92 study trees of different size and age. The study was conducted at four different stands situated between 1000 and 2000 m altitude in the Elmalı Cedar Research Forest of Antalya, SW-Turkey. Sapwood area of the study trees was determined by extracting two tree cores from opposite directions of the stem using an increment borer and by visually assessing the wet part of the core. Parameters measured besides sapwood area were diameter at breast height, stem radius without bark, sapwood depth, tree basal area, tree height, tree age, and projected crown area. Furthermore, at each stand, leaf area index (LAI) was determined using hemispherical photographs of the forest canopy. The most significant relationship was found between stem radius without bark and sapwood area ( $R^2$ : 0.94) followed by tree basal area and sapwood area ( $R^2$ : 0.90). Although it was the second best predictor, tree basal area should be used to estimate sapwood area when estimating stand transpiration since it can be measured faster and without giving damage to the tree. Mean sapwood area and mean site-specific LAI showed a significant positive correlation. The findings of this study can be used in ecophysiological studies when transpiration rates of *C. libani* are measured using sap flow gauges.

**Keywords:** Taurus cedar, sapwood width, sap flow, LAI.

### 1. Introduction

Sapwood is the living and water conducting portion of the stem which transports water and minerals from roots to leaves, and where to a lesser extent energy reserves are stored (Matyssek et al., 2010). With increasing age parenchyma cells die and tracheids and vessels lose their ability to conduct water (Plomion et al., 2001). The non-conductive part of the wood (heartwood) is often infiltrated by tannins which cause a change in color. The proportion between sapwood and heartwood of a stem's cross-section vary between tree species but also among individuals of the same species or a single individual (Matyssek et al., 2010). The amount of sapwood is also an indicator of tree health since stressed trees have less sapwood (Lehmann and Becker, 1993).

In the industrial context (e.g. lumber production), it is important to know about physical and technological properties of the sapwood because they differ from those of the heartwood (Longuetaud et al., 2006). In ecophysiological studies sapwood is an important parameter when measuring sap flow rates and transpiration of single trees or whole stands (Gebauer et al., 2008; Motzer et al., 2005; Phillips et al., 1996; Wullschleger et al., 2004). The amount of sapwood area to leaf area (or leaf biomass) is an indicator about the water conducting capacity of the sapwood in relation to transpiration demand, and about the photosynthetic production relative to respiratory costs (Longuetaud et al., 2006; Mäkelä et al., 1995; Rodriguez- Calcerrada et al., 2015). Several studies have investigated the relationship between sapwood area and other parameters in

<sup>1</sup>University of Hohenheim, Institute of Botany, Stuttgart, Germany.  
\* Corresponding author: [\\*aylinguney13@gmail.com](mailto:*aylinguney13@gmail.com)

Citation: Güney, A. (2018). Sapwood Area Related to Tree Size, Tree Age, and Leaf Area Index in *Cedrus Libani*. Bilge International Journal of Science and Technology Research, 2 (1): 83-91.

various tree species, especially from temperate forests (Ford et al., 2004; Gebauer et al., 2008; Long and Dean, 1986). In *Picea abies* (L.) Karst. for example (Longuetaud et al., 2006), a high positive correlation was found between sapwood width and tree height, and diameter at breast height (DBH). Until now, no study was found that investigated the relationship between sapwood area and tree size, or between sapwood area and tree age of *Cedrus libani* A. Rich.

*C. libani* (Taurus cedar) is a drought tolerant and cold-resistant evergreen conifer of the Pinaceae family. Covering around 600.000 ha, today its largest distribution is found in Turkey (Boydak, 2003). *C. libani* mainly grows at altitudes ranging from 800 to 2100 m a.s.l. where montane Mediterranean climate conditions prevail (Evcimen, 1963). In a recent study published by Messinger et al., (2015), it was shown that planted *C. libani* individuals growing in the Ecological Botanical Gardens of Bayreuth under Central European climate conditions show high adaptation

and good growth performance. The good growth seems mainly to be attributed by the more humid conditions and better water supply during the summer months. In Turkey and outside its natural range, *C. libani* is used for forestation and afforestation projects and discussions about its growth and adaptation potential under different site conditions and future climate scenarios carry on (Boydak 2007; Ducci et al. 2007; Güney et al., 2017). Besides its ecological importance it is one of the most important commercial tree species in Turkey (Boydak, 2003; Kavgacı et al., 2010). Therefore it is of interest to further explore this species, especially in terms of its ecophysiology since only few studies have been carried out so far.

The specific objectives of this study were to investigate (1) the relationship between sapwood area at breast height (1.30 m) and other tree parameters of *C. libani*, and (2) to test if there is a relationship between mean sapwood area and mean leaf area index in *C. libani* stands.

**Table 1.** Characteristics of the study trees selected at four different sampling sites (T1 – T4) within the Elmalı Cedar Research Forest and site-specific leaf area index (LAI). Differences between sites were tested using ANOVA. Significant differences ( $P < 0.05$ ) are indicated by lower case letters.

	T1_1960 m	T2_1665 m	T3_1355 m	T4_1050 m	F-value	P
Latitude	36.58422°N	36.58520°N	36.57771°N	36.57800°N	-	-
Longitude	30.03077°E	30.02035°E	29.98542°E	29.96881°E	-	-
Number of trees (n)	23	24	23	22	-	-
Sapwood area (m <sup>2</sup> )	0.22±0.20 <sup>a</sup>	0.40±0.19 <sup>b</sup>	0.38±0.24 <sup>ab</sup>	0.34±0.26 <sup>ab</sup>	3.20	0.027
Diameter at breast height (cm)	20.1±9.7 <sup>a</sup>	33.9±10.3 <sup>b</sup>	31.3±11.9 <sup>b</sup>	27.8±15.1 <sup>ab</sup>	5.96	0.001
Radius without bark (cm)	9.0±4.9 <sup>a</sup>	14.6±4.5 <sup>b</sup>	14.1±5.5 <sup>b</sup>	12.6±7.3 <sup>ab</sup>	4.66	0.005
Sapwood depth (cm)	4.7±1.2	5.1±1.2	4.9±1.4	5.1±1.1	0.63	0.596
Tree basal area (m <sup>2</sup> )	0.039±0.05 <sup>a</sup>	0.099±0.06 <sup>b</sup>	0.087±0.07 <sup>ab</sup>	0.078±0.08 <sup>ab</sup>	3.67	0.015
Height (m)	7.3±1.8 <sup>a</sup>	18.4±4.8 <sup>b</sup>	18.7±4.7 <sup>b</sup>	12.4±5.3 <sup>c</sup>	35.51	0.000
Age (years)	44.8±25.6 <sup>a</sup>	92.4±23.8 <sup>b</sup>	87.3±25.2 (n=8) <sup>b</sup>	52.2±28.6 <sup>a</sup>	17.23	0.000
Projected crown area (m <sup>2</sup> )	12.9±8.2 <sup>a</sup>	10.7±9.7 (n=9) <sup>a</sup>	30.2±15.6 <sup>b</sup>	22.4±17.6 <sup>ab</sup>	7.81	0.000
Leaf area index (m <sup>2</sup> m <sup>-2</sup> )	1.04±0.45 <sup>a</sup>	2.93±0.46 <sup>b</sup>	3.22±0.89 <sup>b</sup>	2.37±0.65 <sup>c</sup>	42.26	0.000

## 2. Material and Method

### 2.1. Study area and tree selection

The study was conducted during March 2013 and end of 2014 within the Cedar Research Forest in the Elmali district of Antalya located in the southwestern Taurus Mountains. The forested parts exhibit mostly pure stands of *C. libani*, which are sometimes partly mixed with *Juniperus sp.* individuals. The area is characterized by an oro-Mediterranean climate with cold winters and drought periods during summer (Atalay, 1987) with a mean annual precipitation of 640 mm and mean annual temperature of 7.5 °C (Basaran et al., 2008). Our sampling sites (abbreviated as T1, T2, T3, and T4) were located along an altitudinal gradient ranging from approximately 1000 to 2000 m a.s.l. (Table 1). For further details about the characteristics of the sampling sites see Güney et al., (2017).

For analysis of sapwood area, between twenty-two and twenty-four mature *C. libani* trees of different size and age were randomly chosen per sampling site. None of the selected tree individuals had any visible damage (Güney et al., 2016). DBH was measured in two directions and then averaged. Tree height was measured with an ultrasonic distance meter with inclinometer (Vertex III, Haglöf Sweden AB, Langsele, Sweden). Tree basal area (TBA) was measured at breast height (1.30 m) including the bark. The projected crown area for each sample tree was determined by measuring the radius from stem to end of crown perimeter in eight directions (North, Northeast, East, Southeast, South, Southwest, West, and Northwest). Projected crown area was then estimated as a circle of which the diameter was calculated as an average of the eight measured radii (Kantola and Mäkelä, 2004). For T2, data of projected crown area is only available for nine trees.

### 2.2. Sampling and determination of sapwood area

To determine the sapwood area of all sample trees, tree cores were extracted at breast height using an increment borer (Suunto 300/400 mm, Finland). For each tree, two cores were extracted from the north and south facing side of the stem reaching to the pith. Since tree cores were taken during early spring and early winter the stems were assumed to

be fully hydrated and the sapwood was marked right after tree cores were taken as the visibly wet part of the xylem (Long and Dean, 1986). The natural change of color (the heartwood was more reddish brown) did not directly correspond with the boundary of wet to dry wood in most cases and was located closer to the pith. Additionally, several tree cores were stained with Lugol's solution (Rodriguez- Calcerrada et al., 2015) which showed a slight reaction close to the previously marked wet proportion of the cores. Nevertheless, the visibly wet outer part of the cores was taken as the sapwood depth since staining methods can result in high error rates. From the two cores, an average sapwood depth was determined for each tree. Sapwood area at DBH was then calculated as the area of the outer stem ring with a radius that is equal to the average sapwood depth while assuming a uniform circular sapwood (Horna et al. 2011). From the tree cores used for determination of sapwood area, tree age at breast height was defined by counting the number of tree rings, and radius without bark was measured. For mean values of each parameter at each sampling site see Table 1. At T3, exact determination of tree age was only possible for eight trees.

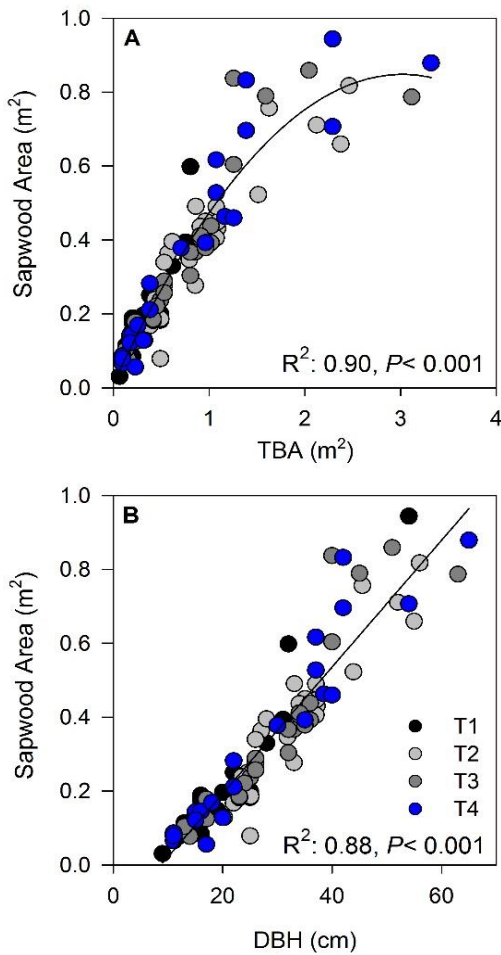


**Figure 1.** Relationship between Sapwood area and (A) tree basal area (TBA), and (B) diameter at breast height (DBH) of *Cedrus libani* at four different sampling sites (black circles: T1\_1960 m; gray circles: T2\_1665 m; dark gray circles: T3\_1355 m; blue circles: T4\_1050 m).

### 2.3. Determination of leaf area index

Leaf Area Index (LAI) is defined as “one half of the total leaf area per unit ground surface area” (Jonckheere et al., 2004). LAI was determined at seventeen different locations within each sampling site. Hemispherical photographs of the forest canopy were taken from the ground which were later analyzed via HemiView image analysis software (1999 Delta-T Devices Ltd, Cambridge, UK). The presented LAI values were published in Güney et al. (2017).

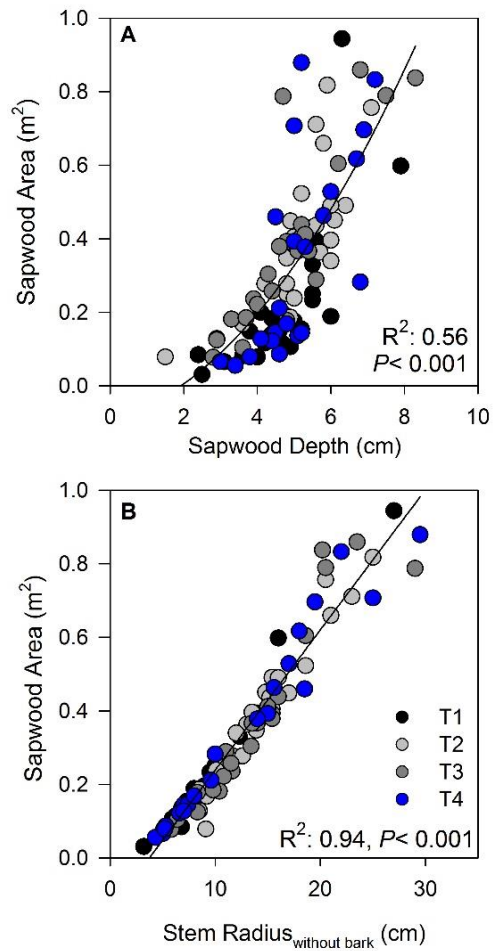


**Figure 2.** Relationship between Sapwood area and (A) sapwood depth, and (B) stem radius without bark of *Cedrus libani* at four different sampling sites (black circles: T1\_1960 m; gray circles: T2\_1665 m; dark gray circles: T3\_1355 m; blue circles: T4\_1050 m).



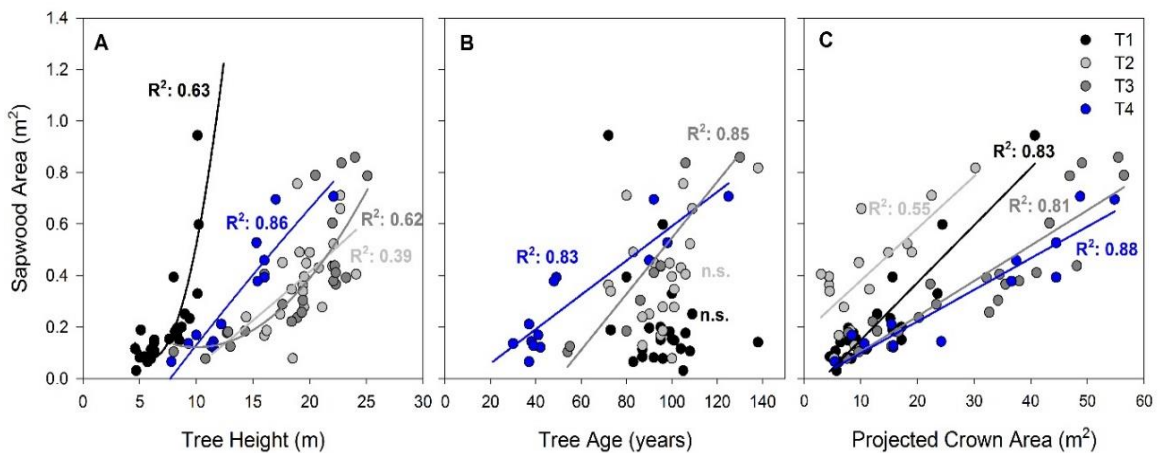


**Figure 3.** Relationship between sapwood area and (A) tree height, (B) tree age at breast height, and (C) projected crown area of *Cedrus libani* at four different sampling sites (black circles: T1\_1960 m; gray circles: T2\_1665 m; dark gray circles: T3\_1355 m; blue circles: T4\_1050 m). Level of significance  $P < 0.05$ . Please note that the scaling of the y-axes are identical.

#### 2.4. Data analysis

Simple regression analysis was used to compare the relationship between sapwood area and other measured parameters. Differences between sites in means of sapwood area and other measured parameters (e.g. DBH, sapwood depth, tree height, LAI, etc.) were tested using ANOVA. Analyses were performed with Sigma Plot 10.0 (Systat software, Inc.) and SPSS 20.0 (SPSS Inc., Chicago, IL, USA) software.

#### 3. Results

ANOVA resulted in significant differences between sites for tree age, LAI, and all measured tree size parameters except for sapwood depth. At all sites, mean sapwood depth was approximately 5 cm (Table 1). Resulting means of the other parameters were generally similar between the sampling sites T2 and T3.

Sapwood area was positively related to TBA and DBH using non-linear (exponential rise to maximum) and linear regression, respectively (Figure 1). Regarding the values obtained from all study trees, TBA was the best predictor for sapwood area explaining 90% of the variation. A high correlation was also found for DBH which accounted for approximately 88% of the variation in sapwood area.

Sapwood area was further related to the tree size parameters sapwood depth and stem radius without bark using non-linear (quadratic) and linear regression, respectively (Figure 2). Stem radius without bark was overall the best predictor for sapwood area explaining 94% of the variation. The quadratic relationship between sapwood area and sapwood depth explained only 56% of the variation.

Regression analysis between sapwood area, tree height, tree age, and projected crown area was done for each sampling site separately (Figure 3). The relationship between sapwood area and tree height was very variable explaining between 39 and 86% of the variation. While no significant correlation was found between sapwood and tree age at the sampling sites T1 and T2, linear regression explained 85 and 83% of the variation for T3 and T4, respectively.

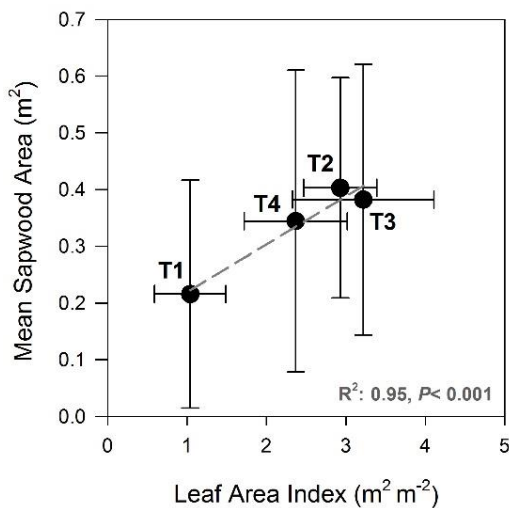


**Figure 4.** Relationship between site-specific mean leaf area index (LAI) and mean sapwood area of *Cedrus libani*. Values are given with standard deviations. T1-T4: Sampling sites, see Table 1.

A high positive correlation was found between sapwood area and projected crown area at T1, T3 and T4. At T2 (values only available for nine trees) it accounted for only 55% of the variation in sapwood area.

A significant positive linear relationship ( $R^2=0.95$ ) was found between site-specific mean sapwood area and LAI (Figure 4). An altitudinal trend for sapwood area was not found.

#### 4. Discussion and Conclusions

In this study, sap wood area of *C. libani* individuals growing at different altitudes in the Elmalı Cedar Research forest was determined by visually assessing the wet part of extracted tree cores. The relationship between sapwood area and different parameters (tree size, age, LAI) was investigated.

##### 4.1. Determination of hydro-active sapwood area

Many techniques and methods are available to determine the sapwood area of the stem, either using tree cores, trees' cross sections or whole tree stems, depending on the study objectives. Determining the sapwood area using computer tomography (portable devices) is non-destructive but measurement devices are expensive. Another

method is to measure the resistance to penetration but it is restricted to areas where frost occurs (Rust 1999). Staining methods are more economical but cannot be performed without causing damage to the tree (Kutscha and Sachs, 1962). Furthermore they are prone for overestimating the sapwood proportion when the transition zone between sapwood and heartwood is also stained, although it almost entirely lost its ability to transport water (Köstner et al., 1998; Rust, 1999). This in turn may lead to overestimating transpiration rates when calculated based on sapwood area. In studies measuring transpiration of trees, a common method is to extract a tree core to the pith of the stem in the early morning hours before transpiration rates rise. Right after coring, a solution including staining reagents (e.g. indigo carmin) is injected into the hole. If necessary the hole is refilled. After a few hours, when the xylem sap including the staining solution should have moved upward, a second core is taken a few cm above the hole of the first extracted tree core. The sapwood can then be determined based on the stained depth of the tree core (Gebauer et al. 2008; Meinzer et al., 2001). It is to mention that in such studies methods including extraction of tree cores should be carried out after all measurements are completed. This way unnecessary disturbance that may influence the measurements can be avoided. If the sapwood area has to be determined in a fast and economical way visual assessment of the wet part, as used in this study, may be the preferred method (Long and Dean 1986; Rust 1999). However, this method should be used only when the stem is fully hydrated (e.g. after rain events, in the early morning hours, preferably during early spring) and the wet part of the tree core has to be marked immediately after extraction. In further studies, different methods could be used to determine the sapwood area of *C. libani* to improve our knowledge in this regard.

##### 4.2. Relationship between sapwood area and different parameters in *C. libani* and its use in ecophysiological studies

Several parameters were measured to find the best predictor to determine sapwood area in *C. libani*. Stem radius without bark explained 94% of the variance, total basal area explained 90%. DBH which is often used as a predictor in other studies, accounted for approximately 88% of the variation in sapwood area. In the study of Vertessy et al. (1995) DBH explained 96% of the variation in sapwood area of mountain ash (*Eucalyptus*

*regnans* F. Muell.). Mean sapwood depth of *C. libani* (approximately 5 cm) was higher than that of Douglas fir (*Pseudotsuga menziesii* (Mirb.) Franco) with approximately 3 cm and lower than sapwood depth of Ponderosa pine (*Pinus ponderosa* Dougl. Ex Laws.) with approximately 12 cm (Barnard et al., 2011). The larger fraction of sapwood area in *P. ponderosa* is hypothesized to be an advantage under drier conditions. Similar sapwood depths (averages mostly range between 4 and 6 cm) were found in mountain pine (*Pinus uncinata* Ram.) trees growing in the Iberian Peninsula (Galván et al., 2012). Tree age, tree height and projected crown area resulted in different good correlations. Especially correlations between sapwood area and tree age were not significant if tree age values did not cover a wide range. Projected crown area was a better predictor, especially when the sampling number was high. The relationship between mean sapwood and mean LAI resulted also in a high positive correlation. Since LAI was not always measured in close proximity to the sampling trees it is only an approximation but it clearly shows the trend how leaf area and sapwood area are correlated. In this context, projected crown area can also be used as an estimator for leaf area. Furthermore, these relationships show the physiological balance between water requirement of the tree (from shoots or leaves) and the water conducting sapwood (Kaufmann and Troendle, 1981).

In studies using sap flow gauges, sapwood area is an important parameter to determine single tree and stand transpiration (Gebauer et al., 2008; Meinzer et al., 2001) or to investigate water storage and transport properties in trees. A study conducted by Rodriguez- Calcerrada et al., (2015) showed how amongst six deciduous species, dominant individuals had higher transpiration rates per unit basal area compared to suppressed individuals mainly because the latter had lower sapwood depth. The findings of this study can be used in ecophysiological studies on *C. libani* to calculate single tree and stand transpiration and to answer other questions related to water use or water transport in this tree species, especially when site and stand characteristics area similar to those in this study.

In conclusion, sapwood area of *C. libani* was visually assessed in extracted tree cores and resulted in significant correlations with the other measured parameters in this study. Stem radius without bark and tree basal area where the best

predictors, but the latter should be preferred since it causes no damage to the tree. Further studies at different sites and using different methods should be carried out to improve our knowledge about *C. libani* sapwood and to enable upscaling of measured sap flow densities from the single tree to the stand level in this species.

### Acknowledgements

This research was carried out during the field studies within the project funded by the German Federal Ministry of Education and Research (01DL12041) and in cooperation with the Southwest Anatolia Forest Research Institute (SAFRI) in Antalya.

### References

- Atalay, İ. (1987). Sedir (*Cedrus libani* A. Rich) Ormanlarının Yayılış Gösterdiği Alanlar ve Yakın Çevresinin Genel Ekolojik Özellikleri ile Sedir Tohum Transfer Rejyonlaması. Tarım Orman ve Köy İşleri Bakanlığı Orman Genel Müdürlüğü Yayını.
- Barnard, D.M., Meinzer, F.C., Lachenbruch, B., McCulloh K.A., Johnson, D.M., Woodruff, D.R. (2011). Climate- related trends in sapwood biophysical properties in two conifers: avoidance of hydraulic dysfunction through coordinated adjustments in xylem efficiency, safety and capacitance. *Plant, cell & environment* 34:643-654.
- Basaran, M. A., Basaran, S., Bas, N., Kaçar, S., Tolunay, D., Makineci, E., Deniz, G. (2008). Determining the actual state of Cedar Research Forest Elmalı by GIS based digital maps. South-West Anatolia Forest Research Institute, Antalya, Turkey, 331..
- Boydak, M. (2003). Regeneration of Lebanon cedar (*Cedrus libani* A. Rich.) on karstic lands in Turkey. *Forest Ecology and Management* 178:231-243.
- Boydak, M. (2007). Reforestation of Lebanon cedar (*Cedrus libani* A. Rich.) in bare karstic lands by broadcast seeding in Turkey. In : Leone V. (ed.), Lovreglio R. (ed.). Proceedings of the international workshop MEDPINE 3: conservation, regeneration and restoration of Mediterranean pines and their ecosystems. Bari : CIHEAM, 2007. p. 33-42 (Options

- Méditerranéennes : Série A. Séminaires Méditerranéens; n. 75).
- Ducci, F, Fusaro, E., Lucci, S., Ricciotti, L. (2007). Strategies for finalizing Conifers experimental tests to the production of improved reproductive materials. In: Proceedings of the Inter. Workshop MEDPINE3“Conservation, Regeneration and restauration of Mediterranean Pines and thei Ecosystems”,(Valenzano-BA, 2005) Options médit., Serie A, 2007. vol 75. pp 99-104.
- Evcimen, B.S. (1963). Türkiye Sedir ormanlarının ekonomik önemi, hasılat ve amenajman esasları.
- Ford, C.R., McGuire, M.A., Mitchell, R.J., Teskey, R.O. (2004). Assessing variation in the radial profile of sap flux density in Pinus species and its effect on daily water use. *Tree physiology* 24:241-249.
- Galván, J, Camarero, J.J., Sangüesa- Barreda, G., Alla, A.Q., Gutierrez, E. (2012). Sapwood area drives growth in mountain conifer forests. *Journal of Ecology* 100:1233-1244.
- Gebauer, T., Horna, V., Leuschner, C. (2008). Variability in radial sap flux density patterns and sapwood area among seven co-occurring temperate broad-leaved tree species. *Tree physiology* 28:1821-1830.
- Güney, A., Küppers, M., Rathgeber, C., Şahin, M., Zimmermann R (2017). Intra-annual stem growth dynamics of Lebanon Cedar along climatic gradients. *Trees* 31:587–606.
- Güney, A, Zimmermann, R., Krupp, A., Haas, K. (2016). Needle characteristics of Lebanon cedar (*Cedrus libani* A. Rich.): degradation of epicuticular waxes and decrease of photosynthetic rates with increasing needle age. *Turkish Journal of Agriculture and Forestry*:40.
- Horna, V., Schuldt, B., Brix, S., Leuschner, C. (2011). Environment and tree size controlling stem sap flux in a perhumid tropical forest of Central Sulawesi, Indonesia. *Annals of Forest Science* 68:1027-1038.
- Jonckheere, I., Fleck, S., Nackaerts, K., Muys, B., Coppin, P., Weiss, M., Baret, F. (2004). Review of methods for in situ leaf area index determination: Part I. Theories, sensors and hemispherical photography. *Agricultural and forest meteorology* 121:19-35.
- Kantola, A., Mäkelä, A. (2004). Crown development in Norway spruce [*Picea abies* (L.) Karst.]. *Trees* 18:408-421.
- Kaufmann, M.R., Troendle, C.A. (1981). The relationship of leaf area and foliage biomass to sapwood conducting area in four subalpine forest tree species. *Forest Science* 27:477-482.
- Kavgacı, A., Başaran, S., Başaran, M. (2010). Cedar forest communities in Western Antalya (Taurus Mountains, Turkey). *Plant Biosystems* 144:271-287.
- Köstner, B., Falge, E.M., Alsheimer, M., Geyer, R., Tenhunen, J.D. (1998). Estimating tree canopy water use via xylem sapflow in an old Norway spruce forest and a comparison with simulation-based canopy transpiration estimates. In: *Annales des sciences forestières*, vol 1-2. EDP Sciences, pp 125-139.
- Kutscha, N.P., Sachs, I.B. (1962). Color tests for differentiating heartwood and sapwood in certain softwood tree species. Madison, Wis.: US Dept. of Agriculture, Forest Service, Forest Products Laboratory.
- Lehmann, J., Becker, G. (1993). Xylem-conductive area of spruce (*Picea abies* (L.) Karst.) of different age and vitality. *Holz als Roh-und Werkstoff* (Germany).
- Long, J.N., Dean, T.J. (1986). Sapwood area of *Pinus contorta* stands as a function of mean size and density. *Oecologia* 68:410-412.
- Longuetaud, F., Mothe, F., Leban, J.M., Mäkelä, A. (2006). *Picea abies* sapwood width: variations within and between trees. *Scandinavian Journal of Forest Research* 21:41-53.
- Mäkelä, A., Virtanen, K., Nikinmaa, E. (1995). The effects of ring width, stem position, and stand density on the relationship between foliage biomass and sapwood area in Scots pine (*Pinus sylvestris*). *Canadian Journal of Forest Research* 25:970-977.
- Matyssek, R., Fromm, J., Rennenberg, H., Roloff, A. (2010). *Biologie der Bäume: von der Zelle zur globalen Ebene* vol 8450. UTB.

- Meinzer, F., Goldstein, G., Andrade, J. (2001). Regulation of water flux through tropical forest canopy trees: do universal rules apply? *Tree physiology* 21:19-26.
- Messinger, J., Güney, A., Zimmermann, R., Ganser, B., Bachmann, M., Remmele, S., Aas, G. (2015). *Cedrus libani*: A promising tree species for Central European forestry facing climate change? *European Journal of Forest Research* 134:1005-1017.
- Motzer, T., Munz, N., Kuppers, M., Schmitt, D., Anhof, D. (2005). Stomatal conductance, transpiration and sap flow of tropical montane rain forest trees in the southern Ecuadorian Andes. *Tree Physiology-Victoria* 25:1283.
- Phillips, N., Oren, R., Zimmermann, R. (1996). Radial patterns of xylem sap flow in non-, diffuse- and ring- porous tree species. *Plant, cell & environment* 19:983-990.
- Plomion, C., Leprovost, G., Stokes, A. (2001). Wood formation in trees. *Plant physiology* 127:1513-1523.
- Rodriguez- Calcerrada, J., López, R., Salomón, R., Gordaliza, G.G., Valbuena- Carabaña, M., Oleksyn, J., Gil, L. (2015). Stem CO<sub>2</sub> efflux in six co- occurring tree species: underlying factors and ecological implications. *Plant, cell & environment* 38:1104-1115.
- Rust, S. (1999). Comparison of three methods for determining the conductive xylem area of Scots pine (*Pinus sylvestris*). *Forestry* 72:103-108.
- Vertessy, R., Benyon, R., O'sullivan, S., Gribben, P. (1995). Relationships between stem diameter, sapwood area, leaf area and transpiration in a young mountain ash forest. *Tree physiology* 15:559-567.
- Wullschleger, S.D., McLaughlin, S.B., Ayres, M.P. (2004). High-resolution analysis of stem increment and sap flow for loblolly pine trees attacked by southern pine beetle. *Canadian Journal of Forest Research* 34:2387-2393.

## Chemical Characterization and Biological Activity Evaluation of Essential Oils of *Achillea sipikorensis*, an Endemic Plant From Turkey

Nuraniye Eruygur<sup>1\*</sup>, Özge Çevik<sup>2</sup>, Mehmet Atas<sup>3</sup>, Mehmet Tekin<sup>4</sup>

**Abstract:** The *Achillea* L. (Asteraceae) are known all over the world and used widely by local people as folk herbal medicine. The species are reported to have anti-inflammatory, antioxidant, diuretic, antispasmodic vs. activities and have been used for the treatment of various ailments in Turkish traditional medicine. This work is the first study on chemical composition and biological activity of essential oil obtained from endemic plant- *A. sipikorensis* Hausskn. Et. Bornm evaluated for their antiradical, antimicrobial and cytotoxic activities. GC/MS analyses showed that cis- chrysanthenol (14.5%), 1, 8-cineol (10.9%), caryophyllene oxide (8.5%), borneol (8.2%), and camphor (6.1%) were the major constituents in the essential oil from aerial part of the plant. The essential oil demonstrated good antioxidant, antimicrobial and cytotoxic activities.

**Keywords:** *Achillea sipikorensis*, Essential oil, Antioxidant, Antimicrobial, Cytotoxicity

### 1. Introduction

The genus of *Achillea* is belongs to Compositae family and comprise of 115 taxa. In Turkish flora, it has 48 species and 54 taxa, among them the half are recorded as endemic. The *Achillea* species are widely used in traditional and folk medicine for treatment of various disease or to maintain good health(Manayi et al., 2012). The majority of *Achillea* species are medicinal plants due to their therapeutic applications. In Turkey, *Achillea* herbal teas are traditionally used for abdominal pain and flatulence(Yaşar and Fakir, 2016).

The previous phytochemical investigations on *Achillea* species indicates that, they contains various secondary metabolites such as flavonoids, essential oils, lignans and terpenic compounds(Karaalp et al., 2009; Saeidnia et al., 2011).

There are many well established reports about the close relationship between increased reactive oxygen species (ROS) in biological system and chronic disease such as diabetes, atherosclerosis, hypertension, and neurodegeneration (Harman, 1992). In this context natural antioxidants play an important role in reducing the risk of degenerative disease. Therefore, plant origin natural antioxidants have great interest attributed to their free radical scavenging abilities.

To the best of our knowledge, there was no available information about antioxidant, antimicrobial and cytotoxic activity of the essential oil of *A. sipikorensis*. The aim of the present work was to evaluate and explore *in vitro* antioxidant, antimicrobial and cytotoxic activity of the essential oil obtained from aerial part of *A. sipikorensis*

<sup>1</sup>Cumhuriyet University, Faculty of Pharmacy, Department of Pharmacognosy, Sivas, Turkey.

<sup>2</sup>Adnan Menderes University, Faculty of Medicine, Department of Biochemistry, Aydın, Turkey.

<sup>3</sup>Cumhuriyet University, Faculty of Pharmacy, Department of Pharmaceutical Microbiology, Sivas, Turkey

<sup>4</sup>Trakya University, Faculty of Pharmacy, Department of Pharmaceutical Botany, Edirne, Turkey

\* Corresponding author : \* [neruygur@cumhuriyet.edu.tr](mailto:neruygur@cumhuriyet.edu.tr)

Citation: Eruygur, N., Çevik, Ö., Atas, M., Tekin, M. (2018). Chemical characterization and biological activity evaluation of essential oils of *Achillea sipikorensis*, an endemic plant from Turkey. *Bilge International Journal of Science and Technology Research*, 2 (1):92-97.



## 2. Material and Method

The study material of *Achillea sipikorensis* were collected at flowering season from gypsous hill at separating section of Kangal-Gürün road, Sivas, Turkey (N 39 07 52,2; E 37 14 33,4;) by botanist Dr. Mehmet Tekin and stored at the herbarium of Faculty of pharmacy, Cumhuriyet University with the collect number of M. Tekin-1736. The plant material were air-dried at shadow place for about two weeks.



**Figure 1.** Habitat image of *A. sipikorensis* (M. Tekin)

### 2.1. Extraction of the essential oil

The essential oil of the dried and grounded aerial part of the *A. sipikorensis* was obtained by hydrodistillation using a Clevenger-type apparatus for 3 h in a yield of 0.5% (v/w). After drying with anhydrous sodium sulphate and filtration, the oil was stored at refrigerator until use.

### 2.2. GC/MS analysis

The analysis of the obtained essential oils was carried out using an Agilent 7809B GC system, equipped with a HP-Innowax capillary column (60m, 0.25mm i.d., 0.25  $\mu$ m film thickness) and a 5977B Mass Selective Detector system. An election ionization system with energy of 70eV used for detection. Helium (0.7mL/min) was used as carrier gas, Injector and detector temperatures were set at 250 °C. The temperature was 60 °C at initial 10 min, then gradually increased to 220 °C at a 4°C/min rate, held for 10 min and finally increased to 240 °C at 1 °C/min. Diluted samples (in 10% hexane, v/v) of 1.0  $\mu$ L were injected manually with 40:1 split rate. Identification of the components was carried out with the retention index determined by injection of a homologous of n -alkane series under the same experimental

conditions. Further identification of the components was performed based on the comparison of their mass spectra with Wiley 9-Nist 1 Mass spectral database system.

### 2.3. Antioxidant activity

The antioxidant activity of the essential oil was evaluated on the basis of the radical scavenging effect of the stable 1, 1-diphenyl-2-picrylhydrazyl (DPPH)-free radical activity by the method of Blois (Blois, 1958) and 2,2'-Azino-bis (3-ethylbenzothiazoline-6-sulphonic acid) (ABTS) radical cation decolorization assay as described by Re et al. (Roberta Re, Nicoletta Pellegrini, Anna Proteggente, Ananth Pannala, Min Yang, 1999).

### 2.4. Antimicrobial activity

The essential oil of *A. sipikorensis* was tested against a panel of microorganisms including *Staphylococcus aureus* (ATCC 29213), *Enterococcus faecalis* (ATCC 29212)), *Pseudomonas aeruginosa* (ATCC 27853), *Escherichia coli* (ATCC 25922)) and *Candida albicans* (ATCC 10231). In order to determine the MIC (minimum inhibition concentration) as recommended by NCCLS. The two-fold dilutions ranging from 5 mg/mL to 0.032 mg/mL of the essential oil was performed in a 96-well plate, and then suspended test strains were inoculated in each well to give a final density of  $5 \times 10^5$  CFU/mL for bacteria and  $0.5-2.5 \times 10^3$  CFU/mL for yeast. Gentamycin and Fluconazole were used as positive control and DMSO was used as negative control. Plates were incubated at 37°C for 24h for bacteria and at 30°C for yeasts. Then 2 mg/mL of 2, 3, 5-Triphenyltetrazolium chloride (TTC) sterile solution was added and further incubated at 37°C for 1h. The microbial growth was indicated by the presence of a red pellet on the well bottom with formation of formazan.

### 2.5. Cytotoxicity

The in vitro cytotoxicity of essential oil was evaluated in the colorimetric 3-(4, 5-dimethylthiazolyl-2)-2, 5-diphenyltetrazolium bromide (MTT) assay. A total of 100  $\mu$ L of the exponential growing MCF-7 and PC-3 cancer cell suspensions are pipetted in to each well of a sterile 96-well microtiter plate in DMEM medium to  $5 \times 10^3$  cells/mL. The plates were incubated for 24h at 37°C in a 5% CO<sub>2</sub> incubator, until the cells were in the exponential phase of growth. On next day,

different concentrations of essential oil (1, 10, 100, and 1000  $\mu\text{g/mL}$ ) prepared in 1% DMSO-growth medium was added. Each dilution concentration was performed in triplicate. The microtiter plates were incubated at 37°C in a 5%  $\text{CO}_2$  incubator for 24 h with essential oils. After incubation, culture medium aspirated carefully and 10  $\mu\text{L}$  of MTT solution was added to each well and further incubated for 4h at same condition. The MTT formazan crystals were dissolved by adding 50  $\mu\text{L}$  of DMSO to each well and the amount of MTT reduction was measured by detecting absorbance in a microplate reader (Epoch, USA) at a wavelength of 570 nm. The  $\text{IC}_{50}$  values were calculated as the concentration of the essential oil resulting in a 50% reduction of absorbance compared to control group which are untreated cells with essential oils.

### 3. Results

The GC/MS method was used for the determination of chemical composition of *A. sipikorensis* essential oil. 29 compounds were identified and constituting 81.2 % of the total oil. The essential oil of *A. sipikorensis* was characterized by a majority of monoterpenes such as Myrteneol (14.5%), 1,8-cineol (10.9%), caryophyllene oxide (8.5%), borneol (8.2%), and camphor (6.1%) (Table 1). Toncer et al. reported that 1,8-cineol, camphor as main principal constituents of the essential oil of *A. biebersteinii*, *A. aleppica*, *A. tenuifolia*, *A. magnifica* and *A. cucullata* (Toncer et al., 2010). Comparing with them, our results reveals that myrteneol, caryophyllene oxide, borneol are the main dominant constituents presented in essential oil of *A. sipikorensis* except for camphor and 1,8-cineol. The great variation in chemical composition of essential oils of *Achillea* species mainly due to their environmental condition and other exogenic factors.

Abundance

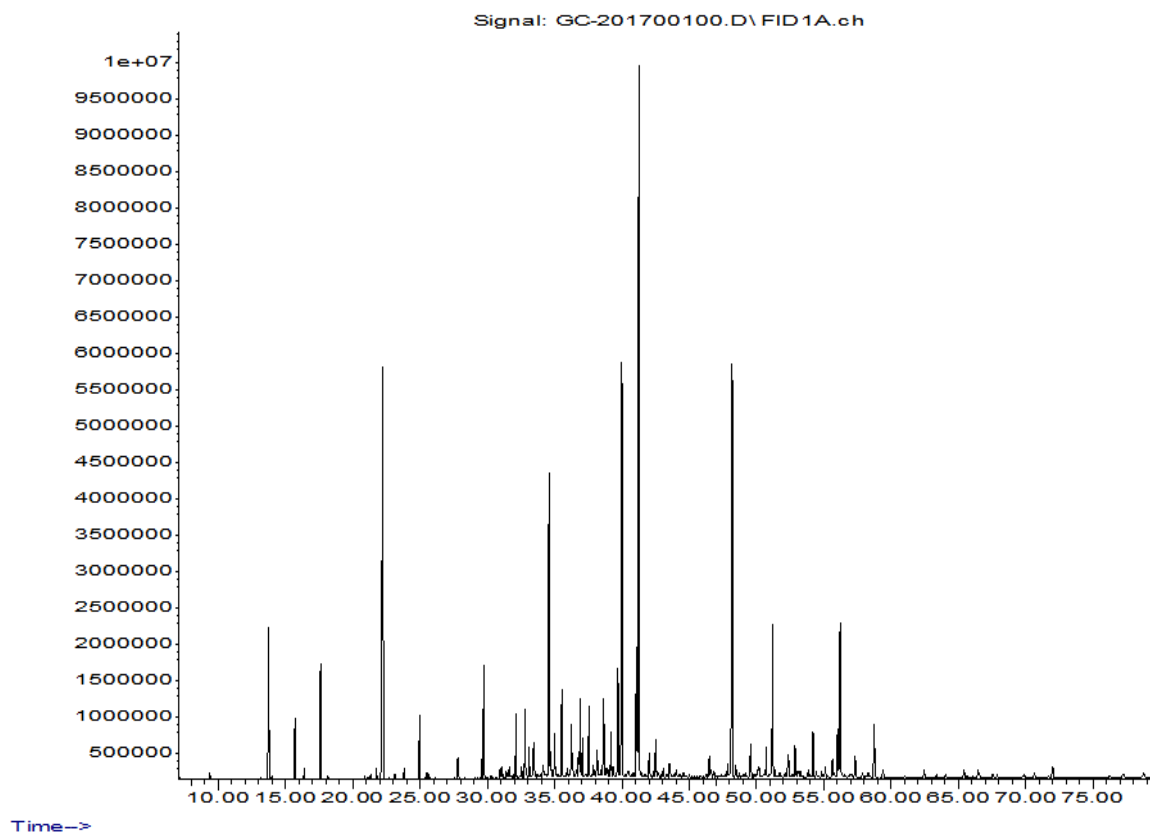


Figure 2. GC/MS chromatogram of essential oil of *Achillea sipikorensis*



**Table 1.** Chemical composition of *Achillea sipikorensis* essential oil

No	Relative Retention Index (RRI) <sup>1</sup>	Compound*	Relative Intensity (%)
1	1035	$\alpha$ -Pinene	2.8
2	1079	Camphene	1.1
3	1121	$\beta$ -Pinene	2.2
4	1222	1,8-Cineole	10.9
5	1284	$\rho$ -Cymene	1.0
6	1405	Santolina alcohol	1.8
7	1474	<i>trans</i> -Sabinene hydrate	1.0
8	1492	2-Ethyl hexanol	1.1
9	1511	Campholenal	0.7
10	1548	Camphor	6.1
11	1576	<i>Trans-p</i> -Menth-2-en-1-ol	1.4
12	1597	Pinocarvone	0.9
13	1620	Terpinen-4-ol	1.3
14	1626	$\beta$ -Caryophyllene	0.6
15	1642	<i>trans</i> -Pinocarveol	1.1
16	1678	$\alpha$ -Terpineol	1.4
17	1713	Borneol	1.7
18	1724	<i>cis</i> -Piperitol	8.2
19	1762	<i>cis</i> -Chrysantheol	2.8
20	1769	Myrteneol	14.5
21	1813	Caryophyllene oxide	0.6
22	2032	Caryophylla -2(12), 6 (13)-dien-5-one	8.5
23	2089	Spathulenol	0.5
24	2154	Spathulenol	2.6
25	2200	Thymol	0.5
26	2265	$\beta$ -Eudesmol	0.9
27	2326	Caryophylla-2(12), 6(13)-dien-5 $\beta$ -ol	1.0
28	2331	Caryophylla-2-(12), 6(13)-dien-5 $\alpha$ -ol	3.5
29	2364	Caryophylla-2(12), 6-dien-5 $\alpha$ -ol	0.5
30	2405	Caryophylla-2(12), 6-dien-5 $\beta$ -ol	1.3
Total			82.5

Antioxidant activity: The radical scavenging activity of DPPH is based on the decolorization of the purple coloured fresh solution of DPPH is bleached by natural antioxidants presented in plants or essential oils and the bleaching degree is proportional to efficiency and amount of antioxidants (Saeed et al., 2012). ABTS also used for radical scavenging properties measurement. In this method, the green/blue coloured ABTS+

cation was generated via the reaction of ABTS with potassium persulfate for 12-16h (Abu Zarin et al., 2016). Antimicrobial activity: The antimicrobial activity of the essential oil was determined and the results are presented in Table 2.

**Table 2.** MIC value of *A. sipikorensis* essential oils on tested 5 microorganism growth

S/No.	Microorganisms	Concentration (mg/ml)
1	<i>E. coli</i>	>5
2	<i>S. aureus</i>	2.5
3	<i>P. aeruginosa</i>	>5
4	<i>E. faecalis</i>	5.0
5	<i>C. albicans</i>	2.5

**Cytotoxicity:** The cytotoxic activity of the essential oil on MCF-7 breast cancer cell line and PC-3 prostate cancer cell line was determined using MTT assay and the results are given in Figure 4. The obtained results suggest that the plant *A. sipikorensis* could be used as valuable resources for bioactive food materials due to its cytotoxic properties.

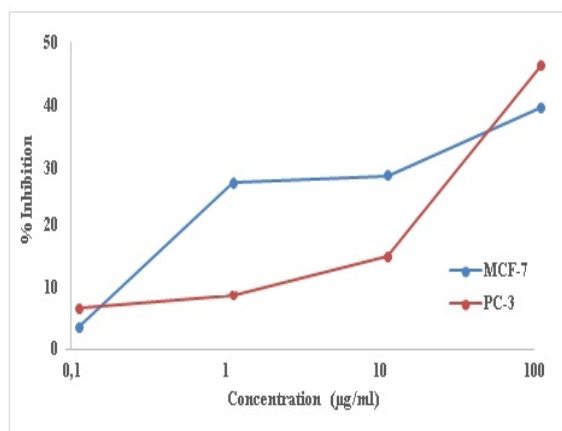


**Figure 3.** Cytotoxic activity of essential oil of *A. sipikorensis* on MCF-7 breast cancer and PC-3 prostate cancer cell lines

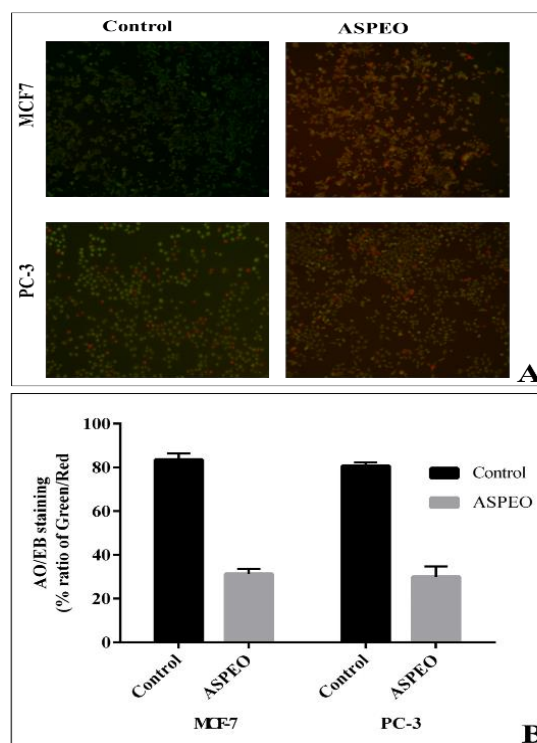


**Figure 4.** Floresans image and AO/EB staining ratio of MCF-7 breast cancer cell line and PC-3 prostate cancer cells 24h incubated with 100 µg/mL *A. Sipikorensis* essential oil

#### 4. Discussion and Conclusions

As to antimicrobial activity of crude herbal extracts, many authors consider that its significant if the MIC value is  $\leq 100$  µg/mL, moderate between 100 and 625 µg/mL, weak if higher than 625 µg/mL (Awouafack et al., 2013). According to this consideration, the essential oil of *A. sipikorensis* had weak antimicrobial activities against the tested five microorganisms. The results obtained from this study showed that essential oil of *Achillea sipikorensis* aerial parts has antiradical, antimicrobial and cytotoxic activity. Therefore, the plant may be useful in treatment of microbial infections or oxidative stress related chronic disease.

#### Acknowledgements

The author wish to thank Cumhuriyet University academic research council for financial support (Grant number CÜBAP-ECZ-020) to carry out this research.

## References

- Abu Zarin, M., Wan, H.Y., Isha, A., Armania, N. (2016). Antioxidant, antimicrobial and cytotoxic potential of condensed tannins from *Leucaena leucocephala* hybrid-Rendang. Food Sci. Hum. Wellness 5, doi:10.1016/j.fshw.2016.02.001
- Awouafack, M.D., McGaw, L.J., Gottfried, S., Mbouangouere, R., Tane, P., Spiteller, M., Eloff, J.N. (2013). Antimicrobial activity and cytotoxicity of the ethanol extract, fractions and eight compounds isolated from *Eriosema robustum* (Fabaceae). BMC Complement. Altern. Med. 13, doi:10.1186/1472-6882-13-289
- Blois, M., (1958). Antioxidant determination by the use of a stable free radical. Nature 181, 1199–1200.
- Harman, D. (1994). Free-Radical Theory of Aging. Annals of the New York Academy of Sciences, 717(1), 1-15.
- Karaalp, C., Yurtman, A.N., Yavasoglu, N.U.K. (2009). Evaluation of antimicrobial properties of *Achillea* L. flower head extracts. Pharm. Biol. 47, 86–91. doi:10.1080/13880200802448682
- Manayi, A., Mirnezami, T., Saeidnia, S., Ajani, Y. (2012). Pharmacognostical Evaluation, Phytochemical Analysis and Antioxidant Activity of the Roots of *Achillea tenuifolia* LAM. Pharmacogn. J. 4, 14–19. doi:10.5530/pj.2012.30.3
- Re, R., Pellegrini, N., Proteggente, A., Pannala, A., Yang, M. (1999). Antioxidant activity applying an improved ABTS radical cation decolorization assay. Free Radic. Biol. Med. 26, 1231–1237.
- Saeed, N., Khan, M.R., Shabbir, M. (2012). Antioxidant activity, total phenolic and total flavonoid contents of whole plant extracts *Torilis leptophylla* L. BMC Complement. Altern. Med. 12, 1174. doi:10.1186/1472-6882-12-221
- Saeidnia, S., Gohari, A., Mokhber-Dezfuli, N., Kiuchi, F. (2011). A review on phytochemistry and medicinal properties of the genus *Achillea*. Daru 19, 173–86.
- Toncer, O., Basbag, S., Karaman, S., Diraz, E. (2010). Chemical Composition of the Essential Oils of some *Achillea* Species Growing Wild in Turkey. Int. J. Agric. Biol. 12, 527–530.
- Yaşar S, Fakir, H. (2016). Effect of reaping time on volatile constituents of *Achillea teretifolia* Willd. Turkish Journal of Forestry 17, 52–55.

## A Study on the Classification of Woody Vegetation in Forest Ecology (Isparta- Yenişarbademli Case)

Esra Özge Kurt<sup>1</sup>, Mehmet Güvenç Negiz<sup>2\*</sup>

**Abstract:** This study was carried out to classify woody vegetation in Yenişarbademli forest areas. The vegetation classification is important to biological diversity conservation and sustainability. In the study, 103 sample plots 20 x 20 m size were taken for inventory. In the study area, woody plant species and environmental factors were recorded in the inventory. Cluster analysis and two way indicator species analysis (TWINSPAN) were performed to distinguish vegetation groups in the study. While cluster analysis and two way indicator species analysis were carried out, present/ absence values of plant species were used. By using the cluster analysis distinctions, a relationship analysis between qualities was also applied. Multi-response permutation procedures (MRPP) analysis was applied to the cluster analysis and TWINSPAN results to determine which groups would use the resulting analyzes. The results obtained from MRPP analysis showed that the best option was provided with TWINSPAN used five indicatory species. As a result of TWINSPAN used five indicatory species, THYSAM, CIRARV, BERVUL, JUNOXY and EUPSPP species were identified as discriminating species. The first group represented 51 and the second group represented 52 sample plots. Discriminating species were determined to be species located in high elevation of the study area. As a result of the analysis, the species in the first group is positive indicators while in the second group is negative indicators. As a result, elevation is the most important variable when discriminating species group and indicator species are identified.

**Keywords:** Indicator Species, Vegetation Classification, Yenişarbademli District, Elevation

### Orman Ekolojisinde Odunsu Vejetasyonun Sınıflandırmasına Yönelik Bir Çalışma (Isparta-Yenişarbademli Örneği)

**Özet:** Bu çalışma Yenişarbademli ormanlık alanlarında odunsu vejetasyonunun sınıflandırılması amacıyla gerçekleştirilmiştir. Vejetasyon sınıflandırması, biyolojik çeşitliliği korumak ve devamını sağlamak adına önemli bilgiler vermektedir. Çalışmada arazi envanteri ile 20x20 metre boyutlarında 103 örnekleme alanı alınmıştır. Her örnekleme alanında odunsu bitki türleri ve yetiştirme ortamı özellikleri envantere kaydedilmiştir. Çalışmada vejetasyon gruplarını ayırabilmek amacıyla kümeleme analizi ve iki yönlü gösterge analizi gerçekleştirilmiştir. Kümeleme analizi ve iki yönlü gösterge analizi gerçekleştirilirken bitki türlerine ait var- yok değerleri kullanılmıştır. Kümeleme analizi ayrımlarından yararlanarak ayrıca nitelikler arası ilişki analizi uygulanmıştır. Yapılan analizler sonucunda hangi grupların kullanacağına karar vermek amacıyla kümeleme analizi ve iki yönlü gösterge analizi sonuçlarına çoklu permütasyon testi (MRPP) analizi uygulanmıştır. MRPP analizinin sonucuna göre iki yönlü gösterge analizinin beş göstergeli ikili grup ayrımı üzerinden yorumların yapılmasının daha uygun olduğuna karar verilmiştir. Vejetasyon sınıflandırmasına yönelik gerçekleştirilen birçok çalışmada iki yönlü gösterge analizinin etkili ve güncel bir yöntem olarak seçilmiş olması elde edilen bu sonucu doğrulamaktadır. İki yönlü gösterge analizinin 5 indikatör ikili grup ayrımı sonucunda THYSAM, CIRARV, BERVUL, JUNOXY, EUPSPP türleri ayrıcı türler olarak tespit edilmiş, ayrıca ikili ayrımın ilk grubunu 51, ikinci grubunu 52 örnekleme alanı temsil etmiştir. Çalışmada

<sup>1</sup>Süleyman Demirel Üniversitesi, Orman Fakültesi, 32100, Isparta, Türkiye.

<sup>2</sup>Süleyman Demirel Üniversitesi, Sütçüler Hasan Gürbüz Meslek Yüksek Okulu, 32950, Isparta, Türkiye.

\*Corresponding author (iletişim yazarı): \*mehmetnegiz@sdu.edu.tr

Citation (Atıf): Kurt, E.Ö., Negiz, M.G. (2018). A Study on the Classification of Woody Vegetation in Forest Ecology (Isparta-Yenişarbademli Case). Bilge International Journal of Science and Technology Research, 2 (1): 98-109.

elde edilen ayırıcı türlerin genel olarak alanın yüksek kesimlerinde dağılım gösteren türler olduğu görülmüştür. Burada ilk grupta bu türler pozitif göstergeler iken, ikinci grupta negatif gösterge niteliğinde olmuştur. Dolayısıyla çalışmanın sonucu olarak; yöredeki grup ayrımlarının oluşmasında ve gösterge türlerinin tespit edilmesinde yükseltinin en önemli değişken olduğunu söylemek mümkün olmuştur.

**Anahtar Kelimeler:** Gösterge Tür, Vegetasyon Sınıflandırması, Yenişarbademli Yöresi, Yükselti

## 1. Giriş

Vejetasyon, bir ülke veya bir bölgenin belirli yetiştirme ortamı koşullarına göre gelişen ve benzer ekolojik isteklere sahip olan bitki türlerinin oluşturdukları bitki toplulukları anlamına gelmektedir (Negiz, 2009).

Orman ekosistemlerinde biyolojik çeşitliliği korumak ve devamlılığını sağlamak için bitki toplumlarının ekolojik özelliklerinin belirlenmesi oldukça önemlidir (Altan vd., 2017). Ancak ekosistem içindeki ilişkilerin çok yönlü olarak belirlenmesi oldukça karmaşık ve zor bir iştir (Özkan ve Negiz, 2011).

Orman ekolojisi çalışmalarında ise vejetasyonun sınıflandırması orman amenajmanı ve silvikültür planlarının yapılmasında, bölgesel ve yöresel tür envanteri ve tür dağılımının tespitinde, orman varlığı envanterlerinin çıkarılmasında büyük önem arz etmektedir. Özellikle vejetasyonun hiyerarşik-analitik değerlendirilmesi üzerine günümüze kadar çok sayıda çalışma yapılmıştır ve birçok araştırmacı tarafından geliştirilen vejetasyon ayırım yöntemleri bulunmaktadır (Williams ve Lamberg, 1959; Pritchard ve Anderson, 1971; Negiz, 2009; Ulsan, 2016).

Söz konusu vejetasyon ayırım yöntemlerinden birliktelik analizi var-yok verileri kullanarak ve örnek çiftleri arasında Ki-kare değerlerinin hesaplanması ile gerçekleştirilmektedir. Birliktelik analizinde elde edilen her ayırım, ayırıcı tür isminde tek bir tür tarafından temsil edilmektedir (Williams ve Lamberg, 1959).

Bitki toplumların ayırımında kullanılan yöntemlerden bir diğeri iki yönlü gösterge (Twinspan) analizidir. İki yönlü gösterge analizi hem var-yok hem de sayısal veriler kullanılarak belirlenebilmektedir. Bu analiz yöntemi ile ayrılan bitki toplumlarının gösterge türleri aynı anda tespit edilebilmektedir (Hill, 1979).

Vejetasyon sınıflandırmasında kullanılan diğer bir yöntem ise kümeleme (Cluster) analizidir. Bu

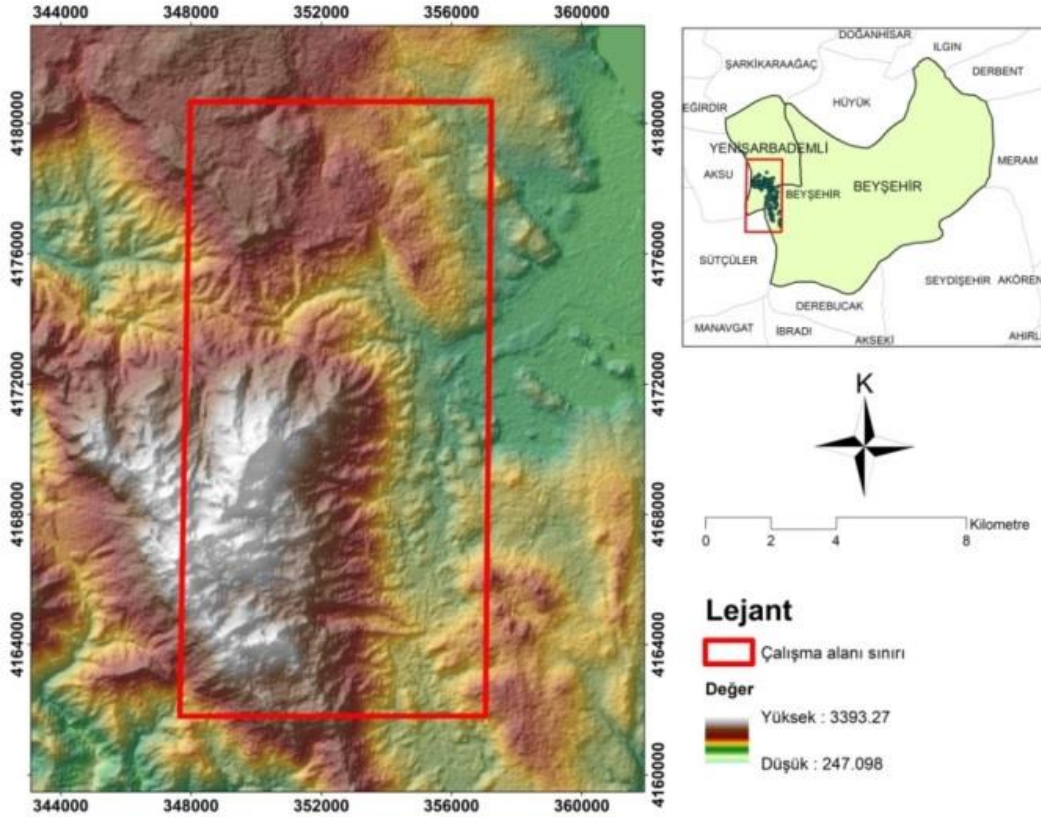
analizde de hem var-yok hem de sürekli veriler kullanılarak gerçekleştirilebilmektedir. Kümeleme analizi gösterge tür vermemektedir. Ancak kümeleme analizi ile bitki toplumlarının ayırımı sonucu nitelikler arası ilişki analizi veya gösterge analizi ile ayrılan grupların gösterge türleri tespit edilebilmektedir (Pritchard ve Anderson, 1971). Vejetasyon toplumlarının sınıflandırılması çalışmalarında genellikle kümeleme analizi veya iki yönlü gösterge analizi tercih edilmektedir (Zavala-Hurtado vd., 1996; Janisova, 2005; Jabeen and Ahmad, 2009; Özkan ve Negiz, 2011; Zhang and Zhang, 2011; Peng vd., 2012; Şentürk vd., 2013).

Yenişarbademli ormanlık alanlarında gerçekleştirilen bu çalışmada ilk aşamada arazi envanteri sonucunda elde edilen bitki türleri kümeleme analizi yöntemi ile gruplandırılmıştır. İkinci aşamada elde edilen gruplara nitelikler arası ilişki analizi uygulanarak gösterge türler belirlenmiştir. Daha sonra ise diğer bir yöntem olarak iki yönlü gösterge analizi yöntemi uygulanmıştır. Böylece, en objektif yaklaşımla bir vejetasyon sınıflandırması gerçekleştirilmeye çalışılmıştır (Fontaine vd., 2007; Özkan vd., 2009; Özkan, 2009).

## 2. Materyal ve Yöntem

### 2.1. Materyal

Çalışma alanı 37°38'35" kuzey 31°21'17" doğu koordinatlarında Akdeniz Bölgesi'nin Göller Yöresinde, Beyşehir Gölü'nün batısında, büyük bölümü Isparta olmak üzere, Isparta-Konya il sınırları içinde yer almaktadır (Şekil 1). Alanda Dedegül Tepe (2992 m), alan içindeki en fazla yükseltiye sahip kısımdır. Kartal Tepe (2983 m), Karaçukur Tepe (2932 m) dağın diğer yüksek tepeleri arasındadır (Çılğın, 2015).



Şekil 1. Çalışma alanına ait yer bulduru haritası

Çalışmanın yürütüldüğü alana ait iklim özelliklerini ifade edebilmek için sahada ve çevresinde yer alan Yenişarbademli Meteoroloji İstasyonunun uzun yıllara ait verilerinden faydalanılmıştır (DMİ,2017). Uzun yıllara ait aylık ortalama sıcaklıklara göre çalışma alanındaki en yüksek sıcaklığa sahip ayın 21,1°C ile Temmuz, en düşük sıcaklığa sahip ayın ise -0.9°C ile Ocak ayı olduğu tespit edilmiştir. Çalışma alanına ait yağış ortalamasına bakıldığında ise yıllık ortalama yağış miktarının 727 mm olduğu belirlenmiştir.

Yörenin iklim tipini belirlemek amacıyla Yenişarbademli (Isparta) meteoroloji istasyonunun verileri Thornthwaite yöntemi ile değerlendirilmiştir (Thornthwaite, 1948; Çepel,

1995). Thornthwaite yöntemi sonucunda çalışma alanının nemli bir iklime sahip olduğu belirlenmiştir.

## 2.2. Yöntem

Çalışmada 20X20m boyutlarında 103 örnekleme alanı alınmıştır. Örnekleme alanlarında yer alan odunsu türler Braun-Blanquet yöntemine göre kaydedilmiştir (r,+1,2,3,4,5), (Barkman,1964). Bu çalışmada odunsu bitki türleri kullanılmıştır. Bitki türleri daha sonra örnekleme alanlarına göre düzenlenmiştir. Bitki türlerinin kodları Çizelge 1’de verilmiştir. Bu çalışmada var/yok değerleri itibariyle veri matrisi düzenlenmiştir.

**Çizelge 1.** Örnekleme alanlarında tespit edilen odunsu bitki türleri ve kodları

<i>Abies cilicica</i> (ANT. ET KOTSCHY) CARR. subsp. <i>isaurica</i> COODE ET CULLEN	ABICIL
<i>Amelanchier parviflora</i> BOISS. var. <i>parviflora</i> BOISS.	AMEPAR
<i>Berberis vulgaris</i> L.	BERVUL
<i>Cedrus libani</i> A. Rich	CEDLIB
<i>Centaurea thirkei</i> SCHULTZ BIP.	CENTHI
<i>Cephalaria speciosa</i> BOISS. ET KOTSCHY	CEPSPE
<i>Cirsium arvense</i> (L.) SCOP. subsp. <i>vestitum</i> (WIMMER ET GRAB.) PETRAK	CIRARV
<i>Cistus laurifolius</i> L.	CISLAU
<i>Clinopodium vulgare</i> L. subsp. <i>vulgare</i> L.	CLIVUL
<i>Colutea cilicica</i> BOISS. ET BAL.	COLCIL
<i>Crataegus monogyna</i> JACQ. subsp. <i>monogyna</i> JACQ.	CRAMON
<i>Crepis</i> sp.	CRESPP
<i>Dianthus zonatus</i> FENZL var. <i>hypochlorus</i> (BOISS. ET HELDR.) REEVE	DIAZON
<i>Digitalis davisiana</i> HEYWOOD	DIGDAV
<i>Euphorbia</i> sp.	EUPSPP
<i>Hypericum</i> sp.	HYPSP
<i>Jasminum fruticans</i> L.	JASFRU
<i>Juniperus excelsa</i> M. BIEB.	JUNEXC
<i>Juniperus oxycedrus</i> L. subsp. <i>oxycedrus</i> L.	JUNOXY
<i>Lamium cariense</i> R. MILL	LAMCAM
<i>Lapsana communis</i> sp.	LAPCOM
<i>Lathyrus laxiflorus</i> (DESF.) O. KUNTZE subsp. <i>laxiflorus</i> (DESF.) O. KUNTZE	LATINF
<i>Laurus nobilis</i> L.	LAUNOB
<i>Melia azedarach</i> L.	MELAZE
<i>Paeonia turcica</i> DAVIS ET CULLEN	PAESPP
<i>Phlomis grandiflora</i> H. S. THOMPSON var. <i>grandiflora</i> H. S. THOMPSON	PHLGRA
<i>Phlomis</i> sp.	PHLSPP
<i>Picea orientalis</i> (L.) LINK	PICORI
<i>Pinus nigra</i> J. F. ARNOLD subsp. <i>nigra</i> var. <i>caramanica</i> (LOUDON) REHDER	PINNIG
<i>Pistacia terebinthus</i> L. subsp. <i>palaestina</i> (BOISS.) ENGLER	POSTER
<i>Populus tremula</i> L.	POPTRE
<i>Prunus divaricata</i> LEDEB. subsp. <i>divaricata</i> LEDEB.	PRUDIV
<i>Pyrus elaeagnifolia</i> PALLAS subsp. <i>elaegnifolia</i> PALLAS	PYRELA
<i>Quercus cerris</i> L. var. <i>cerris</i> L.	QUECER
<i>Quercus coccifera</i> L.	QUECOC
<i>Quercus infectoria</i> OLIVIER subsp. <i>boissieri</i> (REUTER) O. SCHWARZ	QUEINF
<i>Rosa canina</i> L.	ROSCAN
<i>Rubus canescens</i> DC. var. <i>canescens</i> DC.	RUBCAN
<i>Salvia tomentosa</i> Miller	SALTOM
<i>Sambucus ebulus</i> L.	SAMEBU
<i>Sanguisorba minor</i> subsp. <i>muricata</i> (Spach) Briq.	SANMIN
<i>Sideritis condensata</i> BOISS. ET HELDR. APUD BENTHAM.	SIDCON
<i>Silene spergulifolia</i> (DESF.) BIEB.	SILSPE
<i>Sorbus</i> sp.	SORSPP
<i>Teucrium polium</i> L.	TEUPOL
<i>Thymus samius</i> Ronniger. & Rech. Fil	THYSAM
<i>Verbascum</i> sp.	VERSPP
<i>Viscum album</i> L. subsp. <i>album</i> L.	VISALB

Veri seti, kümeleme ve iki yönlü gösterge analizleri ile değerlendirilmiştir. Çalışmada Ward's metoduna göre kümeleme analizi uygulanmıştır. Kümeleme analizinde kesme seviyeleri Özkan (2009) tarafından açıklandığı şekilde gerçekleştirilmiştir. Ayrıca tek indikatör seviyesinden beş indikatör seviyesine kadar her biri için toplam beş adet iki yönlü gösterge analizi

Hill (1979) tarafından açıklandığı şekilde toplamda 6 farklı analiz uygulanmıştır.

Kümeleme analizi ve iki yönlü gösterge analizi ile ayrımı gerçekleştirilen grupların en uygun olanına karar verebilmek için MRPP analizi gerçekleştirilmiştir. MRPP analizinde T, A ve P değerleri karşılaştırılarak en uygun grup ayrımına karar verilmiştir.

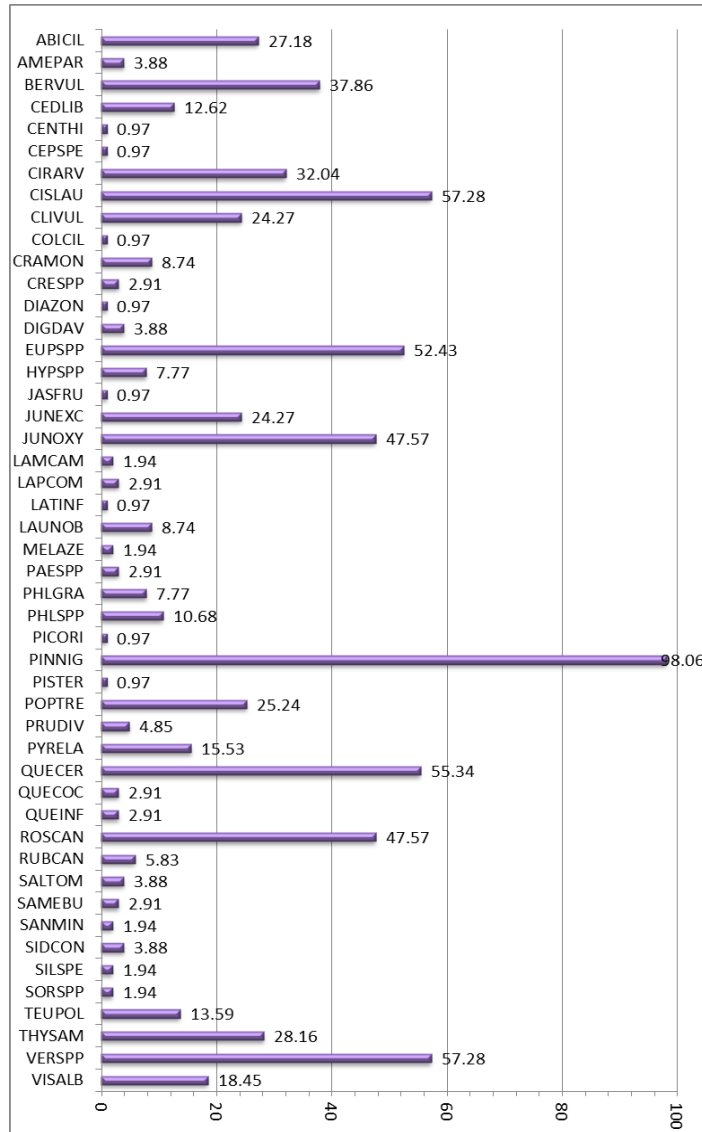
Kümeleme analizi gerçekleştikten sonra örnekleme alanların buldukları grupların gösterge bitki türleri nitelikler arası ilişki analizi kullanılarak belirlenmiştir (Cole, 1949; Poole, 1974; Özkan, 2002; Gülsoy ve Özkan, 2013).

Nitelikler arası ilişki analizi yukarıdaki bilgiler doğrultusunda gerçekleştirilmiştir. Çalışmada gerçekleştirilen analitik değerlendirmeler için PAST (Paleontological Statistics), CAP (Community Analysis Package), PC-ORD, SPSS

(Statistical Package for the Social Sciences) paket programlarından faydalanılmıştır (Seaby ve Henderson, 2004; SPSS, 2010; Hammer vd., 2011; McCune ve Mefford, 2011)

### 3.Bulgular

Yenişarbademli ormanlık alanlarında gerçekleştirilen çalışmada 103 örnekleme alanında toplamda 48 odunsu bitki türü tespit edilmiştir. Envantere kaydedilen odunsu bitki türlerinin frekans değerleri Şekil 2' de gösterilmiştir.

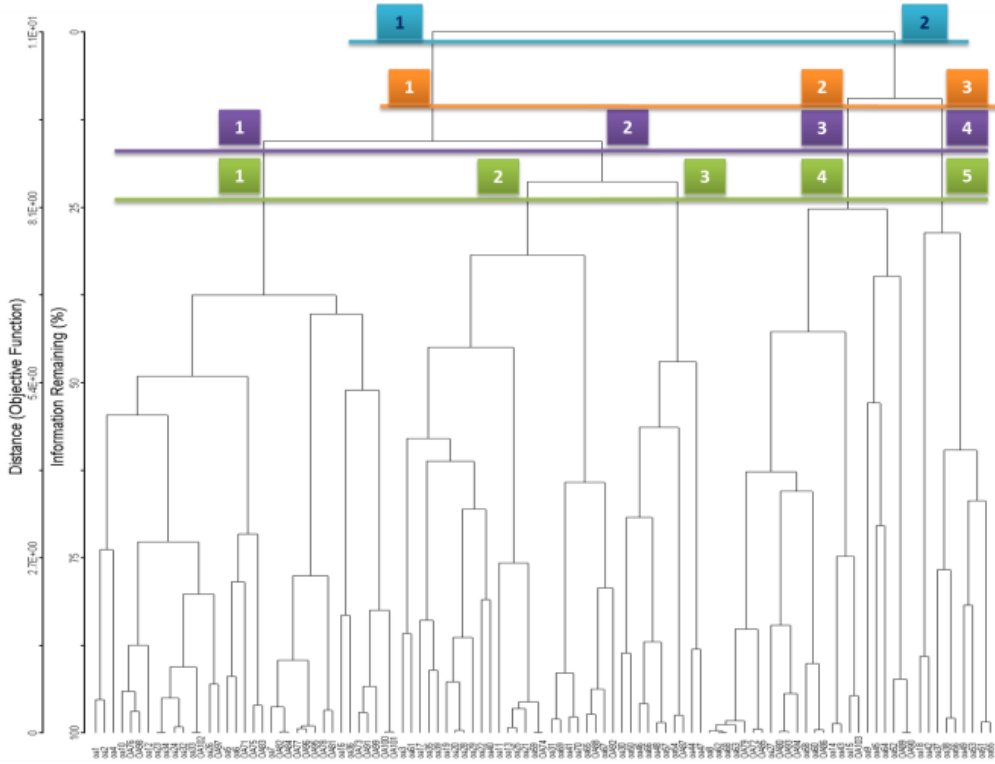


Şekil 2. Arazi envanteri sonucu kaydedilen bitki türlerinin frekans (%) değerleri



Ward's metoduna dayalı olarak gerçekleştirilen kümeleme analizi sonucu 2'li, 3'lü, 4'lü ve 5'li

grup ayrımlarından yararlanılmıştır (Şekil 3).



Şekil 3. Ward's metoduna dayalı gerçekleştirilen kümeleme analizi sonuçları

Kümeleme analizi grupların gösterge bitki türlerini belirlemek için nitelikler arası ilişki analizi uygulanmıştır. Kümeleme analizinin dörtlü grup ayrımlarına uygulanan nitelikler arası olan analizi sonucu Çizelge 2' de verilmiştir. Burada sadece dörtlü grup ayrımlara ait sonuçlarının sunulmasının sebebi ileride MRPP analizleri bölümünde açıklanmıştır.

**Çizelge 2.** Kümeleme analizi sonucu ayrılan grupların nitelikler arası ilişki analizi sonucu elde edilen gösterge türleri

Ayrım grupları	Türler	Ki kare	Önem seviyesi	C3
1	CISLAU	17.515	0.000	0
	JUNOXY	12.097	0.001	0.581
	LAUNOB	5.076	0.024	-0.233
	QUECER	5.552	0.018	0.423
	ROSCAN	26.463	0.000	0.770
	RUBCAN	6.917	0.009	0.198
	SILSPE	3.963	0.047	0.091
	VERSPP	11.182	0.001	0.578
	MELAZE	3.963	0.047	-0.057
	2	AMEPAR	8.085	0.004
BERVUL		6.077	0.014	0.409

	CISLAU	40.052	0.000	0
	CIRARV	12.050	0.001	0.515
	CLIVUL	4.758	0.029	-0.349
	CRESPP	6.003	0.014	0.135
	EUPSPP	42.501	0.000	0.900
	JUNEXC	25.982	0.000	0.614
	JUNOXY	4.966	0.026	0.396
	LAUNOB	19.160	0.000	0.371
	PHLSPP	4.828	0.028	0.222
	POPTRE	14.078	0.000	-0.596
	PRUDIV	10.210	0.001	0.218
	TEUPOL	10.128	0.001	-0.081
	THYSAM	17.895	0.000	0.570
3	BERVUL	8.556	0.003	-0.467
	CEDLIB	4.520	0.034	-0.218
	CISLAU	19.006	0.000	0
	CIRARV	11.164	0.001	-0.517
	EUPSPP	20.001	0.000	-0.642
	HYPSP	7.457	0.006	0.183
	JUNEXC	10.029	0.002	-0.451
	JUNOXY	19.318	0.000	-0.656
	POPTRE	10.163	0.001	0.371
	PYRELA	5.755	0.016	-0.276
	ROSCAN	19.318	0.000	-0.656
	TEUPOL	4.922	0.027	-0.238
	THYSAM	8.902	0.003	-0.447
	VERSPP	36.076	0.000	-0.745
4	ABICIL	26.000	0.000	0.364
	CEDLIB	3.836	0.050	0.098

CISLAU	8.591	0.003	0
CLIVUL	5.151	0.022	0.170
JUNOXY	8.949	0.003	-0.327
LAMCAM	4.355	0.035	0.038
PINNIG	4.355	0.037	-0.038
POPTRE	4.802	0.028	0.167
QUECER	4.376	0.036	-0.236
ROSCAN	5.257	0.022	-0.252
SAMEBU	32.273	0.000	0.119
THYSAM	3.865	0.049	-0.184
VISALB	4.431	0.035	0.132

Kümeleme analizi sonucunda hangi grup ayrımının daha uygun olacağına karar verebilmek amacıyla gerçekleştirilen MRPP analizi sonucunda dörtlü grup ayrımının daha uygun olacağına karar verilmiştir. Ardından gösterge türleri belirlemek amacıyla gerçekleştirilen nitelikler arası ilişki analizi sonuçlarına göre en önemli gösterge türleri sırası ile birinci grupta CISLAU ve ROSCAN, ikinci grupta CISLAU, EUPSPP, JUNEXC, LAUNOB, POPTRE ve THYSAM olarak belirlenmiştir. üç ayırım grubunda CISLAU, EUPSPP, JUNOXY, ROSCAN ve VERSPP olarak ayrılırken, dört ayırım grubunda SAMEBU ve ABICIL en önemli gösterge bitki türleri olmuştur.

İki yönlü gösterge analizi sonuçlarına geldiğimizde ise tek indikatör seviyesinden beş indikatör seviyesine kadar her biri için toplam beş adet iki yönlü gösterge analizi Hill (1979) tarafından açıklandığı şekli ile gerçekleştirilmiştir.

Tek indikatörlü iki yönlü gösterge analizinin ilk ayırım seviyesi için oluşan iki grubun birinde 52 sayıda, diğerinde 51 sayıda örnekleme alan bulunmaktadır. İkili ayırım sonucunda birinci grubun gösterge türü ise EUPSPP olarak belirlenmiştir. Daha aşağı seviyeden kesilen ikinci seviyede dört grup ayrılmıştır. Bunlardan ilk ikisi önceki ilk grubun diğer ikisi ise ilk ayırımdaki ayrılan ikinci grubun alt gruplardır. Burada birinci grupta 15, ikinci grupta 37, üçüncü grupta 38, dördüncü grupta ise 13 sayıda örnekleme alan ayrılmaktadır. Dörtlü grup ayrımı sonrasında ise dördüncü grubun gösterge türü THYSAM, ikinci grubun gösterge türü ABICIL olarak belirlenmiştir.

İki indikatörlü iki yönlü gösterge analizinin ilk ayırım seviyesi için oluşan iki grubun birinde 52 sayıda, diğerinde 51 sayıda örnekleme alanı bulunmaktadır. İkili ayırım sonucunda birinci grubun gösterge türü ise EUPSPP olarak belirlenmiştir. Daha aşağı seviyeden kesilen ikinci seviyede dört grup ayrılmıştır. Bunlardan ilk ikisi ilk ayırımda ayrılan birinci grubun diğer ikisi ise ilk ayırımda ayrılan ikinci grubun alt gruplardır.

Burada birinci grupta 15, ikinci grupta 37, üçüncü grupta 39, dördüncü grupta ise 12 sayıda örnekleme alanı ayrılmaktadır. Dörtlü grup ayrımı sonrasında ise ikinci grubun gösterge türü ABICIL, üçüncü grubun gösterge türü THYSAM, dördüncü grubun gösterge türü ROSCAN olarak belirlenmiştir.

Üç indikatörlü iki yönlü gösterge analizinin ilk ayırım seviyesi için oluşan iki grubun birinde 35 sayıda, diğerinde 68 sayıda örnekleme alanı bulunmaktadır. İkili ayırım sonucunda birinci grubun gösterge türü ise BERVUL, JUNOXY, EUPSPP olarak belirlenmiştir. Daha aşağı seviyeden kesilen ikinci seviyede dört grup ayrılmıştır. Bunlardan ilk ikisi ilk ayırımda ayrılan birinci grubun diğer ikisi ise ilk ayırımda ayrılan ikinci grubun alt gruplardır. Burada birinci grupta 7, ikinci grupta 28, üçüncü grupta 46, dördüncü grupta ise 22 sayıda örnekleme alanı ayrılmaktadır. Dörtlü grup ayrımı sonrasında ise birinci grubun gösterge türü CISLAU, ikinci grubun gösterge türü ABICIL, THYSAM, üçüncü grubun gösterge türü LAUNOB, dördüncü grubun gösterge türü ise ROSCAN olarak belirlenmiştir.

Dört indikatörlü iki yönlü gösterge analizinin ilk ayırım seviyesi için oluşan iki grubun birinde 35 sayıda, diğerinde 68 sayıda örnekleme alanı bulunmaktadır. İkili ayırım sonucunda birinci grubun gösterge türü ise BERVUL, JUNOXY, EUPSPP olarak belirlenmiştir. Daha aşağı seviyeden kesilen ikinci seviyede dört grup ayrılmıştır. Bunlardan ilk ikisi ilk ayırımda ayrılan birinci grubun diğer ikisi ise ilk ayırımda ayrılan ikinci grubun alt gruplardır. Burada birinci grupta 7, ikinci grupta 28, üçüncü grupta 43, dördüncü grupta ise 25 sayıda örnekleme alanı ayrılmaktadır. Dörtlü grup ayrımı sonrasında ise birinci grubun gösterge türü CISLAU, ikinci grubun gösterge türü ABICIL, üçüncü grubun gösterge türü TEUPOL, LAUNOB, THYSAM, dördüncü grubun gösterge türü ise ROSCAN olarak belirlenmiştir.

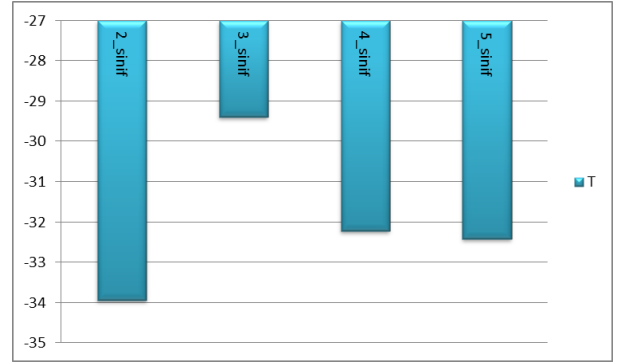
Beş indikatörlü iki yönlü gösterge analizinin ilk ayırım seviyesi için oluşan iki grubun birinde 48 sayıda, diğerinde 55 sayıda örnekleme alanı bulunmaktadır. İkili ayırım sonucunda birinci grubun gösterge türü ise THYSAM, CIRARV, BERVUL, JUNOXY, EUPSPP olarak belirlenmiştir. Daha aşağı seviyeden kesilen ikinci seviyede dört grup ayrılmıştır. Bunlardan ilk ikisi ilk ayırımda ayrılan birinci grubun diğer ikisi ise ilk ayırımda ayrılan ikinci grubun alt gruplardır. Burada birinci grupta 12, ikinci grupta 36, üçüncü

grupta 44, dördüncü grupta ise 11 sayıda örnekleme alanı ayrılmaktadır (Şekil 6). Dörtlü grup ayrımı sonrasında ise birinci grubun gösterge türü ROSCAN, QUECER, CISLAU, ikinci grubun gösterge türü ABICIL, VERSPP, üçüncü grubun gösterge türü ABICIL, LAUNOB, THYSAM, dördüncü grubun gösterge türü ise BERVUL, ROSCAN olarak belirlenmiştir.

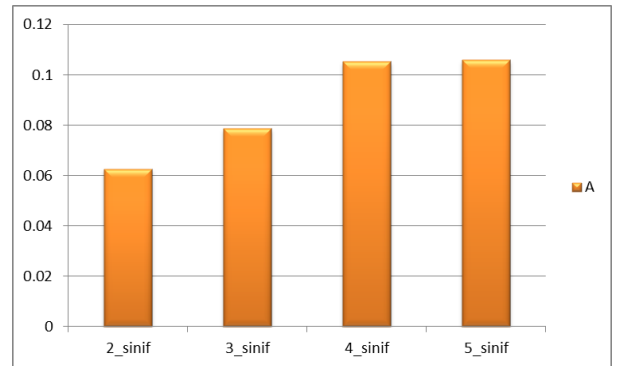
MRPP analiz sonuçları Çizelge 3’de verilmiştir. Bütün kesme seviyelerindeki ayrımlar için T değerleri (-29.38 ile -35.44) aralığında, A değerleri (0.06 ile 0.68) aralığında değişmektedir. Ayrılan grup seviyelerinin ortalamaları da şekilde sütun grafikte gösterilmiştir (Şekil 4, Şekil 5). Burada iki gruplu ayrımların diğer seviye ayrımlarından daha iyi sonuç verdiği görülmektedir. Kümeleme analizine göre iki yönlü gösterge analizinin daha uygun T ve A değerleri içermektedir. Bu sebepten iki yönlü gösterge analizinin ayırım gruplarına odaklanılmasına karar verilmiştir. Her indikatör seviyesi için yapılan iki yönlü gösterge analizinin ikili gruplarına dikkat verilmiştir. Daha sonra her indikatör sayısı için tür grupları incelenmeye başlanmıştır. Beş indikatör ile sınırlandırılmış iki yönlü gösterge analizinin ekolojik anlamda daha anlamlı sonuçlar gösterdiğine karar verilmiştir. Bu sebepten beş indikatörlü iki yönlü gösterge analizi ile bitki türlerinin gruplandırması yapılmış ve Şekil 6’da gösterilmiştir.

**Çizelge 3.** Grupların ayırım seviyeleri için T, A ve P değerleri

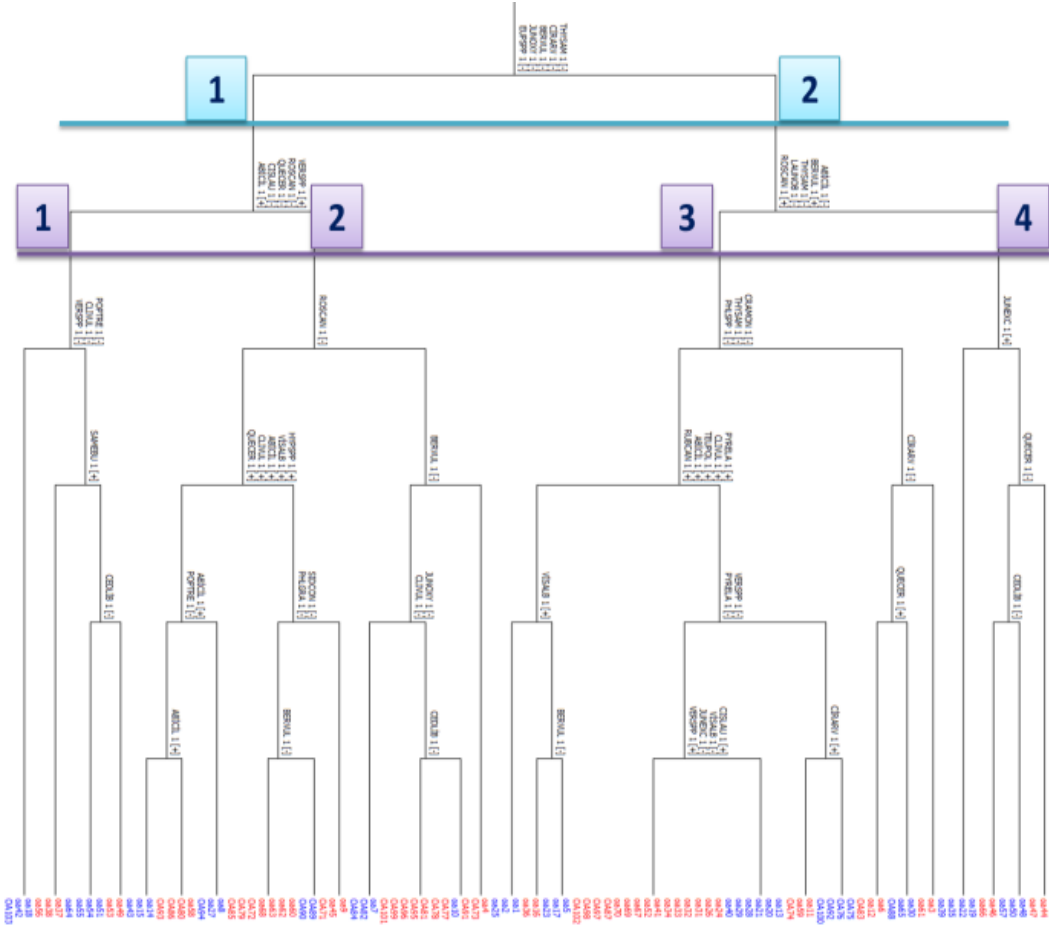
Gruplar	T	A	P
kümeleme_2	-31.7211	0.058680	0
kümeleme_3	-29.3821	0.078724	0
kümeleme_4	-32.8804	0.107194	0
kümeleme_5	-30.6251	0.682980	0
tw_lind_2ayr	-35.2825	0.065075	0
tw_lind_4ayr	-33.0603	0.107483	0
tw_2ind_2ayr	-35.2825	0.065075	0
tw_2ind_4ayr	-32.9771	0.107328	0
tw_3ind_2ayr	-32.9173	0.060852	0
tw_3ind_4ayr	-30.9921	0.101762	0
tw_4ind_2ayr	-32.9173	0.060852	0
tw_4ind_4ayr	-30.9827	0.101663	0
tw_5ind_2ayr	-35.4386	0.065368	0
tw_5ind_4ayr	-32.4105	0.105915	0



**Şekil 4.** Ayrılan grup seviyelerinin ortalama T değerleri



**Şekil 5.** Ayrılan grup seviyelerinin ortalama A değerleri



Şekil 6. Beş indikatör iki ayırım ayırım grupları için iki yönlü gösterge analizi sonuçları

#### 4. Tartışma ve Sonuçlar

Bu çalışma Isparta Yenişarbademli ormanlık alanlarında odunsu vejetasyonun sınıflandırılması ve sınıflandırılan grupların gösterge türlerini tespit etmek amacıyla bitki toplumlarının sınıflandırması için, kümeleme ve iki yönlü gösterge analizleri yapılmıştır. Gerçekleştirilen MRPP analizi sonucunda en iyi ayırım, iki yönlü gösterge analizinin beş indikatörlü ikili grup ayırımı ile elde edilmiştir.

İki yönlü gösterge analizinin beş indikatörlü ayırımına ait analiz çıktısında birinci grup, THYSAM, CIRARV, BERVUL, JUNOXY, EUPSPP türleri ile ifade edilmektedir. Söz konusu bu türler birinci grubu oluşturan 52 örnekleme alanının pozitif gösterge türleri olarak tanımlanmaktadır. Bu türler ikinci grubu oluşturan 51 örnekleme alanı için ise negatif gösterge niteliğindedir. Beş indikatör ikili ayırım incelendiğinde gösterge türlerinin pozitif ilişki

gösterdiği birinci gruba dahil olan örnekleme alanları çalışma sahasının yüksek dağlık kesimlerinde, negatif ilişki gösterdiği ikinci gruba dahil olan örnekleme alanları ise çalışma sahasının düşük yükseltilerinde konumlandığı görülmektedir. Bu durumun sebebi olarak bitki toplumların dağılımında en önemli yetiştirme ortamı faktörünün yükselti olduğu belirlenmiştir. Benzer şekilde, Akdeniz Bölgesi ve Göller bölgesinde daha önceden yapılan çalışmalarda Atalay (1987), Kantarcı (1991), Özkan (2003b), Karatepe (2005), Fontaine vd. (2007), Negiz (2009), Özkan (2009) tür dağılımında en önemli yetiştirme ortamı faktörünün yükselti olduğunu belirtmişlerdir. Bilindiği üzere yöresel boyutta iklim özellikleri yükseltiye bağlı olarak değişim göstermektedir. Ayrıca iklim farklılıkları toprak özelliklerinin de değişmesine sebep olarak gösterilmiştir (Özkan, 2004; Negiz, 2009).

Bunun yanı sıra gerçekleştirilen Kümeleme analizi sonucunda elde edilen grup ayırımından MRPP

analizi ile dörtlü ayrımın yorumlamak için daha uygun olduğuna karar verilmiştir. Kümeleme analizi dörtlü grup ayrımına gerçekleştirilen nitelikler arası ilişki analizi sonucunda; önemli gösterge türleri sırası ile birinci grupta CISLAU ve ROSCAN, ikinci grupta CISLAU, EUPSPP, JUNEXC, LAUNOB, POPTRE ve THYSAM olarak belirlenmiştir. Üç ayrım grubunda CISLAU, EUPSPP, JUNOXY, ROSCAN ve VERSPP olarak ayrılırken, dört ayrım grubunda SAMEBU ve ABICIL olmuştur. Burada da iki yönlü gösterge analizinin gösterge türlerine benzer bir tespit görülmektedir. Dolayısıyla bitki türlerinin dağılımında en önemli yetiştirme ortamı faktörünün yükseltti olduğu nitelikler arası ilişki analizi ile de ortaya konulmuştur.

Özetle; vejetasyon sınıflandırmasında daha güncel ve etkili bir yöntem olması, ayrıca MRPP analizleri ile de en uygun ayrımları sunması sebebiyle iki yönlü gösterge analizinin kullanılabilmesini söylemek yanlış olmayacaktır. Söz konusu bu yöntem gösterge türlerini de tespit ettiği için kümeleme analizinde uygulandığı gibi ayrı bir gösterge analizi uygulamaya gerek duyulmamaktadır. Bu sebeple bitki toplumlarının sınıflandırılmasında daha sade ve anlaşılır sonuçların iki yönlü gösterge analizi ile elde edilebileceği söylenebilir (Negiz, 2009).

Bu çalışmada elde edilen vejetasyon sınıflandırması gelecekte aynı alanda yapılacak olan vejetasyon sınıflandırması ve haritalanması çalışmaları sayesinde geçmiş-bugün kıyaslanmasının yapılabilmesini sağlayacağı, ayrıca gösterge türlerin tespit edilmesi sayesinde türlerin potansiyel yayılış alanlarının belirlenmesi açısından önem arz etmektedir. Çalışmada elde edilen bilgilerin ileride yapılacak vejetasyon dağılım haritalaması ve potansiyel dağılım modellerine katkı sağlayacağı düşünülmektedir.

### Teşekkür

Bu çalışma, SDÜ-BAPKB tarafından desteklenen “Dedegöl (Yenişarbademli) Dağı Yöresinde Alfa Bitkisel Tür Çeşitliliği İle Çevresel Değişkenler Arasındaki İlişkiler” (Proje Numarası: SDU-BAPKB-4817-YL1-16) adlı çalışmadan elde edilen verilerden yararlanılarak hazırlanmıştır. Bu bağlamda, SDÜ-BAPKB’ ne teşekkür ederiz. Ayrıca istatistik analizlerinin seçilmesi ve uygulanmasında çalışmamıza yön veren TÜBİTAK-2229 Bilim İnsanı Destekleme

Programı, Analitik Doğa-Kümeleme ve Ordınasyon Teknikleri Projesine teşekkür ederiz.

### Kaynaklar

- Altan, Y., Aktaş, K., Suveren, Y.M. (2017). Flora of beydere village (Manisa). Bilge International Journal of Science and Technology Research, 1(2), 143-154.
- Atalay, İ. (1987). Sedir (*Cedrus Libani* a. Rich) ormanlarının yayılış gösterdiği alanlar ve yakın çevresinin genel ekolojik özellikleri ile sedir tohum transfer rejyonlaması. Tarım Orman ve Köy İşleri Bakanlığı Orman Genel Müdürlüğü Yayını, 663, (61), 67s., Ankara.
- Barkman, J.J., Doing, H., Segal, S (1964). Kritische bemerkungen und vorschlag zur quantitativen vegetations analyse. Acta Bot Neerl, 13, 394-419
- Cole, L.C. (1949). The measurement of interspecific association. Ecology, 30(4), 411-424.
- Çepel, N. (1995). Orman Ekolojisi. İstanbul Üniversitesi Orman Fakültesi Yayınları, 433 s, İstanbul.
- Çilgın Z. (2015). Dedegöl Dağı kuvaterner buzullaşmaları. Türk Coğrafya Dergisi, 64, 19-37.
- DMİ, (2017). Devlet meteoroloji istasyonu iklim verileri. Ankara.
- Fontaine, M., Aerts, R., Özkan, K., Mert, A., Gülsoy, S., Süel, H., Waelkens, M., Muys, B. (2007). Elevation and exposition rather than soil types determine communities and site suitability in mediterranean mountain forests of southern anatolia, Turkey. Forest Ecology and Management, 247, 18-25.
- Gülsoy, S., Özkan, K., (2013). Determination of Environmental Factors and Indicator Plant Species for Site Suitability Assessment of Crimean Juniper in the Acipayam District, Turkey. Sains Malaysiana, 42(10), 1439–1447.
- Hammer, Ø., Harper, D.A.T., Ryan, P.D. (2001). Past: paleontological statistics software package for education and data analysis. Palaeontologia Electronica, 9, 4(1).
- Hill, M.O. (1979). TWINSpan-a Fortran program for arranging multivariate data in an

- ordered two way table by classification of the individuals and attributes. Cornell University, New York.
- Jabeen T., Ahmad S.S. (2009). Multivariate analysis of environmental and vegetation data of Ayub National Park Rawalpindi. *Soil&Environ*, 28(2), 106-112.
- Janisova, M. (2005). Vegetation-environment relationships in dry calcareous grassland. *Ekologia*, 24(1), 25-44.
- Kantarıcı, M.D. (1991). Akdeniz bölgesi'nin yetişme ortamı bölgesel sınıflandırması. T.C. Tarım Orman ve Köyişleri Bakanlığı Orman Genel Müdürlüğü Yayını, 668, (64), 150.
- McCune, B., Mefford M.J. (2011). PC-ORD multivariate analysis of ecological data, Version 6.0 for Windows.
- Negiz, M.G. (2009). Isparta-Yukarıgökdere (Eğirdir) Yöresi'ndeki odunsu vejetasyonun sınıflandırılması ve haritalanması. Süleyman Demirel Üniversitesi, Fen Bilimleri Enstitüsü, Orman Mühendisliği Anabilim Dalı, Yüksek Lisans Tezi, 101s, Isparta.
- Negiz, M.G. (2013). Gölhisar (Burdur) Yöresinde odunsu tür çeşitliliği ile yetişme ortamı özellikleri arasındaki ilişkiler. Süleyman Demirel Üniversitesi, Orman Fakültesi, Doktora Tezi, 117 s, Isparta
- Özkan, K. (2002). Türler arası birlikteliğin interspesifik korelasyon analizi ile ölçümü. Süleyman Demirel Üniversitesi Orman Fakültesi Dergisi, 2, 71-78.
- Özkan, K. (2003). Beyşehir gölü havzası'nın yetişme ortamı özellikleri ve sınıflandırılması. İstanbul Üniversitesi Fen Bilimleri Enstitüsü Doktora Tezi, 189s.İstanbul.
- Özkan, K. (2004). Prof. Dr. Bekir Sıtkı EVCİMEN Sedir Koruma Ormanı'nda *Toros Sedir*'inin (*Cedrus libani* A. RICH) gelişimi ile yetişme ortamı faktörleri arasındaki ilişkiler. Anadolu Üniversitesi Bilim ve Teknoloji Dergisi, 5(2), 327-332.
- Özkan, K. (2009). Environmental factors as influencing vegetation communities in Acipayam district of Turkey. *Journal Environmental Biology*, 30(5), 741-746.
- Özkan, K., Negiz, M.G. (2011). Isparta Yukarıgökdere Yöresi'ndeki odunsu vejetasyonun hiyerarşik yöntemlerle sınıflandırılması ve haritalanması. Süleyman Demirel Üniversitesi, Orman Fakültesi Dergisi, 12(1), 27-33.
- Özkan, K., Şenol, H., Gülsoy, S., Mert, A., Süel, H., Eser, Y. (2009). Vegetation-environment relationships in mediterranean mountain forests on limeless bedrocks of southern anatolia, Turkey. *Journal of Environmental Engineering and Landscape Management*, 17(3), 154-163.
- Peng W., Song T., Zeng F., Wang K., Du H., Lu S. (2012). Relationships between woody plants and environmental factors in karst mixed evergreen-deciduous broadleaf forest, southwest China. *Journal of Food, Agriculture&Environment*, 10(1), 890-896.
- Poole, R.W. (1974). An Introduction to Quantitative Ecology. McGraw-Hill, 532s, New York.
- Pritchard, N.M., Anderson, A.J.B (1971). Observation on the use of cluster analysis in botany with an ecological example. *The Journal of Ecology*, 59(3), 727-747.
- Seaby, R.M.H., Henderson P.A. (2004). Community analysis package 3.0. Pisces Conservation Ltd., Lympington.
- SPSS (2010). Statistical Package for Windows. Version 17.0, Chicago, IL, USA: SPSS, Inc.
- Şentürk, Ö., Ulsan, MD., Eser, Y., Şenol, A., Özkan, K. (2013). Investigation of relationships between vegetation and environmental factors in the Cariksaraylar district of the sultan mountains. *GeoMed 2013 The 3rd International Geography Symposium*, 597-607.
- Thornthwaite, C.W. (1948). A new and improved classification of climates. *Geographical Review*, 38(1), 55-94.
- Ulsan, M.D. (2016). Akdeniz Bölgesi, Ovacık Dağı Yöresi'nde odunsu vejetasyonun dağılımı ile yetişme ortamı özellikleri arasındaki ilişkilerin ordinasyon metotları ile araştırılması. Süleyman Demirel Üniversitesi, Fen Bilimleri Enstitüsü, Orman Mühendisliği Anabilim Dalı, Doktora Tezi, 152s, Isparta.

- Williams, W.T., Lambert, J.M. (1959). Multivariate methods in plant ecology – 1. Association analysis in plant communities. *The Journal of Ecology*, 47 (1), 83-101.
- Zavala-Hurtado J.A., Valverde P.L., Solis-Diaz A., Vite F., Portilla E. (1996). Vegetation-environment relationships based on a life-forms classification in a semiarid region of Tropical Mexico. *Revista De Biologia Tropical*, 44(2), 581-590.
- Zhang J.T., Zhang F. (2011). Ecological relations between forest communities and environmental variables in the Lishan Mountain Nature Reserve, China. *African Journal of Agricultural Research*, 6(2), 248-259.

## Wildlife Diversity in Reed Beds Around Beyşehir Lake

Ahmet Mert<sup>1\*</sup>, Ahmet Acarer<sup>1</sup>

**Abstract:** This study was carried out to reveal the relation between species diversity calculated by species number data of some mammals and reed beds in northwest of Beyşehir Lake. The study area, which is approximately 1875 ha, is divided into a total of 75 grids measuring 500 x 500 m size. Sign, faeces and tracks of wild mammals were recorded for each grid in the spring and autumn of 2016. Indications of nine wild mammal were detected in 172 points in spring and 290 points in autumn (Jungle cat, Lynx, Wolf, Fox, Coyote, Wild boar, Wild hare, Badger and Beech marten). The Shannon-Wiener diversity index was calculated for each grid using the species number data obtained for spring and autumn. According to the Shannon-Wiener diversity index calculation results, the mapping process was performed by inputting the calculated value of the grid. The total of the data from two period is used in the Shannon-Wiener diversity map of the all area. Shannon-Wiener diversity of all mammals was obtained as  $H_T:1,581$ . When compared to the seasons, this value was calculated as  $H_I=1,418$  in spring and  $H_S=1,56$  in autumn.

**Keywords:** Biodiversity, Reed beds, Shannon-Wiener diversity index, Wildlife.

## Beyşehir Gölü Çevresindeki Sazlık Alanların Yaban Hayatı Çeşitliliği

**Özet:** Bu çalışma Beyşehir Gölü'nün kuzeybatısında bulunan sazlık alanlar ile bazı memeli yaban hayvanlarının birey sayılarıyla hesaplanan tür çeşitliliği arasındaki ilişkilerin ortaya koyulması amacıyla gerçekleştirilmiştir. Yaklaşık 1875 ha olan çalışma alanı 500 x 500 m büyüklüğünde toplam 75 hücreye ayrılmıştır. 2016 yılının ilkbahar ve sonbahar aylarında, çalışma alanı için oluşturulan her bir hücreye gidilerek memeli yaban hayvanlarına ait iz, dışkı ve belirti taraması yapılmıştır. Envanter sonuçlarına göre ilkbahar döneminde 172 noktada, sonbahar döneminde ise 290 noktada 9 farklı (Saz kedisi, Vaşak, Kurt, Tilki, Çakal, Yaban domuzu, Yaban tavşanı, Kaya sansarı ve Porsuk) memeli yaban hayvanına ait belirti tespit edilmiştir. İlkbahar ve sonbahar dönemleri için elde edilen birey sayıları kullanılarak her bir hücre için Shannon-Wiener indisi ile çeşitlilik hesaplanmış ve ait olduğu hücreye hesaplanan değer girilerek haritalama işlemi gerçekleştirilmiştir. Tüm alana ait çeşitlilik haritası içinde iki döneme ait verilerin toplamı kullanılmıştır. Toplam memeli yaban hayvanı tür çeşitliliği  $H_T:1,581$  olarak elde edilirken mevsimlere göre kıyaslandığında ilkbahar döneminde bu değer  $H_I=1,418$  olarak, sonbahar döneminde ise  $H_S=1,56$  olarak hesaplanmıştır.

**Anahtar Kelimeler:** Biyoçeşitlilik, Sazlık alanlar, Shannon-Wiener çeşitlilik indeksi, Yaban hayatı.

### 1. Giriş

Günümüzde sazlık veya bataklık olarak ifade edilen sulak alanlar, ekolojik çeşitlilik açısından tropik ormanlarla beraber yeryüzünün en fazla organik madde üreten ekosistemlerindendir (Williams, 1990; Görmez, 1997; Mitsch ve

Gosselink, 2000). Bir yerin sulak alan olarak ifade edilmesini sağlayan en belirgin özellik, toprak üstü veya toprağın alt tabakasının belirli zaman aralığında suya doymun olması ya da suyla kaplı olmasıdır (Cowardin vd., 1979). Sulak alanlar ekosistemler arası geçiş bölgesi oluşturmakta ve çevresinde bulunan sazlık alanlar sayesinde yaban

<sup>1</sup>Süleyman Demirel Üniversitesi, Orman Fakültesi, 32260, Isparta, Türkiye.

\*Corresponding author (İletişim yazarı): [ahmetmert@sdu.edu.tr](mailto:ahmetmert@sdu.edu.tr)

Citation (Atıf): Mert, A., Acarer A. (2018). Wildlife Diversity in Reed beds Around Beyşehir Lake. Bilge International Journal of Science and Technology Research, 2 (1): 110-119.



hayvanı tür çeşitliliği açısından zengin alanlar olarak tanımlanmaktadır (Batzer ve Wissinger, 1996). Ayrıca sazlık alanlar bulunduğu ortama göre farklı bitki kombinasyonları (nilüfer, şemsiye otu, süsenler vb.) oluşturabilmektedir (Güzelmansur, 2000). Bu nedenle biyolojik çeşitliliğe katkı sağlayan sazlık alanlar, çevresinde bulunan hem flora hem de fauna için yaşam ortamı sağlamaktadır (Katip ve Karaer 2011, Lai vd., 2012).

Bu bağlamda biyolojik çeşitlilik denilince akla; doğal ortamlarında birbirleriyle ilişki içerisinde bulunan organizmaların çeşitliliği gelmektedir. Bu çeşitlilik yaklaşık olarak 15 milyon civarındaki mantar, mikroorganizma, bitki ve yaban hayvan türlerinden oluşmaktadır (Primack, 1995; Mayer, 1995). Doğal ekosistemler içerisinde yer alan kuş ve memeli yaban hayvan türlerinin biyolojik çeşitliliğe katkı sağladığı açık bir şekilde ortadadır (Brooks, 2001, Bibby ve Lunn, 1992). Türkiye mevcut coğrafi konumu sayesinde bitki veya hayvan tür çeşitliliği bakımından son derece zengin bir ülke konumundadır. Sahip olunan bu zenginliği korumak için ülkemiz 1992 yılında imzalamış olduğu “Biyolojik Çeşitlilik Sözleşmesi’ne” taraf olup biyolojik kaynakların küresel ölçekte korunup muhafaza edilmesine destek vermiştir (Güneş, 2011).

Biyolojik Çeşitlilik Sözleşmesi’nde yer alan maddelerin uygulanabilmesi amacıyla başta yaban hayatı üzerine birçok koruma çalışması yapılmaktadır. Fakat yapılan bütün yaban hayatı koruma çalışmalarına rağmen önemli bir başarı sağlanamamıştır (Heywood, 1995; Karagöz, 1998). Koruma çalışmalarında başarılı olabilmek için korunan sahanın özelliklerinin ve burada yaşamlarını sürdüren yaban hayvanlarının habitat isteklerinin ortaya koyulması gerekmektedir (Oruç vd., 2017). Yaban hayvanlarının dağılımını etkileyecek tüm faktörler ile türlerin habitat istekleri göz önüne alınarak yapılacak olan planların daha iyi sonuçlar vereceği ortadadır. Bu bilgiler dahilinde üretilecek haritalar koruma çalışmalarının izlenmesi ve sürdürülebilirliği açısından oldukça önemlidir. Oluşturulacak olan haritalar yaban hayvanlarının tercih ettiği, tür çeşitliliğinin yüksek veya düşük olduğu alanları görsel bir şekilde ortaya koyması açısından kullanıcılara daha kolay izleme imkanı sağlayacaktır.

Doğal ekosistemlerdeki tür çeşitliliğini sayısal değerlerle ifade etmek için farklı indeksler

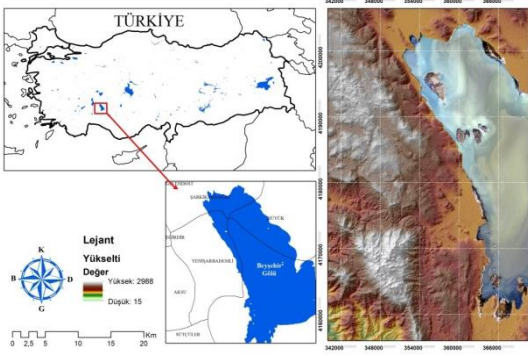
kullanılmaktadır (Warwick ve Clarke, 1995; Desrochers ve Anand, 2004; Özkan, 2016). Örnek alan bazında tür zenginliğini ve yoğunluğunu alfa çeşitliliği ifade etmektedir. Alfa çeşitliliğini belirlemek için birçok indeks kullanılırken, habitat tür çeşitliliğini belirlemek için yaygın olarak bunlar içerisinde Shannon-Wiener indeksi tercih edilmektedir (Aslan, 2008). Yapılan çalışmalar incelendiğinde ise; kuş tür çeşitliliğini, zenginliğini, bolluğunu ve habitat tercihlerini ya da bazı küçük memeli (fareler) tür çeşitliliğini belirlemek için Shannon-Wiener çeşitlilik indeksinin oldukça yaygın kullanıldığını görmek mümkündür (Sullivan vd., 1998; Semere ve Slater, 2007; Aksan ve Mert, 2016; Bibi ve Ali, 2013; Mert ve Yalçınkaya, 2016). Ayrıca diğer iri cüsseli memeli yaban hayvan türlerinin habitat karmaşıklığının yapılandırılması içinde Shannon-Wiener çeşitlilik indeksini kullanan çalışmalara da rastlanmaktadır (August, 1983).

Yapılan bu çalışmada yukarıda bahsedilenlerden farklı olarak; Beyşehir Gölü’nün kuzeybatı kısımlarında bulunan sazlık alanlar ile bazı memeli yaban hayvanlarının birey sayılarından hesaplanan tür çeşitliliği ilişkileri araştırılmıştır. Envanterler sonucu elde edilen yaban hayvanlarına ait var verileri kullanılarak 500 x 500 m (25 ha) büyüklüğündeki hücreler içerisindeki memeli yaban hayvan türlerinin Shannon-Wiener çeşitlilik indeksi hesaplanmış olup, elde edilen veriler ile son aşamada alandaki yaban hayatı çeşitliliği haritalandırılmıştır.

## 2. Materyal ve Yöntem

### 2.1. Çalışma Alanı

Sazlık alanlar birçok memeli yaban hayvanı ve kuş türlerine beslenme, barınma ve üreme ortamı sağlamaktadır. Bu açıdan bakıldığında sazlık alanlar yaban hayvanı tür dağılımını üzerinde etkili olabileceğinden çalışma alanı; sazlıkların yoğun, seyrek ve hiç olmayan bölgelerinin rahatça ayırt edilebileceği Beyşehir Gölü’nün kuzey batı kısmı olarak belirlenmiştir. Beyşehir yöresinde gerçekleştirilen çalışma alanı yaklaşık 1875 ha olup, yükseltisi 1125 - 1355 m arasında değişkenlik göstermektedir (Şekil 1).



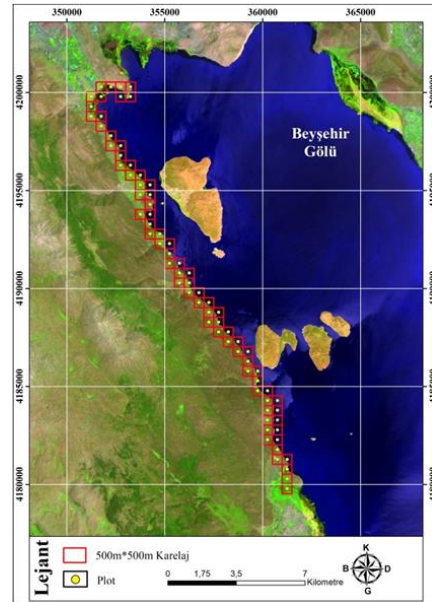
**Şekil 1.** Çalışma alanına ait yer bulduru haritası

Çalışma alanı genel olarak Beyşehir Gölü sınırı ile ulaşım yolu arasında kalmakta olup, bu alan içerisinde yayılış gösteren yaban hayvan türlerini belirlemek amacıyla var-yok taraması gerçekleştirilmiştir. Arazi çalışmalarına ulaşım yolunun diğer tarafının dahil edilmeme nedeni ise, burada bulunan arazi şekli ve vejetasyonun tür dağılımında etkili olacağı ve buradaki tür dağılımının sazlık alan kullanımını yansıtmayacağı düşüncesidir. Yaban hayvan türlerini belirlemek amacıyla kullanılan var-yok taraması ile türlere ait ayak izi, dışkı ve belirtiler fotoğraflanarak daha önceki literatür çalışmaları kapsamında bu verilerin hangi türe ait olduğu yönündeki teşhis işlemleri gerçekleştirilmiştir. Daha sonra yaban hayvanlarına ait elde edilen var verilerinin (iz, dışkı ve belirtilerin) koordinatları GPS yardımıyla alınarak kayıt edilmiştir.

Çalışmanın yapıldığı alanın Akdeniz ve İç Anadolu iklimi arasında olması nedeniyle sert bir iklime sahip olduğunu söylemek mümkündür. Bu nedenle kış aylarında bazı memeli yaban hayvanları yaşamlarını sürdürebilmek için karbonhidrat, protein, vitamin ve mineral ihtiyaçlarını karşılamak zorundadır. Bu gibi besinleri karşılayabilmesi için tabiaten etçil tür bile olsalar bazı mevsimlerde otsu bitkilere yönelmektedir (Oğurlu, 2001; Saatçioğlu 1970). Etçil yaban hayvan türlerinin mevsimsel değişiklikler neticesinde otsu bitkilere yönelmesi ya da besin ihtiyaçlarını karşılamada zorlandıkları için bu durum yaban hayvanlarının habitat tercihlerinde etkili olmaktadır. Aynı zamanda yaz aylarında sulak alanlarda bulunan saz kesimi ya da su seviyesinin azalması nedeniyle bazı sazlık alanlar azalmakta ya da yok olmaktadır. Bazı memeli yaban hayvanlarının da temel besin ihtiyaçlarını karşılamak için yerleşim yerlerinden uzak ormanlık alanları, tarım alanları ve bahçelik

alanları tercih ettikleri literatürde ifade edilmektedir (Virgos vd., 2010). Bu nedenlerden dolayı çalışma alanı içerisinde; kış aylarında görülen dondurucu soğuk ve aşırı kar yağışları, yaz aylarında görülen aşırı sıcaklık ya da kuraklık nedeniyle yaz ve kış mevsimlerinde arazi çalışmaları gerçekleştirilmemiştir.

İki mevsim boyunca gerçekleşen (ilkbahar ve sonbahar) arazi çalışmalarının tamamlanmasının ardından, çalışmada ilk olarak memeli yaban hayvanları tarafından çalışma alanının hangi bölgelerinin daha fazla tercih edildiği tespit edilmeye çalışılmıştır. Bunun için envanter çalışması olarak, Beyşehir Gölü sınırına 50'şer metre aralıklar ile transektler ve transektler üzerinde de 50'şer metre ara ile 114 cm yarıçaplı plotlar atılmıştır (Süel, 2014). Daha sonra her bir plota gidilerek karşılaşılan yaban hayvanlarına ait iz, dışkı ve belirtilerin koordinatları arazi karnelerine kaydedilmiş ve sayısal ortama aktarılmıştır. Çalışmanın ikinci aşamasında yaban hayvanlarına ait var verilerinin sayısal ortama aktarılması sonucunda; alan içerisinde yaban hayvan tür dağılımının haritalanması için çalışma alanı ArcGIS 10.2 yazılımı içerisindeki Create Fishnet eklentisi ile habitat bolluğu ve mekânsal konfigürasyonunun bilgisine dayanılarak Heikkinen vd., (2004) tarafından önerilen 500 x 500 m büyüklüğündeki hücelere ayrılmıştır (Şekil 2).



**Şekil 2.** Çalışma alanına ait 500 x 500 m büyüklüğündeki hücre şebekesi

Plotlar içerisinde tespit edilen yaban hayvanlarına ait veriler ait oldukları hücrelerde birleştirilmiştir. Böylelikle hangi hücrede kaç tür ve bu türlere ait kaç birey olduğu belirlenmiştir. Daha sonra ise 500 x 500 m büyüklüğündeki hücreler içerisinde tür çeşitliliği ve birey sayılarına göre Shannon-Wiener indeksi hesaplanmıştır. Shannon- Wiener çeşitlilik indeksi;

$$H = - \sum \{P_i \ln(P_i)\}$$

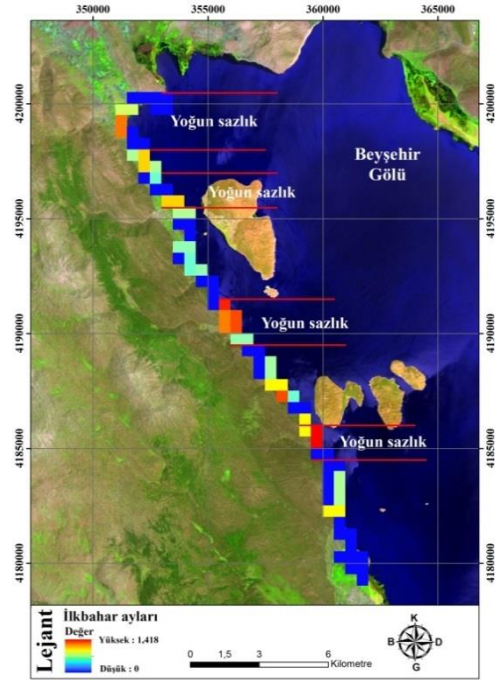
formülü ile hesaplanmıştır. Formülde ilk olarak türlerin oransal değerlerin “ln” değerleri hesaplanır ve bu değer alan içerisindeki tür sayıları ile çarpılmaktadır. Bu işlem alan içerisindeki bütün türlerin kendilerine ait olan tür sayıları ile çarpılarak tekrarlanmaktadır. Daha sonra türlerin kendine ait değerlerinin toplamalarının negatif çarpım değeri alındığında Shannon-Wiener (H) değerini vermektedir (Shannon ve Weaver, 1949; Gülsoy ve Özkan, 2008, Özkan 2016). Shannon-Wiener indeks değerleri doğrultusunda çalışma alanı içerisinde tür zenginliği ile türler arasında birey sayılarının nasıl dağılım gösterdiği haritalandırılmıştır. Haritalandırma işlemi iki mevsim (ilkbahar ve sonbahar) ve toplam olmak üzere üç farklı şekilde gerçekleştirilmiştir.

### 3. Bulgular

Çalışma alanı içerisinde yürütülen ön çalışmalar ve araştırmalar kapsamında; memeli yaban hayvanlarına ait iz, dışkı, ölü birey ve belirtilerden hareketle var-yok taraması gerçekleştirilmiştir. Sahada karşılaşılan iz, dışkı ve belirtiler Elbroch'e (2003) göre belirtilen esaslar kapsamında teşhis edilmiştir. Elde edilen teşhis sonuçlarına göre çalışma alanı içerisinde Saz kedisi (*Felis chaus* L.), Vaşak (*Lynx Lynx* L.), Kurt (*Canis lupus* L.), Tilki (*Vulpes vulpes* L.), Çakal (*Canis aureus* L.), Yaban domuzu (*Sus scrofa* L.), Yaban tavşanı (*Lepus europaeus* L.), Kaya sansarı (*Martes foina* L.) ve Porsuk (*Meles meles* L.) tespit edilmiştir.

Toplam olarak 462 plotta memeli yaban hayvanlarına ait ayak izi, dışkı, kemik ve ölü bireylere rastlanmıştır. Tür bazlı olarak bakıldığında ise; 141 plotta Tilki, 126 plotta Yaban domuzu, 68 plotta Kaya sansarı, 59 plotta Çakal, 22 plotta Saz kedisi, 15 plotta Yaban tavşanı, 12 plotta Porsuk, 10 plotta Vaşak, 9 plotta Kurt türüne ait belirtiler kayıt altına alınmıştır.

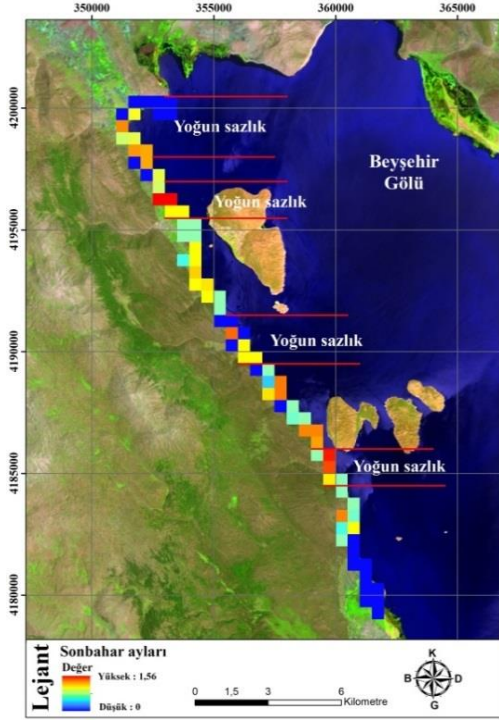
Yaban hayvanlarının habitat tercihlerindeki ana unsurların mekan, besin, örtü ve su olduğu bilinmektedir (Van Horne, 1983; Oğurlu, 2001). Yaban hayvanlarının nereleri hangi amaçla tercih ettiklerinin bilinmesi bu hayvanların korunması açısından önemli bir bilgi kaynağıdır. Bu nedenle çalışma alanı içerisinde ilkbahar ve sonbahar aylarında yapılmış olan envanter sonuçlarına göre Shannon-Wiener indeks haritaları oluşturulmuştur. Ayrıca alan içerisinde tespit edilen tüm türlerin ortak kullanım alanlarını tespit etmek amacıyla toplam iki mevsimin Shannon-Wiener indeks haritası da oluşturulmuştur. Shannon-Wiener çeşitlilik indekslerine göre ilkbahar ( $H_I=1,418$ ), sonbahar ( $H_S=1,56$ ) ve toplam ( $H_T=1,581$ ) olarak belirlenmiştir.



**Şekil 3.** İlkbahar aylarına ait Shannon-Wiener çeşitlilik indeksi haritalaması

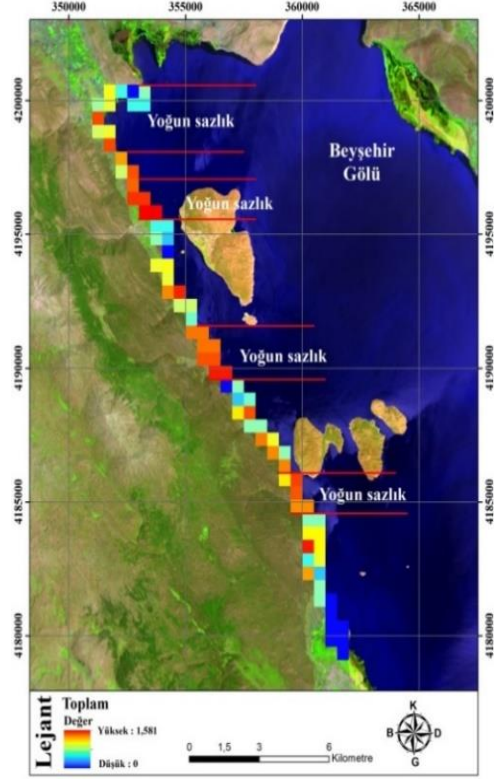
Şekil 3 incelendiğinde ilkbahar aylarında tespit edilen memeli yaban hayvan türlerinin Shannon-Wiener indeksi haritası görülmektedir. İlkbahar aylarında tespit edilen yaban hayvan türlerinin Shannon-Wiener çeşitlilik indeksi değeri toplam  $H_I=1,418$  olarak hesaplanmıştır. Aynı zamanda oluşturulan Shannon-Wiener indeks haritasına göre yaban hayvan tür dağılımının 3 bölgede (kırmızı ve turuncu alanlar) yoğunlaştığı görülmektedir. Yoğunlaştığı üç bölgenin ortak noktasının ise yoğun sazlık alanlar olduğu haritada belirlenmiştir. Bunun yanında yaban hayvan tür dağılımının

çalışma alanı içerisinde bulunan seyrek sazlık alan çevresinde yoğunlaştığı da görülmektedir.



**Şekil 4.** Sonbahar aylarına ait Shannon-Wiener çeşitlilik indeksi haritalaması

Şekil 4 incelendiğinde sonbahar aylarında tespit edilen memeli yaban hayvan türlerinin Shannon-Wiener çeşitlilik indeksi haritası görülmektedir. Elde edilen çeşitlilik haritalamasına göre; sonbahar aylarında tespit edilen yaban hayvan türlerinin Shannon-Wiener çeşitlilik indeksi değeri toplam ( $H_S=1,56$ ) ve ilkbahar aylarına göre daha yüksek olduğu görülmektedir. Sonbahar Shannon-Wiener çeşitlilik indeksi haritasına göre çalışma alanı içerisinde bulunan yaban hayvan çeşitliliğinin yoğun sazlık alanlarda yüksek çıktığı görülmektedir.



**Şekil 5.** Çalışma alanı içerisinde tespit edilen türlere ait toplam Shannon-Wiener çeşitlilik haritalaması

Şekil 5 incelendiğinde çalışma alanı içerisinde iki mevsim boyunca tespit edilen tüm türlerin verileri kullanılarak Shannon-Wiener çeşitlilik indeksi hesaplanmıştır. Shannon-Wiener çeşitlilik hesaplamalarına göre alandaki yaban hayvan türlerinin hangi alanlarda yoğunlaştıklarını belirlemek amacıyla çeşitlilik haritası oluşturulmuştur. Tespit edilen bütün yaban hayvan türlerinin en yüksek Shannon-Wiener çeşitlilik indeksi değerinin toplam  $HT=1,581$  olduğu görülmektedir. Haritaya göre çalışma alanı içerisinde bulunan yaban hayvan türlerinin yoğun sazlık alan çevresinde yoğunlaştığı görülmektedir.





**Şekil 6.** Hücrelerin mevsimlere göre çeşitlilik indeksi değerleri ve Beyşehir Gölü sınırına ait arazi kullanım sınıfları a) İlkbahar ayları b) Sonbahar ayları c) Toplam aylar

Şekil 6 incelendiğinde çalışma alanına ait arazi kullanım sınıfı haritası gözükmemektedir. Şekilde memeli yaban hayvanı türlerinin arazi kullanım sınıflarının ilkbahar ve sonbahar ayları için hesaplanan Shannon-Wiener çeşitlilik indeksi sonuçlarının karşılaştırıldığı görülmektedir. Bu karşılaştırmaya göre; çalışma alanı içerisinde bulunan yoğun sazlık alan, meyve bahçeleri ve tarım alanı çevresinde ilkbahar aylarına göre sonbahar aylarında daha yüksek çıktığı görülmektedir. Ayrıca alan içerisinde bulunan dik yamaçlı kayalık alanların ilkbahar aylarında ve sonbahar aylarında yaban hayvan tür çeşitliliğine negatif etki oluşturduğu açık bir şekilde haritada görülmektedir. İlkbahar ve sonbahar aylarına ait toplam iki harita çakıştırılıp toplam aylara ait renklendirmede şekilde gösterilmektedir.

#### 4. Tartışma ve Sonuçlar

Bu çalışma Beyşehir Gölü'ndeki sazlık alanlar ile bazı memeli yaban hayvanlarının birey sayılarından hesaplanan tür çeşitliliği arasındaki ilişkileri ortaya koymak amacıyla gerçekleştirilmiştir. Bunun için memeli yaban hayvanlarına ait iz, dışkı ve belirti taraması yapılmış ve ilkbahar aylarında toplam 172 noktada ve sonbahar aylarında ise 290 noktada 9 farklı memeli yaban hayvanına ait belirtiler tespit edilmiştir. Shannon-Wiener çeşitlilik indeksi hesaplamaları sonucuna göre çalışma alanı içerisinde bulunan ilkbahar ve sonbahar aylarında yaban hayvan tür dağılımları haritalandırılmıştır. Haritalandırma işlemi sonucunda Beyşehir Gölü'nün kuzeybatı kısımlarında bulunan sazlık alanların bazı memeli yaban hayvanları tür dağılımının üzerinde etkili olduğu sonucuna varılmıştır.

Arazi çalışmaları sırasında çalışma alanı içerisinde bulunan sazlık alanların memeli yaban hayvanları tarafından kullanımı etkileyebilecek bazı olumlu veya olumsuz durumlara bakıldığında; sahadaki bazı sazlık alanların memeli yaban hayvan türlerine ev sahipliği yapacak yoğunlukta olmaması, bazı balık türlerinin yoğun sazlık alanları tercih ettikleri düşüncesiyle olta balıkçıların seyrek sazlık çevresinde yoğunlaşması ve ulaşım yolunun bazı sazlık alanların çok yakınından geçmesi yaban hayvanlarının sazlık alanları kullanımını olumsuz yönde etkileyen başlıca nedenler olarak görülmüştür. Olumlu yönde etkileyebilecek durumlar ise; yoğun sazlıkların çevresinde olta balıkçıların olmalarının takılması sonucu bu alanların tercih edilmemesi ve yöredeki insanlar tarafından "çim sazı" olarak isimlendirilen balıkların balıkçılar tarafından tercih edilmemesi ve sayılarının azalması için yakalanan bu balıkların göl kenarına atılması sonucu ortaya çıkan kolay besin temini şeklindedir.

Bazı memeli yaban hayvan türleri için kolay besin ihtiyacı sağlayan sazlık alanlar içerisinde böcek, balık, amfibi ve sürüngen gibi hayvan türleri barındırmaktadır (Turan, 1990; Nishujima ve Nakata, 2004). Ayrıca sazlık alanların yoğun olduğu yerler göçmen kuş türlerine ev sahipliği yapmakta ve yaban hayvan türleri için besin tercihiinde etkili olmaktadır (Kızıroğlu, 1987; Emerton vd., 2006; Dudley vd., 2005). Ancak sulak alan çevresinde bulunan sazlık alanlar yaban hayatına sağladığı faydaların yanında ekonomik açıdan bakıldığında etrafında yaşayan insanlar ekonomik fayda sağlamasına rağmen hakkettiği değeri görememektedir. Bu nedenle sazlık alanların korunması ve geliştirilmesi bakımından önemini ortaya koymak amacıyla gerçekleştirilen çalışmada sazlık alanların değişik mevsimlerde yaban hayvanları üzerindeki etkisi araştırılmıştır. Bunun için çalışma alanı içerisinde tespit edilen memeli yaban hayvanlarının tür bazında biyolojik çeşitliliğe katkısına bakıldığında, ilkbahar ve sonbahar aylarında Kaya sansarı, Yaban domuzu, Tilki ve Çakal'ın iki mevsimde de aynı alanlar içerisinde bulunduğu ve bu nedenle mevsimler arası beta çeşitliliği bakımından bir fark oluşturmadığı tespit edilmiştir. Saz kedisi, Kurt, Vaşak ve Yaban tavşanının sonbahar aylarında tespit edilmesi sonucunda mevsimler arası beta çeşitliliğine pozitif katkı yaptıkları belirlenmiştir. Bunun yanında Porsuk türünün ise ilkbahar aylarındaki mevsimler arası beta çeşitliliğine en az katkı sağladığı sonucuna varılmıştır.

Bazı memeli yaban hayvanı türlerinin biyolojik çeşitliliğe katkısı üzerine yapılmış olan çalışmalar incelendiğinde; Yaban domuzunun habitat tercihinde en fazla orman içi açıklıklarının (Thurfjell vd., 2009), meyve bahçelerinin, sulak alanların ve sazlık alanların ön plana çıktığı görülmektedir. Ayrıca kayalık alanlarda devamlı bir vejetasyon olmadığı için böylesi alanları yaban domuzlarının tercih etmediği ifade edilmektedir (Küçük ve İkiz, 2004). Türün besin gereksinimini doğal ortamlardan karşılayamadığı zaman yerleşim yerlerine yakın tarım alanlarına yöneldiği belirtilmiştir (Cengiz vd., 2016). Yapmış olduğumuz çalışmada da türün her mevsim alanda bulunduğu için biyolojik çeşitlilik bakımından bir fark oluşturmadığı görülmüştür. Ayrıca benzer özelliklere sahip olan Tilki için mevsimsel farklılığın tür üzerinde etki oluşturmadığı belirlenmiştir. Buna göre Cavallini ve Lovari (1994), çalışmalarında Tilki'nin daha çok sulak ve nemli bölgelerdeki makilik, çimenlik, çayırılık alanları kullandığını ifade etmişlerdir. Ayrıca türün sulak alan ve çevresindeki sürüngen, kuş, ördek gibi canlılarla beslediklerini belirtmişlerdir. Yiğit vd. (1996), Kaya sansarı'nın genellikle yerleşim yerlerine yakın olan bölgeleri, çok fazla ağaçlık olmayan orman kenarlarını, bahçelik yerleri, kaya kovuklarını ve dağların yüksek kesimlerini habitat olarak tercih ettiğini belirtmişlerdir. Ayrıca Çolak vd. (1997), çalışmalarında Türkiye'nin değişik bölgelerinden dokuz Kaya sansarının morfolojik karakterlerini, yayılışını, beslenmelerini ve habitat tercihlerini daha önce yayınlanmış makalelerle uygunluğunu karşılaştırmışlardır. Türün farklı bölgelerde sadece morfolojik açıdan değişiklik gösterdiği sonucuna varmışlardır. Bu gerekçeyle, yapmış olduğumuz çalışmada ise türün habitat tercihinde mevsimsel farklılığın olumsuz bir etki etmediği sonucuna varılmıştır. Ayrıca yapmış olduğumuz çalışmamızda Kaya sansarı türünün ilkbahar ve sonbahar aylarında alan içerisinde bulunduğu görülmektedir. Literatüre göre; Korschgen (1957)'de, Çakal türünün habitat olarak; yerleşim yerlerine yakın, yükseltisi fazla olmayan alanlarda yaşamını sürdürerek buralardaki kümes hayvanlarını, fareleri ve tavşanları yiyerek beslendiklerini belirlemiştir. Diğer yandan yerleşim yerlerine uzak olan tarım arazileri ya da meyve bahçelerini de beslenme amacıyla tercih ettiğini ifade etmiştir. Buna göre alan içerisinde ilkbahar ve sonbahar aylarında tür korunmayan meyve bahçeleri ya da tarım alanlarının olması nedeniyle mevsimsel farklılığın tür üzerinde negatif etki oluşturacağı sonucuna varılmıştır.

Çalışmamızda ise alan içerisinde bulunan sazlık alanların tür için barınmak ya da beslenmek için yeterli yoğunlukta olmaması neticesinde ilkbahar aylarında Saz kedisi tür yoğunluğunun görülmediği belirlenmiştir. Fakat çalışma alanı içerisinde sonbahar aylarında bulunan yoğun sazlık alanlar sayesinde Saz kedisinin habitat tercihinin oluşturduğu için türün bu aylarda biyolojik çeşitliliğe katkı sağladığı sonucuna varılmıştır. Literatüre göre; Majumder vd. (2011), yapmış oldukları çalışmada Saz kedisi türünün hangi alanlarda yoğunlaştığını bulmayı amaçlamışlardır. Saz kedisinin eğimli olmayan arazileri, sulak alanları, yoğun sazlık alanları ve orman içi açıklıkları tercih ettiğini gözlemişlerdir. Bu alanlarda yaşayan kemirgen, balık ve kuş gibi hayvanları besin olarak tercih ettiklerini tespit etmişlerdir. Sonuç olarak, bu türün besin tercihinin bu aylarda maksimum katkıyı küçük kemirgenlerin sağladığını belirlemişlerdir. Bu gerekçeyle yapmış olduğumuz çalışma literatürle uyumluluk göstermektedir. Ayrıca ilkbahar aylarında Vaşak türünün alanda tespit edilmemesi ve sonbahar aylarında alana gelmesi neticesinde türün sonbahar aylarında biyolojik çeşitliliğe katkı sağladığı açıkça ortadadır. Buna göre Major ve Sherburne (1987)'nin Vaşak türünün habitat tercihinin belirlemek amacıyla yapmış olduğu çalışmada türün sonbahar aylarında daha çok iğne yapraklı ormanları ve sulak alan çevrelerini tercih ettiğini bu alanlardaki tavşan, kuş ve ördek gibi hayvanlar ile beslendiklerini ifade etmişlerdir. İlkbahar aylarında çalışma alanında aşırı bir kuraklık görülmediğinden dolayı Yaban tavşanı türünün bu aylarda çalışma alanını tercih etmediği belirlenmiştir. Fakat sonbahar aylarında çalışma alanında oluşan kuraklık neticesinde türün alanı ziyaret etmesi sonucunda biyolojik çeşitliliğe katkı sağladığı sonucuna varılmıştır. Literatüre göre; Carro vd., 2011'de yapmış oldukları çalışmada Yaban tavşanının nemli mevsimlerde dağların yüksek rakımlarına ulaştığını belirtmişlerdir. Buna karşılık olarak kurak mevsimlerde ise türün beslenmesini düşük rakımlardaki önemli bir kısmını bataklık veya sazlık alanlarda oluşan otsu bitkilerin oluşturduğu ifade etmişlerdir. Bu gerekçeyle yapmış olduğumuz çalışmanın literatüre uyumlu olduğu görülmektedir. Ayrıca yapmış olduğumuz çalışmada Kurt türünün alan içerisinde sonbahar aylarında tespit edilmesi sonucunda biyolojik çeşitliliğe katkı sağladığı sonucuna varılmıştır. Literatüre göre; Jedrzejewski vd. (2001), yapmış oldukları çalışmalarında Kurt'un günlük hareket şekillerini ve buldukları alanları kullanım nedenlerini belirlemeyi

amaçlamışlardır. Çalışma alanı içerisinde Kurt'un yiyecek bulma, saklanma ve su ihtiyacını karşılamak için yaklaşık 27 km'lik bir mesafeyi kat ettiğini ve bu ihtiyaçları için yüksek oranda sazlık bölgelerden faydalandığını belirtmiştir. Ayrıca Vos (2000)'da çalışmasında Kurt türünün sonbahar aylarında kolay besin ihtiyacını yüksek rakımlardan karşılayamadığı için düşük rakımlarda bulunan sazlık veya bataklık alanlarda; balık, kuş, porsuk ve bazı memeli türleri avladığını belirtmişlerdir. Buna göre yapmış olduğumuz çalışmanın literatürle uyumlu olduğu açık bir şekilde ortadadır. Sonuç olarak; ilkbahar aylarında alan içerisindeki vejetasyonun yeni canlanması ve sazlıkları kullanan canlıların henüz alana gelmemiş olması nedeniyle yaban hayvanlarının Shannon-Wiener çeşitlilik indeksi değerinin sonbahar aylarına göre daha düşük çıktığı düşünülmektedir.

Bu çalışmadan yola çıkılarak, memeli yaban hayvan tür yoğunluğunu belirlemek amacıyla gerçekleştirilecek olan çalışmalarda; i) Shannon-Wiener çeşitlilik indeksinin yaban hayatı çalışmalarına önemli katkılar sağlayacağı ii) Biyolojik çeşitliliğe katkı sağlayan sazlık alanların yoğunluklarının artırılmasına yönelik çalışmaların yapılması gerekliliği iii) Sulak alan çevresinde yaşayan halkın sazlık alanların yaban hayatı üzerindeki etkileri hakkında bilgilendirilmesinin daha sağlıklı sonuçlara ulaşılmasını sağlayacağı öngörülmektedir. Ayrıca bu çalışma; yaban hayvan tür çeşitliliği ile tür zenginliği arasındaki mevsimsel ilişkilerinin Shannon-Wiener çeşitlilik indeksi sonuçlarına göre haritalanması koruma çalışmalarının hangi mevsimlerde daha yoğun yapılacağına dair önemli bir bilgi kaynağı sağlayacaktır.

### Teşekkür

4750-YL1-16 No'lu Proje ile bu çalışmayı maddi olarak destekleyen Süleyman Demirel Üniversitesi Bilimsel Araştırma Projeleri Yönetim Birimi Başkanlığı'na teşekkür ederiz.

### Kaynaklar

- Aksan, Ş., Mert, A. (2016). Bird species in Isparta-Atabey Plain. *Turkish Journal of Forestry*, 17(2), 153-157.
- Aslan, B. (2008). Comparative Biodiversity Of Carabidae And Tenebrionidae(Coleoptera) Species In Various Habitats Of Kasnak Meşesi Nature Reserve (Isparta) Collected

By Pitfall Traps. *SDU Faculty of ARTS and sciences, Sciences journal*, 3(2). ISO 690.

- August, P. V. (1983). The role of habitat complexity and heterogeneity in structuring tropical mammal communities. *Ecology*, 64(6), 1495-1507.
- Balabanlı, C., Albayrak, S., Türk, M., Yüksel, O. (2006). Some Toxic Plants Growing In Rangelands Of Turkey and Their Effects On Animals. *SDU Faculty of Forestry JournalSeri: A*, (2), 89-96.
- Batzer, D. P., Wissinger, S. A. (1996). Ecology of insect communities in nontidal wetlands. *Annual review of entomology*, 41(1), 75-100.
- Bibby, C.J. Lunn, J. (1982) Conservation of reedbeds and the iravi fauna in England and Wales. *Biological Conservation*, 23, 167-186.
- Bibi, F., Ali, Z. (2013). Measurement of diversity indices of avian communities at Taunsa Barrage Wildlife Sanctuary, Pakistan. *The Journal of Animal, Plant Sciences*, 23(2), 469-474.
- Brooks, R. T. (2001). Effects of the removal of overstory hemlock from hemlock-dominated forests on eastern redback salamanders. *Forest Ecology and Management*, 149(1-3), 197-204.
- Cavallini, P., Lovari, S. (1994). Home range, habitat selection and activity of the red fox in a Mediterranean coastal ecotone. *Acta Theriologica*, 39(3), 279-287.
- Cengiz, G., Ünal, Y., Oğurlu, İ. (2016). Ecological observation on Wild boar (*Sus scrofa* L.) and determination of species habitat relationships: Isparta-Gölcük Natural Park sample *Turkish Journal of Forestry*, 17(2), 158-165.
- Cowardin, L., M., Carter, V., Golet, F., C., Laroe, E., T. (1979). Classification of Wetlands and Deepwater Habitats of the United States. Department of Interior Fish and Wildlife Service, Washington, U.S.A. 45p.
- Çolak, E., Yiğit, N., Kıvanç, E. (1997). Diagnostic Characters and Distribution Of *Meriones Illiger, 1811* Species (Mammalia: Rodentia) in Turkey. *Turkish Journal Of Zoology*, 21(4), 361-374.

- Dardaillon, M. (1986). Seasonal variations in habitat selection and spatial distribution of wild boar (*Sus scrofa*) in the Camargue, Southern France. *Behavioural Processes*, 13(3), 251-268.
- Desrochers, R., Anand, M. (2004). From Traditional Diversity Indices to Taxonomic Diversity Indices, *International Journal of Ecology and Environmental Science* 30: 85-92.
- Dudley, N., Baldock, D., Nasi, R., Stolton, S. (2005). Measuring biodiversity and sustainable management in forests and agricultural landscapes. *Philosophical Transactions of the Royal Society B: Biological Sciences*, 360(1454), 457-470.
- Elbroch, M. (2003). *Mammal Tracks., Sign: A Guide To North American Species*. Stackpole Books. 792p. Mechanisburg.
- Emerton, L., Bishop, J., Thomas, L. (2006). Sustainable Financing of Protected Areas: A global review of challenges and options (No. 13). IUCN.
- Giannatos, G., Marinos, Y., Maragou, P., Catsadorakis, G. (2005). The status of the golden jackal (*Canis aureus* L.) in Greece. *Belgian Journal of Zoology*, 135(2), 145.
- Goszczyński, J., Jedrzejewska, B., Jedrzejewski, W. (2000). Diet composition of badgers (*Meles meles*) in a pristine forest and rural habitats of Poland compared to other European populations. *Journal of Zoology*, 250(4), 495-505.
- Görmez, K. (1997). *Environmental problems and Turkey*. Gazi Bookstore Press, 2nd Edition, Ankara, 17, 53-56.
- Gülsoy, S., Özkan, K. (2008). Importance Of Biodiversity From The Ecological Stand Point And Some Diversity Indexes. *SDU Faculty of Forestry Journal*, 1, 168-178.
- Güneş, G. (2011). The New Approach on Protected area management: Participatory Management Plans. *Economis of Journal*, 3(1).
- Güzelmansur, A. (2000). Erzin İlçesi Sarımsazı-Burnaz Halk Plajları ve Gaziantep Tatil Siteleri Arasındaki Kıyı Şeridinde Kıyı Alan Kullanım Planlaması. Yüksek Lisans Tezi, Çukurova Üniversitesi Fen Bilimleri Enstitüsü, Peyzaj Mimarlığı Anabilim Dalı, Adana.
- Heikkinen, R. K., Luoto, M., Virkkala, R., Rainio, K. (2004). Effects of habitat cover, landscape structure and spatial variables on the abundance of birds in an agricultural-forest mosaic. *Journal of Applied Ecology*, 41(5), 824-835.
- Heywood, V.H. (1995). *Global Biodiversity Assessment*. Published for the united nations Environment Programme. University Pres, 457-542. CAMBRIDGE.
- Jędrzejewski, W., Schmidt, K., Okarma, H., Kowalczyk, R. (2002). Movement Pattern and Home Range Use by The Eurasian Lynx in Białowieża Primeval Forest (Poland). In *Annales Zoologici Fennici* (Pp. 29-41). Finnish Zoological and Botanical Publishing Board.
- Karagöz, A. (1998). Convention On Biological Diversity. *Field Crops Central Research Institute Journal* 7(1).
- Katip, A., Karaer, F. (2011). Assessment of Water Quality of Uluabat Lake in Accordance with Turkish Legislation and International Criteria. *Uludağ University Journal of The Faculty of Engineering and Architecture*, 16(2), s: 25-34, 2011.
- Kızıroğlu, İ. (1987). Kuş Koruması ve Baştankaraların (*Parus* spp.) Biyolojik Savaşta Orman Zararlılarına Etkileri. *Doğa Zooloji Dergisi*, 11, 104-109.
- Korschgen, L. J. (1957). Food habits of the coyote in Missouri. *The Journal of Wildlife Management*, 21(4), 424-435.
- Küçük, F., İkiz, R. (2004). Fish fauna of streams discharging to Antalya Bay. *Ege University, Water Products Journal*, 21(3-4), 287-294.
- Lai, X.J., Huang, Q., ve Jiang, J.H. (2012). Wetland inundation modeling of Dongting Lake using two dimensional hydrodynamic model on unstructured grids. *Procedia Environmental Sciences* 13, 1091 – 1098.
- Major, J. T., Sherburne, J. A. (1987). Interspecific relationships of coyotes, bobcats, and red foxes in western Maine. *The Journal of Wildlife Management*, 606-616.



- Majumder, A., Sankar, K., Qureshi, Q., Asu, S. (2011). Food habits and temporal activity patterns of the Golden Jackal *Canis aureus* and the Jungle Cat *Felis chaus* in Pench Tiger Reserve, Madhya Pradesh. *Journal of Threatened Taxa*, 3(11), 2221-2225.
- Mayer, J. (1995). Nachhaltige Entwicklung – ein Leitbild zur Neuorientierung der Umwelterziehung DGU-Nachrichten 12, 43-56.
- Mert, A., Yalçinkaya, B. (2016). The relation of edge effect on some wild mammals in Burdur-Ağlasun (Turkey) district. *Biological Diversity and Conservation*, ISSN, 1308-8084.
- Mitsch, W. J., Gosselink, J. G. (2000). The value of wetlands: importance of scale and landscape setting. *Ecological economics*, 35(1), 25-33.
- Nishujima, H., Nakata, M. (2004). Relationships between plant cover type and soil properties on Syunkunitai coastal sand dune in Eastern Hokkaido. *Ecological Research*, 19, 581-591.
- Oğurlu, İ. (2001). *Yaban Hayatı Ekolojisi*. Süleyman Demirel Üniversitesi Yayınları, No: 19, Isparta.
- Oruç, M.S., Mert, A., Özdemir, İ. (2017). Modelling Habitat Suitability For Red Deer (*Cervus elaphus* L.) Using Environmental Variables In Çatacak Region. *Bilge International Journal of Science and Technology Research*, 1 (2): 135- 142.
- Özkan, K. (2016). *Biyolojik Çeşitlilik Bileşenleri ( $\alpha$ ,  $\beta$  ve  $\gamma$ ) Nasıl Ölçülür*. Süleyman Demirel Üniversitesi, Orman Fakültesi Yayın, (98).
- Primack, R. B. (1995). *Naturschutz biologie*. Spektrum Akad Verl., Heidelberg.
- Saatçioğlu, F., (1979). *Silvikültür Tekniği*, İ.Ü. Orman Fakültesi Yayınları, İ.Ü. Yayın no:2490, O.F. Yayın no: 268, İstanbul, 556.
- Semere, T., Slater, F. M. (2007). Ground flora, small mammal and bird species diversity in miscanthus (*Miscanthus giganteus*) and reed canary-grass (*Phalaris arundinacea*) fields. *Biomass and Bioenergy*, 31(1), 20-29.
- Shannon, C. E., W. Weaver. (1949). *The mathematical theory of communication* Univ. Illinois Press, Urbana.
- Sullivan, T. P., Wagner, R. G., Pitt, D. G., Lautenschlager, R. A., Chen, D. G. (1998). Changes in diversity of plant and small mammal communities after herbicide application in sub-boreal spruce forest. *Canadian Journal of Forest Research*, 28(2), 168-177.
- Süel, H. (2014). *Isparta-Sütçüler Yöresinde Av Türlerinin Habitat Uygunluk Modellemesi*. Süleyman Demirel Üniversitesi, Fen Bilimleri Enstitüsü Orman Mühendisliği Anabilim Dalı. Doktora Tezi, 151s., Isparta.
- Thurfjell, H., Ball, J. P., Åhlén, P. A., Kornacher, P., Dettki, H., Sjöberg, K. (2009). Habitat use and spatial patterns of wild boar *Sus scrofa* (L.): agricultural fields and edges. *European journal of wildlife research*, 55(5), 517-523.
- Turan, N. (1990). *Türkiye'nin av ve yaban hayvanları* (Vol. 2).
- Van Horne, B. (1983). Density as A Misleading Indicator of Habitat Quality. *J. Wildlife Management*, 47: 893-901.
- Virgos, E., Cabezas-Diaz, S., Mangas, J. G., Lozano, J. 2010. Spatial Distribution Models in A Frugivorous Carnivore, The Stone Marten (*Martes Foina*): Is the Freshyfruit Availability A Useful Predictor? *Animal Biology*, 60(4): 423–43.
- Vos, De P. (2000). Technology of Mammalian Cell Encapsulation. *Advanced Drug Delivery Reviews*, 42(1), 29-64.
- Warwick, R.M., Clarke, K.R. (1995). New biodiversity measures reveal a decrease in taxonomic distinctness with increasing stress. *Marine Ecology Progress Series*, 129, 301– 305.
- Williams, L., H. (1990). Potential Benefits of Diffusible Preservatives for Wood Protection, an Analysis with Emphasis on Building Protection with Diffusible Preservatives, *Forest Product Research Society*, 29-35.

## Yazar rehberi

Makale A4 sayfa boyutunda, Times New Roman yazı tipinde, 10 punto olarak ve düz metin şeklinde yazılmalıdır. Makaleye sayfa ve satır numaraları eklenmelidir.

**Kapak sayfası:** Kapak sayfasında sırasıyla makale başlığı, yazar adı soyadı, yazar iletişim bilgileri bulunmalıdır.

**Başlık ve özet (Türkçe ve İngilizce):** Özet 500 kelimeyi geçmeyecek şekilde yazılmalıdır. Araştırmanın gerekçesini, amaçlarını, uygulanan yöntemi, sonuç ve önerileri içermelidir. Özet sonuna 3-6 kelimedenden oluşan anahtar kelimeler eklenmelidir.

**Ana metin:** Makale ana metni tek satır aralıklı olarak yazılmalı, çizelge ve şekillerle birlikte toplam 15 sayfa geçmemelidir. Konu başlıkları 1., 1.1., 1.1.1., şeklinde numaralandırılmalıdır.

**Dipnotlar:** Metin içerisinde dipnotlardan olabildiğince kaçınılmalıdır. Çizelge ve şekillerde ise gerekli olması halinde ilgili objenin altında yer almalıdır.

**Semboller ve kısaltmalar:** Birim sembolleri Uluslararası Birimler Sistemine (The International System of Units; SI) göre olmalıdır.

**Kaynaklar:** Metin içinde geçen kaynaklar yazarların soyadları ve yayın yılı ile birlikte verilmelidir (Örnek: Özkan vd., 2008; Özdemir, 2015). Metin sonundaki kaynaklar önce alfabetik sonra kronolojik sıraya göre sıralanmalıdır. Bir yazarın aynı yılda birden fazla yayınına atıf yapılmışsa, bu kaynaklar yayının yılından sonra gelecek a, b, c... harfleriyle ayrılmalıdır (Örnek: Kandemir, 1999a; 2000b; 2001).

**Çizelgeler ve şekiller:** Bütün çizelge ve şekiller metin içerisinde atıf sıralarına göre ardışık olarak numaralandırılmalı ve ilgili yere eklenmelidir. Çizelgelerin üzerinde ve şekillerin altında başlıkları yer almalıdır. Çizelge ve şekiller hem elektronik ortamda hem de kağıt baskıda net olarak görünür ve anlaşılabilir olmalıdır. Şekiller en az 300 dpi çözünürlüğünde hazırlanmalıdır. Şekillerde kullanılan karakterler Times New Roman yazı tipinde olmalıdır.

**Makalenin gönderilmesi:** Dergimizin bütün hakemlik ve yayıncılık işlemleri elektronik sistem üzerinden gerçekleştirilmektedir. Dergimize yayın göndermek isteyen yazarların ilk olarak dergimizin “web sitesine” girerek “kayıt” ekranından üye olmaları gerekmektedir. Kayıtlı yazarlarımız sisteme “giriş” yaptıktan sonra, makaleleri ile birlikte ve hakem önerilerini de içeren “Telif Hakkı Devri Formunu” sisteme ek belge olarak yüklemelidirler.

## Instructions for authors

Manuscript should be written in A4 page size, with Times New Roman font and 10 pt font size, as plain text. Page and line numbers should be included into the manuscript.

**Cover page:** Cover page should include title of the manuscript, names and contact information of the authors.

**Title and abstract (Turkish and English):** Abstract should not written exceed 500 words. Explains rationale, goals, methods, results and recommendations of the study. Keywords with 3-6 words should be included at the end of the abstract.

**Main text:** Main body of the manuscript should be written in single line spacing, and it should not exceed a total of 15 pages including tables and figures. Headings should be numbered as follows: 1., 1.1., 1.1.1.

**Footnotes:** Use of footnotes within the text should be avoided as much as possible. If necessary, it can be located below tables and figures.

**Symbols and abbreviations:** Unit symbols should comply with The International System of Units.

**References:** In the text, literature should be given with the last name of the author and year of the publication (For example: Özkan et al., 2008; Özdemir, 2015). At the end of the paper, references should be ordered first alphabetically and then chronologically. If there is more than one paper from the same author for a given year, these references should be identified by the letters a, b, c..., after the year of publication (For example: Kandemir, 1999a; 2000b; 2001).

**Tables and figures:** All tables and figures should be numbered in the order of their citation in the text, and they should be located in suitable places. Titles of the tables should be located above, and titles of the figures should be located below the related table or figure. Tables and figures should be easily visible and understandable both in print and electronic versions. Figures should be prepared in at least 300 dpi resolution. Characters within the figures should be in Times New Roman font type.

**Submission of a manuscript:** In our journal, all review and publishing processes are conducted within an electronic system. Authors who want to submit their manuscript to our journal should first visit our “web page” and “register” as an author. Our registered members can “log in” to the system and then upload their manuscript and “COPYRIGHT RELEASE FORM” as an appendix, containing their suggested referees.

## Kaynaklar

Kaynak kullanımları aşağıda örneklerde belirtilen şekillerde olmalıdır.

## References

Using of references should be in the form as follows.

### Article in periodical journals / Periyodik dergilerde makale

- Akyıldırım, O., Gökce, H., Bahçeli, S., Yüksek, H. (2017). Theoretical and Spectroscopic (FT-IR, NMR and UV-Vis.) Characterizations of 3-p-chlorobenzyl-4-(4-carboxybenzylidenamino)-4,5-dihydro-1H-1,2,4-triazol-5-one Molecule. *Journal of Molecular Structure*, 1127: 114-123.
- Tan, S., Williams, C.T. (2013). An In Situ Spectroscopic Study of Prochiral Reactant–Chiral Modifier Interactions on Palladium Catalyst: Case of Alkenoic Acid and Cinchonidine in Various Solvents. *J. Phys. Chem. C*, 117(35): 18043–18052.

### Book / Kitap

- Özkan, K. (2016). *Biyolojik Çeşitlilik Bileşenleri ( $\alpha$ ,  $\beta$ ,  $\gamma$ ) Nasıl Ölçülür?* Süleyman Demirel Üniversitesi, Orman Fakültesi Yayın No: 98, ISBN: 976-9944-452-89-2, Isparta, 142 s.
- Whittaker, E. T. (1988). *A treatise on the analytical dynamics of particles and rigid bodies*. Cambridge University Press.

### Reference to a chapter in an edited book / Kitapta bölüm

- Westhoff, V., Van Der Maarel, E. (1978). The braun-blanquet approach in classification of plant communities, Reinhold Tüxen (Ed.), *Handbook of Vegetation Science*, Springer Netherlands, pp. 619-704.
- Şencan, A., Sevindir, H.C., Kiliç, M., Karaboyacı, M. (2011). Biosorption of CR+ 6 from Aqueous Solution with Activated Sludge Biosolids (Ref. NO: MT11-OP-475), Gökçekus, H., Türker, U., LaMoreaux, J.W., (Ed, Survival and Sustainability, 973-984.

### Thesis and dissertation / Tez

- Gülsoy, S. (2011). *Pistacia terebinthus* L. subsp. *palaestina* (Boiss.) Enler (Anacardiaceae)'in Göller Yöresi'ndeki Yetiştirme Ortamı Özellikleri ve Yetiştirme Ortamı-Meyve Uçucu Yağ İçeriği Etkileşimleri. SDÜ, Fen Bilimleri Enstitüsü, Orman Mühendisliği Anabilim Dalı, 194 s.
- Özdemir, S. (2015). Ovacık Dağı Yöresi'nde Türk Kekliği (*Origanum onites* L.) ve Büyük Çiçekli Adaçayı (*Salvia tomentosa* Miller) Türlerinin Ekolojik Özellikleri. SDÜ, Fen Bilimleri Enstitüsü, Orman Mühendisliği Anabilim Dalı. 74s.

### Conference proceedings / Konferans bildirisi

- Özkan, K., Kavgacı, A. 2009. Küresel ısınmanın orta dağlık alanlarda tür çeşitliliği üzerine olası etkileri (Acıpayam yöresi örneği). I. Ulusal Kuraklık ve Çölleşme Sempozyumu (Eds: Palta, Ç.), 16-18 Haziran 2009, Konya, Türkiye, 277-284.
- Özkan, K., Negiz, M.G., Şentürk, Ö., Kandemir, H. (2012). Göller Bölgesi'ndeki Bazı Önemli Rekreasyon Alanları ve Onların Ekolojik Özellikleri, I. Rekreasyon Araştırmaları Kongresi 2012, Bildiri Kitabı, 12-15 Nisan, 587-596, Detay Yayıncılık, Kemer-Antalya.

### Electronic reference / Elektronik kaynak

- FAO, (2016). Sustainable Food and Agriculture. Food and Agriculture Organization of the United Nations, Rome, <http://www.fao.org/sustainability/en/>, Accessed: 14.06.2016.
- Milliparklar, (2017). Doğa Koruma ve Milli Parklar Genel Müdürlüğü. <http://www.milliparklar.gov.tr/korunanalanlar/kavramlar.htm>, Erişim Tarihi: 18.06.2017.

Bilge International Journal of Science and Technology Research online ve açık erişimli yayınlanan uluslararası hakemli bir dergidir. Dergi dili İngilizce ve Türkçe'dir. Yılda iki sayı yayınlanan dergide Temel bilimler, Doğa bilimleri, Mühendislik ve Teknoloji bilimleri konularında bilimsel makaleler yayınlanmaktadır. Dergimize gönderilen makalelerin daha önce yayınlanmamış orijinal çalışmalar olması gerekmektedir. Dergide yayımlanacak makalenin atıflarından, bilimsel verilerinden, sonuçlarından ve etik kurallara uygun olup olmadığından yazarlar sorumludur (yazar/yazarlar bu durumu telif hakkı sözleşmesinde kabul eder). Orijinal araştırmaya dayalı çalışmalara öncelik verilmekte, sınırlı sayıda derleme makale yayınlanmaktadır. Dergiye gönderilen makale, yayın kurulu tarafından yayına uygunluk açısından incelendikten sonra en az iki hakeme gönderilir. Hakemlerin değerlendirmeleri sonucunda en az iki yayınlanabilir raporu alan makale, dergi yönetiminin uygun görülen bir sayıda yayımlanır. Hakem raporlarının birisinin olumlu, diğerinin olumsuz olması durumunda makale üçüncü bir hakeme gönderilir. Bu durumda makalenin yayımlanıp yayımlanmamasına üçüncü hakemin raporuna göre karar verilir. Hakemler tarafından düzeltme istenen makaleler gerekli düzeltmeler için yazara geri gönderilir. Düzeltilecek metnin belirtilen sürede dergi sistemine yüklenmesi yazarın sorumluluğundadır. Makalenin yayımlanması konusunda son karar, dergi editörlüğüne aittir.

Bilge International Journal of Science and Technology Research is an online, open access, peer-reviewed, international research journal. Language of the journal is English and Turkish. The journal published two issues a year publishes scientific articles on the subjects of Basic Sciences, Natural Sciences, Engineering and Technology. Authors should only submit original work, which has not been previously published and is not currently considered for publication elsewhere. The authors are responsible for the citations of the article to be published, its scientific data, its results, and whether it is in line with ethical rules (Author / authors accept that in the copyright agreement). Research papers will be given priority for publication while only a limited number of review papers are published in a given issue. The articles are sent to at least two reviewers after examined by the editor board in terms of compliance with the publication. As a result of the evaluations of the reviewers, the article which received at least two publishable reports will be published at a suitable number for the management of the journal. If one of the reviewer reports is positive and the other is negative, the article will be sent a third reviewer. In this case, the publication of the article is decided according to the third report. The articles corrected by the referees are returned to the author for necessary corrections. It is the responsibility of the author to upload the revised text to the journal system for the specified period. The final decision on the publication of the article belongs to chief editor.